

The Synthesis and Characterisation of Polyhedral Oligomeric Silsesquioxane Bound Chromophores

David J. Clarke (MSc.) (BSc.Hons)

Thesis submitted to the Faculty of Science and Engineering of Flinders University in
partial fulfillment of the requirements for the degree of

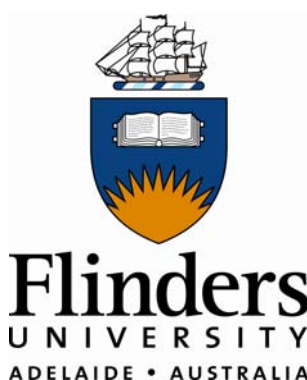
DOCTOR OF PHILOSOPHY

in

CHEMISTRY

Prof Janis Matisons

Prof George Simon



September 2008

Adelaide, South Australia

The Synthesis and Characterisation of Optically Active Polyhedral Oligomeric Silsesquioxanes

David J. Clarke (MSc.) (BSc.Hons)

ABSTRACT

This research involved the synthesis and characterisation of a range of optically active polyhedral oligomeric silsesquioxane (POSS) compounds.

POSS precursor compounds containing functional groups required for subsequent attachment of the desired functional groups have been synthesised. Examples of such precursor compounds include mono-functionalised POSS compounds with periphery aldehyde, azide, amino and pyridyl functional groups.

A variety of POSS compounds, functionalised with a range of optical functionalities, including optical limiters such as fulleropyrrolidine and iminofullerene, and dyes and pigments, including naphthalene, biphenyl, perylene, pyrene and porphyrin have been synthesised.

The reaction of mono-functionalised POSS aldehydes with fullerene (C_{60}) in the presence of N-methylglycine yielded the desired POSS fulleropyrrolidines, whilst reaction of mono-functionalised POSS azide with C_{60} yielded POSS iminofullerenes. All POSS fullerene compounds were characterised by power limiting measurements, exhibiting comparable power limiting to that of parent C_{60} .

The microwave condensation of mono-amino POSS with a range of mono- and bis-anhydrides yielded the POSS imide compounds, which were characterised by UV-Vis and fluorescence spectrophotometry. The perylene POSS imide derivative was further characterised by single crystal x-ray crystallography. The naphtha and biphenyl POSS imides exhibited extremely weak fluorescence, whilst the perylene

POSS imide displayed particularly strong fluorescence, with a quantum yield approaching unity.

The incorporation of a pyridyl group on the periphery of a mono-functionalised POSS cage allowed for the synthesis of the first porphyrin functionalised POSS compound. Mono-porphyrin POSS exhibited comparable absorption properties to other pyridyl ligated ruthenium porphyrins.

Mono-functionalised pyrene POSS compounds were prepared through the reaction of 1-pyrene acid chloride with mono(3-aminopropyl)POSS. This synthetic pathway offered a convenient route to mono-functionalised pyrene POSS, in preference to the multi-substitution associated with Heck coupling. Mono-pyrene POSS was determined to be strongly fluorescent, exhibiting a high quantum yield of fluorescence.

ACKNOWLEDGEMENTS

I would like to thank my supervisors Prof. Janis Matisons and Assoc. Prof. George Simon for the opportunity to undertake this project and their support and assistance. Additionally, I would like to express gratitude to Dr Mark Fisher for his support in the latter stages of the project and the opportunity to work on the biodiesel program, which taught me about chemistry in the real world. I must also thank Dr Stephen Clarke for always making me focus the final hurdle and providing part or my scholarship towards the latter stages the project.

Thanks to Dr Marek Samoc and Dr Anna Samoc at ANU for their help in obtaining the power limiting data and also to Dr Brian Skelton for the x-ray crystallography measurement.

I would also like to thank all the past and present members of the Nanomaterials group at Flinders University. Special thanks must go to Simon Mathew for all his help, ideas and encouragement over my time at Flinders, and for proving that the best ideas are often borne at the pub over a drink. I would also like to say cheers to Rachel Pillar for her help in editing parts of this thesis; it was much appreciated, even if she is a physical chemist.

To my family and Fee, it's been a rough time these past few years but you guys helped me through it, without your love and support there is no way I could have finished this thesis.

Finally, I'd like to dedicate this thesis in part to my late brother in law, Darren. Thanks for the memories mate, I wish you were here to see me finally finish this; it's been a constant source of amusement between us over the years and life isn't the same without you.

‘I certify that this thesis does not incorporate without acknowledgement any material previously submitted for a degree or diploma in any university; and that to the best of my knowledge and belief it does not contain any material previously published or written by another person except where due reference is made in the text’

.....

(D. J. CLARKE)

TABLE OF CONTENTS

LIST OF FIGURES	<i>xi</i>
LIST OF TABLES	<i>xv</i>
LIST OF ABBREVIATIONS	<i>xvi</i>
1 INTRODUCTION	1
1.1 Outline & Aims	1
1.2 Silsesquioxanes	3
1.2.1 Synthesis of POSS Compounds	4
1.2.1.1 Synthesis of Octahydridosilsesquioxane.....	7
1.2.1.2 Synthesis of Octakis(hydridodimethylsiloxy)octasilsesquioxane	8
1.2.1.3 Tetrabutylammonium Fluoride Catalysed Synthesis of POSS.....	9
1.2.1.4 Synthesis of Incompletely Condensed Silsesquioxanes.....	10
1.3 Functionalisation of POSS	14
1.3.1 Hydrosilylation.....	14
1.3.2 Functionalisation of POSS by Hydrosilylation	18
1.4 Functionalisation of POSS by Other Reactions	20
1.4.1 Monosubstituted POSS Derivatives.....	20
1.4.1.1 Method 1	21
1.4.1.2 Method 2.....	22
1.4.1.3 Method 3.....	24
1.4.2 Subsequent Reactions of the R' Group	25
1.4.3 Reaction of the Trisilanol with Mono-Or Dihalide Organosilanes	26
1.4.4 Metal Silsesquioxanes.....	28
1.4.5 Octa-substituted POSS Derivatives.....	28
1.5 POSS Polymers	36
1.6 Summary	36
1.7 References	37
2 POSS BOUND FULLERENES	43
2.1 Outline	43
2.2 Fullerenes	43
2.3 Functionalisation of C₆₀	44
2.3.1 Addition of Diazomethane and Alkyl Azides to C ₆₀	45
2.3.2 Addition of Stabilised α -Halomalonate Anions to C ₆₀	47
2.3.3 Cycloaddition of Azomethine Ylides to C ₆₀	48
2.4 Optical Limiting	49
2.5 Fulleropyrrolidines	53
2.6 Synthesis	58
2.7 Synthetic Pathway 1	59
2.8 Characterisation	60
2.9 Results & Discussion	60
2.9.1 ¹ H NMR	60
2.9.1.1 Mono-vinyl POSS.....	60
2.9.1.2 [2-(4-dimethylsilyl)phenyl]-1,3-dioxolane	62
2.9.1.3 Mono-dioxolane POSS	62
2.9.1.4 Mono-aldehyde POSS.....	64
2.9.1.5 POSS Fulleropyrrolidines	65
2.9.2 ¹³ C NMR	67
2.9.2.1 Mono-vinyl POSS.....	67
2.9.2.2 [2-(4-dimethylsilyl)phenyl]-1,3-dioxalane.....	67
2.9.2.3 Mono-dioxolane POSS	69
2.9.2.4 Mono-aldehyde POSS.....	69

2.9.2.5	POSS Fulleropyrrolidines	71
2.9.3	²⁹ Si NMR.....	72
2.9.4	High Resolution ESI Mass Spectrometry	73
2.9.5	Elemental Analysis of POSS Fulleropyrrolidines.....	74
2.9.6	Optical Properties of POSS Fulleropyrrolidines	74
2.9.6.1	UV-Vis Spectra of POSS Fulleropyrrolidines	74
2.9.6.2	Steady State Spectrofluorometric Emission Studies of POSS Fulleropyrrolidines..	75
2.9.6.3	Power limiting of POSS Fulleropyrrolidines	77
2.10	Synthetic Pathway 2	79
2.11	Results & Discussion	80
2.11.1	FTIR.....	80
2.11.2	¹ H NMR	80
2.11.2.1	Mono-benzyl Chloride POSS.....	80
2.11.2.2	Mono-aldehyde POSS.....	82
2.11.2.3	POSS Fulleropyrrolidines	84
2.11.3	¹³ C NMR	85
2.11.3.1	Mono-benzyl Chloride POSS.....	85
2.11.3.2	Mono-aldehyde POSS.....	85
2.11.3.3	POSS Fulleropyrrolidines	87
2.11.4	²⁹ Si NMR.....	88
2.11.5	High Resolution ESI Mass Spectrometry	89
2.11.6	Elemental Analysis of POSS Fulleropyrrolidines.....	74
2.11.7	Optical Properties of POSS Fulleropyrrolidines	90
2.11.7.1	UV-Vis Spectra of POSS Fulleropyrrolidines.....	90
2.11.7.2	Steady State Spectrofluorometric Emission Studies of POSS Fulleropyrrolidines .	91
2.11.7.3	Power Limiting of POSS Fulleropyrrolidines	92
2.12	Iminofullerenes	94
2.13	Results & Discussion	95
2.13.1	FTIR.....	95
2.13.2	¹ H NMR	95
2.13.2.1	Mono-benzyl Chloride POSS.....	96
2.13.2.2	Mono-azide POSS.....	96
2.13.2.3	POSS Iminofullerene	96
2.13.3	¹³ C NMR	98
2.13.3.1	Mono-benzyl Chloride POSS.....	98
2.13.3.2	Mono-azide POSS.....	99
2.13.3.3	POSS Iminofullerenes.....	99
2.13.4	²⁹ Si NMR.....	101
2.13.5	High Resolution ESI Mass Spectrometry	101
2.13.6	Elemental Analysis of POSS Iminofullerene	102
2.13.7	Optical Properties of POSS Iminofullerene	102
2.13.7.1	UV-Vis Spectrum of POSS Iminofullerene	102
2.13.7.2	Steady State Spectrofluorometric Emission Studies of POSS Iminofullerene..	103
2.13.7.3	Power Limiting of POSS Iminofullerene	104
2.14	Conclusions and Future Work	105
2.15	References	107
3	POSS IMIDES.....	111
3.1	Outline	111
3.2	Perylenes.....	111
3.2.1	Perylenes Incorporated into Sol-gel Matrices	112
3.2.2	Other Anhydrides.....	114
3.3	POSS Imides	115
3.4	Synthesis	117
3.5	Characterisation	118

3.6	Results & Discussion	118
3.6.1	FTIR.....	118
3.6.2	¹ H NMR	118
3.6.2.1	Mono-(3-aminopropyl) POSS.....	120
3.6.2.2	Mono-phthalic POSS Imide.....	120
3.6.2.3	Bis-phthalic POSS Imide	122
3.6.2.4	Octa-(3-chloroammoniumpropyl)POSS	123
3.6.2.5	Octa-phthalic POSS Imide.....	123
3.6.2.6	Mono-naphthalic POSS Imide	124
3.6.2.7	Bis-naphthalic POSS Imide	125
3.6.2.8	Biphenyl POSS Imide.....	126
3.6.2.9	Perylene POSS Imide.....	127
3.6.3	¹³ C NMR	128
3.6.3.1	Mono-(3-aminopropyl)POSS.....	128
3.6.3.2	Mono-phthalic POSS Imide.....	128
3.6.3.3	Bis-phthalic POSS Imide	130
3.6.3.4	Octa-(3-chloroammoniumpropyl) POSS	131
3.6.3.5	Octa-phthalic POSS Imide.....	131
3.6.3.6	Mono-naphthalic POSS Imide	132
3.6.3.7	Bis-naphthalic POSS Imide	132
3.6.3.8	Biphenyl POSS Imide.....	133
3.6.3.9	Perylene POSS Imide.....	133
3.6.4	²⁹ Si NMR.....	134
3.6.5	High Resolution ESI Mass Spectrometry	135
3.6.6	Elemental Analysis of POSS Imides.....	135
3.6.7	UV-Vis Spectra of POSS Imides	136
3.6.7.1	UV-Vis Spectra of Phthalic POSS Imides	136
3.6.7.2	UV-Vis Spectrum of Mono-naphthalic POSS Imide	137
3.6.7.3	UV-Vis Spectrum of Bis-naphthalic POSS Imide	138
3.6.7.4	UV-Vis Spectrum of Biphenyl POSS Imide.....	140
3.6.7.5	UV-Vis Spectrum of Perylene POSS Imide.....	142
3.6.8	Steady State Spectrofluorometric Emission Studies of POSS Imides	145
3.6.8.1	Emission Spectrum of Mono-naphtha POSS Imide.....	145
3.6.8.2	Emission Spectrum of Bis-naphtha POSS Imide.....	146
3.6.8.3	Emission Spectrum of Biphenyl POSS Imide.....	147
3.6.8.4	Emission Spectrum of Perylene POSS Imide	148
3.6.9	Single Crystal X-ray Structure of Perylene POSS Imide.....	149
3.7	Conclusions and Future Work	159
3.8	References:	161
4	POSS BOUND PORPHYRIN	165
4.1	Outline	165
4.2	Porphyryns.....	165
4.3	POSS Ligands	168
4.4	Synthesis	171
4.5	Characterisation	172
4.6	Results & Discussion	172
4.6.1	FTIR.....	172
4.6.2	¹ H NMR	172
4.6.2.1	(3-aminopropyl)POSS.....	172
4.6.2.2	Mono-phenyl POSS	174
4.6.2.3	Isonicotinic Acid Chloride	175
4.6.2.4	Mono-pyridyl POSS.....	176
4.6.2.5	Mono-porphyrin POSS	177
4.6.3	¹³ C NMR	178
4.6.3.1	(3-aminopropyl)POSS.....	178
4.6.3.2	Mono-phenyl POSS	180
4.6.3.3	Isonicotinic acid chloride.....	180

4.6.3.4	Mono-pyridyl POSS.....	180
4.6.3.5	Mono-porphyrin POSS	181
4.6.4	²⁹ Si NMR.....	182
4.6.5	High Resolution ESI Mass Spectrometry	183
4.6.6	Elemental Analysis of Mono-porphyrin POSS and Precursor Compounds....	183
4.6.7	Optical Properties of Mono-porphyrin POSS	184
4.6.7.1	UV-Vis Spectrum of Mono-porphyrin POSS	184
4.7	Conclusions and Future Work	185
4.8	References:	187
5	<i>POSS BOUND PYRENE</i>.....	189
5.1	Outline	189
5.2	Pyrene	189
5.3	Silsesquioxane Bound Pyrene.....	189
5.4	Characterisation	191
5.4.1	FTIR.....	191
5.4.2	¹ H NMR	191
5.4.2.1	(3-aminopropyl)POSS.....	191
5.4.2.2	1-Pyrene Acid Chloride	191
5.4.2.3	Mono-pyrene POSS	193
5.4.3	¹³ C NMR	194
5.4.3.1	(3-aminopropyl)POSS.....	194
5.4.3.2	1-Pyrene Acid Chloride	196
5.4.3.3	Mono-pyrene POSS	196
5.4.4	²⁹ Si NMR.....	197
5.4.5	High Resolution ESI Mass Spectrometry	198
5.4.6	Elemental Analysis of Mono-pyrene POSS	198
5.4.7	Optical Properties of Mono-pyrene POSS	198
5.4.7.1	UV-Vis Spectrum of Mono-pyrene POSS	198
5.4.7.2	Steady State Spectrofluorometric Emission Studies of Mono-pyrene POSS.....	199
5.5	Conclusions and Future Work	201
5.6	References:	202
6	<i>EXPERIMENTAL</i>.....	203
6.1	Instrumentation	203
6.1.1	Nuclear Magnetic Resonance (NMR) Spectroscopy	203
6.1.2	Fourier Transform Infra-Red (FTIR) Spectroscopy.....	203
6.1.3	Mass Spectrometry.....	203
6.1.4	Elemental Analysis	204
6.1.5	UV-Vis Spectrophotmetry	204
6.1.6	Fluorescence Spectrophotmetry	204
6.1.7	Power Limiting	204
6.1.8	Single Crystal X-ray Crystallography	205
6.1.9	Chromatography.....	205
6.2	Chemicals	205
6.3	Synthesis	206
6.3.1	POSS Fulleropyrrolidines: Synthetic Pathway 1	206
6.3.2	POSS Fulleropyrrolidines: Synthetic Pathway 2	212
6.3.3	POSS Iminofullerenes.....	216
6.3.4	POSS Imides	218
6.3.5	POSS Porphyrin	225
6.3.6	POSS Pyrene.....	228
6.4	References:	231
7	<i>CONCLUSIONS & FUTURE WORK</i>.....	232
7.1	POSS Fulleropyrrolidines.....	232
7.1.1	Conclusions.....	232

7.1.2	Future Work	232
7.2	POSS Imides	233
7.2.1	Conclusions	233
7.2.2	Future Work	233
7.3	POSS Porphyrin	234
7.3.1	Conclusions	234
7.3.2	Future Work	234
7.4	POSS Pyrene	235
7.4.1	Conclusions	235
7.4.2	Future Work	235

LIST OF FIGURES

Figure 1.1. Random, ladder, partial and cage conformations of silsesquioxanes	3
Figure 1.2. M, D, T, and Q type silicone units	4
Figure 1.3. Synthesis of POSS through Hydrolytic Condensation	5
Figure 1.4. Proposed mechanism of POSS synthesis	5
Figure 1.5. Synthesis of T_8^H	8
Figure 1.6. Synthesis of $Q_8M_8^H$	9
Figure 1.7. ORTEP representation of tetrabutylammonium octaphenyl	10
Figure 1.8. Examples of incompletely condensed POSS cages	11
Figure 1.9. Hydrolysis of acetonitrile	12
Figure 1.10. Silsesquioxane isomers formed in the hydrolytic condensation of $CySiCl_3$ in acetonitrile	13
Figure 1.11. Acid-mediated cleavage and rearrangement of $Cy_6Si_6O_9$	13
Figure 1.12. Synthesis of incompletely condensed POSS through base-mediated cleavage of fully condensed T_6 cage	14
Figure 1.13. Two possible isomers formed from the hydrosilylation reaction	15
Figure 1.14. Chalk-Harrod mechanism	15
Figure 1.15. Original hydrosilylation mechanism proposed by Lewis	16
Figure 1.16. Improved hydrosilylation reaction mechanism proposed by Lewis	17
Figure 1.17. Hydrosilylation of alkenes onto T_8^H	19
Figure 1.18. Hydrosilylation of vinylferrocene onto $Q_8M_8^H$	20
Figure 1.19. Synthesis of mono-functionalised POSS derivatives (Method 1)	21
Figure 1.20. Synthesis of mono-functionalised POSS derivatives (Method 2)	22
Figure 1.21. Synthesis of mono-functionalised POSS derivatives	22
Figure 1.22. Synthesis of mono-octene POSS	23
Figure 1.23. Synthesis of mono-oligo(ethylene oxide) hydridosilsesquioxane	24
Figure 1.24. Corner capping of incompletely condensed silsesquioxane (Method 3)	25
Figure 1.25. Free radical addition of 3-mercaptopropyl POSS to poly [3-hydroxyalkanoate-co-3-hydroxyalkenoate]	26
Figure 1.26. Mono-functionalised incompletely condensed POSS	27
Figure 1.27. Synthesis of multi-substituted incompletely condensed silsesquioxane derivatives	27
Figure 1.28. Synthesis of disubstituted incompletely condensed silsesquioxane	28
Figure 1.29. Synthesis of octa(nitrophenyl)POSS	29
Figure 1.30. Synthesis of octa(aminophenyl)POSS	29
Figure 1.31. Bromination of octa(phenyl)POSS and subsequent Suzuki coupling	30
Figure 1.32. Radical bromination of octa(vinyl)POSS	31
Figure 1.33. Methoxycarbonylation of octa(vinyl)POSS	31
Figure 1.34. UV addition of phosphanes to octa(vinyl)POSS	31
Figure 1.35. Diels Alder polymerisation of dodeca(cyclopentadienyl)POSS	32
Figure 1.36. Coordination of platinum through phosphine-functionalised POSS	32
Figure 1.37. Radical addition of thiols to octa(vinyl)POSS	33
Figure 1.38. Heck coupling of bromoaromatics with octa(vinyl)POSS	33
Figure 1.39. Arylation and dichlorocarbene addition to octa(vinyl)POSS	34
Figure 1.40. Silylative coupling and cross-metathesis of octa(vinyl)POSS	35
Figure 1.41. 1,3-dipolar cycloaddition of nitrene and nitrile oxides to mono(vinyl) and mono(styryl)POSS	35
Figure 2.1. C_{60} , cyclohexatriene and radialene subunits of C_{60}	44
Figure 2.2. Pyrazoline, fulleroid and methanofullerene derivatives of C_{60}	45
Figure 2.3. Possible isomers of iminofullerenes	46
Figure 2.4. Addition of alkyl azides to C_{60}	46
Figure 2.5. Addition of stabilised α -halomalonate anions to C_{60}	47

Figure 2.6. Addition of α -halomalonate to C_{60}	48
Figure 2.7. Addition of azomethine ylides to C_{60}	49
Figure 2.8. Five-level reverse saturable absorption mechanism.....	51
Figure 2.9. Modified reverse saturable absorption mechanism.....	52
Figure 2.10. Synthesis of 3-(cyclopentadienyl)alkyltriethoxysilane fullerene ¹	54
Figure 2.11. Synthesis of N-[3-(triethoxysilyl)propyl]-2-carbonethoxy fulleropyrrolidine.....	55
Figure 2.12. Synthesis of trimethoxysilyl undecyl fulleropyrrolidine.....	55
Figure 2.13. Synthesis of N-(triethoxysilyl)propyl functionalised fulleropyrrolidine.....	56
Figure 2.14. Synthesis of N-triethoxysilyl functionalised fulleropyrrolidine.....	57
Figure 2.15. Synthesis of silica grafted methanofullerene.....	58
Figure 2.16. Numbering scheme of pyrrolidines.....	59
Figure 2.17. Synthesis of mono-vinyl POSS (2.1, 2.2).....	60
Figure 2.18. Synthesis of [2-(4-dimethylsilyl)phenyl]-1,3-dioxalane (2.3).....	62
Figure 2.19. Synthesis of mono-dioxalane POSS (2.4).....	63
Figure 2.20. Synthesis of mono-aldehyde POSS (2.5, 2.6).....	64
Figure 2.21. Synthesis of POSS-fulleropyrrolidines (2.7, 2.8).....	65
Figure 2.22. Pyrrolidine resonances in the ¹ H NMR spectrum of POSS fulleropyrrolidine 2.7 in CDCl ₃	66
Figure 2.23. Resonance structures of silyl-substituted benzaldehyde.....	70
Figure 2.24. ¹³ C NMR spectrum of POSS fulleropyrrolidine 2.7 in CDCl ₃	71
Figure 2.25. ²⁹ Si NMR spectrum of POSS fulleropyrrolidine 2.7 in CDCl ₃	73
Figure 2.26. UV-Vis spectra of POSS fulleropyrrolidines 2.7 and 2.8 in toluene.....	75
Figure 2.27. Fluorescence and phosphorescence of fullerenes.....	76
Figure 2.28. Fluorescence spectra of POSS fulleropyrrolidines 2.7 and 2.8 in toluene ($\lambda_{exc} = 335$ nm).....	76
Figure 2.29. Power limiting plot for C_{60}	78
Figure 2.30. Power limiting plot for POSS fulleropyrrolidine 2.7.....	78
Figure 2.31. Power limiting plot for POSS fulleropyrrolidine 2.8.....	79
Figure 2.32. Synthesis of mono-benzyl chloride POSS (2.9, 2.10).....	80
Figure 2.33. Synthesis of mono aldehyde POSS (2.11, 2.12).....	82
Figure 2.34. ¹ H NMR of mono-aldehyde POSS 2.11 in CDCl ₃	83
Figure 2.35. Synthesis of POSS fulleropyrrolidines (2.13, 2.14).....	84
Figure 2.36. ¹³ C NMR of POSS fulleropyrrolidine 2.13 in CDCl ₃	88
Figure 2.37. ²⁹ Si NMR of POSS fulleropyrrolidine 2.12 in CDCl ₃	89
Figure 2.38. UV-Vis absorption spectra of POSS fulleropyrrolidines 2.13 and 2.14 in toluene.....	91
Figure 2.39. Emission spectra of POSS fulleropyrrolidines 2.13 and 2.14 in toluene.....	92
Figure 2.40. Power limiting plot of POSS fulleropyrrolidine 2.13.....	93
Figure 2.41. Power limiting plot of POSS fulleropyrrolidine 2.14.....	93
Figure 2.42. Synthesis of literature POSS azides.....	94
Figure 2.43. Synthesis of POSS azide (2.16).....	95
Figure 2.44. Synthesis of POSS iminofullerene (2.16).....	97
Figure 2.45. ¹ H NMR of POSS iminofullerene 2.16 in CDCl ₃	98
Figure 2.46. ¹³ C NMR of POSS iminofullerene 2.16 in CDCl ₃	100
Figure 2.47. Open [5,6] and closed [6,6] iminofullerenes.....	100
Figure 2.48. ²⁹ Si NMR of POSS iminofullerene 2.16 in CDCl ₃	101
Figure 2.49. UV-Vis spectra of POSS iminofullerene 2.16 in toluene.....	103
Figure 2.50. Fluorescence spectrum of POSS iminofullerene 2.16 in toluene.....	104
Figure 2.51. Power limiting plot of POSS iminofullerene 2.18.....	105
Figure 3.1. Benzene, naphthalene, biphenyl and perylene functional groups.....	111
Figure 3.2. Ethoxysilane substituted perylene derivatives.....	112
Figure 3.3. Structure of Perylene Orange.....	113
Figure 3.4. Synthesis of bis-(propyltriethoxysilyl)peryene diimide.....	113
Figure 3.5. Self-assembly of bis(propyltriethoxysilyl)peryene diimide.....	114
Figure 3.6. Synthesis of bis(propyltriethoxysilyl)phthalic diimide.....	114

Figure 3.7. Synthesis of mono(3-aminopropyl)POSS	115
Figure 3.8. Synthesis of octa(chloroammoniumpropyl)POSS.....	115
Figure 3.9. Synthesis of octa(propylsuccinimide) POSS.....	116
Figure 3.10. Synthesis of mono-phthalic POSS imide (3.2).....	120
Figure 3.11. Structure of N-[3-(isobutylPOSS)propyl]bis(benzyloxybenzamide)	121
Figure 3.12. ¹ H NMR of mono-phthalic POSS imide 3.2 in CDCl ₃	122
Figure 3.13. Synthesis of bis-phthalic POSS imide (3.3).....	123
Figure 3.14. Synthesis of octa-phthalic POSS imide (3.5).....	124
Figure 3.15. Synthesis of mono-naphthalic POSS imide (3.6).....	125
Figure 3.16. Synthesis of bis-naphthalic POSS imide (3.7).....	126
Figure 3.17. Synthesis of biphenyl POSS bis-imide (3.8).....	127
Figure 3.18. Synthesis of POSS perylene bis-imide (3.9).....	128
Figure 3.19. ¹³ C NMR of mono-phthalic POSS imide 3.2 in CDCl ₃	130
Figure 3.20. Succinimide, maleimide and phthalic imide functional groups.....	132
Figure 3.21. ²⁹ Si NMR of mono-phthalic POSS imide 3.2 in CDCl ₃	135
Figure 3.22. UV-Vis spectra of phthalic POSS imides 3.2, 3.3 and 3.5 in toluene	137
Figure 3.23. UV-Vis spectrum of mono-naphtha POSS imide 3.6 in toluene	137
Figure 3.24. Literature examples of mono-naphtha imides	138
Figure 3.25. Naphthalic imide used for absorption calculations.....	138
Figure 3.26. UV-Vis spectrum of bis-naphtha POSS imide 3.7 in toluene	139
Figure 3.27. Bis-naphtha diimide examples	139
Figure 3.28. Literature examples of bis-naphtha imides.....	140
Figure 3.29. UV-Vis spectrum of biphenyl POSS imide 3.8 in toluene	141
Figure 3.30. Literature biphenyl bis-imides.....	142
Figure 3.31. UV-Vis spectrum of perylene POSS imide 3.9 in toluene	142
Figure 3.32. HOMO (top) and LUMO (bottom) of perylene bisimides	143
Figure 3.33. Emission spectrum of mono-naphtha POSS imide 3.6 in toluene.....	145
Figure 3.34. Examples of mono-naphtha imides	146
Figure 3.35. Emission spectrum of bis-naphtha POSS imide 3.7 in toluene	147
Figure 3.36. Emission spectrum of biphenyl POSS imide 3.8 in toluene.....	148
Figure 3.37. Emission spectrum of perylene POSS imide 3.9 in toluene	148
Figure 3.38. Single crystal x-ray structure of perylene POSS imide 3.9	151
Figure 3.39. Unit cell diagram of perylene POSS imide 3.9	152
Figure 3.40. Numbering scheme used for perylene POSS imide 3.9.....	152
Figure 3.41. Empirical variation of perylene absorption maximum.....	157
Figure 3.42. Transverse and longitudinal displacements of perylenes	158
Figure 3.43. Overlay of perylene regions	158
Figure 4.1. The unsubstituted porphyrin macrocycle	165
Figure 4.2. Synthesis of TPP	166
Figure 4.3. Porphyrins employed in solid matrices.....	167
Figure 4.4. Synthesis of ruthenium functionalised POSS.....	168
Figure 4.5. Synthesis of platinum functionalised POSS.....	169
Figure 4.6. Synthesis of octa-terpyridyl functionalised POSS.....	169
Figure 4.7. Synthesis of POSS based ruthenium metallodendrimers	170
Figure 4.8. Synthesis of Ru(TPP)(CO)(Rpy).....	171
Figure 4.9. Synthesis of octa-(phenyl amide) POSS.....	171
Figure 4.10. Synthesis of mono-phenyl POSS amide (4.1)	174
Figure 4.11. Structure of N-[3-(isobutylPOSS)propyl]bis(benzyloxybenzamide)	175
Figure 4.12. Synthesis of isonicotinic acid chloride (4.2)	175
Figure 4.13. Synthesis of mono-pyridyl POSS (4.3)	176
Figure 4.14. Synthesis of mono-porphyrin POSS (4.3).....	177
Figure 4.15. Non-equivalence in isobutyl resonances in ¹ H NMR spectrum of mono-porphyrin POSS 4.4 in CDCl ₃	178
Figure 4.15. Non-equivalence in isobutyl resonances in ¹³ C NMR spectrum of mono-porphyrin POSS 4.4 in CDCl ₃	181

Figure 4.16. Aromatic region in ^{13}C NMR spectrum of mono-porphyrin POSS 4.4 in CDCl_3 ..	182
Figure 4.17. ^{29}Si NMR of mono-porphyrin POSS (4.4)	183
Figure 4.18. UV-Vis spectrum of POSS porphyrin 4.4 in dichloromethane	184
Figure 5.1. Synthesis of octa-pyrene substituted POSS.	190
Figure 5.2. Synthesis of pyrene acid chloride (5.1)	193
Figure 5.3. Synthesis of mono-pyrene POSS (5.2)	193
Figure 5.4. ^1H NMR of mono-pyrene POSS 5.2 (pictured) in CDCl_3	194
Figure 5.5. ^{13}C NMR of mono-pyrene POSS 5.2 (pictured) in CDCl_3	197
Figure 5.6. ^{29}Si NMR of mono-pyrene POSS 5.2 in (pictured) CDCl_3	197
Figure 5.7. UV-VIS spectrum of mono-pyrene POSS (5.2) and pyrene in toluene	199
Figure 5.8. Emission spectrum of mono-pyrene POSS 5.2 in toluene ($\lambda_{\text{exc}} = 365\text{nm}$)	200
Figure 5.9. Oligo-ether functionalised pyrene	200
Figure 6.1. Structure of 4-Bromophenyldioxalane	206
Figure 6.2. Structure of 2-(4-(Dimethylsilyl)phenyl)-1,3-dioxalane (2.3)	207
Figure 6.3. Structure of mono-vinyl POSS (2.1, 2.2)	208
Figure 6.4. Structure of mono-dioxalane POSS (2.4)	209
Figure 6.5. Structure of mono-aldehyde POSS (2.5, 2.6)	210
Figure 6.6. Structure of POSS fulleropyrrolidines (2.7, 2.8)	211
Figure 6.7. Structure of mono-benzyl chloride POSS (2.9, 2.10)	213
Figure 6.8. Structure of mono-aldehyde POSS (2.11, 2.12)	214
Figure 6.9. Structure of POSS Fulleropyrrolidines (2.13, 2.14)	216
Figure 6.10. Structure of mono-benzyl azide POSS (2.17)	217
Figure 6.11. Structure of POSS iminofullerene (2.16)	218
Figure 6.12. Structure of (3-aminopropyl)POSS (3.1)	219
Figure 6.13. Structure of octa(3-chloroammoniumpropyl)POSS (3.4)	219
Figure 6.14. Structure of mono-phthalic POSS imide (3.2)	220
Figure 6.15. Structure of bis-phthalic POSS imide (3.3)	221
Figure 6.16. Structure of octa-phthalic POSS imide (3.5)	222
Figure 6.17. Structure of mono-naphthalic-POSS imide (3.6)	223
Figure 6.18. Structure of bis-naphthalic-POSS imide (3.7)	223
Figure 6.19. Structure of biphenyl POSS imide (3.8)	224
Figure 6.20. Structure of perylene POSS imide (3.9)	225
Figure 6.21. Structure of mono-phenyl POSS (4.1)	226
Figure 6.22. Structure of isonicotinic acid chloride (4.2)	226
Figure 6.23. Structure of mono-pyridyl POSS (4.3)	227
Figure 6.24. Structure of mono-porphyrin POSS (4.4)	228
Figure 6.25. Structure of pyrene acid chloride	229
Figure 6.26. Structure of mono-pyrene POSS (5.2)	230

LIST OF TABLES

Table 1.1. Yields of T ₈ silsesquioxane cages obtained from the corresponding trilkoxysilane with tetrabutylammonium fluoride.....	9
Table 2.1. ¹ H NMR resonances of POSS fulleropyrrolidines and precursor compounds (synthetic pathway 1)	61
Table 2.2. ¹³ C NMR resonances of POSS fulleropyrrolidines and precursor compounds (synthetic pathway 1)	68
Table 2.3. ²⁹ Si NMR of POSS fulleropyrrolidines and precursor compounds	72
Table 2.4. High resolution ESI mass spectrometry results of POSS fulleropyrrolidines and precursor compounds.....	73
Table 2.5. Elemental analysis of POSS fulleropyrrolidines.....	74
Table 2.6. ¹ H NMR of POSS fulleropyrrolidines and precursor compounds (synthetic pathway 2)	81
Table 2.7. ¹³ C NMR of POSS fulleropyrrolidines and precursor compounds (synthetic pathway 2)	86
Table 2.8. ²⁹ Si NMR of POSS fulleropyrrolidines and precursor compounds	89
Table 2.9. High resolution ESI mass spectrometry results of POSS fulleropyrrolidines and precursors (synthetic pathway 2).....	90
Table 2.10. Elemental analysis of POSS fulleropyrrolidines.....	90
Table 2.11. ¹ H NMR of POSS iminofullerenes and precursor compounds	95
Table 2.12. ¹³ C NMR of POSS iminofullerenes and precursor compounds	99
Table 2.13. ²⁹ Si NMR of POSS iminofullerenes and precursor compounds	101
Table 2.14. ESI mass spectrometry of POSS iminofullerenes and precursor compounds ...	102
Table 3.1. FTIR of POSS Imides	118
Table 3.2. ¹ H NMR of POSS imides.....	119
Table 3.3. ¹³ C NMR of POSS imides	129
Table 3.4. ²⁹ Si NMR of POSS imides.....	134
Table 3.5. ESI mass spectroscopy of POSS imides	135
Table 3.6. Elemental analysis of POSS imides.....	136
Table 3.7. UV-Vis data of bis-naphthalic imides	140
Table 3.8. UV-Vis data of various N-substituted perylenes in CHCl ₃	144
Table 3.9. Fluorescence data of various N-substituted perylenes in chloroform.....	149
Table 3.10. X-ray parameters	150
Table 3.11. Bond distances of POSS perylene and literature perylene bis-imides	153
Table 3.12. Bond Angles of bis(POSS)perylene diimide	154
Table 3.13. Bond distances and angles of POSS crystal structures	155
Table 4.1. ¹ H NMR of POSS porphyrin and precursor compounds	173
Table 4.2. ¹³ C NMR of POSS porphyrin and precursor compounds	179
Table 4.3. ²⁹ Si NMR of POSS porphyrin and precursor compounds.....	182
Table 4.4. ESI mass spectrometry of POSS porphyrin and precursor compounds.....	183
Table 4.5. Elemental analysis POSS porphyrin and precursor compounds.....	183
Table 5.1. ¹ H NMR of mono-pyrene POSS (5.2) and precursor compounds	192
Table 5.2. ¹³ C NMR of mono-pyrene POSS (5.2) and precursor compounds	195

ABBREVIATIONS AND PARAMETER DEFINITIONS

ϵ	(epsilon) molar extinction coefficient
λ	(lambda) wavelength
\AA	Angstrom
δ	(delta) chemical shift in ppm
ppm	parts per million
${}^xJ_{A-B}$	coupling constant between nuclei A and B over x bonds in Hz
FTIR	Fourier Transform InfraRed
NMR	Nuclear Magnetic Resonance
UV-VIS	Ultraviolet visible
HOMO	Highest Occupied Molecular Orbital
LUMO	Lowest Unoccupied Molecular Orbital
Ph	Phenyl
Cy	Cyclohexyl
Cp	Cyclopentyl
λ_{\max}	wavelength of maximum absorption
λ_{exc}	wavelength of excitation
Φ_F	quantum yield
κ	dielectric constant
M_n	mean molecular weight
<i>o</i>	ortho
<i>m</i>	meta
<i>p</i>	para
vs	very strong
s	strong
m	medium
w	weak

1 INTRODUCTION

1.1 Outline & Aims

Polyhedral Oligomeric Silsesquioxanes (POSS) are a versatile class of three-dimensional building block units for the synthesis of new materials. Recent improvements in the synthesis of organofunctionalised POSS compounds have led to a significant increase in research activities.¹ A range of POSS compounds with optically active functionalities, such as pyrene,^{2,3} liquid crystalline mesogens⁴⁻⁷ and photodimeric coumarins have previously been synthesised.⁸

A range of optically active functional groups were desired to be attached to the periphery of POSS cages. One such class of compounds were fullerenes (C_{60}), as it has been well established that fullerene solutions exhibit optical limiting behaviour derived from a Reverse Saturable Absorber (RSA) mechanism.^{9,10} Fullerene derivatives, such as methanofullerenes and fulleropyrrolidines, have been ascertained to be equally useful for optical limiting purposes and also possess improved solubility.^{11,12}

Another functional group of interest was perylenes, which have been used as pigments in products such as in automotive finishes due to their insolubility, migrational stability, light- and weather-fastness, thermal stability, chemical strength, high photostability, high fluorescence quantum yield and high tinctorial strength, with hues ranging from red to black.^{13,14} More recently, perylenes have been used in electronic applications and are among the best available *n*-type semiconductors.^{15,16}

The third functionality of interest was pyrene, which possesses long monomer lifetimes and efficient excimer formation.¹⁷ Pyrene derivatives have been used as fluorescent probes, due to the high quantum yield of fluorescence and photostability generally exhibited in dilute solutions.¹⁸ POSS bound pyrene compounds have previously been synthesised with a range of substitutions, where they have been reported to be effective hole transport materials in organic light emitting diodes (OLED's).^{2,3}

Porphyrins were the final class of compounds of interest, being fluorescent crystalline pigments widely used in a range of applications, such as molecular electronics,¹⁹⁻²² solar energy conversion,²³ photochemical water splitting^{24,25} and donor-acceptor systems.^{20,26-28}

A detailed description of POSS chemistry is reviewed in **Chapter 1**, together with the general chemistry of siloxanes, followed by detailed review of the scientific literature pertaining to the synthesis and properties of condensed and incompletely condensed POSS compounds and methods of derivitisation. Hybrid organic-inorganic materials derived from POSS compounds are also discussed.

The remaining chapters are split into the relevant compound classes; fullerenes, imides, pyrene and porphyrin. Each chapter contains a brief review of the scientific literature of the chemistry and properties of that particular class of compounds. This distinction was made in order to improve the readability of the thesis as some sections, such as optical limiting, are only relevant to a specific chapter.

Chapter 2 details the chemistry and properties of fullerenes, followed by a summary of the scientific literature referring to fullerene functionalisation, the optical properties of fullerenes and the mechanism of optical limiting. This is followed by discussion of the synthesis, characterisation and optical properties of the POSS-fullerene derivatives and associated precursor compounds.

The properties of optically active groups covalently linked to POSS, including pyromellitic, naphthalene, biphenyl and perylene diimides and methods of functionalisation of such groups for use in sol-gel applications is discussed in **Chapter 3**. The synthesis, characterisation and optical properties of the synthesised POSS imides are detailed, followed by discussion of the single crystal x-ray structure of the POSS perylene imide.

Chapter 4 includes a review of the scientific literature pertaining to the properties of metallo-porphyrins and ligands previously incorporated on the periphery of POSS cages and the synthesis of subsequent metal functionalised POSS compounds and metallodendrimers using a central POSS template. The synthesis, characterisation

and optical properties of mono-functionalised porphyrin POSS will also be presented within this chapter.

Chapter 5 details the properties of pyrene, related compounds included in sol-gel systems and silsesquioxane bound pyrene, followed by a discussion on the synthesis, characterisation and optical properties of mono-functionalised pyrene POSS.

The chemicals used in the synthesis of the compounds presented in this thesis and the methods of characterisation employed are discussed in **Chapter 6**. The synthetic procedures and characterisation data are also presented within this chapter.

Chapter 7 presents the conclusions of the research contained within this thesis and examines possible avenues of further research.

1.2 Silsesquioxanes

Silsesquioxane is the IUPAC name for a range of polycyclic compounds consisting of silicon and oxygen. The name silsesquioxane is derived from *siloxane* (compounds of silicon and oxygen) and *sesqui* (Latin, meaning one and a half). This general name reflects the ratio of silicon and oxygen in the completely condensed silsesquioxanes, $(\text{RSiO}_{1.5})_n$, with examples of R including hydrogen, alkene and aryl, where n is an even integer. The silsesquioxanes consist of four main types of structures; random, ladder, partial cage and cage (**Figure 1.1**).²⁹

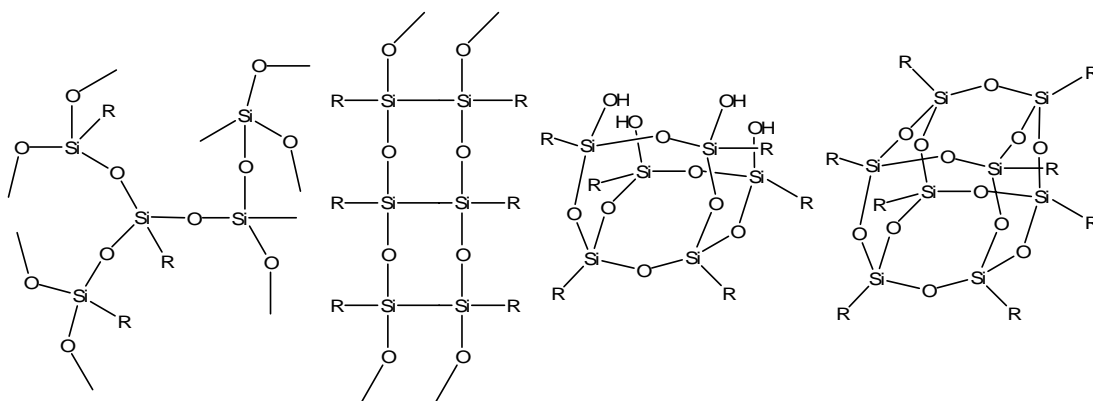


Figure 1.1. Random, ladder, partial and cage conformations of silsesquioxanes²⁹

Silsesquioxanes comprise of tetrahedral units where a silicon atom is bonded to three oxygen atoms and one R group. The oxygen atoms act as bridges between the silicon atoms from different tetrahedral units. The empirical formulae SiO_4 , RSiO_3 , R_2SiO_2 and R_3SiO are generally abbreviated as mono- (M), di- (D), tri- (T) and quaternary (Q) (**Figure 1.2**), where R can be a range of groups. The M, D, T and Q units are easily identified by ^{29}Si NMR, where siloxanes exhibit resonances in the range δ 13 to -114, referenced to tetramethylsilane (TMS) at 0 ppm. The resonance ranges for unsubstituted M, D, T and Q units are well separated at δ ~6, ~-20, ~-67 and ~-105 respectively.³⁰

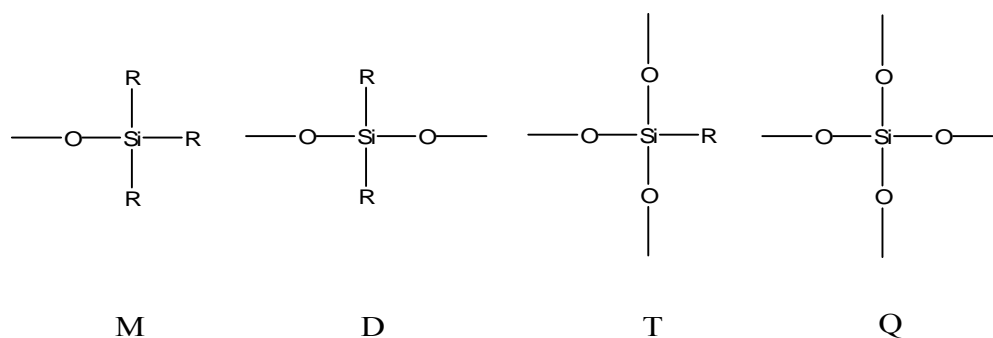


Figure 1.2. M, D, T, and Q type silicone units³¹

Silsesquioxanes are part of the larger family of silicon-oxygen compounds, commonly referred to as spherosilicates. The first report on oligomeric silsesquioxanes was published by Scott³² in 1946, describing the synthesis of $(\text{MeSiO}_{1.5})_n$ through the thermolysis of polymeric products obtained from the co-hydrolysis of MeSiCl_3 and Me_2SiClH . In 1955, Barry *et al.*³³ isolated compounds of the type $\text{R}_8\text{Si}_8\text{O}_{12}$, where R = Et, from the thermolysis of the hydrolysis products of EtSiCl_3 , further confirming the existence of polyhedral silsesquioxanes and providing the basis for further research of these molecules.

1.2.1 Synthesis of POSS Compounds

The most common method of synthesis is through the hydrolytic condensation of RSiX_3 , where X = Cl or alkoxy, which can be represented by the equations shown in **Figure 1.3**.³⁴

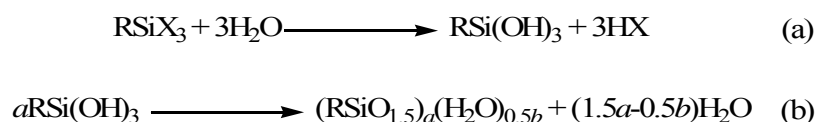


Figure 1.3. Synthesis of POSS through Hydrolytic Condensation

(a) Hydrolysis of RSiX_3 ; (b) Condensation of RSi(OH)_3 ³⁴

Hydrolysis of the monosilane (a) to give the corresponding trisilanol occurs rapidly.³⁵ Subsequent condensation of the trisilanol (b) occurs more slowly and yields a range of silsesquioxane species. The hydrolytic condensation of RSiX_3 has been studied, in 1965 by Sprung and Gunther^{36,37} and Brown and Vogt.³⁵ In the cases where $\text{R} = \text{Me}, \text{Et}, \text{Ph}$ and Cy , a mechanism of formation involving consecutive condensation of the monomeric trisilanol to linear, cyclic, polycyclic and polyhedral silsesquioxane intermediates (**Figure 1.4**) was postulated.³⁶⁻³⁹ In the case of $\text{Ph}_8\text{Si}_8\text{O}_{12}$, the proposed mechanism involved the consecutive formation of dimer, cyclic, tetramer and cubic silsesquioxanes.³⁶⁻³⁹

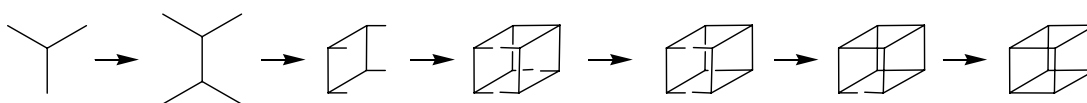


Figure 1.4. Proposed mechanism of POSS synthesis³⁶⁻³⁹

The energy barriers for the initial hydrolysis of HSiCl_3 to HSi(OH)_3 and the successive formation of the dimer $\text{H}_2\text{Si}_2\text{O(OH)}_4$, the cyclic trimer $\text{H}_3\text{Si}_3\text{O}_3(\text{OH})_3$ and cyclic tetramer $\text{H}_4\text{Si}_4\text{O}_4(\text{OH})_4$ have been calculated using *ab initio* quantum mechanical methods.^{40,41} The presence of a single water molecule greatly reduces energy barriers for the initial hydrolysis, implying that the reaction solvent plays a significant role during synthesis.

Many factors have been found to influence the synthesis of silsesquioxanes, including the nature of the R group, the nature of the leaving group (X), the reaction solvent, the concentration of RSiX_3 , the rate of addition and quantity of H_2O , temperature, pH and reaction time.^{31,34}

Steric and electronic effects influence the thermodynamics and kinetics of the condensation reaction. The formation of the incompletely condensed silsesquioxanes is favoured by the use of bulky R groups such as cyclohexyl⁴² and cyclopentyl.⁴³ For smaller groups, such as methyl^{36,39} and hydrogen,⁴⁴ the formation of fully condensed silsesquioxanes is favoured. These examples indicate that the steric bulk of the R group determines the level of condensation of the product. The nature of the leaving group has a minor influence on the reaction as the leaving group reacts during the first step of the hydrolysis. When the leaving group is a halide, the hydrolysis is much faster than for an alkoxy moiety.³⁸ Also, the hydrolysis of trichlorosilanes gives rise to the formation of HCl, which can catalyse successive condensation reactions.

Polar solvent molecules are able to hydrogen bond with the silanol groups, stabilising the incompletely condensed intermediates, and thus favouring the formation of incompletely condensed products.³⁴ Solvent has also been used to influence reaction kinetics through interaction with transition state intermediates, e.g. the interaction of the intermediate species with a polar solvent molecule can stabilise the system, leading to the formation of higher silsesquioxanes such as T₁₀ and T₁₂.⁴⁰

The initial concentration of RSiX₃ as well as the quantity and rate of addition of water can influence the reaction kinetics in the synthesis of POSS. High starting concentrations of RSiX₃ can lead to the formation of polymeric silsesquioxanes,³¹ whilst the precise effects of the rate of addition of water have not yet been quantified.³⁴

The temperature of the hydrolytic condensation reaction can influence the reaction kinetics and also the solubility of species in solution. High reaction temperatures have been demonstrated to favour the formation of highly condensed polymeric species.³⁸ The nature of the R group dictates the required reaction temperature, as bulky R groups generally require heating of the reaction mixture, however the reaction of smaller R groups is usually performed at room temperature.³¹

When the hydrolytic condensation reaction is finished prior to the ideal reaction time, the formation of incompletely condensed silsesquioxane products is generally

favoured, as they are generated by the rapid condensation of the intermediate products.

The catalyst employed in the hydrolytic condensation reaction can be acidic or basic in nature. Low pH has been shown to favour the formation of oligomeric silsesquioxanes. In contrast, high pH has been seen to assist the formation of polymeric species.³⁶ A variety of POSS compounds have been synthesised through the use of acid catalysts, such as R = H,⁴⁵⁻⁴⁷ Me,⁴⁸ cyclopropyl,⁴⁹ *n*-Bu⁵⁰ and *m*-MeC₆H₄⁵¹ and basic catalysts, such as R = Me,⁵² Ph⁵³ and Me₂NC₆H₄.⁵⁴

1.2.1.1 Synthesis of Octahydridosilsesquioxane

As previously discussed, POSS can be synthesised with a variety of R groups. One of the most useful of these groups is the silyl (Si-H) group, as it readily undergoes further reaction to enable functionalisation of the cage with a variety of groups. Major advances in the synthesis of hydrido-functionalised POSS have enabled the use of these compounds as precursors to functionalised POSS materials, as detailed in **Section 1.3**.

In 1959, Muller *et al.*⁵⁵ first described the synthesis of octahydridosilsesquioxane (T₈^H), albeit with a yield of less than 1 %. The conditions employed involved the hydrolysis of trichlorosilane with 80 % sulphuric acid (H₂SO₄) in the presence of hexamethyldisiloxane (Me₃SiOSiMe₃). In 1970, Frye and Collins⁴⁴ reported a modified procedure, with an increased yield of approximately 13 %, involving the use of trimethoxysilane as the silane monomer, concentrated aqueous hydrochloric acid (HCl_(aq)) as a catalyst and cyclohexanone/acetic acid as the solvent. HCl_(aq) was used in preference to H₂SO₄ due to the sensitivity of T₈^H to concentrated H₂SO₄. Agaskar⁴⁵ later reported an improved procedure, yielding 17.5 % T₈^H. This method involved the ‘scarce-water’ hydrolysis of trichlorosilane through the use of a partially hydrated metal salt, in this case, hydrated ferric chloride (FeCl₃·3H₂O). A biphasic reaction mixture was used, with the non-polar toluene/hexane phase containing trichlorosilane and the polar MeOH/HCl_(aq) phase containing FeCl₃. Further modifications to this procedure have been developed, increasing the yield to

approximately 23 % (**Figure 1.5**).^{46,47}

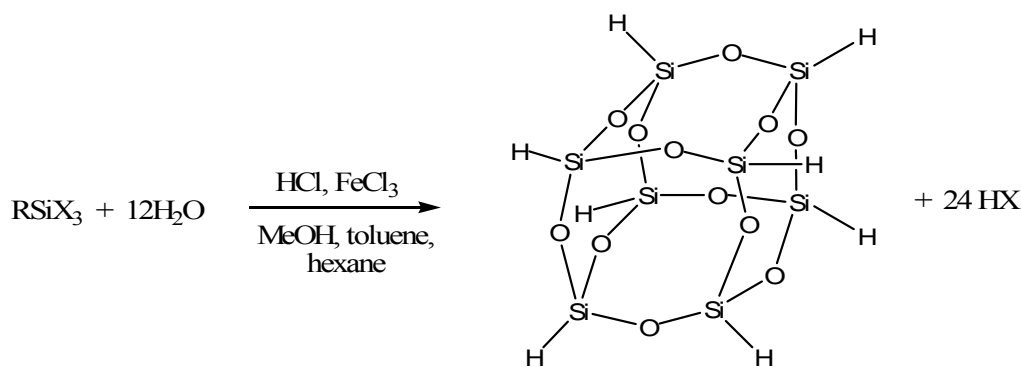


Figure 1.5. Synthesis of T_8^{H} ^{46,47}

1.2.1.2 Synthesis of Octakis(hydridodimethylsiloxy)octasilsesquioxane

Octakis(hydridodimethylsiloxy)octasilsesquioxane ($\text{Q}_8\text{M}_8^{\text{H}}$) is related to T_8^{H} as it contains the central Si_8O_{12} core, however $\text{Q}_8\text{M}_8^{\text{H}}$ has siloxy groups at each corner of the cage and thus contains both Q and M type silicon atoms, giving rise to its abbreviated name. Whilst technically not a silsesquioxane, $\text{Q}_8\text{M}_8^{\text{H}}$ is often included in this class of compounds due to its structural and physical resemblance to POSS. The synthesis of $\text{Q}_8\text{M}_8^{\text{H}}$ involves the preparation of a polyhedral silicate anion, $[\text{Si}_8\text{O}_{20}]^{8-}$ and functionalisation of the anion with dimethylchlorosilane (**Figure 1.6**). The anion was first synthesised in via the reaction of aqueous tetramethylammonium hydroxide with silica gel, yielding $[(\text{CH}_3)_4\text{N}]_8[\text{Si}_8\text{O}_{20}].69\text{H}_2\text{O}$,^{56,57} which was subsequently reacted with trimethylsilyl chloride, yielding the product $(\text{Me}_3\text{SiO})_8\text{Si}_8\text{O}_{12}$. $[\text{Si}_8\text{O}_{20}]^{8-}$ has also been synthesised in aqueous⁵⁸ and methanolic⁵⁹ solvents. The synthesis of $[\text{Si}_8\text{O}_{20}]^{8-}$ has recently been achieved from the pyrolysis residues of silica-containing organic substances, the most common example being rice hull ash.⁶⁰ Worldwide rice hull production is estimated at 80 million tonnes per year, with much of this combusted for electric power generation, producing over 3 million tonnes of rice hull ash annually.⁶⁰ The depolymerization of rice hull ash in aqueous alcohol, in the presence of bases, such as quaternary ammonium compounds, under ambient conditions, yielded the desired silsesquioxane anions.⁶⁰

$[\text{Si}_8\text{O}_{20}]^{8-}$ has proven to be difficult to functionalise through conventional chemistry, due to the presence of the alkylammonium cations and the high ordering of

crystallisation.⁶⁰ $[\text{Si}_8\text{O}_{20}]^{8-}$ proved unreactive towards alkyl halides, tosylates, anhydrides and other substrates normally receptive to nucleophilic attack.⁶⁰ The only known method of functionalisation of the $[\text{Si}_8\text{O}_{20}]^{8-}$ anion is through silylation, e.g. with dimethylvinylchlorosilane or dimethylchlorosilane, to yield $\text{Q}_8\text{M}_8^{\text{H}}$ (Figure 1.6).⁶¹

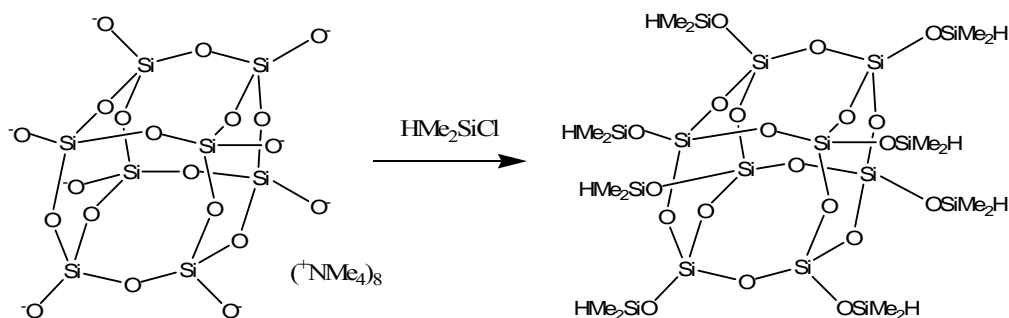


Figure 1.6. Synthesis of $\text{Q}_8\text{M}_8^{\text{H}}$ ⁶¹

1.2.1.3 Tetrabutylammonium Fluoride Catalysed Synthesis of POSS

The hydrolysis of trialkoxysilanes in the presence of tetrabutylammonium fluoride (TBAF) as a catalyst has been the focus of recent studies by Bassindale *et. al.*⁶² This synthetic procedure takes advantage of the fact that TBAF contains ~5 % water; as increasing the amount of water in the reaction leads to a slower rate of reaction and lower yields of the desired cage products.⁶²

Table 1.1. Yields of T_8 silsesquioxane cages obtained from the corresponding trialkoxysilane with tetrabutylammonium fluoride⁶²

R in $\text{RSi}(\text{OEt})_3$	T_8 yield (%)	Other T cages present
Hexyl	44	T_{10}
Octyl	65	T_{10}
4-Carboxymethyl-3,3-dimethylbutyl	20	T_{10}
Isobutyl	26	T_{10}
Cyclopentyl	95	-
Cyclohexyl	84	-
Phenyl	49	T_{12}
2-Bicyclopentyl	56	-
Methyl	0	-
Vinyl	1	$\text{T}_{10}, \text{T}_{12}$
Allyl	3	$\text{T}_{10}, \text{T}_{12}$
<i>tert</i> -Butyl	0	-

Interaction of the fluoride ion of TBAF with the silanol groups caused an increase in the nucleophilicity of the silanol groups, leading to Si-O-Si bond formation.⁶² The yields associated with the various R groups are detailed in **Table 1.1**.

The synthetic procedure generally involved precipitation of the cage product with acetone. However, in the case of R = Ph, if the reaction solvent was removed *in vacuo*, a fluoride ion was found to be included in the cage centre (**Figure 1.7**).⁶³ This was confirmed by ²⁹Si NMR, negative-ion Fast Atom Bombardment (FAB) mass spectrometry and single crystal x-ray crystallography. The presence of the fluoride ion slightly distorted the cage structure, whilst a significant increase in the solubility of the octa-phenyl cage product was exhibited.^{63,64}

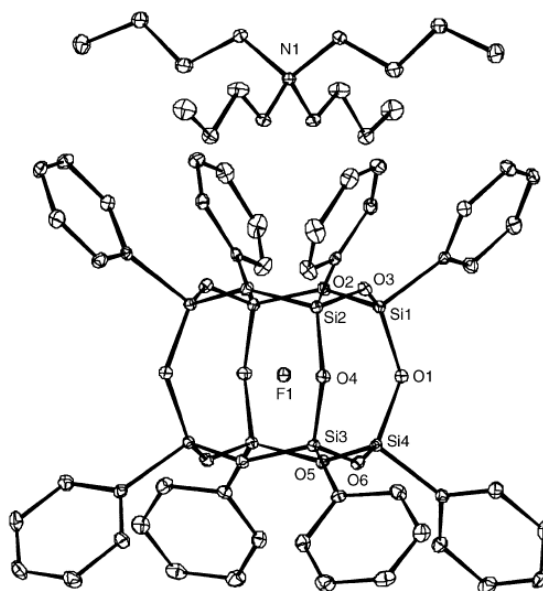


Figure 1.7. ORTEP representation of tetrabutylammonium octaphenyl octasilsesquioxane fluoride⁶⁴

1.2.1.4 Synthesis of Incompletely Condensed Silsesquioxanes

Incompletely condensed silsesquioxanes can also be synthesised by the hydrolytic condensation of silanes, such as RSiX_3 where X = Cl or alkoxy. A number of factors such as the nature of the R group, the nature of the X group, the reaction solvent, the concentration of RSiX_3 , the rate of addition and quantity of H_2O , temperature, pH and reaction time have been found to be significant in the condensation reaction, as

discussed previously in **Section 1.2.1**. The combination of these factors essentially determined whether the synthetic procedure yielded fully or incompletely condensed POSS cages, examples of which are depicted in **Figure 1.8**.⁴³

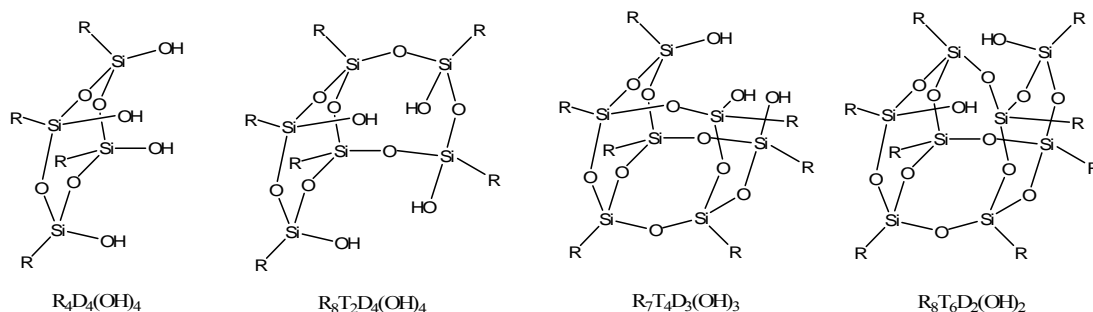


Figure 1.8. Examples of incompletely condensed POSS cages⁴³

The hydrolytic condensation of bulky silanes, such as R = *tert*-butyl, Ph, Cy generally yields incompletely condensed silsesquioxanes. The kinetic hydrolytic condensation of cyclohexyltrichlorosilane (CySiCl₃) in aqueous acetone was shown to produce the trisilanol product [Cy₇Si₇O₉(OH)₃].³⁹ Other bulky silanes have also been used, such as cyclopentyltrichlorosilane (CpSiCl₃).⁴² Incompletely condensed silsesquioxanes produced from Cy and Cp silanes are useful as they allow for cage mono-functionalisation via the corner-capping reaction. The main problems associated with the synthesis of these trisilanol compounds were the long preparation times and the required use of bulky trichlorosilanes, both of which severely restricted the scope of the synthetic procedure. Hydrolytic condensation of silanes with smaller R groups, such as R = H and Me, generally yielded fully condensed silsesquioxanes.⁶⁵⁻⁶⁷

The reaction solvent was particularly important in determining the level of condensation in the final product, as discussed previously in **Section 1.2.1**. Solvents of high dielectric constant and dipole moment caused stabilisation of silanol containing silsesquioxanes, favouring the synthesis of incompletely condensed silsesquioxanes over less polar, fully condensed silsesquioxane species.^{34,68}

The use of acetonitrile as a reactive solvent of high polarity ($\kappa = 37.5$) in the formation of incompletely condensed silsesquioxanes has been investigated.⁶⁸ Hydrolysis of the alkyltrichlorosilane yielded hydrochloric acid, which caused

hydrolysis of acetonitrile to occur (**Figure 1.9**). The resultant ammonium chloride resulted in phase separation of the solvent. The preferential solvation of ammonium chloride by water, relative to that of silsesquioxane or acetonitrile, caused the condensation reaction of alkyltrichlorosilane to be driven to the formation of condensed species in particular. The formation of ammonium chloride through the hydrolysis of acetonitrile caused a partial neutralisation of the reaction mixture, resulting from consumption of HCl in solution, therefore the reaction rate was slowed and the precipitation of poorly soluble species, such as incompletely condensed silsesquioxanes, was favoured.⁶⁸



Figure 1.9. Hydrolysis of acetonitrile⁶⁹

Acetonitrile is of a higher polarity ($\kappa = 37.5$) than other solvents, such as acetone ($\kappa = 20$),⁴³ previously used for the synthesis of incompletely condensed silsesquioxanes. The use of a highly polar solvent provided superior stabilisation of the incompletely condensed silsesquioxanes through interaction with the silanol groups. The formation of incompletely condensed silsesquioxanes over the completely condensed silsesquioxanes was favoured when acetonitrile was used as the reaction solvent. This synthesis was selective to the formation of the trisilanol derivative $\text{R}_7\text{Si}_7\text{O}_9(\text{OH})_3$ where $\text{R} = \text{Cp}$. When $\text{R} = \text{Cy}$, a mixture of incompletely condensed structures was formed, (**Figure 1.10**), with the lower selectivity associated with the higher solubility of the cyclohexyl silsesquioxane intermediates.⁶⁹

Feher *et al.*⁷⁰⁻⁷² recently devised methods of cleaving the POSS molecule at a single corner in a fully condensed $\text{R}_8\text{Si}_8\text{O}_{12}$ framework through the use of acid or base catalysis. The first of these reported examples detailed the controlled cleavage of $\text{R}_8\text{Si}_8\text{O}_{12}$, where $\text{R} = \text{Cy}$, through the addition of excess tetrafluoroboric acid dimethyl ether ($\text{HBF}_4 \cdot \text{OMe}_2$) and boron trifluoride etherate ($\text{BF}_3 \cdot \text{OEt}_2$) to a solution of $\text{Cy}_8\text{Si}_8\text{O}_{12}$ in C_6D_6 or CDCl_3 .⁷³ Further investigation with other strong acids revealed that was not the formation of a silicon-fluorine bond, but rather the strong acidity of HBF_4 , that drove the cleavage of the Si-O-Si framework.

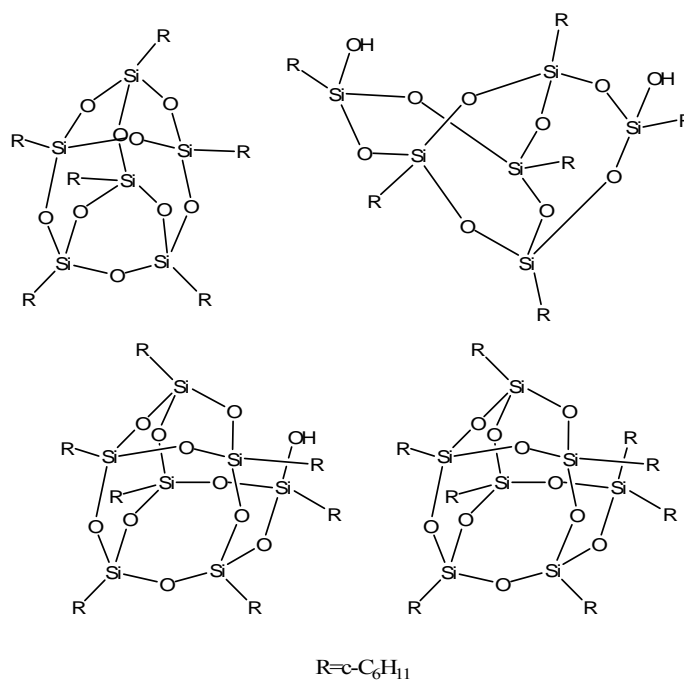


Figure 1.10. Silsesquioxane isomers formed in the hydrolytic condensation of CySiCl₃ in acetonitrile⁶⁹

Acid-catalysed cleavage has also been performed on the T₆ type cages, such as C₆Si₆O₉ (**Figure 1.11**), through reaction with triflic acid and methanesulfonic acid to yield Cy₆Si₆O₈(X)₂, where X = triflate (OTf) or mesylate (OMs).⁷⁴ Further reaction of these compounds yielded a variety of incompletely condensed silsesquioxanes Cy₆Si₆O₈(X)₂, where X = OH, OSiMe₂H, F, NMe₂ or C≡CPh. If the acid used for cleavage was HBF₄·OMe₂/BF₃·OEt₂, the product was the C₂-symmetric tetrafluoride obtained through irreversible cleavage of the Si-O framework.⁷⁴

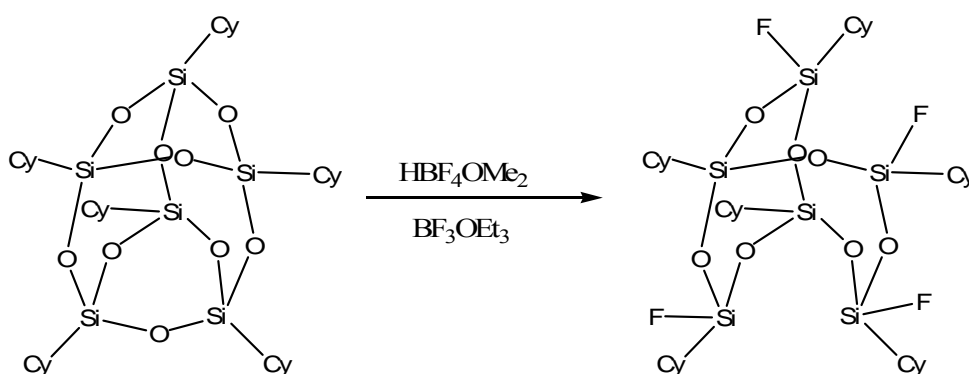


Figure 1.11. Acid-mediated cleavage and rearrangement of Cy₆Si₆O₉⁷⁴

The synthesis of incompletely condensed silsesquioxanes has also been achieved through base-mediated cleavage of fully condensed systems. The reaction of $C_6Si_6O_9$ with aqueous tetraammonium hydroxide in tetrahydrofuran yielded the *endo*- C_{2h} - $Cy_6Si_6O_7(OH)_4$, which was then hydrolysed to $CySi(OH)_3$ fragments. These fragments were able to react with an intermediate *endo*- C_{2h} - $Cy_6Si_6O_7(OH)_4$ to yield *endo*- C_3 - $C_7Si_7O_9(OH)_3$ (**Figure 1.12**).⁷⁰

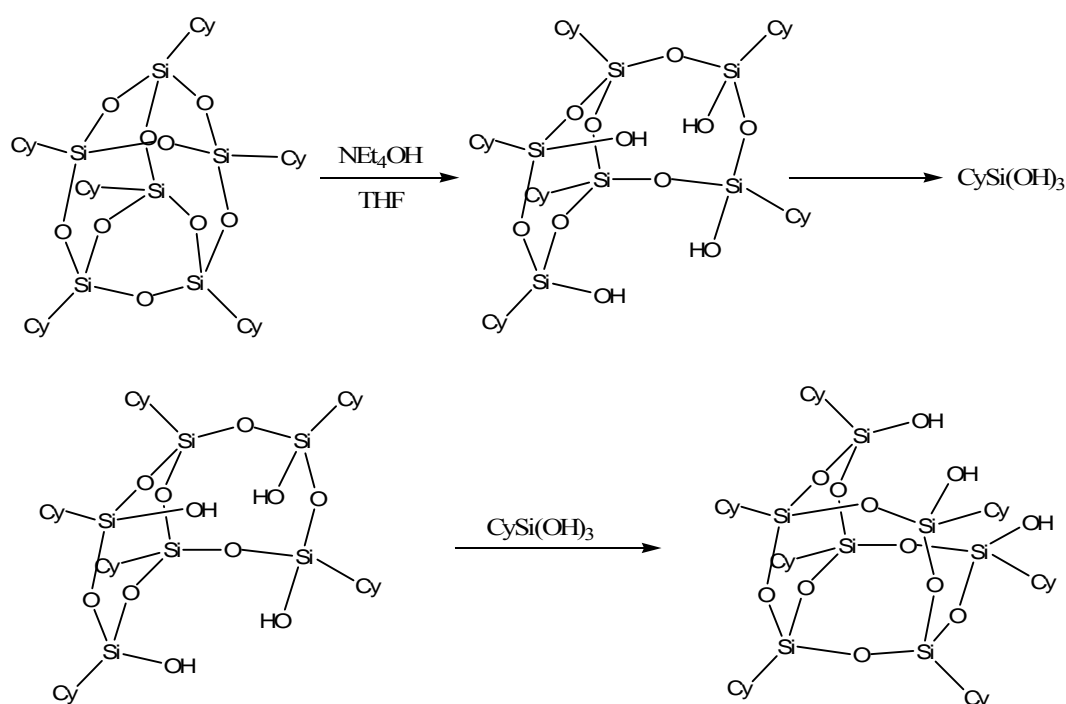


Figure 1.12. Synthesis of incompletely condensed POSS through base-mediated cleavage of fully condensed T_6 cage⁷⁰

1.3 Functionalisation of POSS

1.3.1 Hydrosilylation

Hydrosilylation involves the addition of hydrosilanes to unsaturated bonds. The reaction can be catalysed by ultraviolet light, γ -irradiation, electrochemical discharge or catalysts such as nucleophiles (tertiary amines), Lewis acids, metals reduced *in situ* or metal complexes.⁷⁵ The most active catalysts are platinum-based, with Speier's (H_2PtCl_6) ⁷⁶ and Karstedt's (Platinum(0)-1,3-divinyl-1,1,3,3-tetramethyldisiloxane)⁷⁷ catalysts being the two most common catalysts used. The addition of alkenes to silanes using the hydrosilylation reaction can generate both α - and β -isomers, with the β -adduct being the major product (**Figure 1.13**).⁷⁸

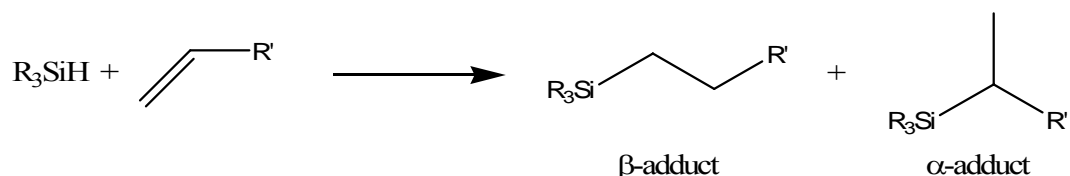


Figure 1.13. Two possible isomers formed from the hydrosilylation reaction⁷⁸

The traditional mechanism for platinum catalysed hydrosilylation is the Chalk-Harrod mechanism (**Figure 1.14**).⁷⁹ This mechanism proceeds in four main stages:

1. complex formation of alkene with metal centre;
2. oxidative addition of hydrosilane to metal centre;
3. *cis*-rearrangement of the metal silane complex, and
4. reaction with alkene to produce alkyl silane by reductive elimination, regenerating the metal-alkene complex.

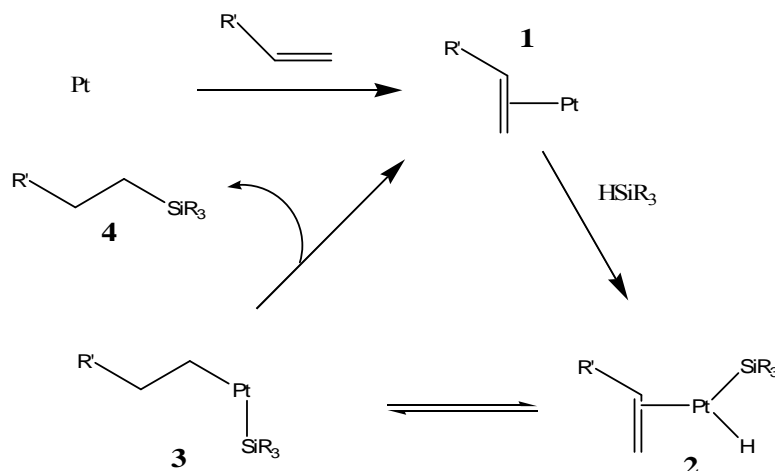


Figure 1.14. Chalk-Harrod mechanism⁷⁹

There are a number of phenomena that remained unexplained by the Chalk-Harrod mechanism. These included the presence of an induction period, the formation of colloidal platinum upon reaction completion despite the presence of competing equilibria and the requirement of oxygen for some hydrosilane/alkene reactions. In addition, some of the platinum complexes proposed in the Chalk-Harrod mechanism were not observed with highly active catalysts.

A novel mechanism based on platinum colloids as the active species was later proposed **Figure 1.15**.⁸⁰⁻⁸² Lewis *et al.*⁸⁰⁻⁸² attributed the induction period to the formation of colloidal platinum species, which required the presence of trace amounts of oxygen. These colloidal species were thought to be responsible for the coloured bodies at the completion of some hydrosilylation reactions.

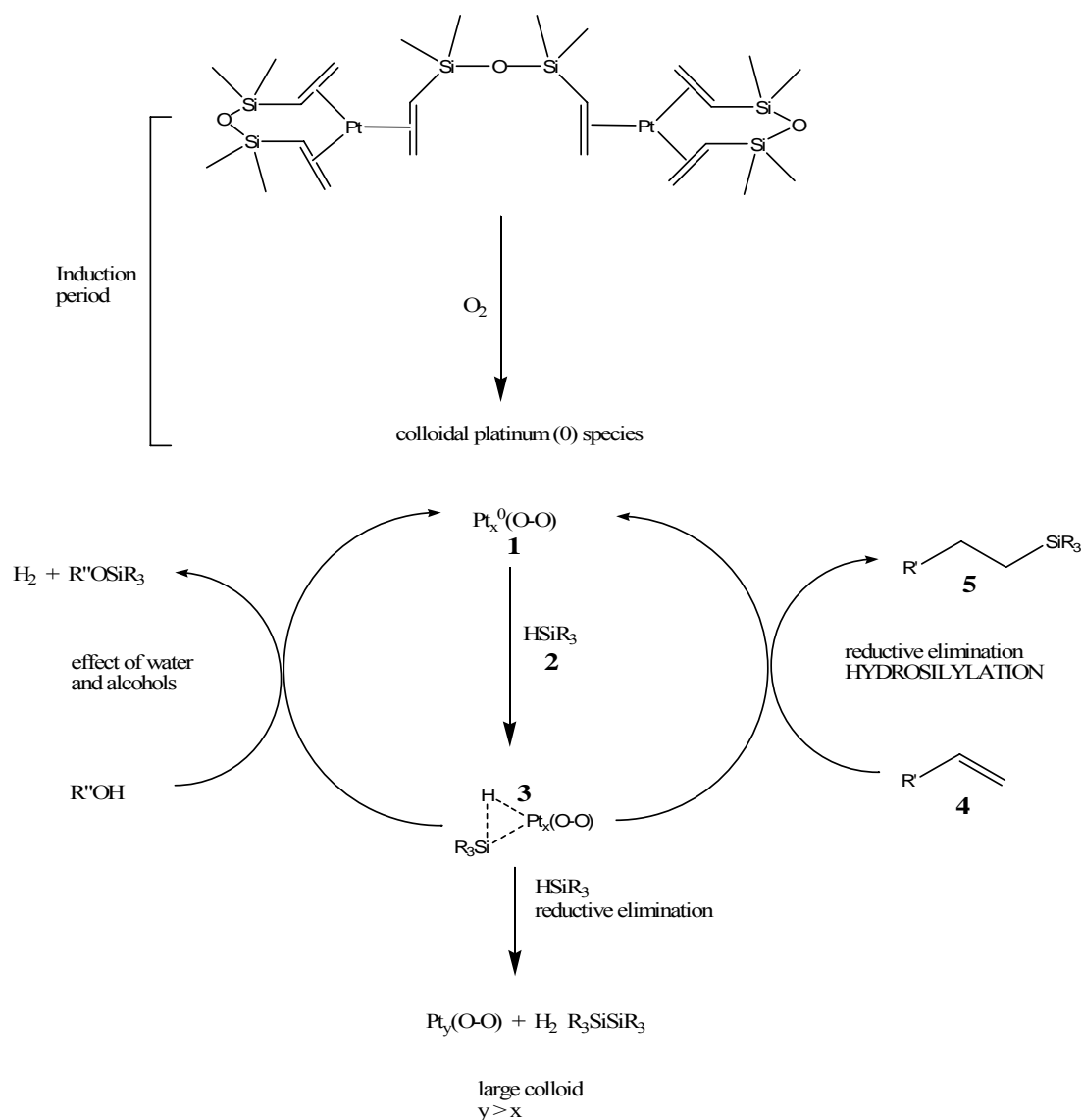


Figure 1.15. Original hydrosilylation mechanism proposed by Lewis⁸⁰⁻⁸²

During the induction period, the platinum species were reduced by the hydrosilane to form colloidal species stabilised by oxygen (1). The platinum colloid undergoes reaction with the hydrosilane (2) to form a platinum species, which was coordinated via a three-centre two-electron bond to the hydrosilane (3). Nucleophilic attack by the alkene (4) then generated the hydrosilylation reaction products (5). However no

in situ evidence for the formation of colloidal species during the catalytically active part of reaction was observed.⁸³

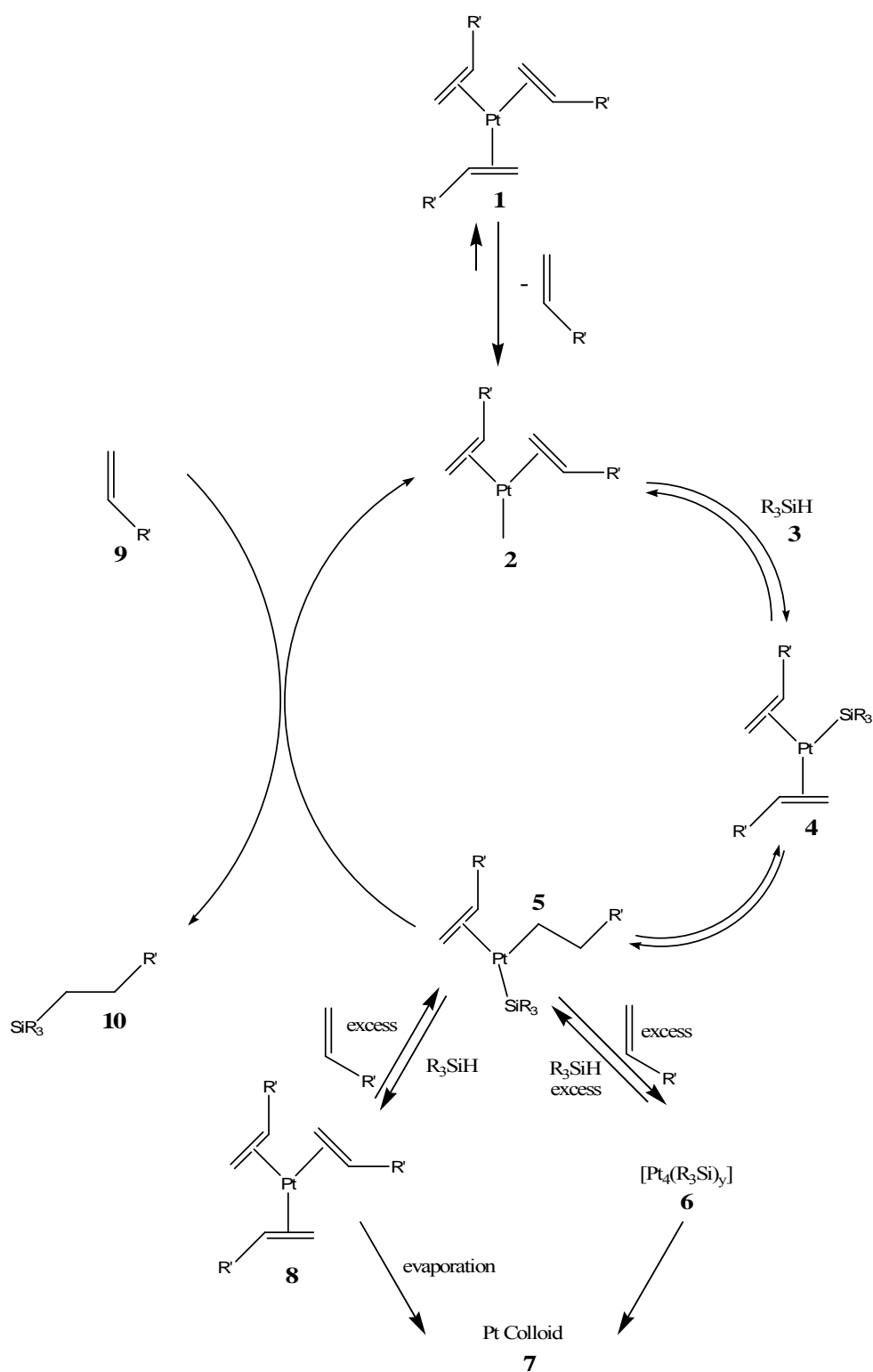


Figure 1.16. Improved hydro-silylation reaction mechanism proposed by Lewis⁸³

This proposed mechanism was based on Transmission Electron Microscopy (TEM) and High Resolution Electron Microscopy (HREM) images of evaporated solutions after reaction completion.^{80,82,84,85} The presence of colloidal platinum at reaction completion implied that colloidal platinum was the active species in the reaction.

The Lewis group later published a paper refuting their earlier work, concluding that a Pt(II) complex was involved in the reaction mechanism. Lewis *et al.*⁸³ reported studies in which the platinum species were structurally characterised during hydrosilylation through *in situ* investigation of hydrosilylation reactions involving Karstedt's catalyst. The use of Extended X-ray Absorption Fine Structure (EXAFS) spectroscopy, Small Angle X-ray Scattering (SAXS) and X-ray Photoelectron Spectroscopy (XPS) during the catalysis confirmed the presence of mononuclear platinum species during the catalytic reaction stage. From this data, a new mechanism was proposed (**Figure 1.16**) uniting aspects of the previous colloidal and Chalk-Harrod mechanisms.⁸³

The induction period involved dissociation of the platinum catalyst (1) to form a mononuclear, two-coordinate complex (2). This was followed by oxidative addition of the hydrosilane (3) to form a platinum(II) complex (4) and subsequent migratory olefin insertion into the platinum-hydrogen bonds (5). Excess hydrosilane gave rise to a multinuclear platinum cluster (6), formed with silyl ligands, leading to the formation of colloidal platinum (7). Excess alkene yielded a platinum-alkene complex (8), decreasing the overall yield of the hydrosilylation product. The catalytic cycle was completed with the reaction of additional alkene (9) with the intermediate, leading to the desired alkylsilanes (10) via reductive elimination and regeneration of the platinum(II) complex (1).⁸³

1.3.2 Functionalisation of POSS by Hydrosilylation

The first hydrosilylation reaction on T_8^H was reported by Herren *et. al* (**Figure 1.17**).⁸⁶ 1-hexene and methylenecyclohexane were hydrosilylated onto T_8^H through the use of Speier's catalyst, with yields of 90 %, although there was no discussion of whether the β isomer was the only observed product.

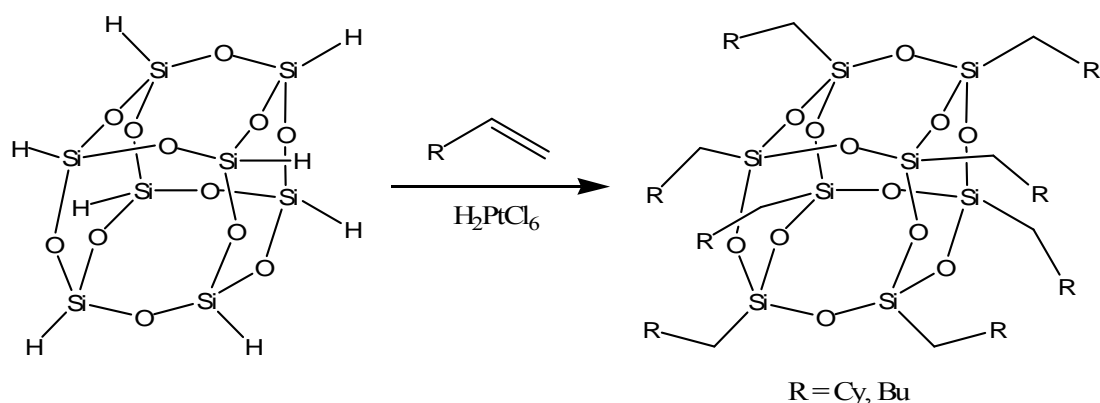


Figure 1.17. Hydrosilylation of alkenes onto T_8^H ^{H86}

Following this pioneering work, several hydrosilylation reactions were reported, mainly employing platinum catalysts, such as Speier's, Karstedt's, Pt/C or platinum(II) oxide.^{46,47,87,88} Bassindale and Gentle^{47,88} reported the hydrosilylation of T_8^H with hex-1-ene, dec-1-ene, tetradec-1-ene, octadec-1-ene and vinyl siloxane ($(\text{BuSi}(\text{Me})_2[\text{OSi}(\text{Me})_2]_3\text{CH}=\text{CH}_2)$). ¹³C and ²⁹Si NMR indicated that the addition of alkenes to T_8^H resulted in the exclusive formation of the β -adduct, however hydrosilylation of the vinyl siloxane to T_8^H yielded both α - and β -adducts. Gel Permeation Chromatography (GPC) indicated a small amount of impurity, resulting from vinyl/H exchange on silicon and subsequent formation of a POSS dimer.

A homologous series of octa-alkyl substituted silsesquioxanes was synthesised via the hydrosilylation of alkenes onto T_8^H in the presence of Speier's catalyst. Analysis by ¹³C NMR indicated that the β -adduct was the sole product.⁸⁹ The hydrosilylation of 1-hexene to T_8^H was also studied through ²⁹Si NMR, which indicated that both α - and β -adducts were present; with the β -adduct being the major product. This study concluded that steric hindrance involved with the organic substituents played an important role in the hydrosilylation reaction onto T_8^H .⁴⁶

The difficulty in synthesising large quantities of T_8^H has led to the use of $Q_8M_8^H$ for many reactions. Other examples of hydrosilylation reactions have involved the addition of silanes to alkene functionalised POSS compounds. The first reported hydrosilylation onto $Q_8M_8^H$ was the addition of vinylferrocene in the presence of Karstedt's catalyst (**Figure 1.19**).⁹⁰

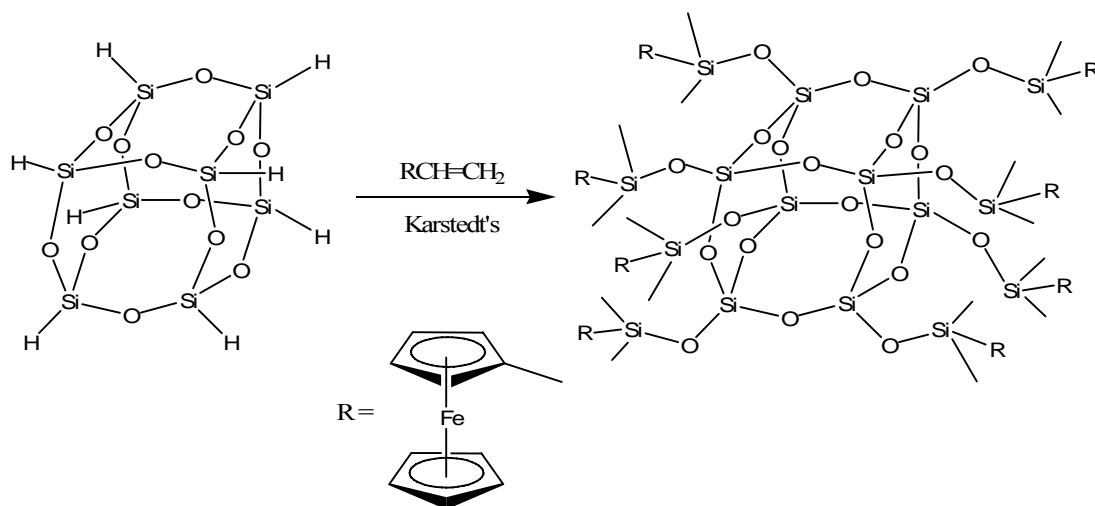


Figure 1.18. Hydrosilylation of vinylferrocene onto $Q_8M_8^{H 90}$

Examples of classes of compounds that have been successfully hydrosilylated onto POSS are long chain alkenes,⁸⁹ allyloxycoumarin,⁸ methyl terminated tetraethyleneglycol,⁹¹ bis-, tri-, tetra- and hexa-ethylene glycol,⁹² allyl bromide,⁹³ allyl alcohol,⁹⁴ *m*-isopropenyl- α,α' -dimethylbenzyl isocyanate⁹⁵ and vinyl epoxide.⁹⁶⁻¹⁰⁰ Thus, a wide range of reactive functionalities have been introduced to the periphery of POSS cages through the hydrosilylation reaction.

1.4 Functionalisation of POSS by Other Reactions

The corners of both mono- and octa-functionalised cages can be functionalised by a variety of methods, such as reaction of the trisilanol with mono-, di- or tri- halide or alkoxy organosilanes or metals, and reaction of the R groups.

1.4.1 Monosubstituted POSS Derivatives

Monosubstituted POSS compounds, of the general formula $R^1R_7Si_8O_{12}$, possess one reactive (often organic) group, whilst the remaining seven groups are relatively inert. Hybrid materials containing these singularly functionalised compounds have been employed in applications such as surface modification.³⁸ Mono-functionalised octasilsesquioxanes are generally synthesised by one of three general methods,

monomer polycondensation (Method 1), functionalisation of mono-functionalised silsesquioxane precursors (Method 2) and corner capping of incompletely condensed POSS cages (Method 3). Method 1 (**Figure 1.19**) involves monomer polycondensation in order to synthesise the desired mono-substituted silsesquioxanes. However, a mixture of hetero-substituted compounds, which are often unable to be separated, is generally obtained if this reaction is carried out in the presence of monomers containing different R groups. Method 2 (**Figure 1.20**) involves functionalisation of mono-functionalised silsesquioxane precursors, where R' is generally H or SiMe₂H. Method 3 (**Figure 1.21**) involves the reaction of a trisilanol POSS with a trichloro- or trialkoxy-silane, commonly referred to as the corner-capping method, and was initially developed by the Feher group.⁴²

1.4.1.1 Method 1

The first reported synthesis of a mono-substituted silsesquioxane via method 1 involved the co-hydrolysis of RSiX₃ and R' SiX₃, where R = H, R' = organic group and X = Cl or alkoxy (**Figure 1.19**).³¹ A complex mixture of isomers, containing all possible ratios of R and R', was obtained. The hydrolysis was, as previously discussed, influenced by a variety of reaction conditions, including the nature of the X group and the nature of the R and R' groups. In particular, for examples where R = Me, Et and X = Cl, OMe, the ratio of R to R' in the final product and the yield of reaction were greatly influenced by the concentrations of alkali and water in the reaction mixture.¹⁰¹ Mono-functionalised octasilsesquioxanes of the type R' R₇Si₈O₁₂ have also been synthesised through the co-hydrolysis of HSiCl₃ and PhSiCl₃, yielding PhH₇Si₈O₁₂.¹⁰²

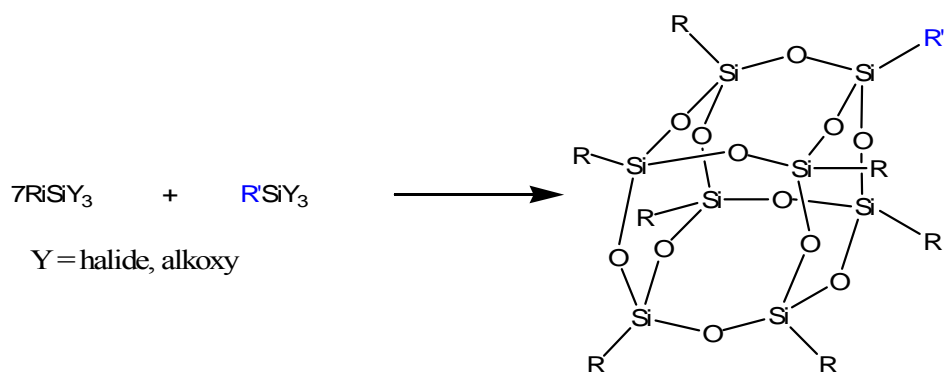


Figure 1.19. Synthesis of mono-functionalised POSS derivatives (Method 1)^{31,101,102}

1.4.1.2 Method 2

One of the simplest and most efficient routes of synthesis for mono-substituted octasilsesquioxanes is through the reaction of a reactive functional group (Method 2), such as $R' = H$ or $OSiMe_2H$ (**Figure 1.20**).

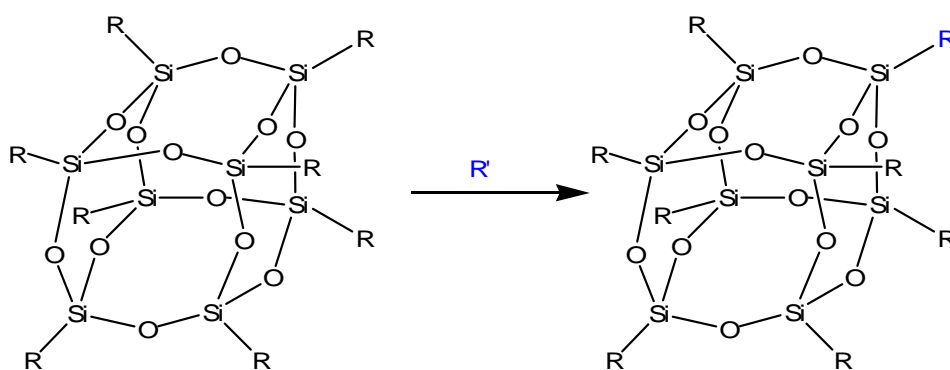


Figure 1.20. Synthesis of mono-functionalised POSS derivatives (Method 2)

The silane can be hydrosilylated with a range of alkenes, in the presence of a platinum catalyst. A variety of alkenes, such as $(\eta-C_5H_5)Fe(\eta-C_5H_4CH=CH_2)$, $PhCH=CH_2$, $PhC\equiv CH$ and 1-hexene have been hydrosilylated onto $R_7Si_8O_{12}(OSiMe_2H)$ (**Figure 1.21**).¹⁰³⁻¹⁰⁵

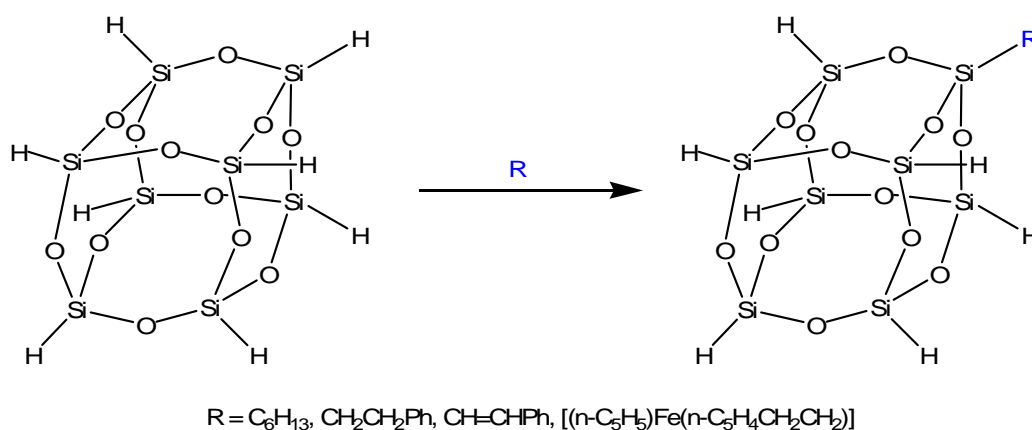


Figure 1.21. Synthesis of mono-functionalised POSS derivatives¹⁰³⁻¹⁰⁵

Examples of mono-functionalised POSS compounds prepared by hydrosilylation also include $R' =$ octene and allyl(polyethylene oxide).^{106,107} Mono-octene functionalised POSS was obtained via the mono-hydrosilylation of dibrominated decadiene onto T_8^H . The seven remaining silyl groups were then reacted with ethene. Subsequent

debromination yielded the desired octane functionalised POSS, which was then used in homo- and co-polymerisation reactions with ethene and propene, to synthesise high molecular weight polymers containing pendant POSS cages (**Figure 1.22**). Thermal analysis of these polymers indicated that the incorporation of POSS improved the thermal stability of the polymers.

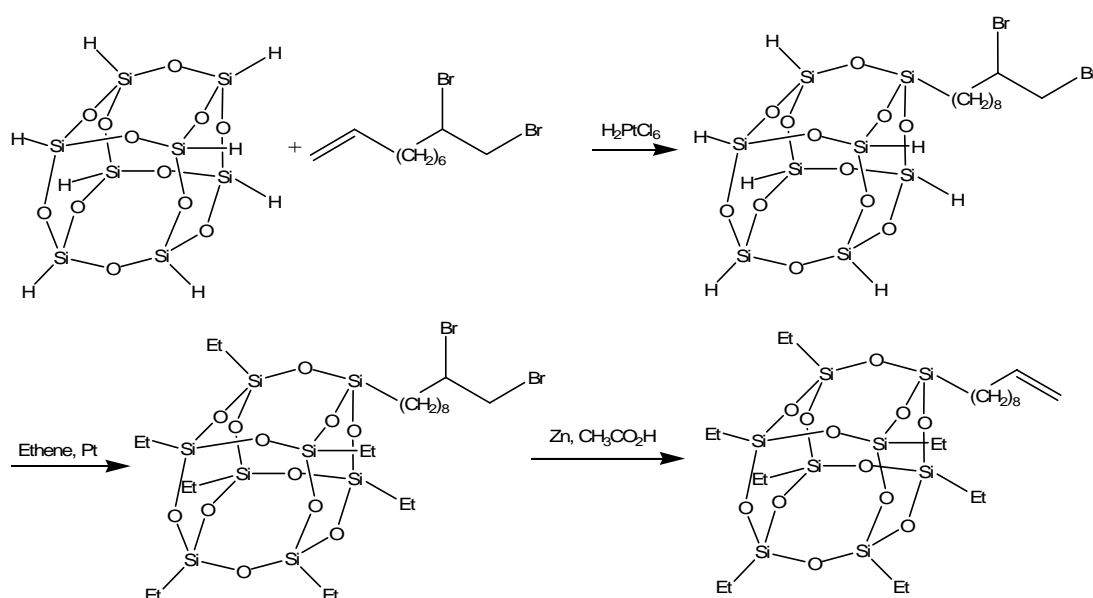


Figure 1.22. Synthesis of mono-octene POSS^{106,107}

A mono-(polyethylene oxide) POSS derivative was synthesised via the hydrosilylation of $\text{H}_7\text{Si}_8\text{O}_{12}\text{R}$ and allyl functional (polyethylene oxide), with a mean molecular weight (M_n) of $750 \text{ g}\cdot\text{mol}^{-1}$, in the presence of Speier's catalyst (**Figure 1.23**).¹⁰⁷ This particular POSS molecule possessed intriguing amphiphilic properties; as a relatively hydrophobic silsesquioxane core was covalently linked to a hydrophilic (polyethylene oxide) chain. Aggregation of the uncondensed amphiphile demonstrated the potential use of these compounds to prepare novel core/shell type nanoparticles.¹⁰⁷

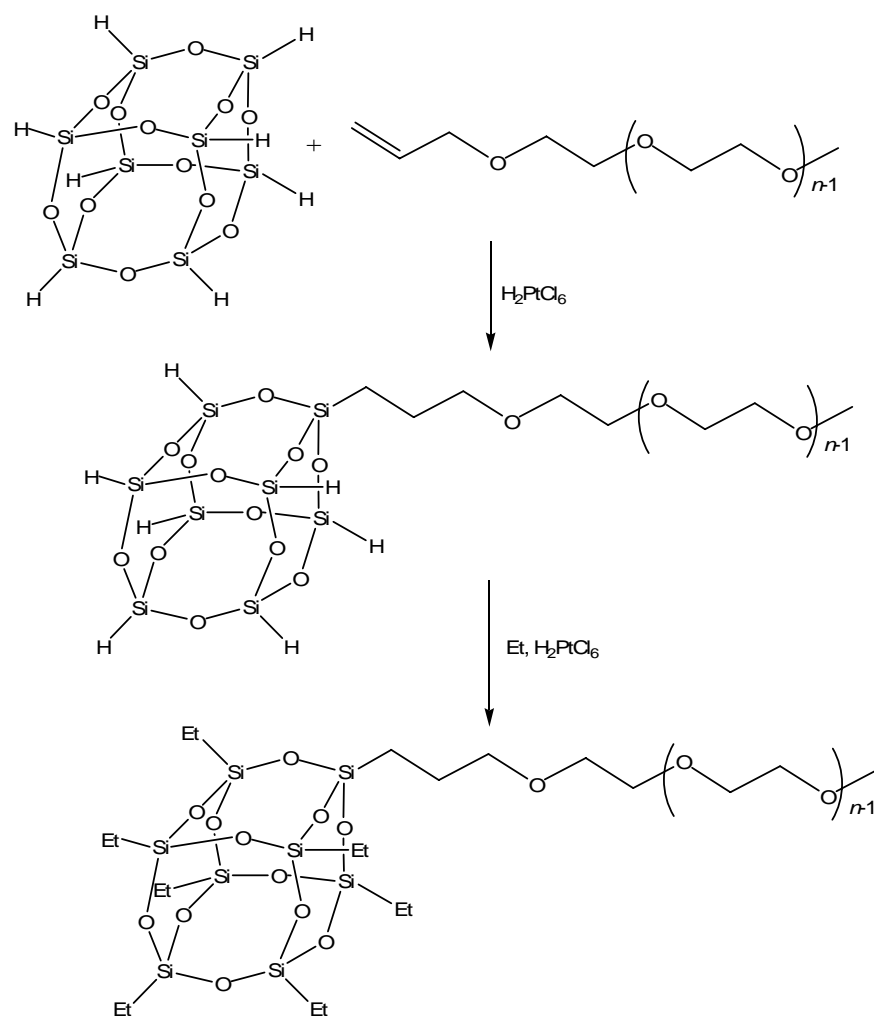
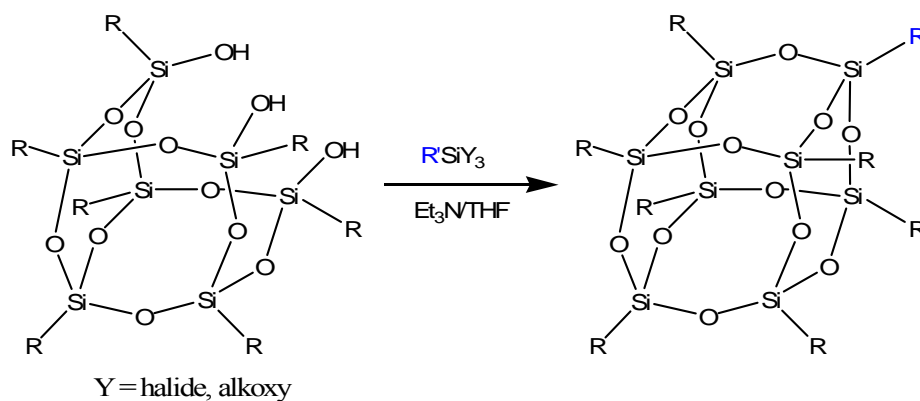


Figure 1.23. Synthesis of mono-oligo(ethylene oxide) hydridosilsesquioxane¹⁰⁷

1.4.1.3 Method 3

The corner capping reaction represents a method of synthesising mono-substituted silsesquioxanes. This method was developed by the Feher group¹⁰⁸⁻¹¹¹ and involves the use incompletely condensed silsesquioxanes of the type R₇Si₇O₉(OH)₃. The silanol groups in this molecule are very reactive and thus can be reacted with trichloro- or trialkoxysilanes, to obtain the fully condensed product (**Figure 1.24**). A range of functionalities have been incorporated via this method, such as hydrogen,¹¹² halides,¹¹²⁻¹¹⁶ alkenes,^{49,112,117} methacrylates,^{115,118,119} alkyl groups,¹¹⁵ amines^{115,120} and thiols.^{116,121}



**Figure 1.24. Corner capping of incompletely condensed silsesquioxane
(Method 3)**^{49,112-121}

1.4.2 Subsequent Reactions of the R' Group

Subsequent modifications of the R' group enabled the synthesis of a variety of mono-functionalised precursors. Examples include compounds such as $\text{Cy}_7\text{Si}_8\text{O}_{12}\text{Cl}$ or $\text{Cy}_7\text{Si}_8\text{O}_{12}\text{H}$, which are able to be subsequently reacted with alkyl and aryl phosphine ylides, such as Me_3PCH_2 and Ph_3PCH_2 , to yield $\text{Cy}_7\text{Si}_8\text{O}_{12}(\text{CHPR}_3)$ where R = Me, Ph.¹²² These compounds were then able to undergo further reaction with a variety of aldehydes, acting as Wittig reagents.

The reaction of (3-mercaptopropyl)trimethoxysilane with $\text{iBu}_7\text{Si}_7\text{O}_9(\text{OH})_3$, in the presence of *p*-toluenesulfonic acid as a catalyst, yielded mono-(3-mercaptopropyl)POSS derivative.¹²¹ The free radical addition of mono-(3-mercaptopropyl)isobutyl-POSS to the side chain double bonds of poly[3-hydroxyalkanoate-*co*-3-hydroxyalkenoate] has been reported (**Figure 1.25**).¹²³ 3-mercaptopropyl-POSS has also been used as a ligand for the coordination of transition metal ions, such as Rh(II), Hg(II), Pb(II) and Au(I).^{116,121}

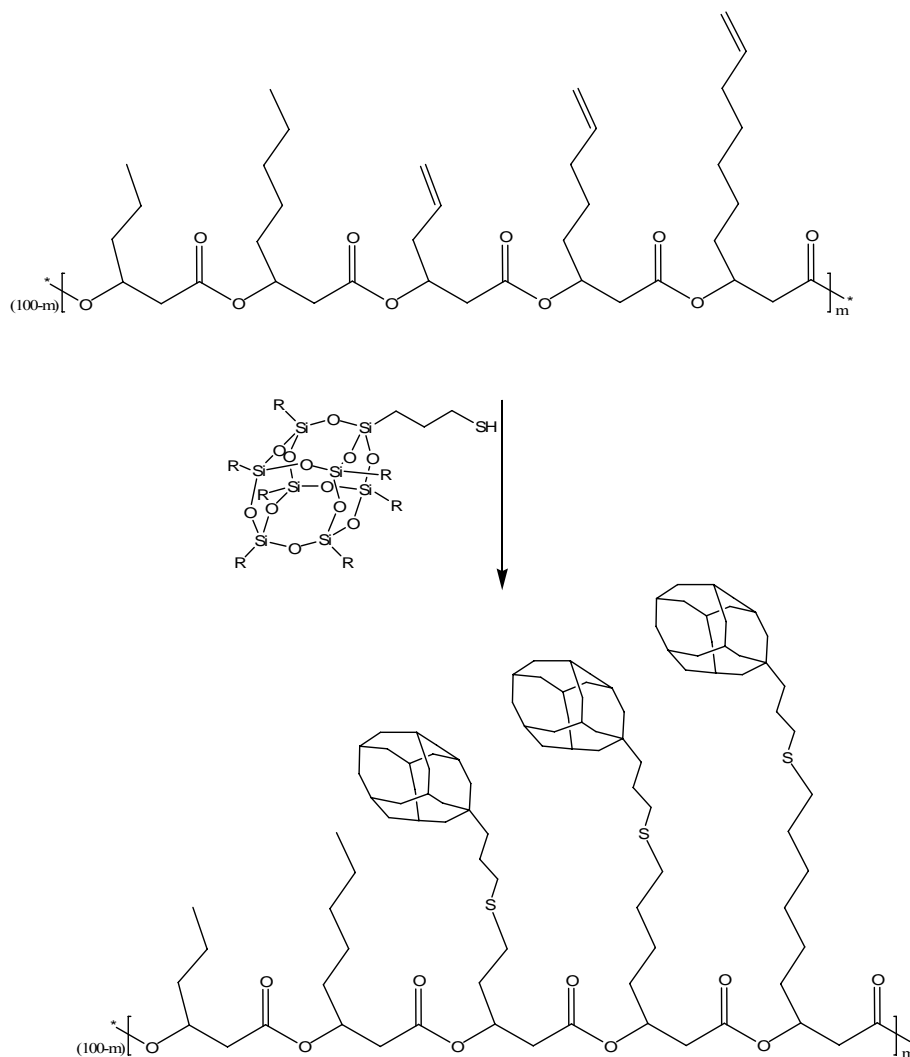


Figure 1.25. Free radical addition of 3-mercaptopropyl POSS to poly [3-hydroxyalkanoate-co-3-hydroxyalkenoate]¹²³

1.4.3 Reaction of the Trisilanols with Mono-Or Dihalide Organosilanes

The reaction of mono-halide or mono-alkoxy organosilanes, such as Me_3SiCl ,^{42,122,124,125} Me_2PhSiCl ,¹²⁴ MePh_2SiCl ,¹²⁵ $(\text{CH}_2=\text{CH})\text{Me}_2\text{SiCl}$,¹²⁵ $(\text{CH}_2=\text{CHCH}_2)\text{Me}_2\text{SiCl}$ ¹²⁶ and $(\text{EtO})\text{Si}(\text{CH}_3)_2\text{CH}_2\text{CH}_2\text{PPh}_2$,¹²⁷ with incompletely condensed silsesquioxanes yielded the substituted disilanol derivatives. A similar reaction has also been performed by reacting *tert*-BuMe₂Si(OTf) with an incompletely condensed trisilanol silsesquioxane, in the presence of triethylamine, to yield the substituted disilanol derivative (**Figure 1.26**).¹²⁸

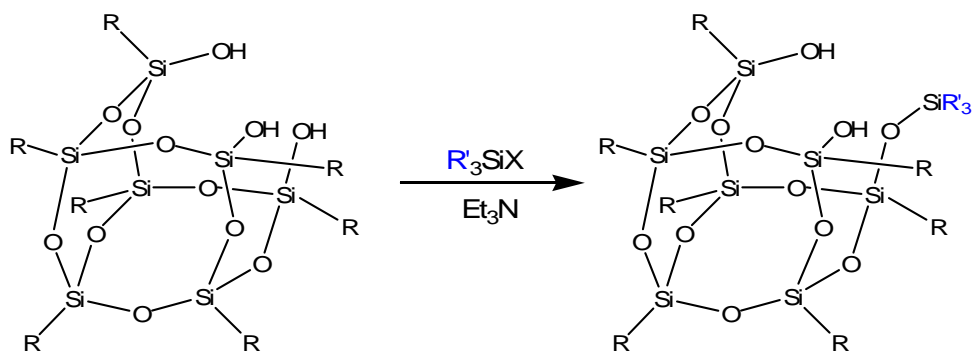


Figure 1.26. Mono-functionalised incompletely condensed POSS^{42,122,124-128}

Changing the stoichiometric ratio enabled the formation of disubstituted incompletely condensed silsesquioxane derivatives, where $R' = \text{SiMe}_3$ ^{42,122,124,129} and SiMe_2Ph ,¹²⁹ and trisubstituted derivatives, such as $R' = \text{SiMe}_3$,^{42,129} $\text{SiMe}_2(\text{CH}=\text{CH}_2)$,¹³⁰ $\text{SiMe}_2(\text{CH}_2\text{CH}=\text{CH}_2)$ ¹³¹ and $\text{SiMe}_2\text{CH}_2\text{CH}_2\text{PPh}_2$ (Figure 1.27).¹²⁷

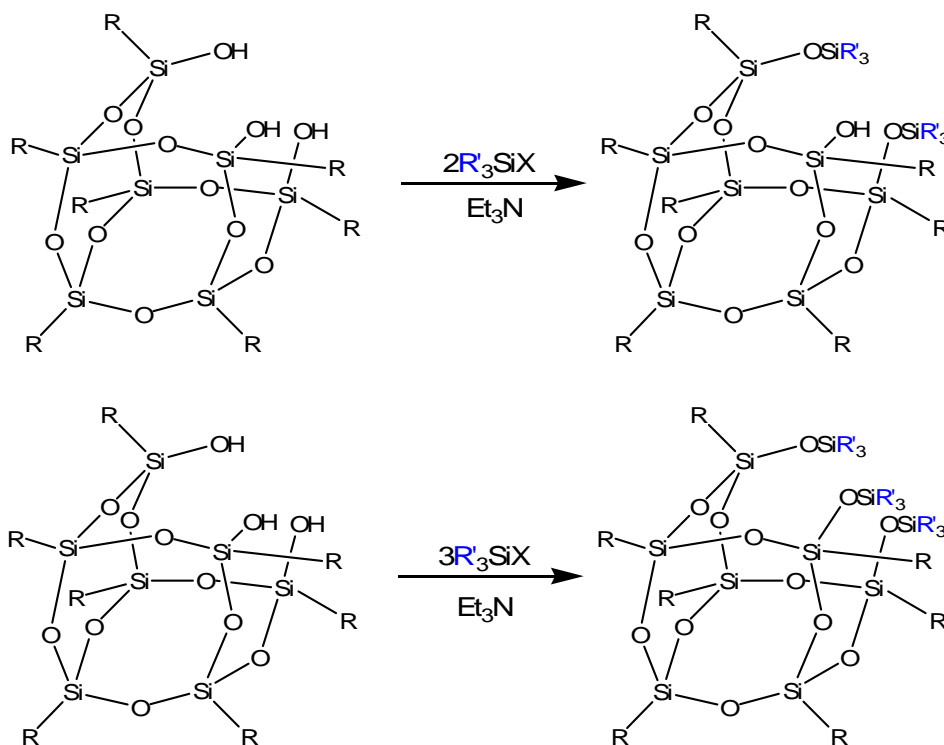


Figure 1.27. Synthesis of multi-substituted incompletely condensed silsesquioxane derivatives^{42,122,124,129-131}

The reaction of dihalide organosilanes with incompletely condensed silsesquioxanes has led to the formation of disubstituted incompletely condensed silsesquioxanes with one remaining silanol group (Figure 1.28).¹³²

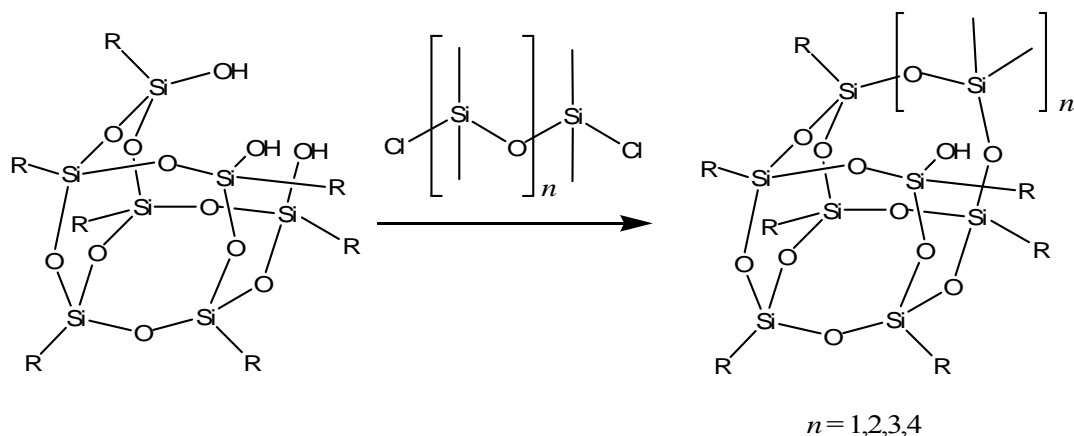


Figure 1.28. Synthesis of disubstituted incompletely condensed silsesquioxane¹³²

1.4.4 Metal Silsesquioxanes

The Feher group¹⁰⁸ initiated the use of silsesquioxanes as ligands for main and transition metals in the late 1980's, by investigating the use of silsesquioxanes as models for industrially used silica supports. Subsequent research has seen the coordination of a range of elements spanning the periodic table, including Na,¹³³ Li,^{128,134-137} Ti,^{131,138-140} Fe,¹⁴¹⁻¹⁴³ Al,^{141,144,145} Au,^{116,121} and Pt^{116,125,146} to silsesquioxane ligands.

1.4.5 Octa-substituted POSS Derivatives

A large range of methods exist for the reaction of the R' group in mono-substituted POSS compounds, as discussed in **Section 1.4.2**. Similarly, octa-substituted POSS derivatives can also be further functionalised through a variety of other reactions. The first synthesis of products derived from T₈^H involved photochlorination to obtain Cl₈Si₈O₁₂.¹⁴⁷ Subsequent methoxylation with methyl nitrite yielded (MeO)₈Si₈O₁₂. Single crystal x-ray studies confirmed that the stereochemical configuration of the central Si₈O₁₂ core was retained following methoxylation. Methoxylation was also attempted with ionic reagents, such as methyllithium or sodium methoxide, however degradation of the cage occurred.¹⁴⁷

The complete mono-nitration of octa(phenyl)silsesquioxanes was first described by Olsson and Gronwell,⁵⁰ however the resultant product was poorly characterised and reported to be unreactive. The procedure was modified by Laine *et. al.*,¹⁴⁸ yielding octa(nitrophenyl)POSS (ONPS) with *meta*- or *para*- substitution (**Figure 1.29**).

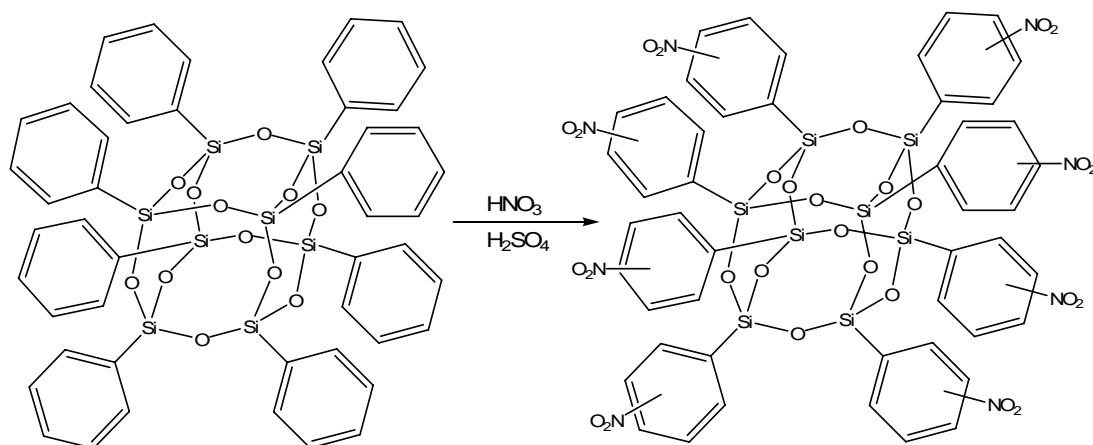


Figure 1.29. Synthesis of octa(nitrophenyl)POSS¹⁴⁸

Mild reduction of the ONPS with Pd/C and H₂, produced octa(aminophenyl)POSS (OAPS), which can be further reacted with a variety of functional groups (**Figure 1.30**).¹⁴⁸

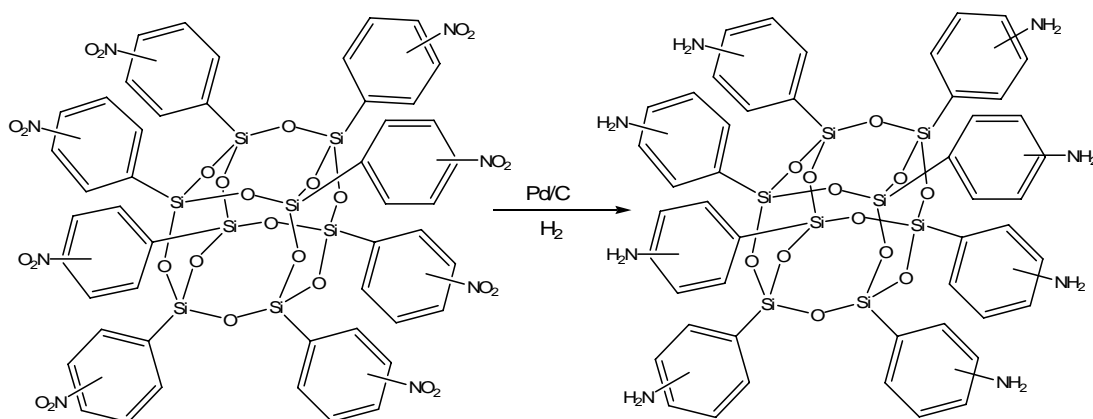


Figure 1.30. Synthesis of octa(aminophenyl)POSS¹⁴⁸

Octa(bromophenyl)POSS has been synthesised via bromination of octa(phenyl)POSS with Br₂/Fe (**Figure 1.31**).¹⁴⁹ Suzuki coupling was subsequently performed on this compound to synthesise phenyl, biphenyl, naphthyl, 9,9-dimethylfluorene and thiophene derivatives of octa(phenyl)POSS.¹⁵⁰

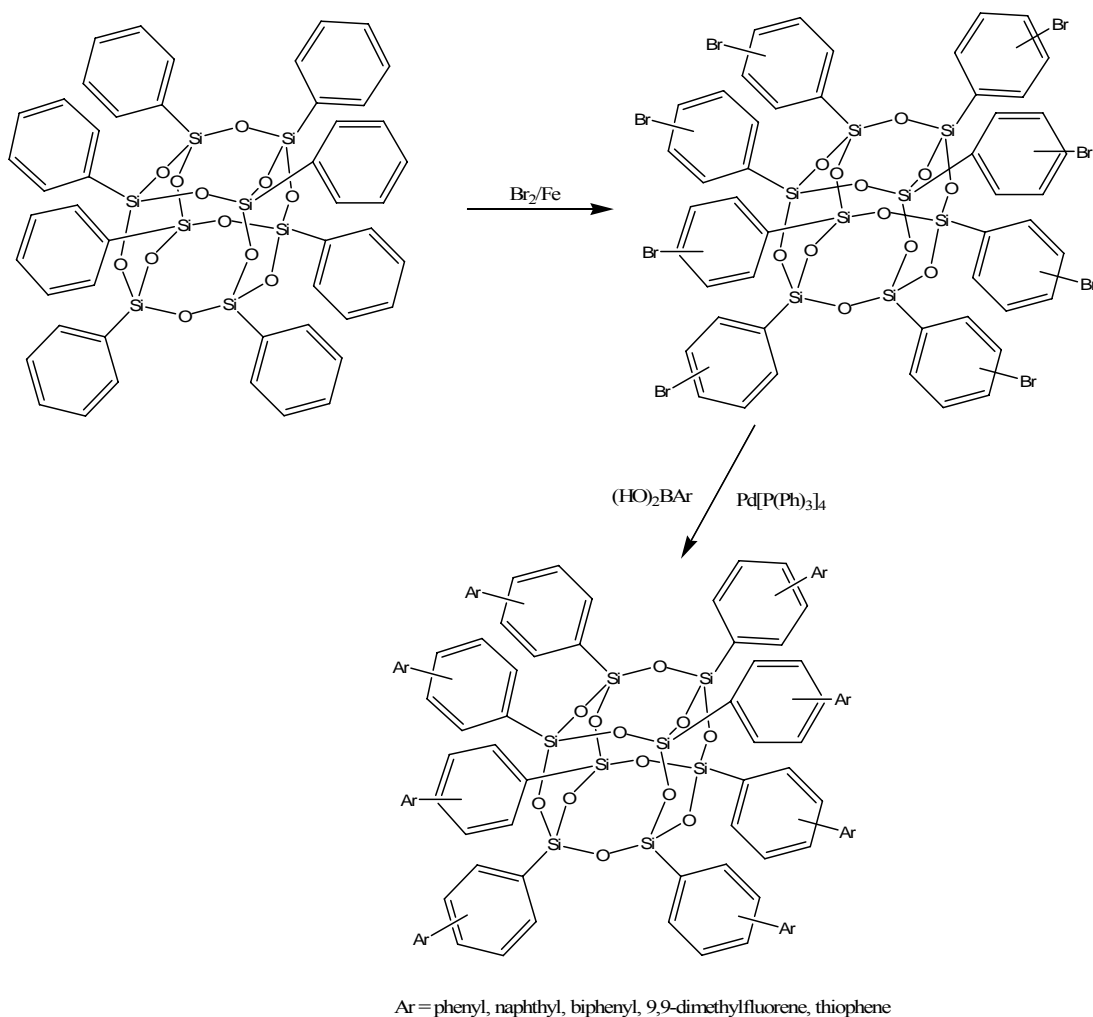


Figure 1.31. Bromination of octa(phenyl)POSS and subsequent Suzuki coupling^{149,150}

The formation of a range of POSS imides and polyimides has been achieved through the reaction of mono-,^{5,72,113} bis-¹⁵¹ and octa-^{100,148,152} POSS amines with a variety of mono- and bis-anhydrides. The synthesis and properties of POSS imides are discussed in greater depth in **Chapter 3**.

The bromination of POSS has also been achieved through radical addition. The reaction of hydrogen bromide and benzoyl peroxide with octa(vinyl)POSS yielded octa(2-bromoethyl)POSS (**Figure 1.32**).¹⁵³

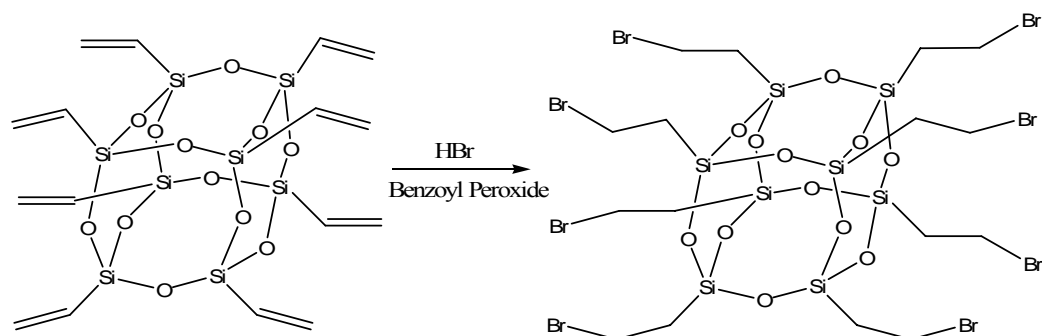
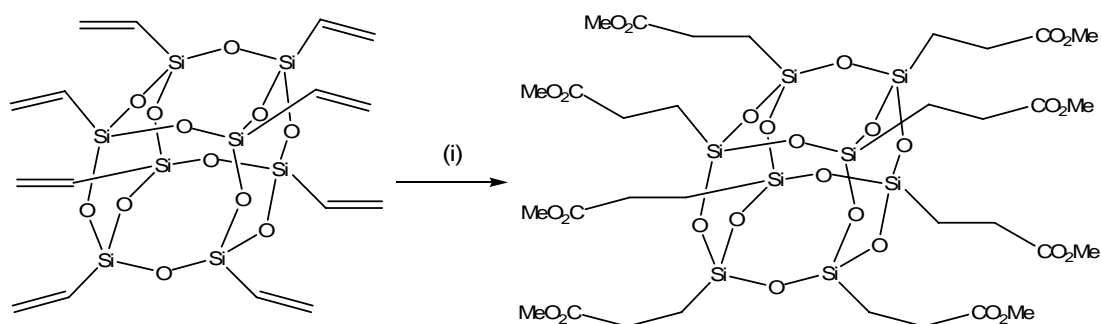


Figure 1.32. Radical bromination of octa(vinyl)POSS¹⁵³

The introduction of methyl ester groups onto the periphery of the POSS cage has been achieved through palladium catalysed methoxycarbonylation of octa(vinyl)POSS to form an octa-functionalised silsesquioxane containing methyl propanoate groups, with the reaction performed under a 30 bar CO atmosphere at 80 °C in an autoclave (**Figure 1.33**).¹⁵³



(i) Pd₂(dba)₃, 1,2-bis(di-*tert*-butylphosphinomethyl)benzene, MeOH, methanesulfonic acid, CO

Figure 1.33. Methoxycarbonylation of octa(vinyl)POSS¹⁵³

POSS has also been functionalised through the UV addition of phosphanes to carbon-carbon double bonds, such as those in octa(vinyl)POSS (**Figure 1.34**). The resulting silsesquioxanes were able to be used as precursors to organometallic gels or dendritic macromolecules.¹⁵⁴

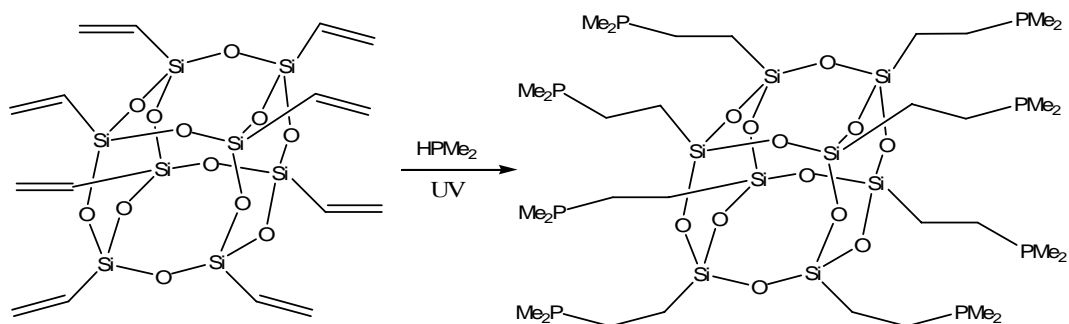


Figure 1.34. UV addition of phosphanes to octa(vinyl)POSS¹⁵⁴

Cyclopentadienyl functionalised POSS molecules have been synthesised via hydrolytic condensation of dodeca(cyclopentadienyl)POSS ($\text{Cp}_{10}\text{Si}_{10}\text{O}_{15}$) (**Figure 1.35**). Diels Alder polymerisation has been performed with these compounds to generate new polymeric POSS materials.¹⁵⁵ Metallation of the free Cp groups offer a potential route for the preparation of controlled pore size metal-containing materials.

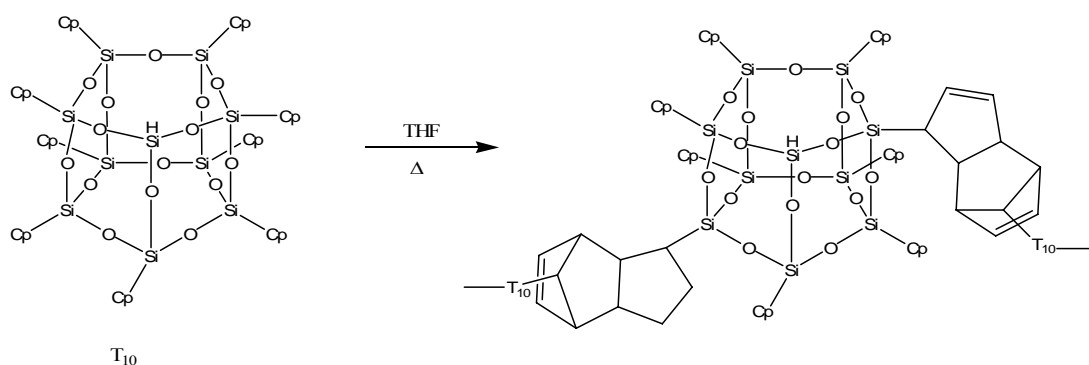


Figure 1.35. Diels Alder polymerisation of dodeca(cyclopentadienyl)POSS¹⁵⁵

Nucleophilic substitution reactions have been performed on octa(3-chloropropyl)silsesquioxane with reactants such as NaI, NaSCN, KPPH_2 and NaSCH_3 .^{116,156}

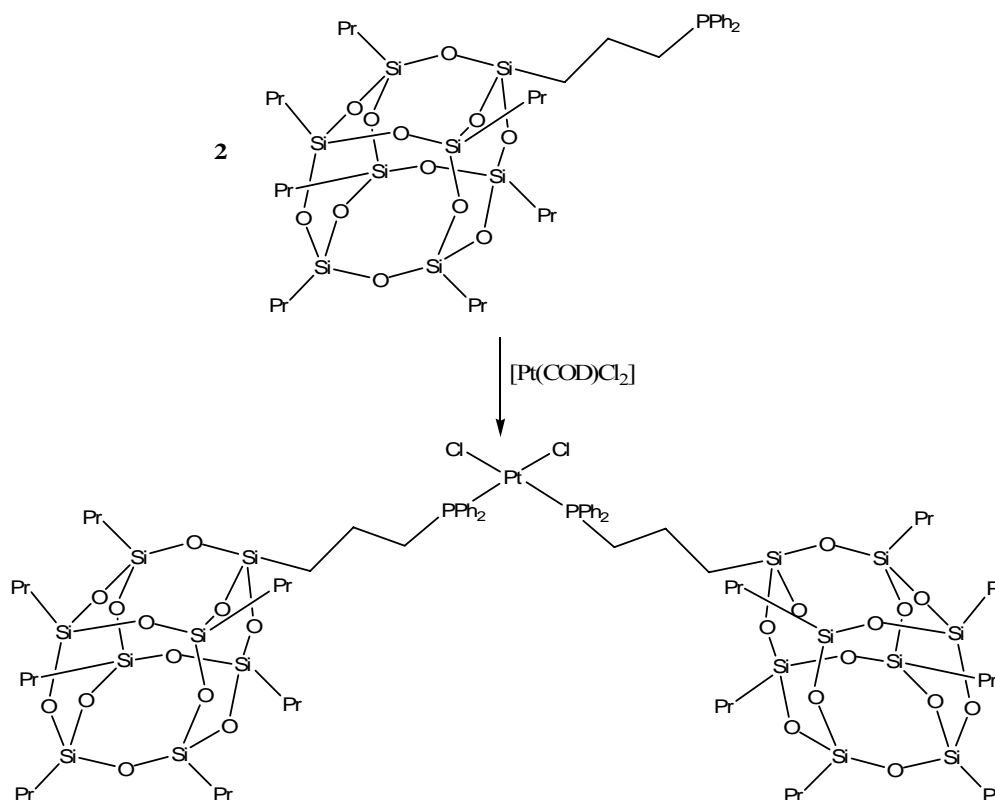


Figure 1.36. Coordination of platinum through phosphine-functionalised POSS¹¹⁶

The addition of KPPH_2 enabled the coordination of transition metals, such as platinum, through the phosphine ligand (**Figure 1.36**).¹¹⁶

The radical addition of thiols to POSS has been demonstrated in the addition of thioglycosides to octa(vinyl)POSS (**Figure 1.37**).⁸³

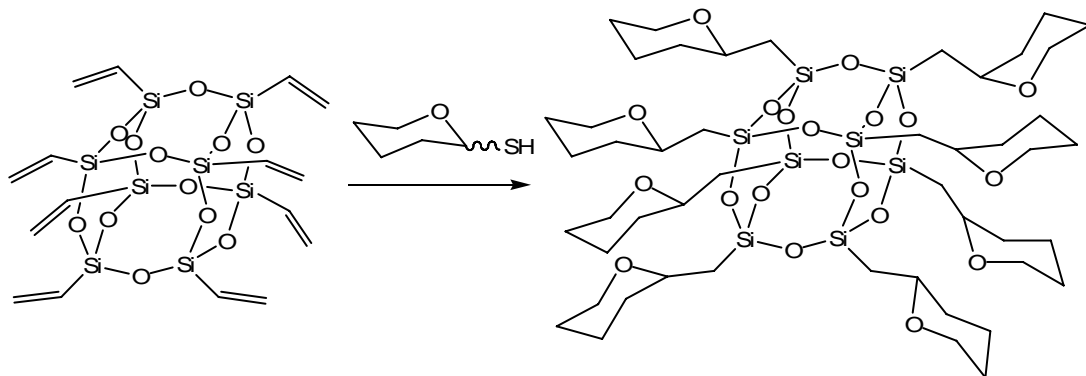


Figure 1.37. Radical addition of thiols to octa(vinyl)POSS⁸³

Heck coupling of octa(vinyl)POSS with aromatic halogens (Cl, Br, I) has been reported, with a large variety of polycyclics, including naphthalene, pyrene, anthracene and dimethylfluorene (**Figure 1.38**).^{3,157} Characterisation by Matrix-Assisted Laser Desorption/Ionisation - Time-of-Flight Mass Spectrometry (MALDI-TOF) and ^{29}Si NMR indicated a distribution of products ranging from six to ten substitutions, whilst the presence of nine and ten substitutions were indicative of di-substituted vinyl groups.^{158,159}

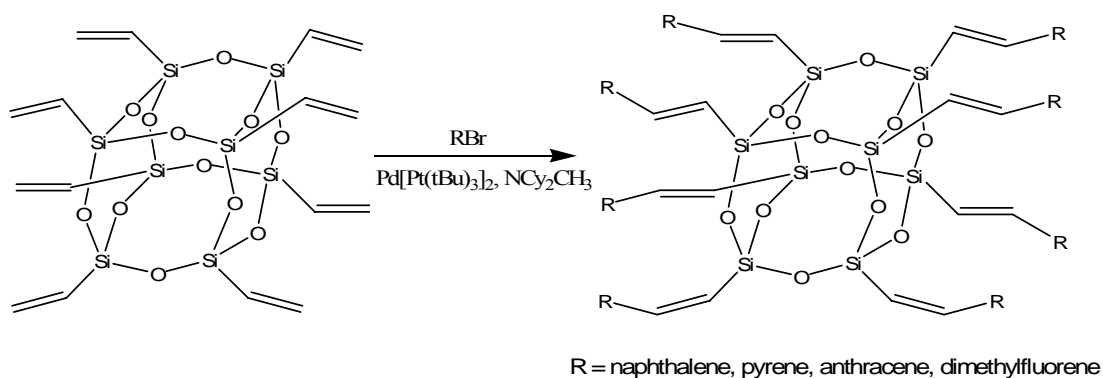


Figure 1.38. Heck coupling of bromoaromatics with octa(vinyl)POSS^{158,159}

Friedel-Crafts alkylation has previously been performed on octa(vinyl)POSS. The

addition of benzene in the presence of aluminium chloride has been reported, along with dichlorocarbene addition to the vinylic double bonds, which was accomplished under basic conditions, employing tetrabutylammonium halide as a catalyst, in order to form dichlorocyclopropane functionalized POSS compounds (**Figure 1.39**).¹⁶⁰

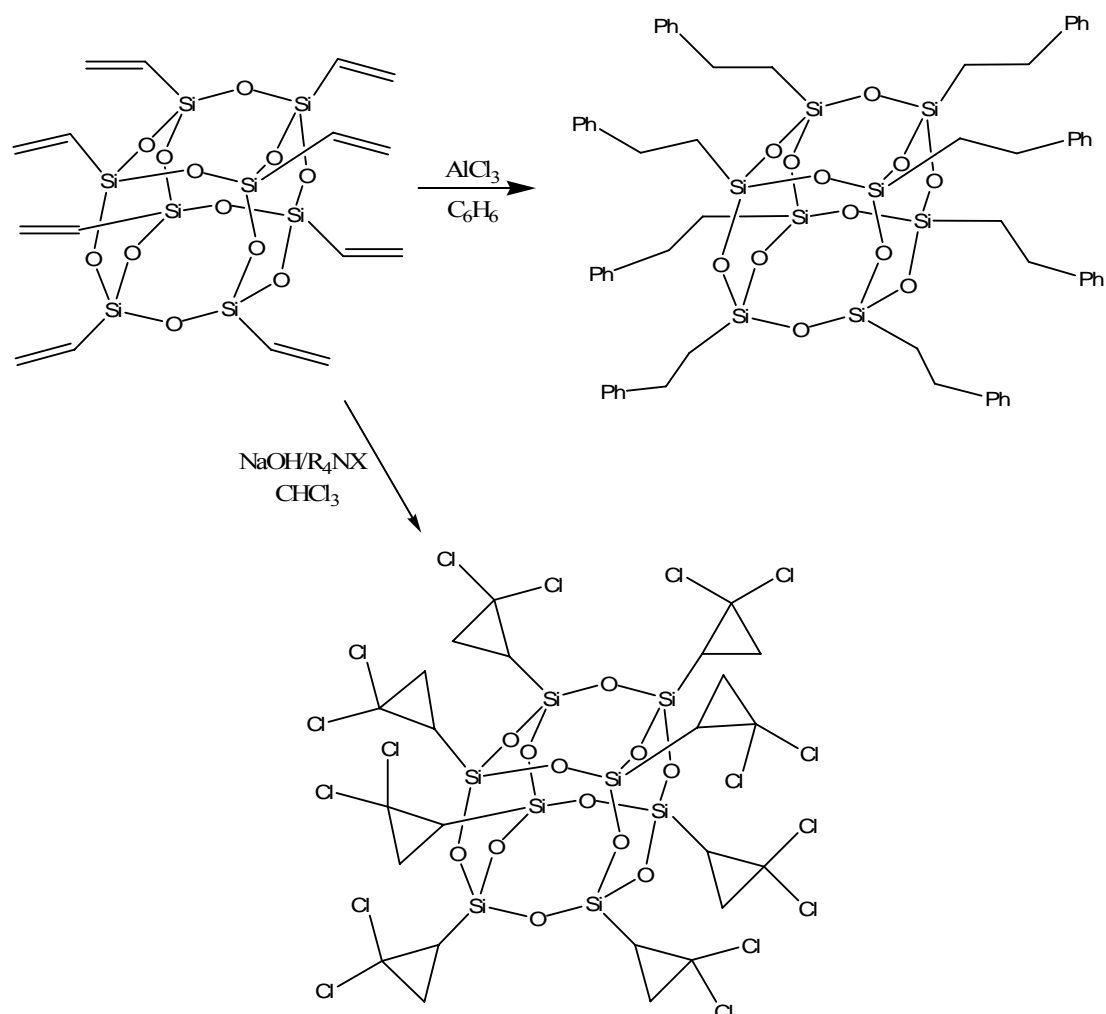


Figure 1.39. Arylation and dichlorocarbene addition to octa(vinyl)POSS¹⁶⁰

Functionalisation of octa(vinyl)POSS has been achieved through ruthenium catalysed silylative coupling and cross-metathesis on substituted silsesquioxanes with a range of β -substituted vinyl groups, such as styrene, 1-hexene, vinyltrimethylsilane, allyltrimethylsilane and vinyl ethers (**Figure 1.40**).¹⁶¹

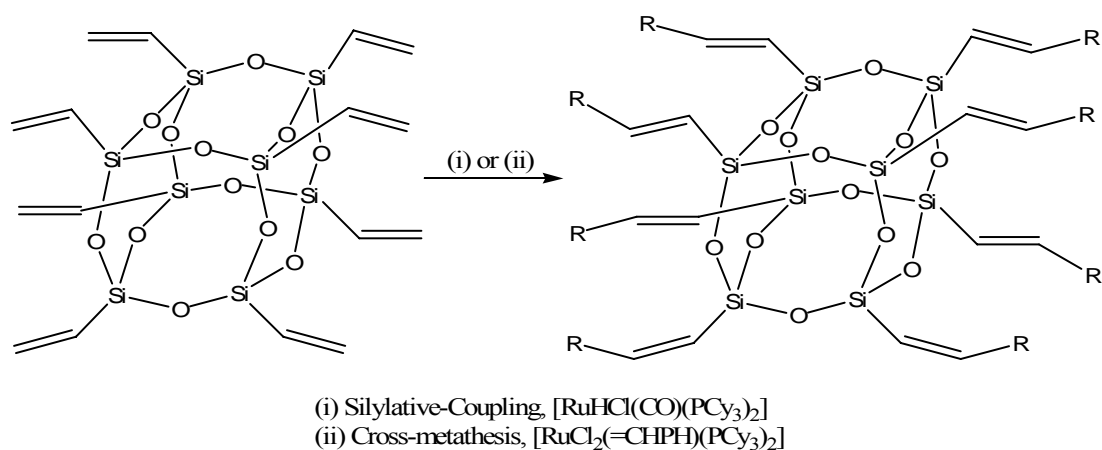


Figure 1.40. Silylative coupling and cross-metathesis of octa(vinyl)POSS¹⁶¹

The conversion of mono-vinyl and mono-styryl silsesquioxanes into isoxazole derivatives has been performed via the microwave assisted 1,3-dipolar cycloaddition of nitrene and nitrile oxides (**Figure 1.41**).¹⁶² The presence of the isoxazole ring offered a possible avenue to new functionalised derivatives, through modification of the N,O ring.

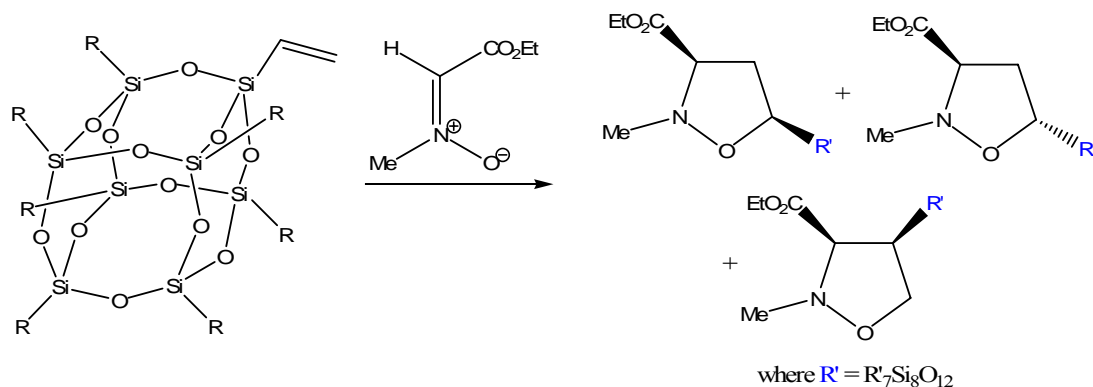


Figure 1.41. 1,3-dipolar cycloaddition of nitrene and nitrile oxides to mono(vinyl) and mono(styryl)POSS¹⁶²

A large range of both mono- and octa-functionalised POSS compounds have been synthesised by a variety of reaction pathways, including nitration,^{50,148} bromination,^{149,153} Suzuki coupling, radical addition,⁸³ Heck coupling,^{3,157} UV addition,¹⁵⁴ Diels Alder reaction,¹⁶³ nucleophilic substitution,^{116,156} Friedels-Craft alkylation,¹⁶⁰ silylative coupling¹⁶¹ and dipolar cycloaddition.¹⁶²

1.5 POSS Polymers

POSS based hybrid materials have recently emerged as unique materials due to their enhanced physical and mechanical properties, such as temperature and oxidation resistance, surface hardening, mechanical properties, reduced flammability, diminished exothermicity on combustion and reduced viscosity during processing, however oxygen permeability has been shown to increase.^{94,148,164,165}

The reinforcement of organic polymers has been achieved through the covalent linkage of functionalised POSS cages to the polymer matrix, which was attained through the attachment of either single or multiple polymerisable groups to the periphery of the POSS cage. Subsequent copolymerisation of the functionalised POSS cage and the desired monomer yielded the hybrid material. Systems synthesised via this methodology include polysiloxane,¹⁶⁶ poly(methyl methacrylate),¹⁶⁷ poly(4-methyl styrene),^{117,168} epoxy,^{112,169} polynorborene^{170,171} and polyurethane.^{95,172}

The synthesis of organic-inorganic hybrid materials can also be achieved through the employment of functionalisation of POSS cages containing eight polymerisable groups. Polymerisation of the POSS can then be undertaken with or without other monomers. A range of functional groups have been employed in the preparation of such materials, including epoxy,^{98,173,174} amino,¹⁴⁸ methacryloyl,⁹⁴ vinyl¹⁶⁴ and isocyanato.⁹⁵

1.6 Summary

Polyhedral oligomeric silsesquioxanes are flexible molecules that have been used in a wide range of applications. The synthesis, functionalisation and properties of POSS molecules have been discussed in detail within this chapter. The coupling of a range of optical functionalities was desired to produce a range of POSS molecules with unique properties, as discussed in the following chapters.

1.7 References

- (1) R. H. Baney; M. Itoh; A. Sakakibara; T. Suzuki *Chem. Rev.* **1995**, *95*, 1409.
- (2) M. Y. Lo; C. Zhen; M. Lauters; G. E. Jabbour; A. Sellinger *J. Am. Chem. Soc.* **2007**, *129*, 5808.
- (3) M.-Y. Lo; K. Ueno; H. Tanabe; A. Sellinger *Chem. Rec.* **2006**, *6*, 157-168.
- (4) G. H. Mehl; I. M. Saez *Appl. Organometal. Chem.* **1999**, *13*, 261.
- (5) M.-C. Gravel, C. Z., M. Dinderman, R. M. Laine *Appl. Organometal. Chem.* **1999**, *13*, 329.
- (6) K.-M. Kim; Y. Chujo *J. Polym. Sci. A. Polym. Chem.* **2001**, *39*, 4035.
- (7) I. M. Saez; J. W. Goodby *J. Mater. Chem.* **2001**, *11*, 2845.
- (8) M. Fujiwara; K. Shiokawa; N. Kawasaki; Y. Tanaka *Adv. Funct. Mater.* **2003**, *13*, 371.
- (9) R. Signorini; R. Bozio; M. Prato In *Fullerenes: From Synthesis to Optoelectronic Properties*; D. M. Guldi, Martin, N., Eds.; Kluwer Academic Publishers: Netherlands, 2002, p 395.
- (10) R. C. Hollins *Curr. Opin. Sol. State Mater. Sci.* **1999**, *4*, 189.
- (11) D. M. Guldi; M. Prato *Acc. Chem. Res.* **2000**, *33*, 695.
- (12) Tutt, L.; Kost, A. *Nature* **1992**, *356*, 225.
- (13) W. Herbst; Hunger, K. *Industrial Organic Pigments: Production Properties, Applications*; 2nd Edn. ed.; Wiley-VCH: Weinheim, 1997.
- (14) G. Geissler; Remy, H.; Hoechst AG: DE, 1959.
- (15) C. D. Dimitrakopoulos; P. R. L. Malenfant *Adv. Mater.* **2002**, *14*, 99.
- (16) C. W. Struijk; A. B. Sieval; J. E. J. Dakhorst; M. van Dijk; P. Kimkes; R. B. M. Koehorst; H. Donker; T. J. Schaafsma; S. J. Picken; A. M. van de Craats; J. M. Warman; H. Zuilhof; E. J. R. Sudholter *J. Am. Chem. Soc.* **2000**, *122*, 11057.
- (17) K. Kalyanasundaram; J. K. Thomas *J. Am. Chem. Soc.* **1977**, *99*, 2039.
- (18) V. de Halleux; W. Mamdouh; S. De Feyter; F. De Schryver; J. Levin; Y. H. Geerts *J. Photochem. Photobiol. A: Chem.* **2006**, *178*, 251.
- (19) A. Tsuda; S. Sakamoto; K. Yamaguchi; T. Aida *J. Am. Chem. Soc.* **2003**, *125*, 15722.
- (20) K. Li; D. I. Schuster; D. M. Guldi; M. A. Herranz; L. Echegoyen *J. Am. Chem. Soc.* **2004**, *126*, 3388.
- (21) A. J. Myles; N. R. Branda *J. Am. Chem. Soc.* **2001**, *123*, 177.
- (22) T. D. Lash; P. Chandrasekar *J. Am. Chem. Soc.* **1996**, *118*, 8767.
- (23) T. Hasobe; P. V. Kamat; V. Troiani; N. Solladie; T. K. Ahn; S. K. Kim; D. Kim; A. Kongkanand; S. Kuwabata; S. Fukuzumi *J. Phys. Chem. B* **2005**, *109*, 19.
- (24) J. R. Darwent, P. D., A. Harriman, G. Porter, M.-C. Richoux *Coordination Chemistry Reviews* **1982**, *44*, 833.
- (25) S. Funyu; T. Isobe; S. Takagi; D. A. Tryk; H. Inoue *J. Am. Chem. Soc.* **2003**, *125*, 5734.
- (26) D. Sun; F. S. Tham; C. A. Reed; L. Chaker; M. Burgess; P. D. W. Boyd *J. Am. Chem. Soc.* **2000**, *122*, 10704.
- (27) F. T. Tat; Z. Zhou; S. Macmahon; F. Song; A. L. Rheingold; L. Echegoyen; D. I. Schuster; S. R. Wilson *J. Org. Chem.* **2004**, *69*, 4602.

- (28) P. A. Liddell; G. Kodis; A. L. Moore; T. A. Moore; D. Gust *J. Am. Chem. Soc.* **2002**, *124*, 7668.
- (29) R. H. Baney; X. Cao *Silicon-Containing Polymers*, 2000.
- (30) R. K. Harris; J. D. Kennedy; W. McFarlane In *NMR and the Periodic Table*; R. K. Harris, B. E. Mann, Eds.; Academic Press Inc.: London, 1978.
- (31) M. G. Voronkov; Larentyev, V. I. *Topics of Current Chemistry* **1982**, *102*, 199-236.
- (32) Scott, D. W. *J. Am. Chem. Soc.* **1946**, *68*, 356.
- (33) A. J. Barry; Daudt, W. H.; Domicone, J. J.; Gilkey, J. W. *J. Am. Chem. Soc.* **1964**, *86*, 1120.
- (34) P. P. Pescarmona; T. Maschmeyer *Aust. J. Chem.* **2001**, *54*, 583.
- (35) J. F. Brown; L. H. Vogt *J. Am. Chem. Soc.* **1965**, *87*, 4313.
- (36) Sprung, M. M.; Guenther, F. O. *J. Am. Chem. Soc.* **1965**, *87*, 3990.
- (37) Sprung, M. M.; Gunther, F. O. *J. Am. Chem. Soc.* **1965**, *87*, 3996.
- (38) Harrison, P. G. *Journal of Organometallic Chemistry* **1997**, *542*, 141 - 183.
- (39) Brown, J. F.; Vogt, L. H. *J. Am. Chem. Soc.* **1965**, *87*, 4313.
- (40) Kudo, T.; Gordon, M. S. *J. Am. Chem. Soc.* **2000**, *104*, 4058.
- (41) Kudo, T.; Gordon, M. S. *J. Am. Chem. Soc.* **1998**, *120*, 11432.
- (42) F. J. Feher; D. A. Newman; J. F. Walzer *J. Am. Chem. Soc.* **1989**, *111*, 1741.
- (43) F. J. Feher; T. A. Budzichowski; R. L. Blanski; K. J. Weller; J. W. Ziller *Organomet.* **1991**, *10*, 2526.
- (44) Frye, C. L.; Collins, W. T. *J. Am. Chem. Soc.* **1970**, *92*, 5586.
- (45) Agaskar, P. A. *Inorganic Chemistry* **1991**, *30*, 2707-2708.
- (46) Crivello, J. V.; Malik, R. *Journal of Polymer Science: Part A: Polymer Chemistry* **1997**, *35*, 407.
- (47) Bassindale, A. R.; Gentle, T. E. *J. Mater. Chem.* **1993**, *3*, 1319.
- (48) P. A. Agaskar; W. G. Klemperer *Inorg. Chim. Acta* **1995**, *229*, 355.
- (49) T. N. Martynova; V. P. Korchkov; P. P. Semyannikov *J. Organomet. Chem.* **1983**, *258*, 277-282.
- (50) Olsson, K.; Gronwall, C. *Arkiv. Kemi.* **1961**, *17*, 529.
- (51) F. J. Feher; T. A. Budzichowski *J. Organomet. Chem.* **1989**, *373*, 153.
- (52) Vogt, L. H.; Brown, J. F. *Inorganic Chemistry* **1962**, *2*, 189.
- (53) J. F. Brown; L. H. Vogt; P. I. Prescott *J. Am. Chem. Soc.* **1964**, *86*, 1120.
- (54) R. Tacke; A. Lopez-Mras; W. S. Sheldrick; A. Sebald *Z. Anorg. Allg. Chem.* **1993**, *619*, 346.
- (55) Muller, R.; Kohne, R.; Sliwinski, S. *J. Prakt. Chem* **1959**, *9*, 71.
- (56) Hoebbel, D.; Wicker, W. *Anorg. Allg. Chem* **1971**, *384*, 83.
- (57) Smolin, I. Y. *Sov. Phys. Crystallogr.* **1970**, *23*.
- (58) Moran, M.; Casdo, C.; Guadrado, I. *Organometallics* **1993**, *12*, 4327.
- (59) Hasegawa, I.; Sakka, S.; Sugahara, Y.; Kuroda, K.; Kato, C. *Chem. Comm.* **1989**, 208.
- (60) M. Z. Asuncion; I. Hasegawa; J. W. Kampf; Laine, R. M. *Journal of Materials Chemistry* **2005**, *15*, 2114.
- (61) I. Hasegawa; K. Ino; H. Ohnishi *Appl. Organomet. Chem.* **2003**, *17*, 287.
- (62) A. R. Bassindale; Z. Liu; I. A. MacKinnon; P. G. Taylor; Y. Yang; M. E. Light; P. N. Horton; M. B. Hursthouse *J. Chem. Soc., Dalton Trans.* **2003**, 2945.

- (63) A. R. Bassindale; H. Chen; Z. Liu; I. A. MacKinnon; D. J. Parker; P. G. Taylor; Y. Yang; M. E. Light; P. N. Horton; M. B. Hursthouse *J. Organomet. Chem.* **2004**, 689, 3287.
- (64) A. R. Bassindale; M. Pourny; P. G. Taylor; M. B. Hursthouse; M. E. Light *Angew. Chem. Int. Ed.* **2003**, 42, 3487.
- (65) N. Winkhofer; H. W. Roeski; M. Noltemeyer; W. T. Robinson *Angew. Chem. Int. Ed.* **1992**, 31, 599.
- (66) T. Takiguchi *J. Am. Chem. Soc.* **1959**, 81, 2359.
- (67) H. Ishida; J. L. Koenig *J. Polym. Sci., Polym. Phys. Ed.* **1979**, 17, 1807.
- (68) P. P. Pescarmona; J. C. van der Waal; T. Maschmeyer *Eur. J. Inorg. Chem.* **2004**, 5, 978.
- (69) Paolo P. Pescarmona, J. C. v. d. W., Thomas Maschmeyer *Eur. J. Inorg. Chem.* **2004**, 5, 978.
- (70) Feher, F. J.; Terroba, R.; Ziller, J. W. *Chem. Comm.* **1999**, 2309.
- (71) F. J. Feher; D. Soulivong; F. Nguyen *Chem. Comm.* **1998**, 1279.
- (72) Feher, F. J.; Nguyen, F.; Souvilong, D.; Ziller, J. W. *Chem. Comm.* **1999**, 1705.
- (73) F. J. Feher; D. Soulivong; A. G. Eklund *Chem. Comm.* **1998**, 399.
- (74) Feher, F. J.; Souvilong, D.; Nguyen, F. *Chem. Comm.* **1998**, 1279.
- (75) B. Marciniak *Silicon Chem.* **2002**, 1, 155-172.
- (76) J. W. Ryan; J. L. Speier *J. Am. Chem. Soc.* **1964**, 86, 895.
- (77) B. D. Karstedt 1974.
- (78) I. Ojima In *The Chemistry of Organic Silicon Compounds*; S. Patai, Z. R., Ed.; John Wiley & Sons Ltd: 1989, p 1479-1526.
- (79) A. J. Chalk; Harrod, J. F. *J. Am. Chem. Soc.* **1965**, 87, 16.
- (80) Lewis, L. N.; Lewis, N. J. *J. Am. Chem. Soc.* **1986**, 108, 7228.
- (81) Lewis, L. N.; Uriarte, R. J. *Organometallics* **1990**, 9, 621.
- (82) Lewis, L. N.; Uriarte, R. J.; Lewis, N. J. *J. Mol. Cat.* **1991**, 66, 105.
- (83) J. Stein; L. N. Lewis; Y. Gao; Scott, R. A. *J. Am. Chem. Soc.* **1999**, 121, 3693-3703.
- (84) L. N. Lewis *J. Am. Chem. Soc.* **1990**, 112, 5998.
- (85) Lewis, L. N.; Lewis, N. J. *Chem. Mater.* **1989**, 1, 106.
- (86) D. Herren; H. Burgy; G. Calzaferri *Helv. Chim. Acta* **1991**, 74, 24.
- (87) N. Sabourault; G. Mignani; A. Wagner; C. Mioskowski *Org. Lett.* **2002**, 4, 2117.
- (88) T. E. Gentle; A. R. Bassindale *J. Inorg. Organomet. Polym.* **1995**, 5, 281.
- (89) C. Bolln; A. Tsuchida; H. Frey; R. Mulhaupt *Chem. Mater.* **1997**, 9, 1475.
- (90) M. Morh; C. M. Casado; I. Cuadrado; J. Losada *Organomet.* **1993**, 12, 4327.
- (91) J. Huang; C. He; X. Liu; Y. Xiao; K. Yi Mya; J. Chai *Langmuir* **2004**, 20, 5145.
- (92) E. Markovic; M. Ginic-Markovic; S. Clarke; J. Matisons; M. Hussain; G. Simon *Macro.* **2007**, 40, 2694.
- (93) A. Provatas; M. Luft; J. C. Mu; A. H. White; J. G. Matisons; B. W. Skelton *J. Organomet. Chem.* **1998**, 565, 159.
- (94) C. Zhang; R. M. Laine *J. Am. Chem. Soc.* **2000**, 122, 6979.

- (95) D. Neumann; M. Fisher; L. Tran; J. G. Matison *J. Am. Chem. Soc.* **2002**, *124*, 13998.
- (96) A. Sellinger; R. M. Laine *Chem. Mater.* **1996**, *8*, 1592.
- (97) J. Choi; A. F. Yee; R. M. Laine *Macro.* **2003**, *36*, 5666.
- (98) C. Zhang; R. M. Laine *J. Organomet. Chem.* **1996**, *521*, 199.
- (99) J. Huang; Y. Xiao; K. Yi Mya; X. Liu; C. He; J. Daib; Y. Ping Siow *J. Mater. Chem.* **2004**, *14*, 2858.
- (100) R. Tamaki; J. Choi; R. M. Laine *Chem. Mater.* **2003**, *15*, 793.
- (101) T. N. Martynova; T. I. Chupakbina *J. Organomet. Chem.* **1988**, *345*, 10.
- (102) G. Calzaferri; C. Marcolli; R. Imhof; K. W. Tornroos *J. Chem. Soc., Dalton Trans.* **1996**, 3313.
- (103) C. Marcolli; G. Calzaferri; R. Imhof *Microchim. Acta* **1997**, *14*, 493.
- (104) G. Calzaferri; D. Herren; R. Imhof *Helv. Chim. Acta* **1991**, *74*, 1278.
- (105) G. Calzaferri; R. Imhof *J. Chem. Soc., Dalton Trans.* **1992**, 3391.
- (106) A. Tsuchida; C. Bolln; F. G. Sernetz; H. Frey; R. Mulhaupt *Macro.* **1997**, *30*, 2818.
- (107) R. Knischka; F. Dietsche; R. Hanselmann; H. Frey; R. Mulhaupt *Langmuir* **1999**, *15*, 4752.
- (108) F. J. Feher *J. Am. Chem. Soc.* **1986**, *108*, 3850.
- (109) F. J. Feher; R. L. Budzichowski; K. K. Weller *J. Am. Chem. Soc.* **1989**, *111*, 7288.
- (110) F. J. Feher; K. J. Weller *Organomet.* **1990**, *9*, 2638.
- (111) F. J. Feher; K. Weller *Inorg. Chem.* **1991**, *30*, 880.
- (112) E. G. Shockey; A. G. Bolf; P. F. Jones; J. J. Schwab; K. P. Chaffee; T. S. Haddad; J. D. Lichtenhan *Appl. Organomet. Chem.* **1999**, *13*, 311.
- (113) C.-M. Leu; G. M. Reddy; K.-H. Wei; C.-F. Shu *Chem. Mater.* **2003**, *15*, 2261.
- (114) C. M. Leu; Y. T. Chang; K. H. Wei *Macro.* **2003**, *36*, 9122.
- (115) J. Carsten, K. A. 2003.
- (116) B. J. Hendan; H. C. Marsmann *Appl. Organomet. Chem.* **1999**, *13*, 287.
- (117) T. S. Haddad; J. D. Lichtenhan *Macro.* **1996**, *29*, 7302.
- (118) J. D. Lichtenhan; Y. A. Otonari; M. J. Cam *Macro.* **1995**, *28*, 8435.
- (119) K.-M. Kim; Y. Chujo *J. Mater. Chem.* **2003**, *13*, 1384.
- (120) F. J. Feher; Kevin D. Wyndham *Chem. Comm.* **1998**, 323.
- (121) G. Schmid; R. Pugin; J.-O. Malm; J.-O. Bovin *Eur. J. Inorg. Chem.* **1998**, *1998*, 813.
- (122) F. J. Feher; K. J. Weller; J. J. Schwab *Organomet.* **1995**, *14*, 2009.
- (123) R. Hany; R. Hartmann; C. Bohlen; S. Brandenberger; J. Kawada; C. Lowe; M. Zinn; B. Witholt; R. H. Marchessault *Polymer* **2005**, *46*, 5025.
- (124) F. J. Feher; T. A. Budzichowski; K. Rahimian; J. W. Ziller *J. Am. Chem. Soc.* **1992**, *114*, 3859.
- (125) H. C. L. Abbenhuis; R. A. van Santen; A. D. Burrows; M. T. Palmer; H. Kooijman; M. Lutz; A. L. Spek *Chem. Comm.* **1998**, 2627.
- (126) K. Wada; M. Bundo; D. Nakabayashi; N. Itayama; T. Kondo; T. Mitsudo *Chem. Lett.* **2000**, 628.
- (127) K. Wada; D. Izuhara; M. Shiotsuki; T. Kondo; T. Mitsudo *Chem. Lett.* **2001**, *30*, 734.

- (128) P. L. Arnold; A. J. Blake; S. N. Hall; B. D. Ward; C. Wilson *J. Chem. Soc., Dalton Trans.* **2001**, 488.
- (129) F. J. Feher; D. A. Newman *J. Am. Chem. Soc.* **1990**, *112*, 1931-1936.
- (130) V. Lorenz; M. Spoida; A. Fischer; F. T. Edelmann *J. Organomet. Chem.* **2001**, *625*, 1-6.
- (131) K. Wada; D. Izuhara; K. Yamada; M. Shiotsuki; T. Kondo; T. Mitsudo *Chem. Comm.* **2001**, 1802.
- (132) R. Duchateau; T. W. Dijkstra; R. A. van Santen; G. P. A. Yap *Chem. Eur. J.* **2004**, *10*, 3979.
- (133) F. J. Feher; T. A. Budzichowski *Polyhedron* **1995**, *14*, 3239.
- (134) V. Lorenz; A. Fischer; S. Gießmann; J. W. Gilje; Y. Gunko; K. Jacob; F. T. Edelmann *Coord. Chem. Rev.* **2000**, *206-207*, 321.
- (135) J. Annand; H. C. Aspinall; A. Steiner *Inorg. Chem.* **1999**, *38*, 3941.
- (136) N. Maxim; A. Overweg; P. J. Kooyman; J. H. M. C. van Wolput; R. W. J. M. Hanssen; R. A. van Santen; H. C. L. Abbenhuis *J. Phys. Chem. B* **2002**, *106*, 2203.
- (137) V. Lorenz; A. Fischer; F. T. Edelmann *Inorg. Chem. Comm.* **2000**, *3*, 292.
- (138) P. Smet; J. Riondato; T. Pauwels; L. Moens; L. Verdonck *Inorg. Chem. Comm.* **2000**, *3*, 557.
- (139) K. Wada; N. Watanabe; K. Yamada; T. Kondo; T. Mitsudo *Chem. Comm.* **2005**, *1*, 95.
- (140) Edelmann, F. T.; Gießmann, S.; Fischer, A. *Journal of Organometallic Chemistry* **2001**, *620*, 80-89.
- (141) G. Gerritsen; R. Duchateau; R. A. van Santen; G. P. A. Yap *Organometal.* **2003**, *22*, 100-110.
- (142) P. A. Shapley; W. S. Bigham; M. T. Hay *Inorg. Chim. Acta* **2003**, *345*, 255.
- (143) Volker Lorenz, A. F. F. T. E. *Zeitschrift für anorganische und allgemeine Chemie* **2000**, *626*, 1728-1730.
- (144) M.D. Skowronska-Ptasinska; R. Duchateau ; R. A van Santen; G. P. A Yap *Eur. J. Inorg. Chem.* **2001**, *2001*, 133.
- (145) Edelmann, F. T.; Gun'ko, Y. K.; Giessmann, S.; Olbrich, F.; Jacob, K. *Inorg. Chem.* **1999**, *38*, 210-211.
- (146) N. Mintcheva; M. Tanabe; K. Osakada *Organomet.* **2006**, *25*, 3776.
- (147) V. W. Day, W. G. K., V. V. Mainz,; Millar, D. M. *J. Am. Chem. Soc.* **1985**, *107*, 8262-8264.
- (148) R. Tamaki; Y. Tanaka; M. Z. Asuncion; J. Choi; R. M. Laine *J. Am. Chem. Soc.* **2001**, *123*, 12416.
- (149) C. H. Chou; S. L. Hsu; K. Dinakaran; M. Y. Chiu; K. H. Wei *Macro.* **2005**, *38*, 745.
- (150) C. M. Brick; Y. Ouchi; Y. Chujo; R. M. Laine *Macro.* **2005**, *38*, 4661.
- (151) C.M. Leu; Y. T. Chang; K. H. Wei *Macromolecules* **2003**, *36*, 9122-9127.
- (152) J. Huang; C. He; Y. Xiao; K. Yi Mya; J. Dai; Y. Ping Siow *Polymer* **2003**, *44*, 4491.
- (153) E. A. Drylie; C. D. Andrews; M. A. Hearshaw; C. Jimenez-Rodriguez; A. Slawin; D. J. Cole-Hamilton; R. E. Morris *Polyhedron* **2006**, *25*, 853.
- (154) Lucke, S.; Stopekk-Langer, K. *Applied Surface Science* **1999**, *144-145*, 713-715.

- (155) M. Bent; Y. Gun'ko *J. Organomet. Chem.* **2005**, 690, 463.
- (156) U. Dittmar; B. J. Hendan; U. Florke; C. Heinrich; C. Marsmann *Journal of Organometallic Chemistry* **1995**, 489, 185-194.
- (157) A. Sellinger; R. Tamaki; R. M. Laine; K. Ueno; H. Tanabe; E. Williams; G. E. Jabbour *Chem. Comm.* **2005**, 3700.
- (158) K. Itami; Y. Ohashi; J. I. Yoshida *J. Org. Chem.* **2005**, 70, 2778.
- (159) K. Itami; Y. Ushioji; T. Nokami; Y. Ohashi; J. Yoshida *Org. Lett.* **2004**, 6, 3695.
- (160) E. O. Dare, G. A. O., D. S. Ogunniyi *Polish Journal of Chemistry* **2005**, 79, 101.
- (161) Y. Itami; B. Marciniec; Kubicki, M. *Chem. Eur. J.* **2004**, 10, 1239-1248.
- (162) M. Chiacchio; L. Borrello; G. Di Pasquale; A. Pollicino; F. A. Bottino; A. Rescifina *Tetrahedron* **2005**, 61, 7986.
- (163) M. Bent; Y. Gun'ko *J. Organomet. Chem.* **2005**, 690, 463.
- (164) C. Zhang; F. Babonneau; C. Bonhomme; R. M. Laine; C. L. Soles; H. A. Hristov; A. F. Yee *J. Am. Chem. Soc.* **1998**, 120, 8380.
- (165) R. O. R. Costa; W. L. Vasconcelos; R. Tamaki; R. M. Laine *Macro.* **2001**, 5398.
- (166) J. D. Lichtenhan; N. Q. Vu; J. A. Carter *Macro.* **1993**, 26, 2141.
- (167) F. Gao; B. M. Culbertson; Y. Tong; S. R. Schricker *Polym. Prepr.* **2001**, 41, 580.
- (168) A. Romo-Uribe; P. T. Mather; T. S. Haddad; J. D. Lichtenhan *J. Polym. Sci. B. Polym. Phys.* **1998**, 36, 1857.
- (169) A. Lee; J. D. Lichtenhan *Macro.* **1998**, 31, 4970.
- (170) R. K. Bharadwaj; R. J. Berry; B. L. Farmer *Polymer* **2000**, 41, 7209.
- (171) P. T. Mather; H. G. Jeon; A. Romo-Uribe; T. S. Haddad; J. D. Lichtenhan *Macro.* **1999**, 31, 1194.
- (172) B. X. Fu; B. S. Hsiao; H. White; M. Rafailovich; P. T. Mather; H. G. Jeon; S. Phillips; J. Lichtenhan; J. Schwab *Polym. Int.* **2000**, 49, 437.
- (173) J. Choi; J. Harcup; A. F. Yee; Q. Zhu; R. M. Laine *J. Am. Chem. Soc.* **2001**, 123, 11420.
- (174) R. M. Laine; J. Choi; I. Lee *Adv. Mater.* **2001**, 13, 800.

2 POSS BOUND FULLERENES

2.1 Outline

This chapter is divided into two sections, with the first reviewing functionalised fullerene literature, focusing on the properties of C₆₀ and its derivatives and the optical limiting mechanism of fullerenes in both solution and the solid state. The second section of this chapter discusses the three synthetic pathways employed and characterisation of the resultant POSS bound fullerenes. Full experimental conditions, general characterisation techniques used and sample data are detailed in **Chapter 6**.

2.2 Fullerenes

In 1985 Smalley, Curl and Kroto¹ discovered that elemental carbon could exist as highly stable spheres, later termed fullerenes. The most abundant of the fullerenes is buckminsterfullerene, commonly referred to as C₆₀. It was not until 1990 that macroscopic quantities of C₆₀ were produced through the extraction of condensed soot, produced from evaporated graphite.²

The spherical shape of the unsaturated carbon network present in C₆₀ causes the carbon atoms to be pyramidalised, introducing a large amount of strain energy, thus fullerenes are thermodynamically less stable than diamond and graphite. The deviation from planarity, introduced by rehybridisation from the sp² σ and π orbitals, as pure p character of π orbitals is possible only in strictly planar situations, caused double bond localisation, in contrast to benzene, and for the carbon-carbon double and single bonds to be unequal in length. The C₆₀ surface contains 20 hexagons and 12 pentagons, with all rings fused and all double bonds conjugated. Common nomenclature refers to the carbon-carbon bonds within C₆₀ by the nature of the rings that the two carbon atoms of the bond are associated with. Subsequently, bonds at the junctions of two hexagons are commonly referred to as [6,6] bonds and bonds at the junction of a pentagon and a hexagon are referred to as [5,6] bonds, with [6,6] bonds being shorter than [5,6] bonds.³

Topologically, C_{60} has a localised structure where each hexagon resembles a cyclohexatriene unit and each pentagon displays a [5]-radialene character (**Figure 2.1**).³ C_{60} possesses a polyenic-type structure, with all the double bonds occurring within the six-membered rings.⁴

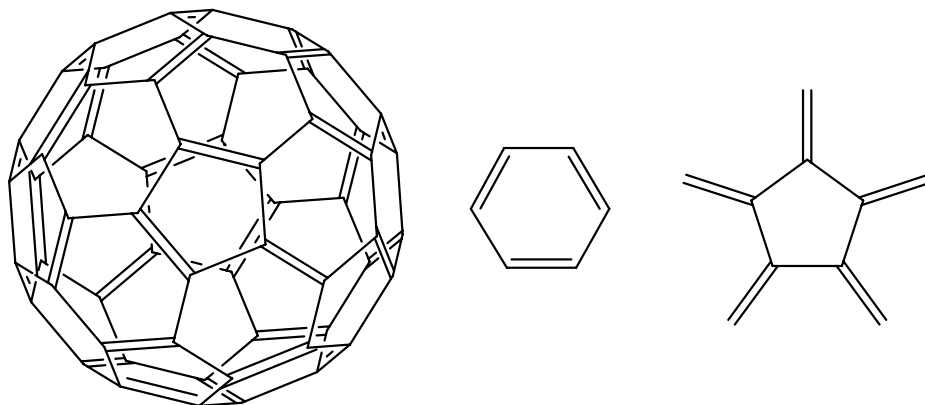


Figure 2.1. C_{60} , cyclohexatriene and radialene subunits of C_{60} ³

The electron-deficient character of C_{60} stems from its low-lying Lowest Unoccupied Molecular Orbital (LUMO), causing all cage embedded olefins, i.e. [6,6]-ring junctions, to act as strong electrophiles.^{5,6} The strain in the carbon-carbon bonds also provides a driving force for their reactivity, not only as 2π electron partners in cycloaddition reactions, but also as electrophiles susceptible to nucleophilic and free radical addition.^{7,8}

One of the major drawbacks of C_{60} is its low solubility; C_{60} is essentially insoluble in polar and/or protic solvents. The solvents of choice are aromatics, such as toluene and 1,2-dichlorobenzene, and some non-aromatics, such as carbon disulfide, however, derivitisation of C_{60} significantly improves solubility.³

2.3 Functionalisation of C_{60}

A variety of methods have been employed in the functionalisation of fullerenes, such as the addition of diazomethane, alkyl azides, α -halomalonate anions and the cycloaddition of azomethine ylides, as detailed herein.

2.3.1 Addition of Diazomethane and Alkyl Azides to C₆₀

The addition of diazomethane derivatives to C₆₀ can yield two different structures, commonly termed fulleroids and methanofullerenes (**Figure 2.2**).⁷ The first step of the reaction involved the 1,3-dipolar cycloaddition of a diazomethane to C₆₀, yielding an unstable pyrazoline derivative (**Figure 2.2**), which was isolated only in the case of diazomethane.⁹ Extrusion of nitrogen generally yielded a mixture of the [5,6] open fulleroid and the [6,6]-closed methanofullerene. The conversion of fulleroids to methanofullerenes has been achieved thermally,^{10,11} electrochemically,¹² photochemically¹³ or by acid catalysis.¹⁴

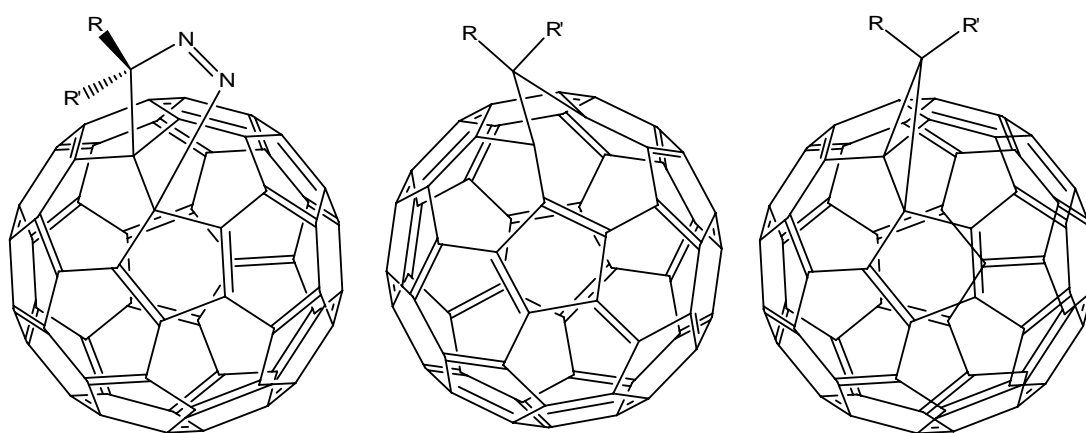


Figure 2.2. Pyrazoline, fulleroid and methanofullerene derivatives of C₆₀⁷

Iminofullerenes can be synthesised through two different synthetic routes, the first being through a direct [2+1] cycloaddition to C₆₀ of oxycarbonylnitrenes produced *in situ* by base catalysed α -elimination of O-4-nitrophenylsulfonylhydroxamic acid derivatives.¹⁵⁻¹⁷ Iminofullerenes have also been synthesised through a 1,3-dipolar cycloaddition of organic azides to C₆₀, followed by extrusion of nitrogen either thermally or photochemically.¹⁸⁻³³ Depending on the mode of addition, one of four isomers can be formed, the open [5,6], closed [5,6], open [6,6] or closed [6,6] (**Figure 2.3**). The addition of oxycarbonylnitrenes to C₆₀ yields predominantly the closed [6,6] isomer as the major product, with up to 10 % of the open [5,6] product as the minor product.³⁴

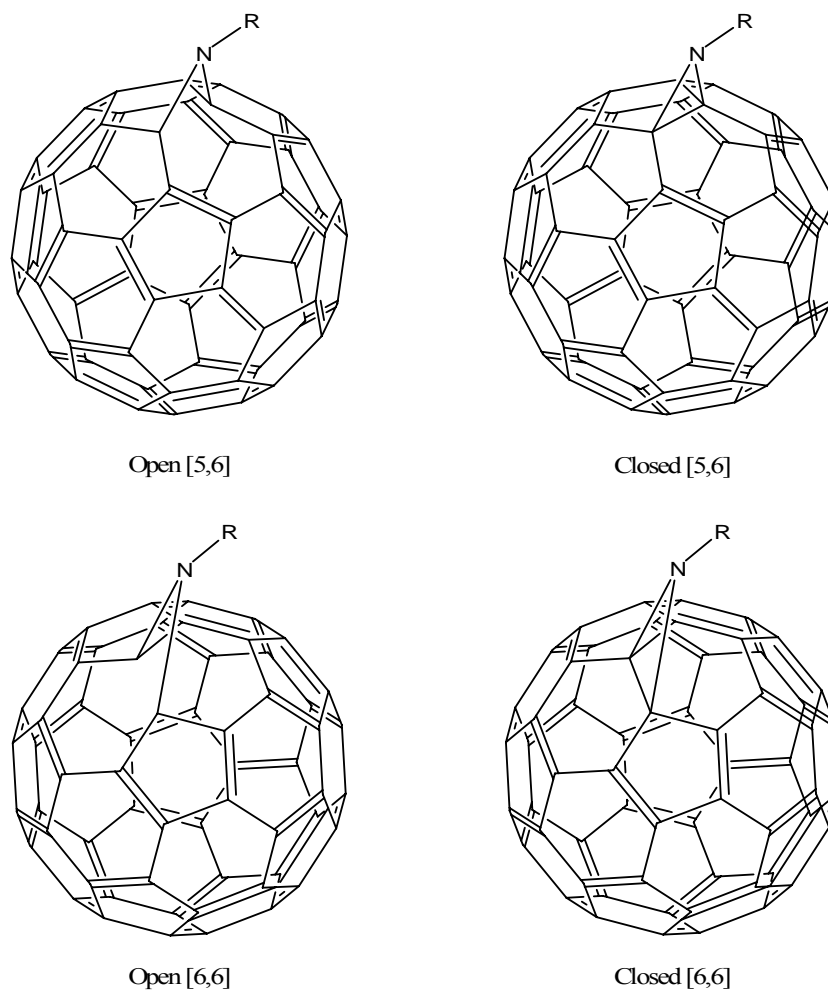


Figure 2.3. Possible isomers of iminofullerenes¹⁵⁻³⁴

Experimental results indicate that the organic azide initially attacked C_{60} at the [6,6] ring junctions, yielding a [6,6]-triazoline intermediate.^{18-33,35} This intermediate extruded N_2 upon heating, to yield the closed [5,6] iminofullerene as the major, and often exclusive, product (**Figure 2.4**).³⁴

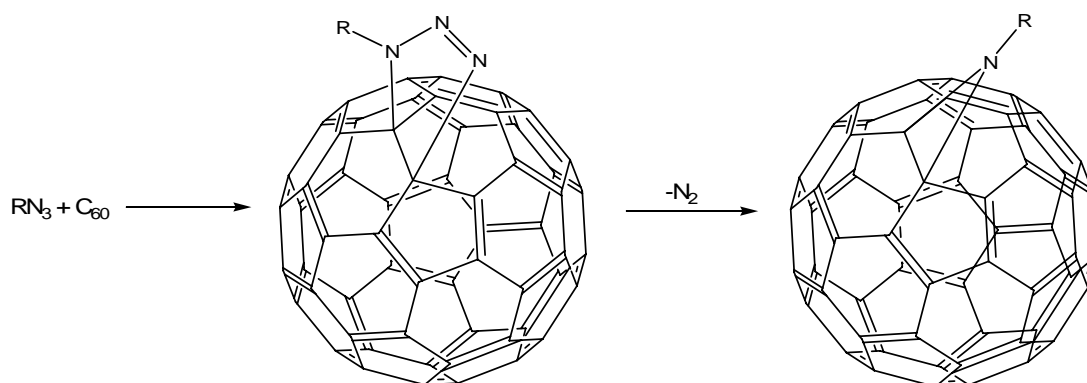


Figure 2.4. Addition of alkyl azides to C_{60} ³⁴

2.3.2 Addition of Stabilised α -Halomalonate Anions to C_{60}

The chemical reactivity of C_{60} is typical of an electron deficient olefin and C_{60} therefore reacts readily with nucleophiles. Bingel³⁶ demonstrated that the addition of stabilised α -halomalonate anions to C_{60} was followed by an intramolecular displacement of the halide by the anionic centre generated on the fullerene core to give the corresponding methanofullerenes (**Figure 2.5**).

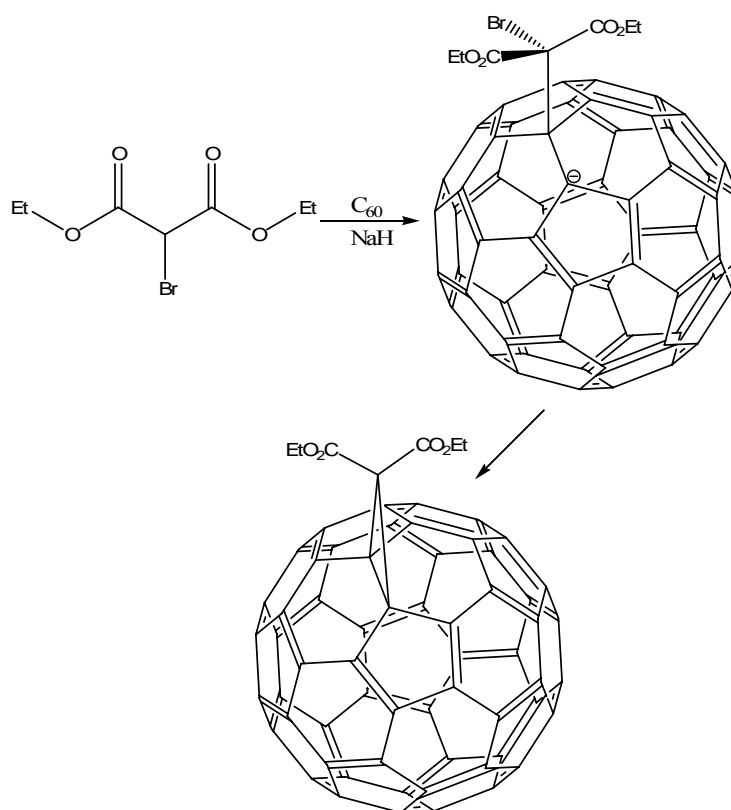


Figure 2.5. Addition of stabilised α -halomalonate anions to C_{60} ³⁶

Nucleophilic cyclopropanation of C_{60} can also be achieved through using non-halogenated malonates. The α -halomalonate was generated *in situ* and direct treatment of C_{60} with malonates in the presence of I_2 ³⁷ or CBr_4 ³⁸ and base afforded the corresponding methanofullerene (**Figure 2.6**).

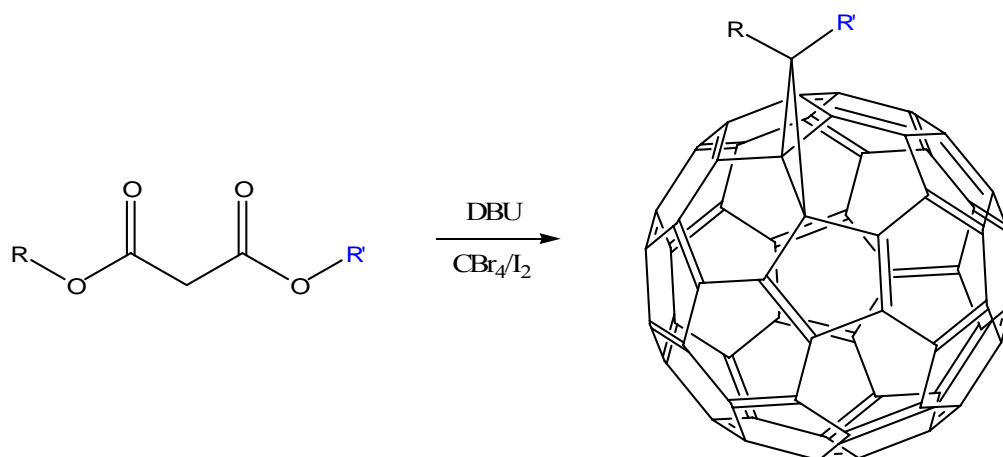


Figure 2.6. Addition of α -halomalonate to C_{60} ^{37,38}

2.3.3 Cycloaddition of Azomethine Ylides to C_{60}

Azomethine ylides are organic 1,3-dipoles possessing a carbanion next to an ammonium ion. The ylides can be generated in several ways, the easiest of which is through the decarboxylation of immonium salts generated from the condensation of α -amino acids with aldehydes or ketones. The azomethine ylide [3+2] cycloaddition, developed by Prato³⁹ is a one-pot reaction where the reactive 1,3-dipole is generated *in situ* from an aldehyde and an amino acid (**Figure 2.7**). Azomethine ylides have also been generated from the thermal ring opening of aziridines.^{39,40} Subsequent [3+2] cycloaddition of the azomethine ylide across the [6,6] double bond of C_{60} yields the desired fulleropyrrolidine. The advantages of this synthesis are that:

- mono-functionalisation affords a single regioisomer;
- the use of functionalised aldehydes yielded 2-substituted fulleropyrrolidines, whereas the use of N-functionalised amino glycines yielded N-substituted fulleropyrrolidines. The combination of these reagents allowed for concurrent introduction of two functional groups in one reaction step;
- the reaction was compatible with other functional groups, and
- when $R' \neq H$, a new stereocentre was generated at position 2 on the pyrrolidine ring.

The reaction required careful control of reagent stoichiometry and reaction conditions to minimise the formation of multiple addition compounds. This generally resulted in reaction yields lower than 50%; however the excess C₆₀ can be recycled.⁴¹

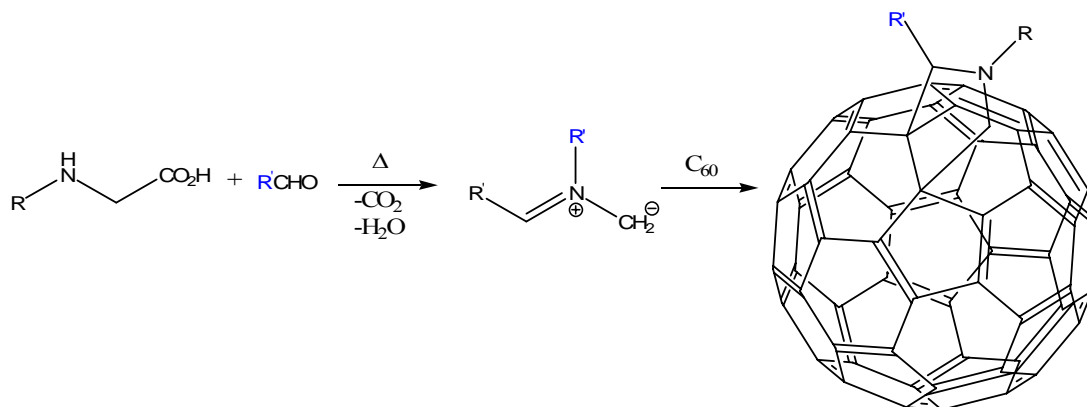


Figure 2.7. Addition of azomethine ylides to C₆₀³⁹⁻⁴¹

2.4 Optical Limiting

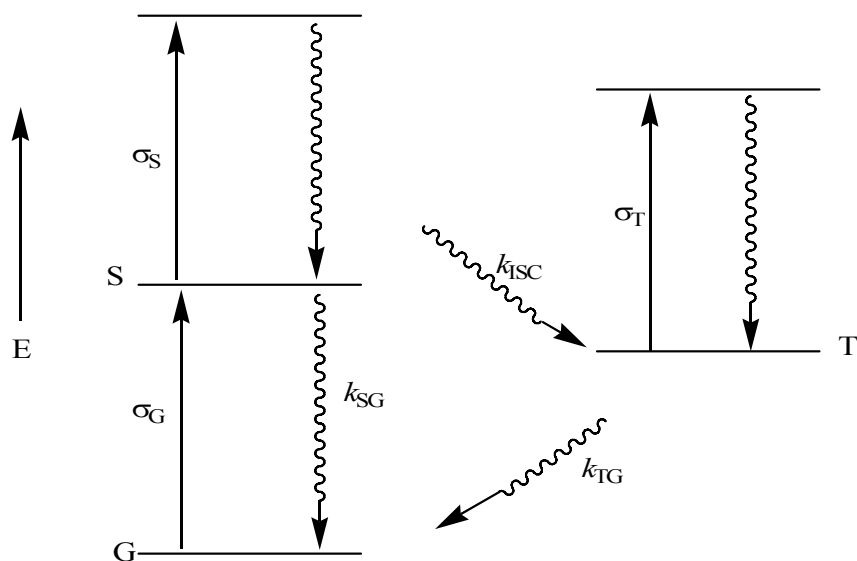
The use of lasers is prevalent in a variety of scientific, industrial, medical and military field. The emission wavelength of lasers can be tuned from the visible to the near-infrared (NIR) region and the radiation can be emitted either as continuous wave or in a pulsed mode, with pulse duration ranging from microseconds to femtoseconds. Protection of operating personnel and technical components against pulsed tunable lasers is a high priority. Eye protection is critical, as the retina is vulnerable in the visible and NIR spectral range.⁴²

An ideal optical limiter exhibits linear transmission below a certain input light fluence threshold, but above the threshold the output light fluence is fixed at a constant level. Promising optical limiting materials, also known as Reverse Saturable Absorbers (RSA), are those that exhibit strong nonlinear absorptions. The primary mechanism for nonlinear absorptive optical limiting is a large ratio of excited-state to ground-state absorption cross sections. Thus, potent RSA's are usually molecules with weak ground-state absorptions, such as metallophthalocyanines, mixed metal complexes and clusters, and fullerenes.⁴³

It is well established that C₆₀ solutions exhibit optical limiting behaviour derived from a RSA mechanism.^{42,44} C₆₀ exhibits a broad absorption spectrum, characterised by strong absorptions in the ultraviolet region and weaker absorptions that extend over the majority of the visible region.⁴⁵ These weak absorptions allow for optical pumping using a broad range of laser wavelengths. The excited state dynamics and the large quantum yield for intersystem crossing allow for population build up in either the singlet or triplet excited states, depending on the duration of the laser pulse. C₆₀ also possesses excited state absorption cross sections that are larger than those of the ground state over the complete visible section.⁴⁴ Different fullerene derivatives, such as methanofullerenes and fulleropyrrolidines, exhibit diverse electronic properties. The ground state absorptions of such derivatives vary in the UV-Vis region, as methanofullerenes display a major absorption band at 500 nm, whilst fulleropyrrolidines display reduced absorption in this spectral region. However, the triplet-triplet absorption is stronger for methanofullerenes than fulleropyrrolidines, thus making them equally useful for optical limiting purposes.⁴⁶

Tutt and Kost⁴⁷ measured the first optical limiting performances of C₆₀ and C₇₀ in dichloromethane and toluene solutions with a nanosecond Nd:YAG laser pulse at 532 nm. This study concluded that C₆₀ possessed better optical limiting performance than the majority of known optical limiting materials available at that time. Since then many investigations have been performed on C₆₀ and its derivatives. The focus on using functionalised fullerene derivatives arose from the improved solubility of these derivatives in polar solvents. Breaking the high symmetry of the fullerene allows a new transition, at approximately 690 nm, so that the fullerene derivatives extend their absorption into the NIR.⁴⁷

The optical limiting properties of fullerenes have previously been described using a five-level RSA mechanism (**Figure 2.8**). For example, McLean *et al.*^{48,49} utilised the five-level model to correlate the observed optical limiting response of C₆₀ in room temperature toluene solution with the ground and excited state absorption cross sections of C₆₀. For limiting nanosecond pulses at 532 nm, there was near quantitative agreement between the experimental results and the five-level model for light fluences of up to ~1 Jcm⁻². This agreement strongly supported the use of the RSA mechanism to describe the optical limiting properties in fullerenes.



where k = rate constant, σ = cross section, S = singlet, T = triplet, G = ground,
 ISC = intersystem crossing

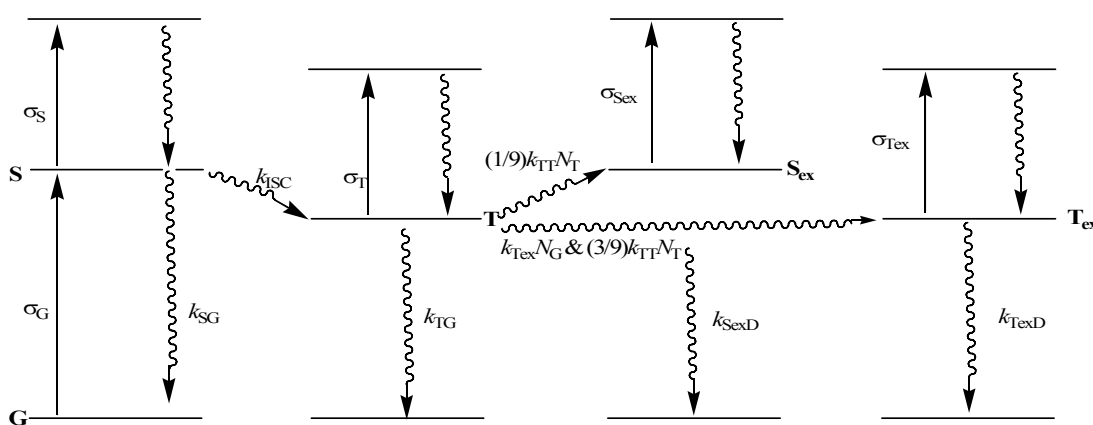
Figure 2.8. Five-level reverse saturable absorption mechanism^{48,49}

Both the excited singlet and triplet absorption cross sections have been determined to be larger than the ground state absorption cross section for C_{60} in room temperature toluene.⁴⁹ This implies that nonlinear absorption contributes to C_{60} 's observed optical limiting response. Alternative optical limiting mechanisms have been postulated for C_{60} , taking into account the fact that optical limiting responses consist of significant contributions from other nonlinear processes, such as nonlinear scattering.⁵⁰⁻⁵⁴ These mechanisms have been investigated due to inconsistencies between the RSA mechanism and the experimental optical limiting results of C_{60} and its derivatives.

Among the most significant inconsistencies is the performance of C_{60} in solid matrices, such as poly(methyl methacrylate) (PMMA),⁵⁵ and the medium viscosity dependence of a methanofullerene derivative observed by Riggs and Sun.⁴³ The optical limiting responses of C_{60} dispersed in a PMMA matrix⁵⁵ are much weaker than those displayed for C_{60} in room temperature toluene solution.⁵⁶ This difference in optical limiting performance could not be attributed to changes in the nonlinear absorptive behaviour, as the ground-state and triplet-triplet transient absorption spectra of C_{60} in PMMA polymer film were similar to those in room temperature toluene solution.⁵⁵ This implied that different mechanisms or mechanistic processes

dominated the optical limiting properties of C₆₀ in both solution and in a solid matrix. Further complications arose from the fact that the optical limiting results of C₆₀ and its derivatives in solution were strongly dependent on the fullerene solution concentration.⁴³

The RSA mechanism alone does not explain the optical limiting results of C₆₀ and mono-functionalised C₆₀ derivatives quantitatively and consistently. In order to account for the concentration dependence, a modified RSA mechanism for fullerenes in solution that includes both unimolecular and bimolecular excited state processes was proposed by Riggs and Sun⁴³ (**Figure 2.9**). The contributions of bimolecular processes were subject to a concentration threshold. The threshold represented the minimum fullerene concentration required for the bimolecular excited-state processes to be significant, with respect to optical limiting toward nanosecond laser pulses. Below this threshold, the optical limiting properties of fullerenes were dominated by the simple five-level RSA mechanism. The five-level RSA model may be considered as the unimolecular RSA model for fullerenes, with the concentration dependence accounted for through the excited triplet state bimolecular processes, including self-quenching of the fullerene excited triplet state by ground-state fullerene molecules, and triplet-triplet annihilation.



where k = rate constant, σ = cross section, S = singlet, T = triplet, G = ground, ISC = intersystem crossing, S_{ex} = singlet excimer-like state, T_{ex} = triplet excimer like state, N = number of transitions

Figure 2.9. Modified reverse saturable absorption mechanism⁴³

Fullerenes in polymer films or solid matrices also displayed significantly weaker

optical limiting responses. This was attributed to the effective impossibility of diffusional and pseudodiffusional processes on the nanosecond time scale. This absence of optical limiting contributions associated with excited triplet-state bimolecular processes was postulated to be responsible for the reduced optical limiting responses of C₆₀ and its derivatives in solid matrices, such as PMMA films.⁵⁵ The optical limiting results in polymer films are therefore usually be modelled by the simple five-level mechanism (**Figure 2.8**). Experimental data has shown that the behaviour of fullerene derivatives in PMMA films is similar to that of C₆₀ in room temperature solution below the concentration threshold. The bimolecular processes are absent for fullerenes in polymer films due to a lack of molecular diffusion.⁴³ Bimolecular processes are also absent in dilute solutions as the concentrations are too low to support meaningful bimolecular processes on the excited-state time scale.⁴³

2.5 Fulleropyrrolidines

Fullerene solutions are efficient optical limiters,⁴⁹ however the use of solid devices is preferred for practical applications. Crystalline films of C₆₀ have previously been studied, although they proved to be inefficient against pulses longer than tens of picoseconds, ascribed to fast excited state de-excitation due to interactions of neighbouring C₆₀ molecules in the solid phase. Studies have revealed that C₆₀ retained its optical limiting properties after inclusion in solid matrices, such as sol-gel glasses,⁵⁷⁻⁶² PMMA⁵⁶ and glass-polymer composites.⁶³ In sol-gel glasses, faster de-excitation dynamics and reduced triplet yields were typically observed in comparison to C₆₀ solutions. The reduction in triplet yield occurred for two main reasons; perturbation of the energy levels due to interactions with the sol-gel matrix, and reduced interactions between neighbouring fullerene spheres associated with aggregation.⁶⁴

Fullerene derivatives bearing covalently linked silicon alkoxide groups have been homogeneously dispersed in a sol-gel matrix, preventing large-scale fullerene aggregation in the final glass due to covalent bonding of the fullerene to the oxide

matrix. A wide range of fullerene derivatives bearing covalently-linked silicon alkoxide groups have been detailed in the literature, examples of which follow.^{39,40,62,65-70}

Reaction of the cyclopentadiene anion with 3-chloropropyl trimethoxysilane yielded 3-(cyclopentadienyl)alkyltriethoxysilane, which was reacted with C_{60} to yield the 3-(cyclopentadienyl)alkyltriethoxysilane fullerene derivative (**Figure 2.10**).⁶⁵ The cyclopentadiene fullerene derivative underwent cycloreversion back to C_{60} ; and therefore exhibited a short shelf-life and is unsuitable for use in sol-gel applications.⁶²

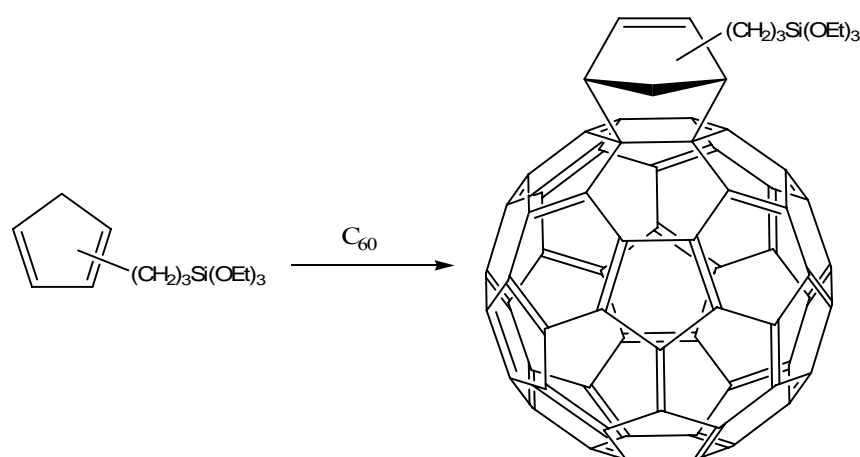


Figure 2.10. Synthesis of 3-(cyclopentadienyl)alkyltriethoxysilane fullerene^{62,65}

As discussed previously in this chapter, azomethine ylides have been generated through the thermal ring opening of aziridines.^{39,40} Thus, when N-[3-(triethoxysilyl)propyl]-2-carbonethoxy aziridine was refluxed with C_{60} on chlorobenzene, N-[3-(triethoxysilyl)propyl]-2-carbonethoxy fulleropyrrolidine was isolated (**Figure 2.11**).⁷⁰

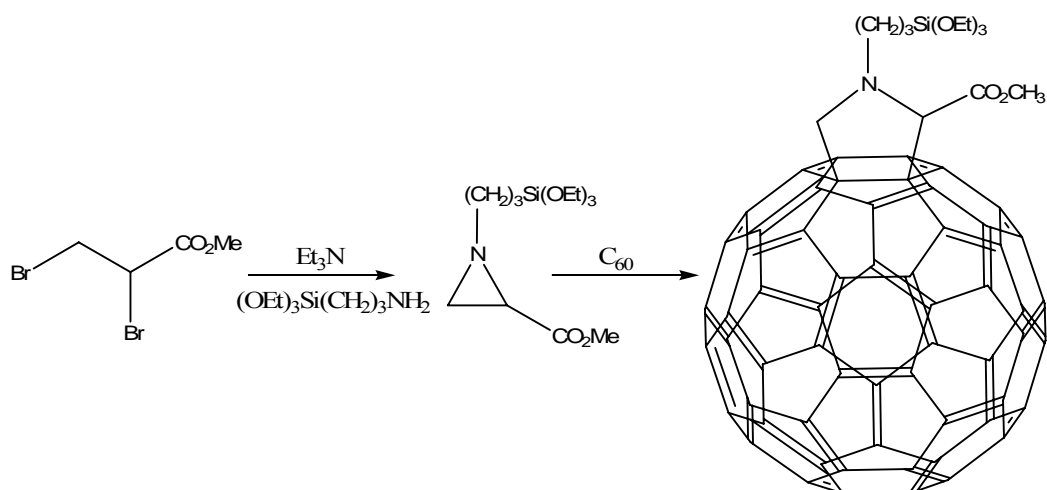


Figure 2.11. Synthesis of N-[3-(triethoxysilyl)propyl]-2-carbonethoxy fulleropyrrolidine⁷⁰

Trialkoxysilyl functionalised aldehydes or amino glycines have also been used to generate azomethine ylides *in situ*, with the trimethoxysilyl undecyl aldehyde example depicted in **Figure 2.12**.

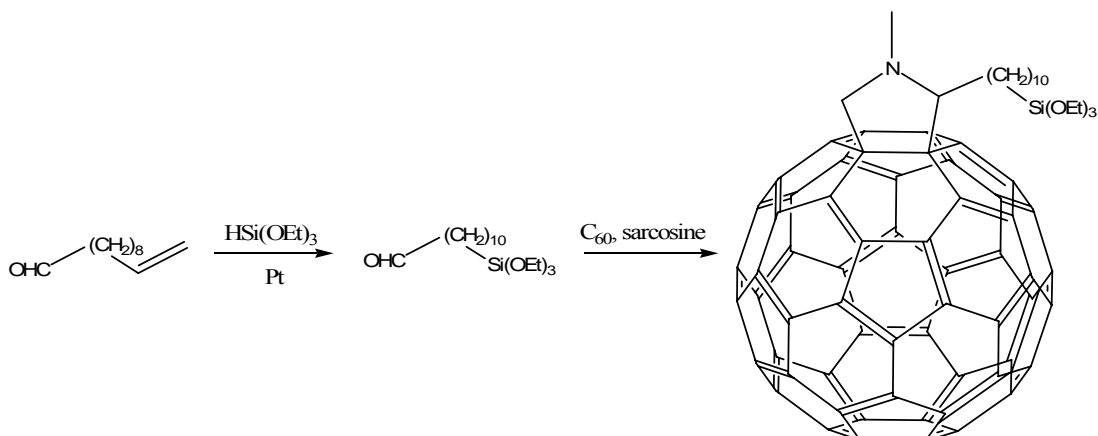


Figure 2.12. Synthesis of trimethoxysilyl undecyl fulleropyrrolidine⁶²

Synthesis of the aldehyde was complex, as hydrosilylation was able to occur at both the carbon-oxygen and carbon-carbon double bonds, leading to a polymeric product. Protection the aldehyde was possible, however the presence of the reactive alkoxy silane implied that deprotection was often problematic.⁶²

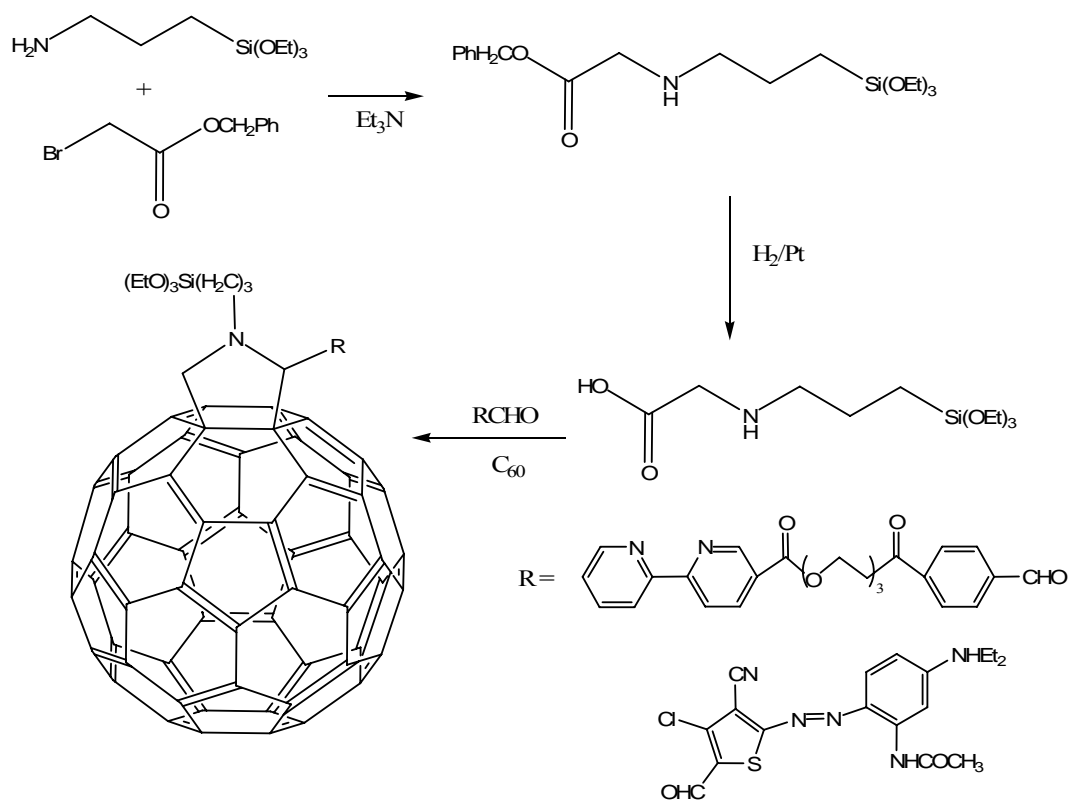


Figure 2.13. Synthesis of N-(triethoxysilyl)propyl functionalised fulleropyrrolidine^{68,69}

N-[3-(triethoxysilyl)propyl]glycine has been used to synthesise a variety of N-[3-(triethoxysilyl)propyl] fulleropyrrolidines (**Figure 2.13**).^{68,69} The glycine was synthesised via the reaction of (3-aminopropyl)triethoxysilane with benzyl bromoacetate. The benzyl protecting group was removed via platinum catalysed hydrogenation to yield the desired glycine, which was subsequently reacted with a variety of aldehydes to synthesise the desired fulleropyrrolidines.

Fulleropyrrolidines have also been synthesised bearing an N-protected aminoalkyl chain, which was then deprotected and reacted further to attach the trialkoxysilane moiety (**Figure 2.14**).⁶⁷ The N-*tert*-butoxycarbonyl (N-Boc) protected glycine was reacted with the desired aldehyde to yield an N-Boc protected fulleropyrrolidine. Deprotection of the amine was undertaken through treatment with trifluoroacetic acid (TFA), and subsequent reaction with (3-isocyanatopropyl)triethoxysilane yielded the desired fulleropyrrolidine derivative.⁶⁷

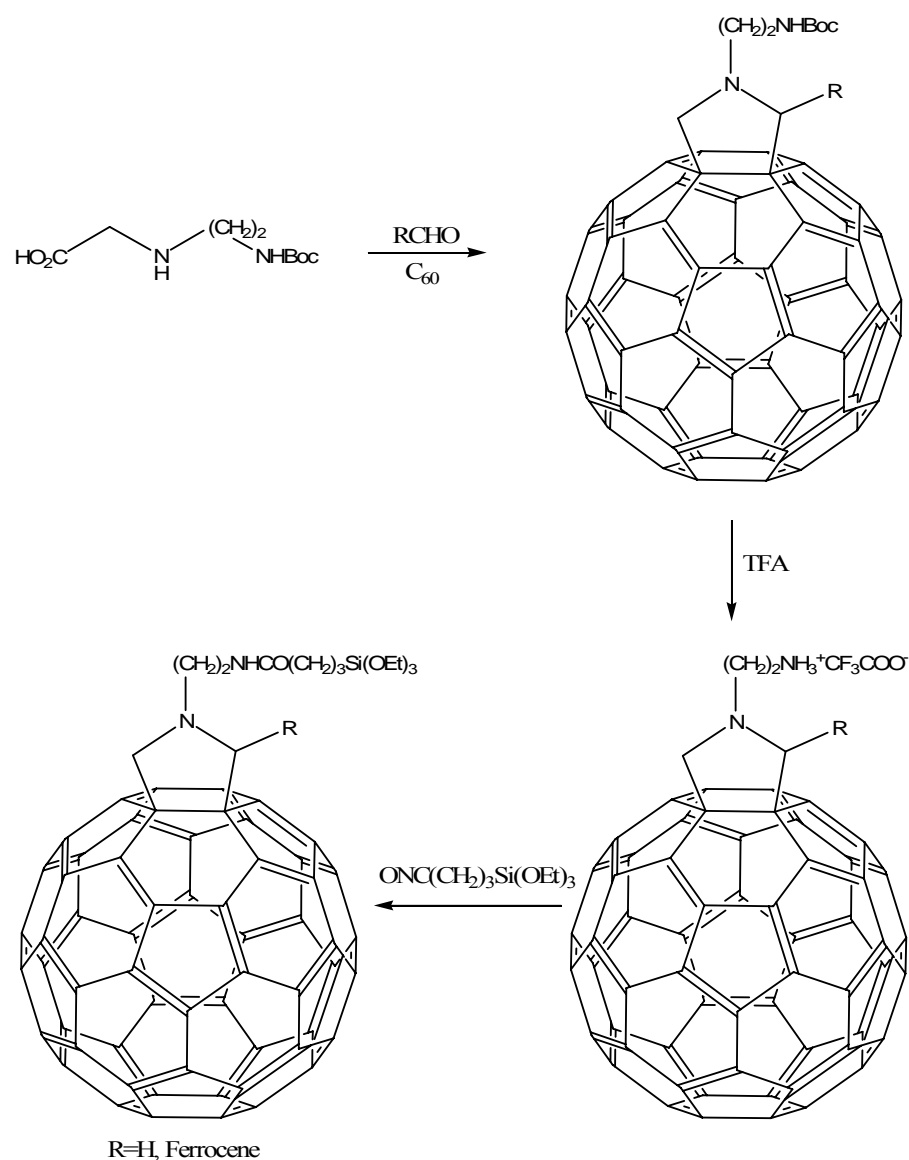


Figure 2.14. Synthesis of N-triethoxysilyl functionalised fulleropyrrolidine⁶⁷

Trialkoxysilyl functionalised methanofullerenes have been synthesised through the Bingel reaction.⁶⁶ Reaction of a *tert*-butyl protected malonate with C₆₀, deprotection of the carboxylic acid group, and subsequent reaction with 3-(isocyanato)propyl trimethoxysilane yielded the desired methanofullerene. Silica grafted fullerene was then obtained through the reaction of the trimethoxysilane methanofullerene with silica (Figure 2.15).

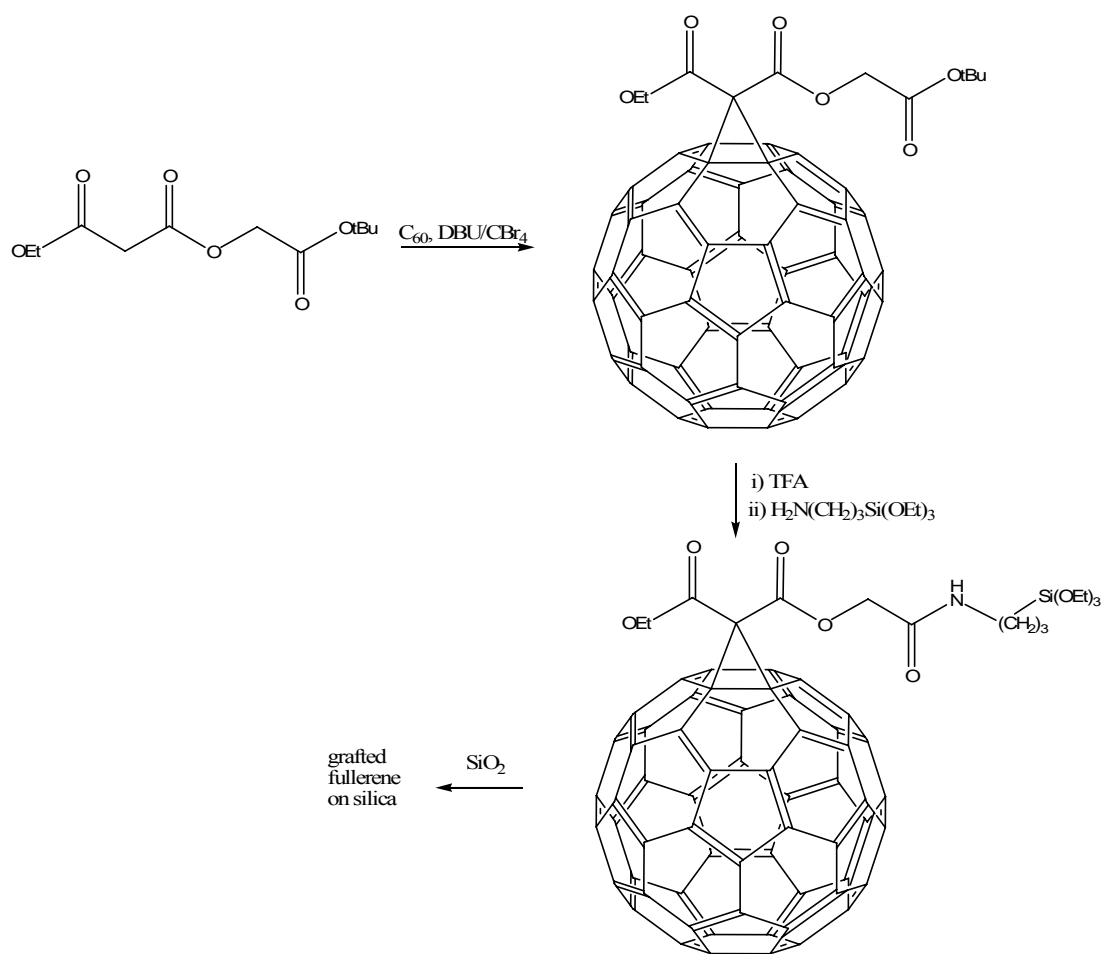


Figure 2.15. Synthesis of silica grafted methanofullerene⁶⁶

2.6 Synthesis

As discussed previously, one of the most widely accessible pathways to fullerene substitution was the Prato reaction,³⁹ i.e. the generation of azomethine ylides *in situ* from an aldehyde and an amino acid, followed by a [6,6] cycloaddition to C_{60} . The numbering scheme of the pyrrolidine moiety is depicted in **Figure 2.16**. The use of functionalised aldehydes yielded 2-substituted fulleropyrrolidines, whereas the use of N-functionalised amino glycines yielded N-substituted fulleropyrrolidines. The synthesis of mono- and octa-functionalised aldehyde functionalised POSS has previously been detailed in the literature.^{71,72} A monosubstituted aldehyde was used in the research contained within this chapter in preference to an octa-substituted aldehyde, as a large excess of aldehyde and amino acid is required to generate a

mono-fulleropyrrolidine adduct. This implied that the formation of an octa-substituted fulleropyrrolidine derivative was unlikely; with a mixed distribution of products the likely result.

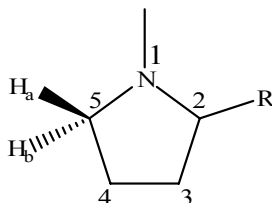


Figure 2.16. Numbering scheme of pyrrolidines

2.7 Synthetic Pathway 1

In the present work, monosubstituted POSS aldehydes have been synthesised previously by two methods, the first of which involved the hydrosilylation of a silyl dioxolane.⁷² Protection of the aldehyde functionality was required during the synthesis to prevent unwanted reaction during generation of the Grignard reagent and to prevent undesired O-silylation in the subsequent hydrosilylation reaction. Protection was achieved through the employment of the dioxolane group, which was generated through the condensation of 4-bromobenzaldehyde with ethylene glycol, to obtain 2-(4-bromophenyl)-1,3-dioxolane.⁷³ The dioxolane was reacted with magnesium to generate a Grignard reagent, which was reacted with chlorodimethylsilane to yield [2-(4-dimethylsilyl)phenyl]-1,3-dioxolane.⁷² Monovinyl POSS was synthesised by the reaction of vinyltrichlorosilane with $R_7Si_7O_9(OH)_3$ in the presence of triethylamine, where $R = iBu$ and Ph .⁷⁴ Platinum catalysed hydrosilylation was then performed with [2-(4-dimethylsilyl)phenyl]-1,3-dioxolane and monovinyl POSS in diethyl ether, to yield the desired mono-dioxolane POSS derivative. Subsequent deprotection through the use of pyridinium *p*-toluenesulfonate yielded the POSS aldehyde. The aldehyde was then reacted with N-methylglycine and C_{60} to yield the desired POSS fulleropyrrolidine after purification by column chromatography. Synthetic pathway 2 is discussed in **Section 2.10**.

2.8 Characterisation

Characterisation was performed by ^1H , ^{13}C and ^{29}Si NMR, UV-Vis and fluorescence spectrophotometry, Electrospray Ionisation (ESI) mass spectrometry and power limiting measurements, the details of which are detailed in **Chapter 6**.

2.9 Results & Discussion

2.9.1 ^1H NMR

^1H NMR resonances of the POSS fulleropyrrolidines and precursor compounds are detailed herein.

2.9.1.1 Mono-vinyl POSS

Mono-vinyl POSS was synthesised according to the literature procedure (**Figure 2.17**).^{74,75} The ^1H NMR spectrum of monovinyl POSS (R = iBu, **2.1**) exhibited a multiplet at δ 5.87-6.01 (3H, CH=CH₂). Resonances of the POSS isobutyl chains were apparent at δ 0.60 (m, 14H, CH₂) and 0.94 (m, 42H, CH₃), with a nonseptet at 1.86 (n, $^3J_{\text{H-H}} = 10.2$ Hz, 7H, CH). The resonances were consistent with those detailed in the literature.⁷⁴

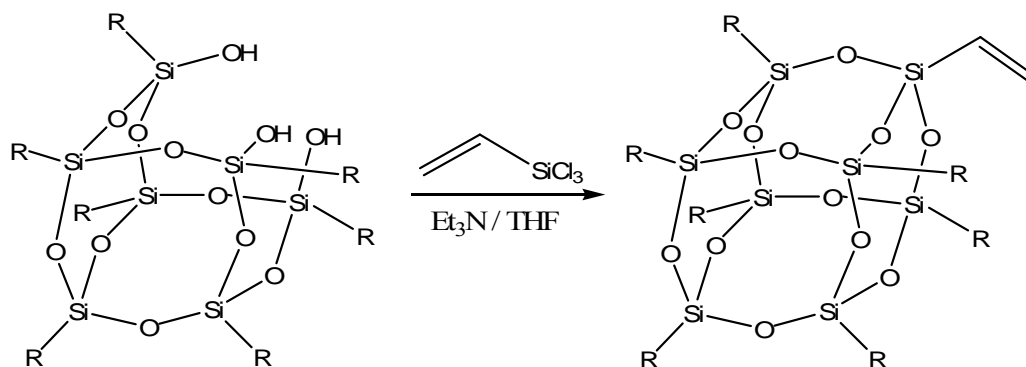


Figure 2.17. Synthesis of mono-vinyl POSS (**2.1**, **2.2**)

Table 2.1. ¹H NMR resonances of POSS fulleropyrrolidines and precursor compounds (synthetic pathway 1)

Compound	POSS	SiCH ₃	SiCH ₂	CH ₂	Ph	Dioxolane	CHO	Pyrrolidine
2.1	0.60, 0.94, 1.86 n (10.2Hz) ^a	-	5.87-6.01		-	-	-	-
2.2	7.30-7.50, 7.75-7.80	-	5.85-6.20		-	-	-	-
2.3	-	0.35	-	-	7.48 d (8.1Hz), 7.58 d (8.1Hz) ^a	4.01, 4.44 sept. (5.7 Hz), ^a 5.85	-	-
2.4	0.61, 0.97, 1.86	0.35	Obs.	Obs.	7.49, 7.51	4.04-4.14, 5.84	-	-
2.5	0.59 d (9.9 Hz), 0.95 d (9.9 Hz), 1.85 d (9.9 Hz) ^a	0.29	Obs.	Obs.	7.66 d (12.0 Hz), 7.84 d (12.0 Hz) ^a	-	10.02	-
2.6	7.34-7.58, 7.73-7.80	0.25	0.69-0.74	0.89-0.94	-	-	9.97	-
2.7	0.55- 0.59, 0.91-0.96, 1.75-1.90	0.24	Obs.	Obs.	7.42 d (11.4Hz), 7.76 d (11.4 Hz) ^a	-	-	2.82, 4.27 d (1H, 14.1Hz), ^b 4.93 (2H), 4.99 d (1H, 14.1 Hz) ^b
2.8	7.34-7.49, 7.70-7.74	0.23	0.53-0.59	0.82-0.90	-	-	-	2.83, 4.25-4.28, 4.92, 4.98-5.00

^a = ³J_{H-H}, ^b = ²J_{H-H}

Similarly, in the case where R = Ph (**2.2**), the ^1H NMR spectrum exhibited the vinyl resonance as a multiplet at δ 5.85-6.20 (3H), with the cage bound phenyl ring resonances apparent as broad multiplets at δ 7.30-7.50 (21H) and 7.75-7.80 (14H). The resonances were again consistent with those displayed in **2.1** and the literature.⁷⁴

2.9.1.2 [2-(4-dimethylsilyl)phenyl]-1,3-dioxolane

[2-(4-dimethylsilyl)phenyl]-1,3-dioxolane (**1.3**) was synthesised according to the literature procedure (**Figure 2.18**).⁷² ^1H NMR exhibited a doublet associated with the methyl groups attached to the silicon atom δ 0.35 (d, $^3J_{\text{H-H}} = 5.7$ Hz, 6H). Resonances of the dioxolane functionality were present at δ 4.01 (m, 4H, $\text{OCH}_2\text{CH}_2\text{O}$), and 5.85 (1H, OCHO). The silyl group exhibited a resonance at δ 4.44 (sept, $^3J_{\text{H-H}} = 5.7$ Hz, 1H), with the resonances associated with the phenyl ring apparent as doublets at δ 7.48 (d, $^3J_{\text{H-H}} = 8.1$ Hz, 2H) and 7.58 (d, $^3J_{\text{H-H}} = 8.1$ Hz, 2H). The ^1H NMR resonances were consistent with those evident in the literature.⁷²

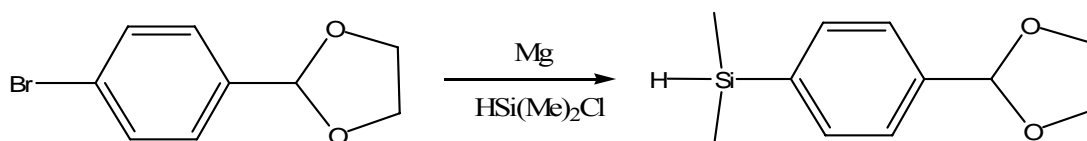


Figure 2.18. Synthesis of [2-(4-dimethylsilyl)phenyl]-1,3-dioxolane (**2.3**)

2.9.1.3 Mono-dioxolane POSS

Synthesis of the mono dioxolane POSS was achieved through hydrosilylation of mono-vinyl POSS with the silyl dioxolane (**Figure 2.19**). Disappearance of the vinyl and silyl peaks in ^1H , ^{13}C and ^{29}Si NMR were evident, indicating that the hydrosilylation reaction had proceeded to completion. ^1H NMR of **2.4** (R = iBu) was expected to exhibit new peaks due to the presence of the two CH_2 groups adjacent to the silicon cage following reaction of the vinyl group, however these peaks were obscured by the broad resonances of the isobutyl groups, which were apparent at δ 0.61 (16H, $\text{SiCH}_2/\text{iBu CH}_2$), 0.97 (44H, $\text{CH}_2\text{Si}/\text{iBu CH}_3$) and 1.86 (7H, iBu CH). The silicon bound methyl groups displayed a resonance at δ 0.35 (6H). Resonances of the dioxolane moiety were evident at δ 4.04-4.14 (m, 1H, CH) and 5.84 (4H,

OCH₂CH₂O), with the phenyl ring resonances apparent at δ 7.49 (2H, CH) and 7.51 (2H, CH). Little change was present in the resonances of the dioxolane moiety, in comparison with the resonances of the silyl dioxolane precursor, with only the resonance of the aromatic protons at position 3 exhibiting an upfield shift (0.07 ppm). A similar upfield shift (0.05 ppm) was previously observed in the resonances of the octa-substituted dioxolane derivative, in comparison with the corresponding resonance of the silyl dioxolane.⁷²

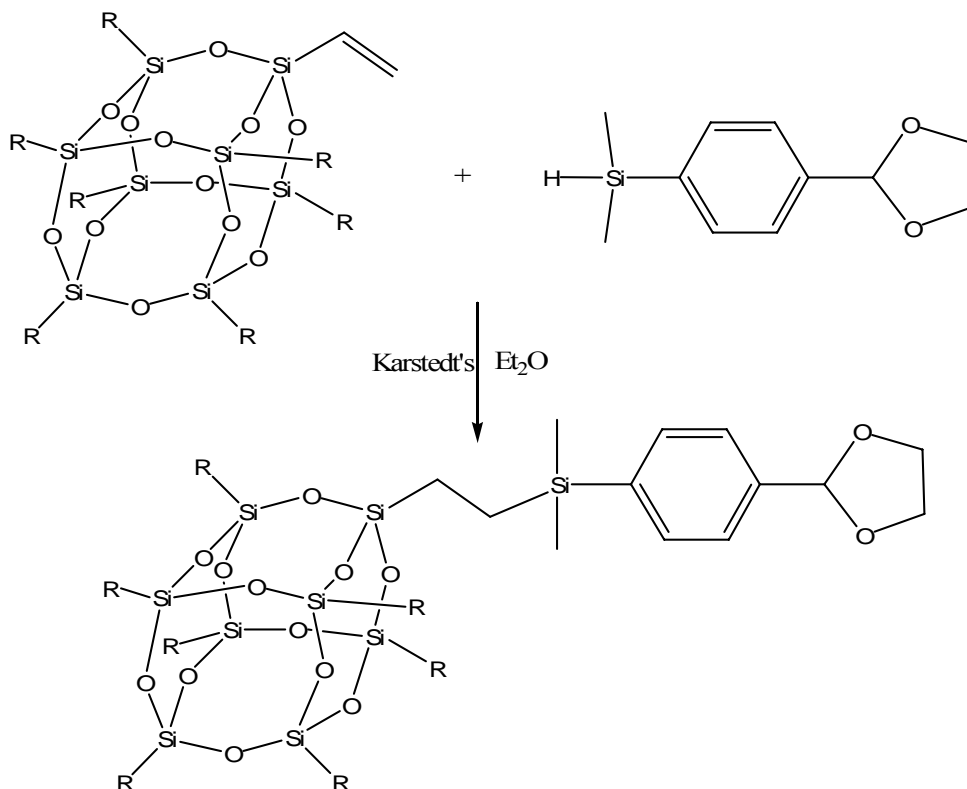


Figure 2.19. Synthesis of mono-dioxolane POSS (2.4)

The product was not isolated in the case of R = Ph, due to partial deprotection of the subsequent aldehyde occurring under the specified reaction conditions, evident by the presence of both aldehyde and dioxolane resonances at δ 4.05-4.14 (m, CH), 5.83 (OCH₂) and 10.02 (CHO).

2.9.1.4 Mono-aldehyde POSS

Mono-dioxolane POSS was deprotected through reflux with pyridinium *p*-toluenesulfonate in acetone, in order to generate the desired aldehyde functionality (**Figure 2.20**).

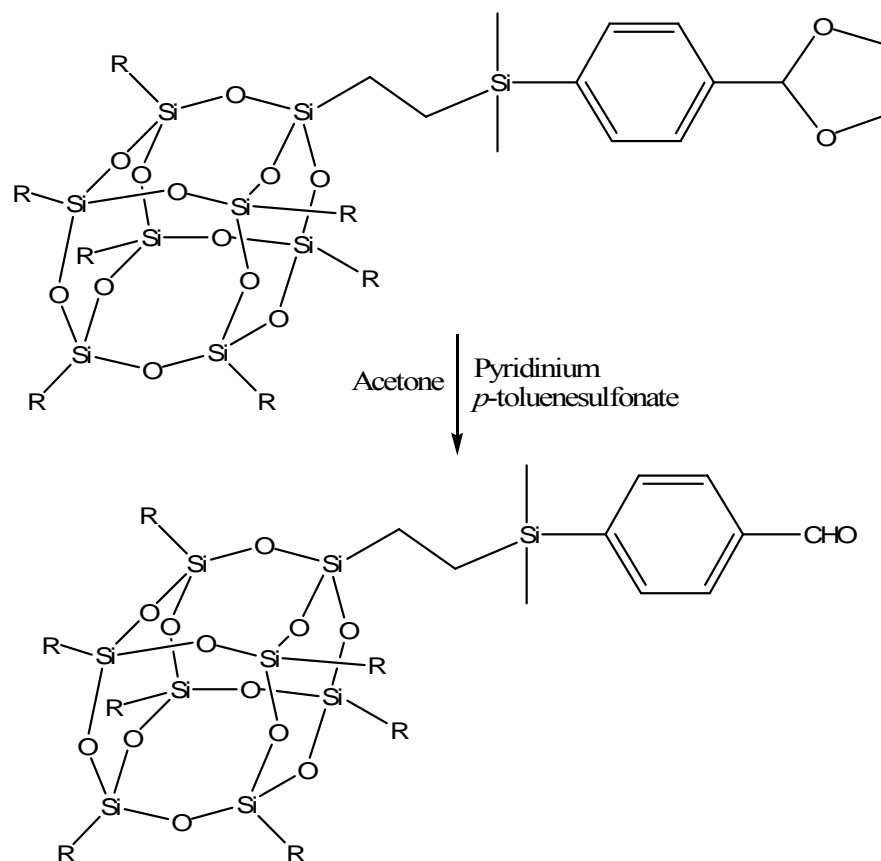


Figure 2.20. Synthesis of mono-aldehyde POSS (2.5, 2.6)

^1H NMR of **2.5** ($\text{R} = \text{iBu}$) exhibited isobutyl resonances at δ 0.59 (d, $^3J_{\text{H-H}} = 9.9$ Hz, 16H, $\text{SiCH}_2/\text{iBu CH}_2$), 0.95 (d, $^3J_{\text{H-H}} = 9.9$ Hz, 44H, $\text{CH}_2\text{Si}/\text{iBu CH}_3$) and 1.85 (n, $^3J_{\text{H-H}} = 9.9$ Hz, 7H, iBu CH). The SiCH_3 resonance was evident at δ 0.29, with the resonances of the ethylene spacer obscured. The disappearance of the dioxolane peaks, previously apparent at δ 4.04-4.14 and 5.84, in conjunction with the appearance of the aldehyde resonance at δ 10.02 (1H, CHO) confirmed that deprotection of the dioxolane had proceeded to completion. The phenyl resonances were apparent at δ 7.66 (d, $^3J_{\text{H-H}} = 12.0$ Hz, 2H, CH) and 7.84 (d, $^3J_{\text{H-H}} = 12.0$ Hz, 2H, CH), resulting in downfield shifts of 0.17 and 0.33 ppm, relative to the corresponding resonances in **2.4**, due to the increased deshielding experienced by the protons, associated with electronic effects of the aldehyde functionality. Similar downfield shifts were evident in the phenyl resonances of the octa-aldehyde derivative (0.15 and 0.27 ppm), relative to the corresponding resonances of the octa-dioxolane precursor.⁷²

Similarly, ^1H NMR of **2.6** ($\text{R} = \text{Ph}$) exhibited the cage bound phenyl resonances as broad multiplets at δ 7.34-7.58 (23H, CH), and 7.73-7.80 (16H, CH). The aldehyde resonance was evident at δ 9.97 (1H), confirming that the deprotection reaction had proceeded to completion, whilst the phenyl resonances were obscured by the broad resonances associated with the POSS cage phenyl rings. The SiCH_3 resonance was displayed at δ 0.25 (6H), with the ethylene spacer resonances observed at δ 0.69-0.74 (2H, SiCH_2) and 0.89-0.94 (2H, CH_2).

2.9.1.5 POSS Fulleropyrrolidines

The mono POSS-aldehyde was reacted with N-methylglycine and C_{60} to generate the desired POSS-fulleropyrrolidine product (**Figure 2.21**).

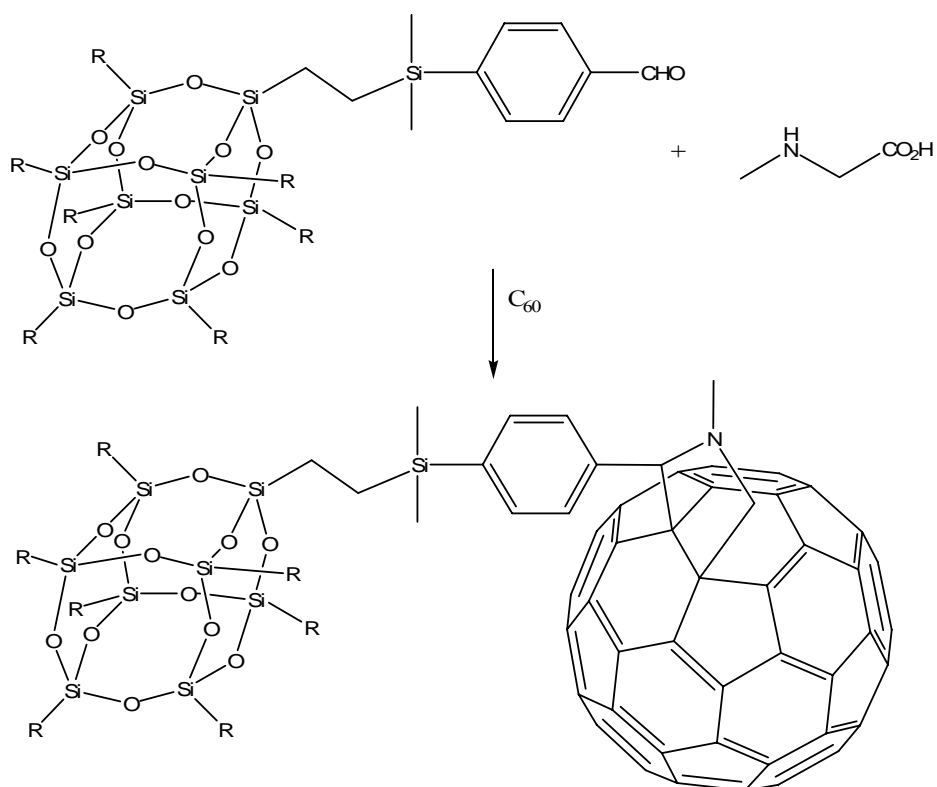


Figure 2.21. Synthesis of POSS-fulleropyrrolidines (2.7, 2.8)

The ^1H NMR spectrum of **2.7** ($\text{R} = \text{iBu}$) (**Figure 2.22**), exhibited the cage bound isobutyl resonances at 0.53-0.59 (14H, CH_2), 0.91-0.96 (42H, CH_3) and 1.75-1.90 (7H, CH), with the $\text{Si}(\text{CH}_3)_2$ resonance evident at δ 0.24 (6H). Resonances of the phenyl ring were apparent at δ 7.42 (d, $^3\text{J}_{\text{H-H}} = 11.4$ Hz, 2H, CH) and 7.76 (d, $^3\text{J}_{\text{H-H}} =$

11.4 Hz, 2H, CH), corresponding to upfield shifts by 0.24 and 0.08 ppm, relative to the corresponding resonances in **2.5**. The resonance shift occurred due to increased deshielding associated with the close proximity to the carbon sphere.²⁰ The upfield shifts are analogous to those present of 2-phenyl fulleropyrrolidine (0.21 and 0.06 ppm), relative to the corresponding resonances of benzaldehyde.⁷⁶ The disappearance of the aldehyde resonance, previously displayed at δ 10.02, coupled with the appearance of the pyrrolidine resonances, confirmed that the occurrence of the cycloaddition reaction. Pyrrolidine resonances were apparent at δ 2.82 (3H, NCH₃) and 4.93 (1H, NCH), together with an AB quartet, consisting of doublets at δ 4.27 and 4.99 (²J_{H-H} = 14.1 Hz, 2H, NCH₂). The presence of the AB quartet was indicative of geminal coupling between the protons at the 5 position of the pyrrolidine ring. The dramatic difference in resonance position was associated with the dissimilar deshielding effects each proton experienced due to the proximity of the carbon sphere.^{9,39,77,78}

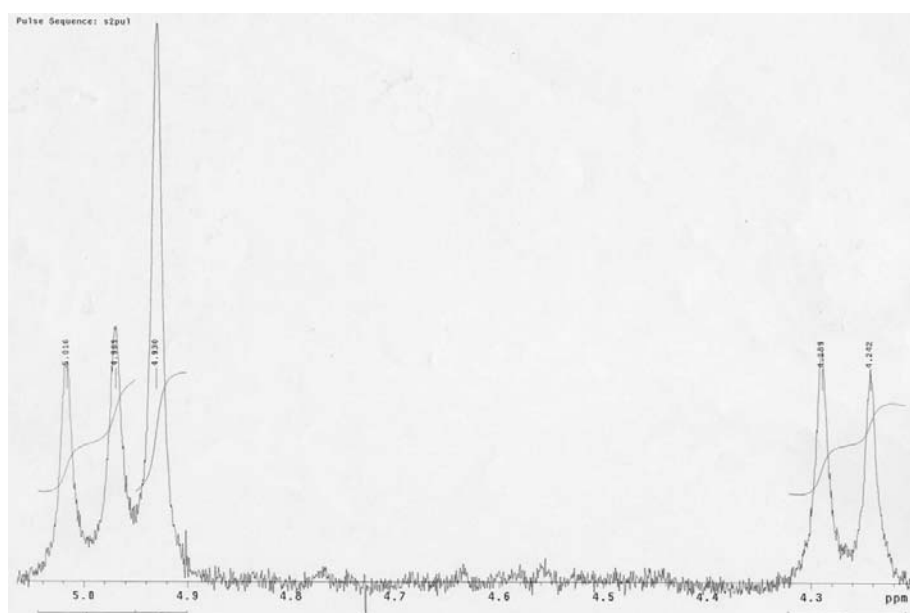


Figure 2.22. Pyrrolidine resonances in the ¹H NMR spectrum of POSS fulleropyrrolidine **2.7 in CDCl₃**

Likewise, ¹H NMR of **2.8** (R = Ph), exhibited little change from the resonances present in the aldehyde precursor, with the Si(CH₃)₂ resonance apparent at δ 0.23 (6H). The ethylene spacer resonances were observed at δ 0.54-0.59 (2H, SiCH₂) and 0.82-0.90 (2H, CH₂), with the cage bound phenyl resonances displayed at δ 7.34-7.49 (23H, CH) and 7.70-7.74 (16H, CH). Resonances of the pyrrolidine moiety were

evident at δ 2.83 (3H, NCH₃), 4.25-4.28 (1H, NCH₂), 4.92 (1H, NCH) and 4.98-5.00 (1H, NCH₂). The AB system was again present in the resonances at δ 4.25-4.28 and 4.98-5.00; however the broad nature of the resonances inferred that coupling constants were unable to be determined in this instance.

2.9.2 ¹³C NMR

¹³C NMR resonances of the POSS fulleropyrrolidines and precursor compounds are detailed in **Table 2.2**.

2.9.2.1 *Mono-vinyl POSS*

¹³C NMR of **2.1** (R = iBu) exhibited resonances of the isobutyl carbons at δ 22.64, 24.09 and 25.90, with the vinyl carbons exhibiting resonances at 130.16 and 136.03. Similarly, in **2.2** (R = Ph), the resonances of the POSS bound phenyl carbons were displayed at δ 127.89, 130.72 and 134.34, with the vinyl resonances being obscured. The resonances of **2.1** and **2.2** were consistent with those evident in the literature.^{74,75}

2.9.2.2 *[2-(4-dimethylsilyl)phenyl]-1,3-dioxolane*

¹³C NMR of **2.3** exhibited the Si(CH₃)₂ resonance at δ -3.72 (SiCH₃), with the dioxolane resonances apparent at δ 65.39 (OCH₂CH₂O) and 103.73 (OCHO). The phenyl resonances were evident at δ 125.39 (CH), 134.15 (CH), 138.75 (CSi) and 139.00 (CCH). The resonances were consistent with those detailed in the literature.⁷²

2.9.2.3 *Mono-dioxolane POSS*

¹³C NMR of **2.4** exhibited resonances of the isobutyl chains at δ 22.65, 24.01 and 25.83. Resonances of the dioxolane functionality were observed at δ 65.42 (OCH₂CH₂O) and 103.86 (CH). The Si(CH₃)₂ resonance was evident at δ -3.53, with the ethylene spacer resonances apparent at δ 4.56 (SiCH₂) and 6.82 (CH₂Si). Phenyl

Table 2.2. ^{13}C NMR resonances of POSS fulleropyrrolidines and precursor compounds (synthetic pathway 1)

Compound	POSS	SiCH ₃	SiCH ₂	CH ₂	Ph	Dioxolane	CHO	Fulleropyrrolidine
2.1	22.64, 24.09, 25.90	-	130.16	136.03	-	-	-	-
2.2	127.89, 130.72, 134.34	-	Obs.	Obs.	-	-	-	-
2.3	-	-3.71	-	-	125.39, 134.15, 138.75, 139.00	65.39, 103.73	-	-
2.4	22.65, 24.01, 25.83	-3.53	4.56	6.82	125.86, 133.80, 138.53, 140.57	65.42, 103.86	-	-
2.5	22.62, 24.00, 25.80	-3.27	4.55	6.70	128.75, 134.25, 136.59, 148.30	-	192.87	-
2.6	127.85, 128.00, 130.18, 130.42, 130.76, 134.16	-3.79	4.24	6.51	147.96	-	192.62	-
2.7	22.62, 24.00, 25.87	-3.56, -3.47	4.57	7.09	Obs.	-	-	40.26, 69.25, 70.25, 83.78, 127.75-156.41
2.8	127.80, 128.860, 130.25, 130.74, 134.20	-3.56	4.21	7.04	Obs.	-	-	40.14, 68.84, 79.77, 83.47, 133.91-153.02

resonances were displayed at δ 125.86, 133.80 (CH), 138.53 (CSi) and 140.57 (CC).

The majority of resonances associated with the dioxolane moiety experienced shifting following the hydrosilylation reaction. Downfield shifts of 0.19, 0.13 and 1.57 ppm were observed in the SiCH₃, CH (dioxolane) and CC resonances, relative to the corresponding resonances of **2.2**, with upfield shifts of 0.30 and 0.27 ppm observed in the CH and CSi phenyl resonances. Similar shift patterns were previously observed in the resonances of the octa-substituted dioxolane derivative,⁷² which exhibited downfield shifts of 0.2 and 1.5 ppm in the Si(CH₃)₂ and quaternary carbon (CC) resonances, along with upfield shifts of 0.4 and 0.2 ppm in the CH and CSi phenyl resonances, relative to the corresponding resonances of the octa-dioxolane precursor.

The product was not isolated in the case of R = Ph, due to partial deprotection to the subsequent aldehyde occurring under the specified reaction conditions, evident by the presence of both aldehyde and dioxolane resonance in ¹³C NMR with resonances evident at δ 65.42 (OCH₂CH₂O), 103.86 (CH), 192.62 (CHO). The mixture of products was unable to be separated, therefore deprotection was undertaken immediately to enable complete conversion of the dioxolane to the desired aldehyde.

2.9.2.4 *Mono-aldehyde POSS*

¹³C NMR of **2.5** (R = iBu) exhibited isobutyl resonances at δ 22.62, 24.00 and 25.80. The disappearance of the dioxolane resonances, coupled with the appearance of the aldehyde resonance at δ 192.87 (CHO), confirmed that deprotection of the dioxolane had occurred. The Si(CH₃)₂ resonance was observed at δ -3.72, with the ethylene spacer resonances evident at δ 4.55 (SiCH₂) and 6.70 (CH₂Si). Upfield shifts of 0.19 and 0.12 ppm were observed in the SiCH₃ and CH₂ resonances, relative to the corresponding resonances of **2.4**. The upfield shifting of these resonances was comparable with that exhibited in the octa-aldehyde derivative (0.2 and 0.1 ppm), relative to the octa-dioxolane precursor.⁷² The phenyl resonances were displayed at δ 128.75 (CH) and 134.25 (CH), 136.59 (CSi) and 148.30 (CC), with the downfield shifts apparent in the CH resonances of 2.89 and 0.45 ppm, similar to that detailed in

the octa-aldehyde derivative (2.9 ppm).⁷² The quaternary carbon resonance (CSi) exhibited an upfield shift of 1.94 ppm, again comparable to that detailed in the octa-aldehyde derivative (4.5 ppm).⁷² The resonance of quaternary carbon (CC) exhibited a substantial upfield shift of 7.73 ppm. The resonance positions of **2.5** were comparable to the corresponding resonances detailed in 4-trimethylsilylbenzaldehyde (δ 128.6, 133.8, 136.4 and 149.2),⁷⁹ with the shifts in the quaternary carbon resonances associate with the formation of resonance structures in the benzaldehyde structure (**Figure 2.23**). The resonance structure led to the generation of a partial positive charge on the C-Si quaternary carbon, with the resultant decrease in electron density resulting in an upfield resonance shift. Similarly, a partial negative charge was generated on the C-C quaternary carbon, with the resultant increase in electron density causing a downfield resonance shift.

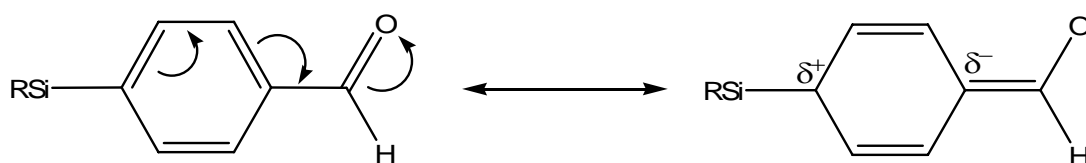


Figure 2.23. Resonance structures of silyl-substituted benzaldehyde

¹³C NMR of **2.6** (R = Ph) exhibited the Si(CH₃)₂ and ethylene spacer resonances at δ -3.79 (SiCH₃), 4.24 (SiCH₂) and 6.51 (CH₂Si). The cage bound phenyl ring resonances were evident at δ 127.85, 128.00, 130.18, 130.42, 130.76 and 134.16, obscuring the majority of the phenyl resonances of the aldehyde moiety. The resonance of the quaternary carbon (CC) was apparent at δ 147.96, analogous to that previously detailed for **2.5** (148.20) and 4-trimethylsilylbenzaldehyde (149.2),⁷⁹ with the aldehyde resonance apparent at δ 192.62.

2.9.2.5 POSS Fulleropyrrolidines

The ¹³C NMR spectrum of **2.7** (R = iBu) (**Figure 2.24**) exhibited the Si(CH₃)₂ and ethylene spacer resonances at δ -3.56 and -3.47 (SiCH₃), 4.57 (SiCH₂) and 7.09 (CH₂Si). A slight downfield shift of 0.39 ppm was present in the resonance of the CH₂Si of the ethylene spacer, relative to the corresponding resonance in **2.5**. The resonance shift was indicative of the increased deshielding effect associated with the

proximity of the carbon sphere.²⁰ Resonances of the cage bound isobutyl chains were evident at δ 22.62, 24.00 and 25.87. Resonances associated with the fulleropyrrolidine moiety were observed at δ 40.26 (NCH₃), 69.25 (CH₂), 70.25 (sp³ C), 83.78 (CH) and 127.75 to 156.41.

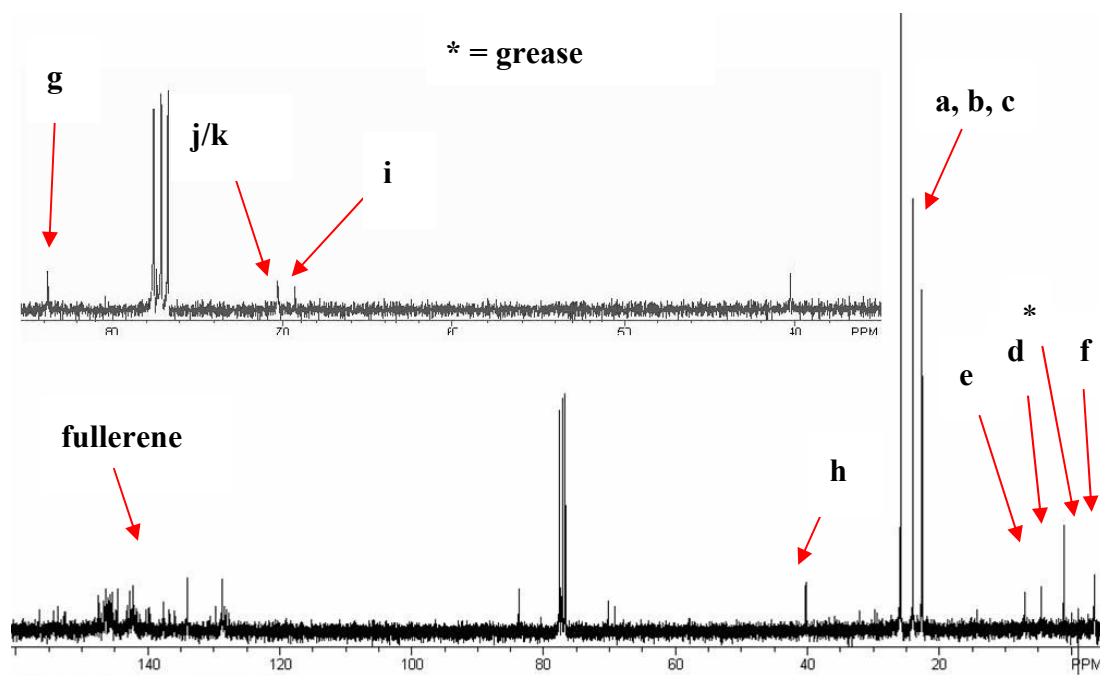
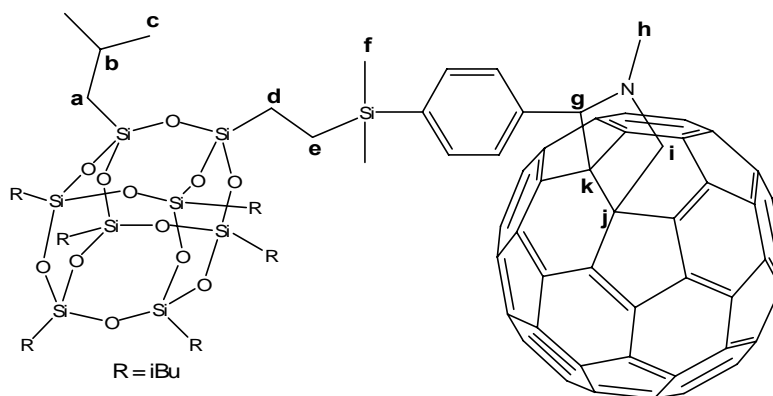


Figure 2.24. ¹³C NMR spectrum of POSS fulleropyrrolidine 2.7 in CDCl₃

¹³C NMR of **2.8** (R = Ph) displayed the Si(CH₃)₂ and ethylene spacer resonances at resonances at δ -3.56 (SiCH₃), 4.21 (SiCH₂) and 7.04 (CH₂Si). A downfield shift of 0.53 ppm was evident in the CH₂Si resonance, relative to the corresponding resonance in **2.6**, similar to the shift previously detailed for **2.7** (0.39 ppm). Resonances of the pyrrolidine moiety were observed at δ 40.14 (NCH₃), 68.84 (CH₂), 69.77 (sp³ C) and 83.47 (CH), with fullerene resonances displayed from δ 133.91 to

153.02. Resonances of the cage bound phenyl rings were apparent at δ 127.80, 128.60, 130.25, 130.45, 130.74 and 134.20.

2.9.3 ^{29}Si NMR

The ^{29}Si NMR resonances of the POSS fulleropyrrolidines and precursor compounds are detailed in **Table 2.3**.

Table 2.3. ^{29}Si NMR of POSS fulleropyrrolidines and precursor compounds

Compound	^{29}Si NMR
2.1	-67.79, -68.26
2.2	-65.14, -78.88, -79.13
2.3	-17.60
2.4	-1.51, -67.60, -68.04, -68.36
2.5	-0.66, -67.89, -68.03, -68.33
2.6	-0.54, -65.12, -78.84, -79.16
2.7	-1.66, -67.65, -68.13, -68.4
2.8	-1.19, -65.28, -78.85, -78.92, -79.19

The silyl dioxolane (**2.3**) displayed a resonance at δ -17.60, associated with the Si-H group. This resonance disappeared upon hydrosilylation, along with the appearance of a resonance at δ -1.51 (R = iBu, **2.4**), typical of a SiC_4 system, confirming that the reaction had gone to completion. This resonance was shifted upfield upon deprotection to the aldehyde, associated with the resonance structure of the aldehyde as discussed previously in **Section 2.9.2.4**. The SiC_4 resonance was shifted downfield in the resultant fulleropyrrolidines, indicative of the increased deshielding effect associated with the proximity of the carbon sphere.²⁰ All POSS compounds exhibited multiple peaks for the T type silicon atoms, indicative of the mono-functionalisation and the retention of the cage structure during reaction.^{74,80} The ^{29}Si NMR spectrum for **2.7** (**Figure 2.25**) exhibited resonances at δ -1.66, -67.70, -68.14 and -68.43, with all other spectra being analogous in appearance.

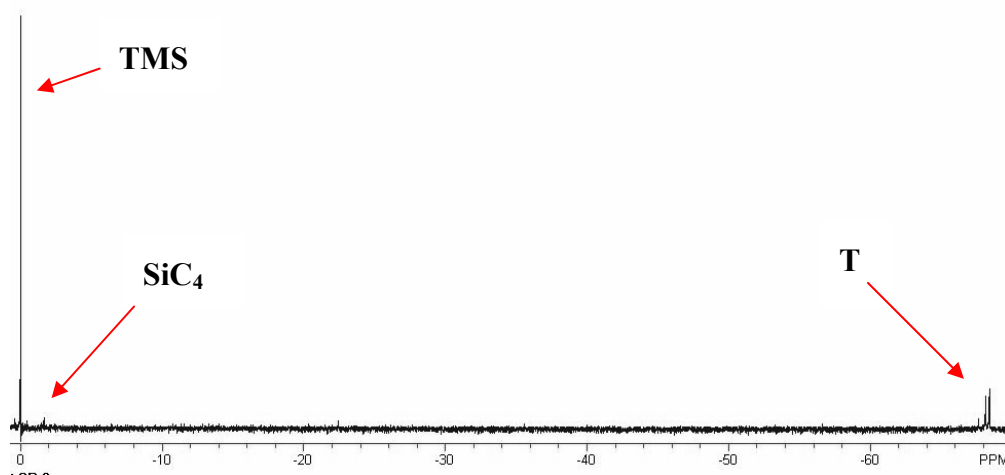


Figure 2.25. ^{29}Si NMR spectrum of POSS fulleropyrrolidine 2.7 in CDCl_3

2.9.4 High Resolution ESI Mass Spectrometry

The theoretical and experimental high resolution ESI mass spectrometry results are depicted in **Table 2.4**. The close correlation between the experimental and theoretical results offered unequivocal evidence of the formation of the desired compounds. ESI of the mono-aldehyde (R = iBu, **2.5**) was unobtainable due to product decomposition.

Table 2.4. High resolution ESI mass spectrometry results of POSS fulleropyrrolidines and precursor compounds

Compound	Experimental	Theoretical
2.1	865.2615	865.2505
2.2	1005.0421	1005.0415
2.4	1073.3510	1073.3526
2.6	1169.0200	1169.1073
2.7	1754.3888	1754.3872
2.8	1894.1723	1894.1681

2.9.5 Elemental Analysis of POSS Fulleropyrrolidines

The theoretical and experimental elemental analysis results of POSS fulleropyrrolidines **2.7** and **2.8** are depicted in **Table 2.5**. The close correlation between the experimental and theoretical results offered further evidence of

formation of the desired compounds.

Table 2.5. Elemental analysis results of POSS fulleropyrrolidines

Compound	Experimental (C, H, N)	Theory (C, H, N)
2.7	69.10, 4.77, 0.80	69.81, 5.67, 0.46
2.8	72.87, 2.92, 0.74	70.29, 3.12, 0.75

2.9.6 Optical Properties of POSS Fulleropyrrolidines

2.9.6.1 UV-Vis Spectra of POSS Fulleropyrrolidines

As C₆₀ contains 30 conjugated double bonds, multiple absorption bands were observed in the UV-Vis spectrum, corresponding to S₀→S_n electronic transitions.⁸¹ Derivatisation caused the conversion of some of the vibronic-forbidden states to the allowed states, thus increasing their population and transition probabilities.

Fulleropyrrolidines exhibit broad absorption spectra analogous to C₆₀, which exhibited strong absorptions in the ultraviolet range and a weaker absorption band between 430 and 630 nm, associated with the numerous forbidden transitions of C₆₀.^{82,83} In C₆₀, the allowed transitions, which occur in the UV below 400 nm, arose via excitation from the HOMO to the second excited configuration, LUMO+1, as well as from the HOMO-1 to LUMO excitations. The forbidden transitions in the visible region, induced by Herzberg-Teller vibronic interactions, occurred via the lower energy excitation from HOMO to LUMO.⁸⁴

Fulleropyrrolidines exhibit a broader range of absorption, up to 800 nm, with a sharp peak at approximately 430 nm and a broader band at approximately 700 nm due to the triplet-triplet absorption. These features are characteristic of [6,6] ring-closed fullerene derivatives, which exhibit a singlet-triplet quantum yield near unity, similar to C₆₀.⁸⁵ The absorption spectra of the fulleropyrrolidine derivative **2.7** (Figure 2.26) exhibited absorption maxima at 433 and 705 nm, with molar extinction coefficients of 3005 and 235, respectively. Analogously, the absorption spectra of **2.8** (Figure 2.26) displayed absorption maxima at 432 and 705 nm, with molar extinction coefficients of 4935 and 343, respectively.

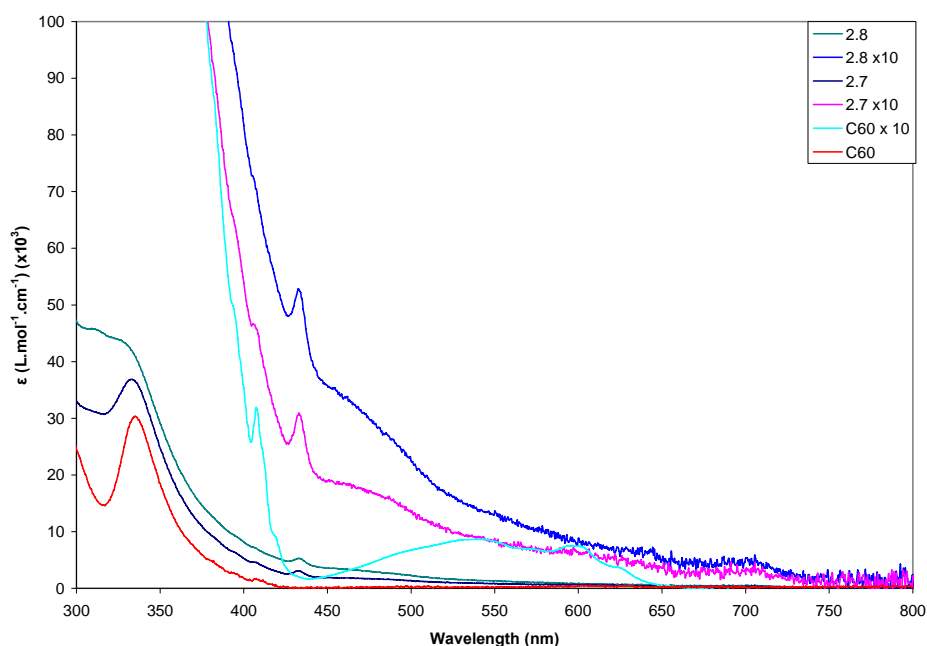


Figure 2.26. UV-Vis spectra of POSS fulleropyrrolidines 2.7 and 2.8 in toluene

2.9.6.2 *Steady State Spectrofluorometric Emission Studies of POSS Fulleropyrrolidines*

The fluorescence and phosphorescence of fullerenes and their derivatives can be discussed by referring to the energy level diagram below (**Figure 2.27**). At room temperature, the majority of molecules reside in the lowest vibrational level of the ground state. Light induced transitions occur upward from this level, where transitions to particular vibrational levels can appear in the absorption spectrum as separate bands (1 and 2). Following excitation to any of the upper vibrational levels of the first excited state, most molecules undergo rapid energy degradation down to the lowest vibrational level via fluorescent emission (${}^10 \rightarrow 0$) (4). Photoexcited molecules are also able to return to the ground state via intersystem crossings to the triplet state, and subsequent phosphorescence (5).⁸⁶

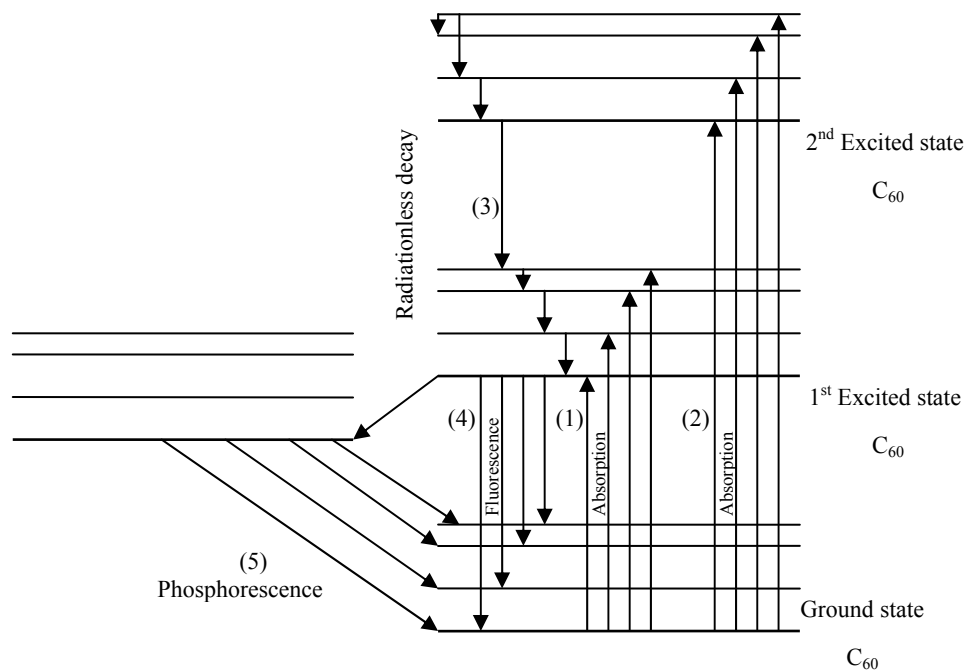


Figure 2.27. Fluorescence and phosphorescence of fullerenes⁸⁶

Excitation of **2.7** and **2.8** ($\lambda_{\text{exc}} = 335 \text{ nm}$) produced emission bands with maxima at approximately 719 nm (**Figure 2.28**), which correspond to the fullerene excited singlet state emission ($^1\text{C}_{60}^*$), characteristic of a fullerene-based emission.^{68,86-89}

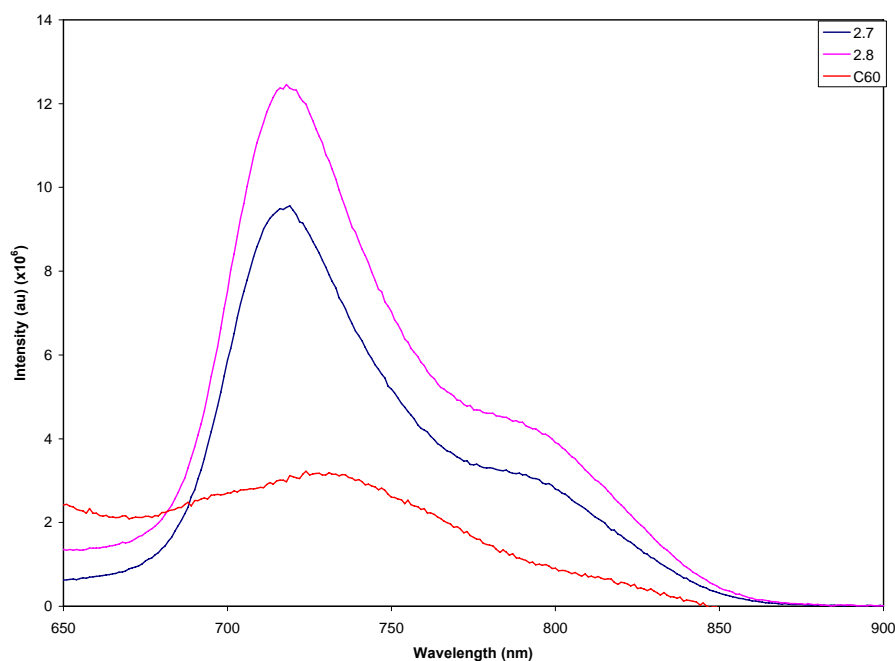


Figure 2.28. Fluorescence spectra of POSS fulleropyrrolidines 2.7 and 2.8 in toluene ($\lambda_{\text{exc}} = 335 \text{ nm}$)

The fluorescence of C_{60} in room temperature toluene solution was both weak and broad, as the high icosahedral (I_h) symmetry of C_{60} was nearly preserved due to the weak interactions between C_{60} and toluene.⁸⁷ Methanofullerenes generally exhibit an emission band at approximately 705 nm compared to the fulleropyrrolidines at approximately 720 nm. This red-shifting reflected the greater electron-withdrawing effect induced by the functional groups and the different ring sizes.^{82,87,90}

Monofunctionalised fullerenes exhibited a significant increase in the fluorescent intensity relative to C_{60} . The intensity of the emission in **2.7** was three times that of C_{60} , whilst the intensity of the emission in **2.8** was approximately four times greater than that for C_{60} . This is consistent with other fullerene derivatives, which exhibited emissions from three to four times the intensity of C_{60} .⁸¹ This was, in part, due to the change in symmetry from I_h (C_{60}) to one n-fold axis of symmetry and a vertical plane (C_{2v}) (monoadducts).⁸¹

2.9.6.3 Power limiting of POSS Fulleropyrrolidines

Figure 2.29, **Figure 2.30** and **Figure 2.31** exhibit the results obtained for the three compounds. In the three cases examined; for solutions of C_{60} , **2.7** and **2.8**, there was distinct power limiting of the transmission with the onset of a power level of approximately 200 mJ/cm². In all three cases strong thermal effects were seen at fluences above ca 1 J/cm², evident from increased scattering which was contributed to the power limiting effect.

The power limiting properties of **2.7** and **2.8** were essentially identical to those of C_{60} . While the results for **2.7** and **2.8** were obtained at higher concentrations by weight, the molar concentrations of C_{60} and **2.7** and **2.8** were similar, thus leading to comparable number densities of the C_{60} moieties.

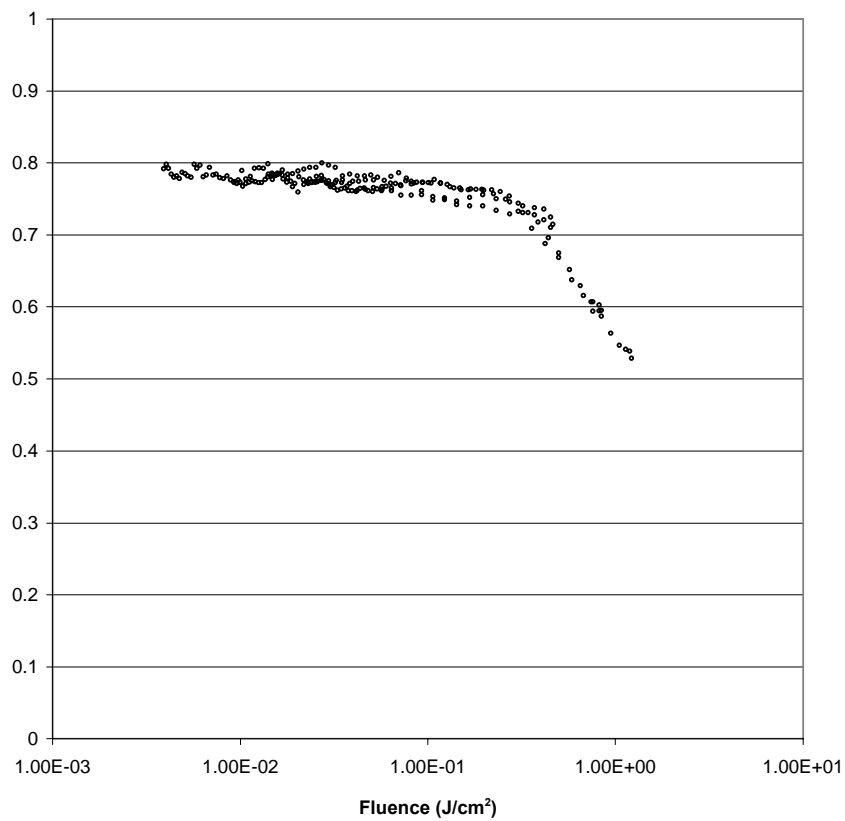


Figure 2.29. Power limiting plot for C₆₀

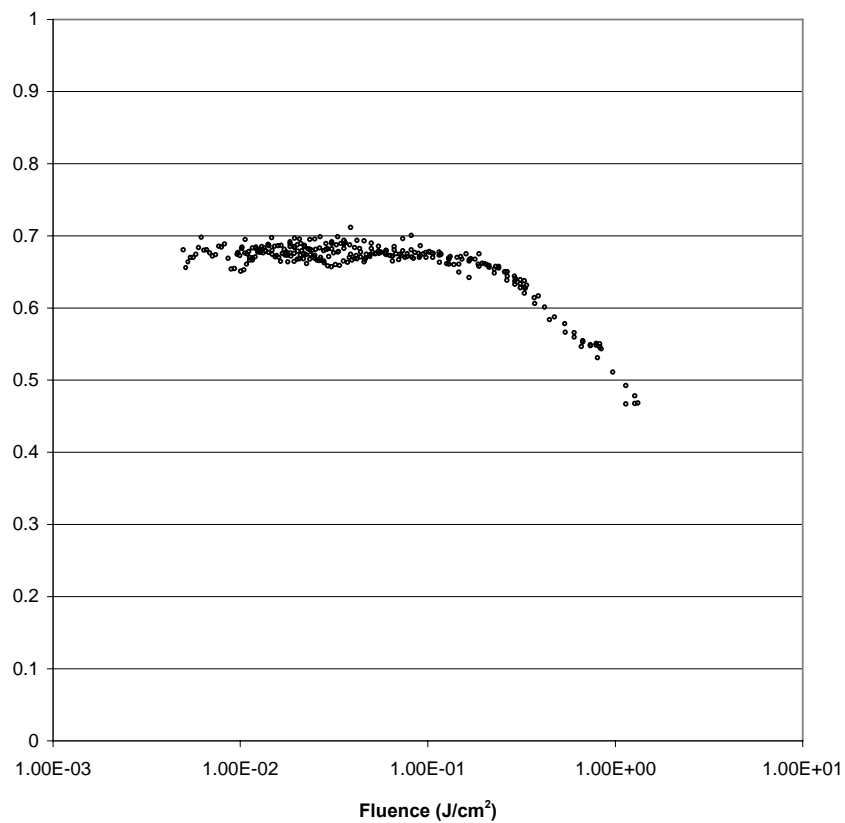


Figure 2.30. Power limiting plot for POSS fulleropyrrolidine 2.7

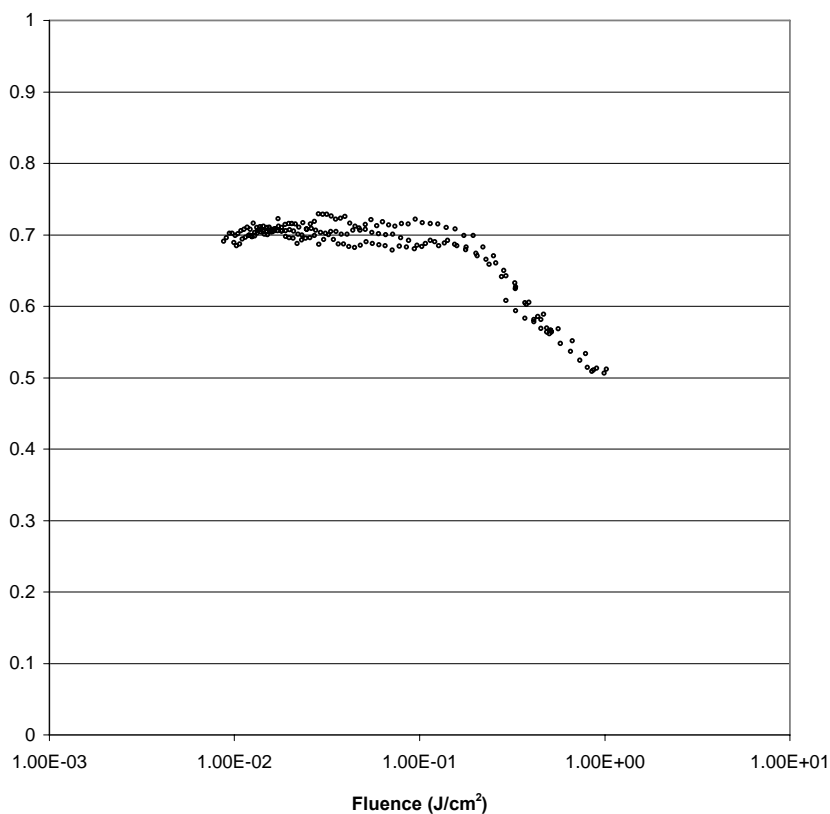


Figure 2.31. Power limiting plot for POSS fulleropyrrolidine 2.8

2.10 Synthetic Pathway 2

An aldehyde functionality on the periphery of a POSS cage has previously also been synthesised via nucleophilic substitution of benzyl chloride functionalised POSS.⁷¹ Incompletely condensed trisilanol POSS was reacted with trichloro[4-(chloromethyl)phenyl]silane to yield mono benzyl chloride POSS. Nucleophilic substitution of the chloride functionality with 4-hydroxybenzaldehyde was performed to yield the desired POSS aldehyde.⁷¹ This POSS aldehyde was subsequently reacted with N-methylglycine and C₆₀ to yield the desired POSS fulleropyrrolidine.

2.11 Results & Discussion

2.11.1 FTIR

Nucleophilic substitution of the chloride functionality with 4-hydroxybenzaldehyde was evident in the FTIR, with the appearance of a carbonyl stretching band at 1697 cm^{-1} indicative of the aldehyde functionality.

2.11.2 ^1H NMR

The ^1H NMR resonances of the POSS fulleropyrrolidines and precursor compounds are detailed in **Table 2.6**.

2.11.2.1 Mono-benzyl Chloride POSS

The synthesis of mono-benzyl chloride POSS was performed according to the literature procedure (**Figure 2.32**).⁷¹ ^1H NMR, in the case where $\text{R} = \text{iBu}$ (**2.9**), exhibited the cage bound isobutyl resonances at δ 0.58-0.62 (14H, CH_2), 0.93-0.97 (42H, CH_3) and 1.85-1.91 (7H, CH). The benzyl chloride moiety displayed resonances at δ 4.59 (2H, CH_2Cl), 7.39 (d, $^3\text{J}_{\text{H-H}} = 7.50\text{ Hz}$, 2H, CH) and 7.64 (d, $^3\text{J}_{\text{H-H}} = 7.50\text{ Hz}$, 2H, CH), with the resonances consistent with those detailed in the literature.⁷¹

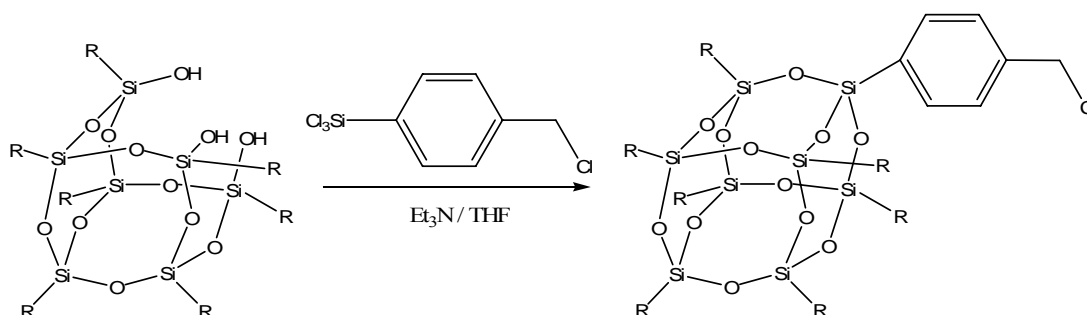


Figure 2.32. Synthesis of mono-benzyl chloride POSS (**2.9**, **2.10**)

Table 2.6. ¹H NMR of POSS fulleropyrrolidines and precursor compounds (synthetic pathway 2)

Compound	POSS	CH ₂ -X	Ph	CHO	Fulleropyrrolidine
2.9	0.58-0.62, 0.93-0.97, 1.85-1.91	4.59	7.39 (d, 7.5 Hz), 7.64 (d, 7.5 Hz) ^a	-	-
2.10	0.99-1.04, 1.52-1.56, 1.76-1.78	4.60	7.40 (d, 7.8 Hz), 7.67 (d, 7.8 Hz) ^a	-	-
2.11	0.63-0.66, 0.94-0.99, 1.83-1.93	5.17	7.08 (d, 8.7 Hz), 7.44 (d, 7.5 Hz), 7.71 (d, 7.5 Hz), 7.85 (d, 8.7 Hz) ^a	9.90	-
2.12	0.99-1.04, 1.51-1.56, 1.77	5.17	7.08 (d, 8.7 Hz), 7.43 (d, 7.5 Hz), 7.71 (d, 7.5 Hz), 7.84 (d, 8.7 Hz) ^a	9.88	-
2.13	0.65-0.66, 0.96-1.01, 1.86-1.93		6.85-7.07, 7.43-7.50, 7.68-7.84	-	2.80, 4.26-4.27, 4.91, 4.96-5.21
2.14	1.03, 1.54, 1.78		7.04, 7.43, 7.69	-	2.80, 4.25-4.27, 4.91-5.13

^a = ³J_{H-H}

Similarly, in the ^1H NMR spectrum of **2.10** ($\text{R} = \text{Cp}$), resonances of the cage bound cyclopentyl rings were evident at δ 0.99-1.04 (7H, CH), 1.52-1.56 (42H, CH_2) and 1.76-1.78 (14H, CH_2). Resonances of the benzyl chloride moiety were apparent at δ 4.60 (s, CH_2Cl), 7.40 (d, $^3J_{\text{H-H}} = 7.8$ Hz) and 7.67 (d, $^3J_{\text{H-H}} = 7.8$ Hz). The ^1H NMR resonances were again consistent with those evident in the literature.⁷¹

2.11.2.2 Mono-aldehyde POSS

Mono-aldehyde POSS (2.11, 2.12) was synthesised through the reaction of mono-benzyl chloride POSS (2.9, 2.10) with 4-hydroxybenzaldehyde (**Figure 2.33**). ^1H NMR of **2.11** ($\text{R} = \text{iBu}$) (**Figure 2.34**) exhibited little change in the resonances of the cage bound isobutyl groups, with resonances evident at δ 0.63-0.66 (14H, CH_2), 0.94-0.99 (42H, CH_3) and 1.83-1.93 (7H, CH). The benzyl resonance was observed at δ 5.17 (2H, CH_2O), resulting in a downfield shift of 0.59 ppm, relative to the corresponding resonance of **2.9**. The resonance shift was associated with the increased deshielding effect of the aryl aldehyde in comparison to the chloride, and was consistent with the spectroscopic literature for the nucleophilic substitution of an alkyl chloride with phenoxy group system, where a downfield shift of approximately 0.7 ppm was generally evident.⁹¹ The resonance shift is also comparable with the literature synthesis of **2.12** ($\text{R} = \text{Cp}$) (0.64 ppm).⁷¹ The aldehyde functionality exhibited a resonance at δ 9.90, with the phenyl resonances (**Figure 2.34**) displayed at δ 7.08 (d, $^3J_{\text{H-H}} = 8.70$ Hz, 2H, CH), 7.44 (d, $^3J_{\text{H-H}} = 7.50$ Hz, 2H, CH), 7.71 (d, $^3J_{\text{H-H}} = 7.50$ Hz, 2H, CH) and 7.85 (d, $^3J_{\text{H-H}} = 8.70$ Hz, 2H, CH). The displayed resonances were consistent with those described in the literature.⁷¹

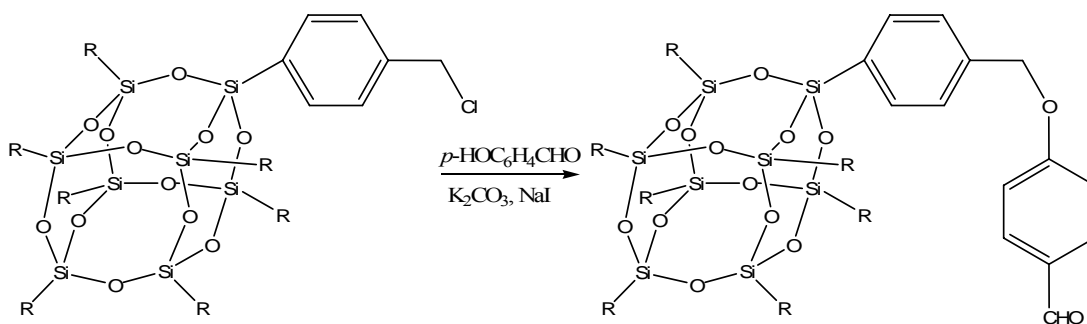


Figure 2.33. Synthesis of mono aldehyde POSS (2.11, 2.12)

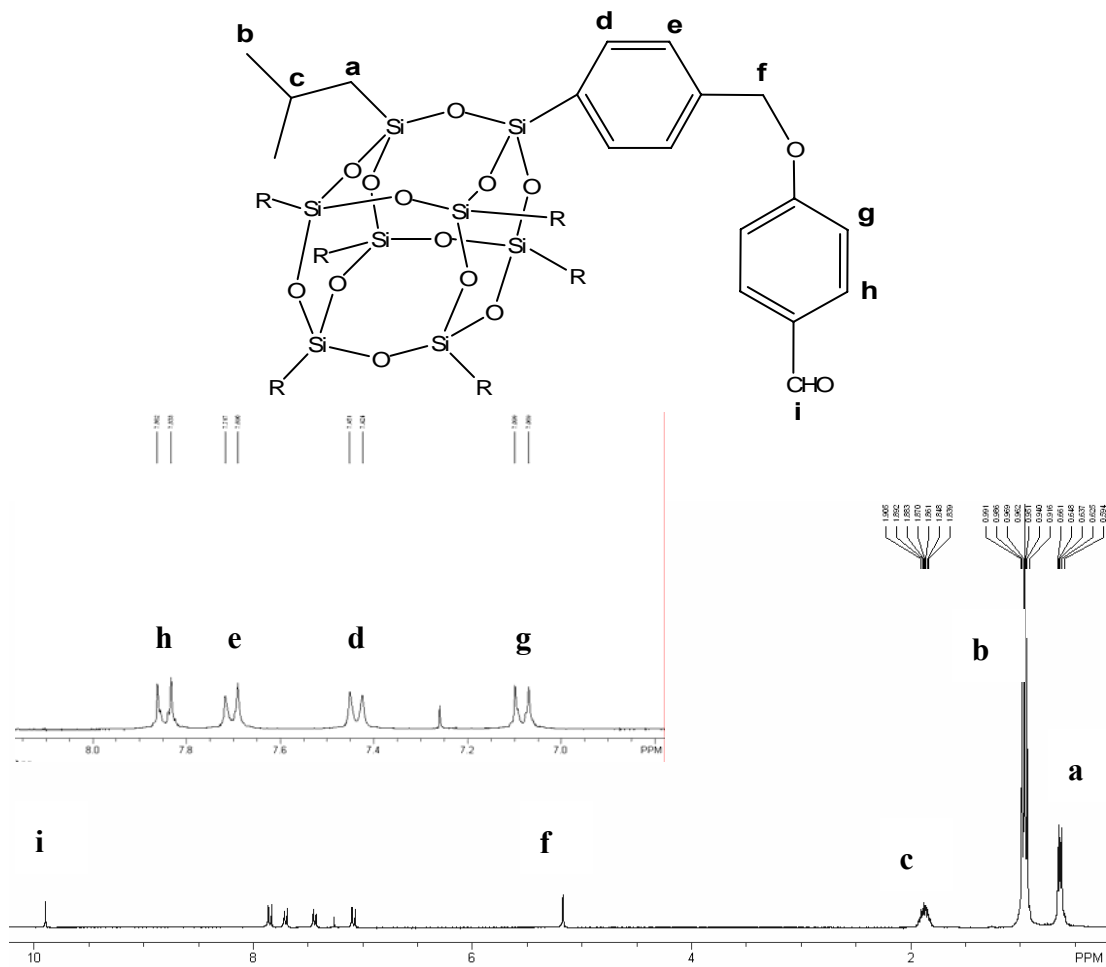


Figure 2.34. ¹H NMR of mono-aldehyde POSS 2.11 in CDCl₃

Similarly, in the case where R = Cp (**2.12**), ¹H NMR exhibited the resonances of the cage bound cyclopentyl groups at δ 0.99-1.04 (7H, CH), 1.51-1.56 (42H, CH₂) and 1.77 (14H, CH₂). The benzyl resonance was present at δ 5.17, resulting in a downfield shift of 0.57 ppm, relative to the corresponding resonance in **2.10**, similar to that detailed for **2.11** (0.59 ppm). The aldehyde resonance was displayed at δ 9.88 (1H), with the phenyl resonances present at δ 7.08 (d, $^3J_{\text{H-H}} = 8.70$ Hz, 2H, CH), 7.43 (d, $^3J_{\text{H-H}} = 7.50$ Hz, 2H, CH), 7.71 (d, $^3J_{\text{H-H}} = 7.50$ Hz, 2H, CH) and 7.84 (d, $^3J_{\text{H-H}} = 8.70$ Hz, 2H, CH). The displayed resonances were consistent with **2.11** and those detailed in the literature.⁷¹

2.11.2.3 POSS Fulleropyrrolidines

Mono-aldehyde POSS was reacted with N-methylglycine and C₆₀ in order to synthesise the desired POSS fulleropyrrolidine product (**Figure 2.35**). ¹H NMR of fulleropyrrolidine **2.13** (R = iBu) exhibited isobutyl resonances at δ 0.65-0.66 (14H, CH₂), 0.96-1.01 (42H, CH₃) and 1.86-1.93 (7H, CH). Resonances of the two phenyl rings were evident at δ 6.85-7.07 (2H, CH), 7.43-7.50 (2H, CH) and 7.68-7.84 (2H, CH), with the broadness associated with restricted rotation around the pyrrolidine-phenyl bond. A similar phenomenon has been witnessed previously in a variety of compounds containing phenyl rings adjacent to the pyrrolidine ring in the literature.^{78,92-99} The disappearance of the aldehyde resonance, coupled with the appearance of new resonances of the pyrrolidine moiety confirmed that the cycloaddition reaction had occurred. Resonances of the pyrrolidine moiety were apparent at δ 2.80 (3H, NCH₃), 4.25-4.27 (1H, NCH₂), 4.91 (1H, NCH) and 4.96-5.21 (1H, CH₂), with the AB quartet coupling constants unable to be determined due to the broadness of the resonance associated with restricted rotation, as detailed previously.

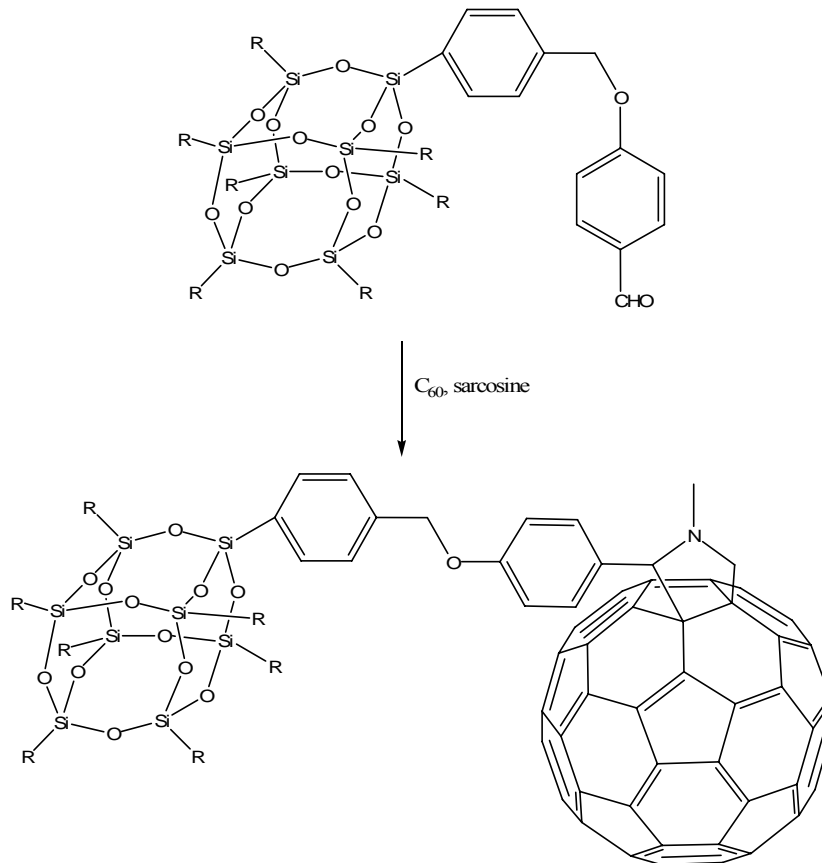


Figure 2.35. Synthesis of POSS fulleropyrrolidines (**2.13**, **2.14**)

Similarly, in the case where R = Cp (**2.14**), comparable resonances to that of the aldehyde precursor were evident, with the cyclopentyl resonances apparent at δ 1.03 (7H, CH), 1.54 (42H, CH₂) and 1.78 (14H, CH₂). Resonances of the phenyl rings were evident as broad resonances, as detailed for **2.13**, at δ 7.04 (2H, CH), 7.43 (2H, CH) and 7.69 (2H, CH). The pyrrolidine resonances were apparent at δ 2.80 (3H, NCH₃), 4.25-4.27 (1H, NCH₂) and 4.91-5.13 (3H, NCH/NCH₂), with coupling constants again unable to be determined.

2.11.3 ¹³C NMR

¹³C NMR resonances of the POSS fulleropyrrolidines and precursor compounds are detailed in **Table 2.7**.

2.11.3.1 Mono-benzyl Chloride POSS

¹³C NMR of **2.9** (R = iBu) exhibited resonances of the cage bound isobutyl chains at δ 22.37, 22.46, 23.85 and 25.69, in addition to the resonances of the benzyl chloride moiety which were apparent at δ 46.09 (CH₂Cl), 127.68, 132.13, 134.44 and 139.28 (CH). The resonances were consistent with those detailed in the literature.⁷¹

Similarly, for **2.10** (R = Cp), resonances of the cyclopentyl groups were displayed at δ 22.22, 26.96, 27.02 and 27.30. Resonances of the benzyl chloride moiety were apparent at δ 46.13 (CH₂Cl), 127.70, 132.54, 134.49 and 139.22 (CH), with all resonances displayed consistent with those described in the literature.⁷¹

2.11.3.2 Mono-aldehyde POSS

¹³C NMR of **2.11** (R = iBu) exhibited resonances of the isobutyl carbons at δ 22.44, 22.48, 22.57, 23.03, 23.66 and 25.68. The benzyl resonance was observed at δ 70.04 (CH₂O), resulting in a downfield shift of 23.95 ppm, relative to the corresponding resonance of **2.9**. The resonance shift was again associated with the increased

Table 2.7. ¹³C NMR of POSS fulleropyrrolidines and precursor compounds (synthetic pathway 2)

Compound	POSS (iBu/Cp)	CH₂X	Ph	C=O	Fulleropyrrolidine
2.9	22.37, 22.46, 23.85, 25.69	46.09	127.68, 132.13, 134.44, 139.28		
2.10	22.22, 26.96, 27.02, 27.30	46.13	127.70, 132.54, 134.49, 139.22		
2.11	22.44, 22.48, 22.57, 23.03, 23.66, 25.68	70.04	114.81, 116.03, 129.61, 132.13, 132.46, 164.36	191.17	
2.12	22.44, 22.47, 27.20, 27.26, 27.60	70.42	115.42, 115.41, 126.74, 130.40, 132.25, 132.62, 134.72, 138.12, 163.68	190.74	
2.13	22.62, 22.71, 24.02, 25.86	70.12	115.14		40.14, 69.15, 83.32, 126.75-159.04
2.14	22.40, 27.13, 27.18, 27.46	70.13	115.10		40.13, 69.12, 83.28, 126.75-159.00

deshielding effect of the aryl aldehyde group and was comparable to that exhibited in the literature for **2.12** (24.3 ppm).⁷¹ Resonances of the phenyl rings were evident at δ 114.81, 116.03, 129.61, 132.13, 132.46 and 164.36, along with the resonance of the aldehyde functionality, which was observed at δ 191.17.

¹³C NMR of **2.12** (R = Cp) exhibited resonances of the cyclopentyl carbons at δ 22.44, 22.47, 27.20, 27.26 and 27.56. Downfield shifts of 0.22, 0.24, 0.24 and 0.26 were apparent in the cyclopentyl resonances, relative to the corresponding resonances in **2.10**. compared to shifts of 0.2, 0.3, 0.1, 0.2 and 0.2 ppm detailed in the literature synthesis of **2.12**.⁷¹ The benzyl resonance was apparent at δ 70.42, resulting in a downfield shift of 24.29 ppm, with the resonance shift similar to that detailed previously for **2.11** (23.95 ppm) and in the literature report of **2.12** (24.3 ppm). Resonances of the phenyl rings were present at δ 115.42, 116.41, 126.74, 130.40, 132.25, 132.62, 134.72, 138.12 and 163.68, with the aldehyde resonance evident at δ 190.74. Both **2.11** and **2.12** exhibited resonances consistent with those displayed in the literature for **2.12**.⁷¹

2.11.3.3 POSS Fulleropyrrolidines

¹³C NMR of **2.13** (R = iBu) (**Figure 2.36**) exhibited resonances of the cage bound isobutyl carbons at δ 22.62, 22.71, 24.02 and 25.86, resulting in downfield shifts of 0.18, 0.14/0.23, 0.36 and 0.18 ppm, relative to the corresponding resonances in **2.11**. The resonance shift was associated with the increased deshielding associated with the close proximity to the carbon sphere.²⁰ Resonances associated with the pyrrolidine moiety were evident at δ 40.14 (NCH₃), 69.15 (CH) and 83.32 (CH), with the sp³ carbon resonance obscured by the benzyl CH₂O resonance, which was present at δ 70.12. The peak broadness associated with the restricted rotation of the phenyl rings, as previously detailed in the ¹H NMR discussion in **Section 2.11.2.3**, was again evident in the broad resonance at δ 115.14. The remaining resonances of the phenyl carbons were obscured by the large number of resonances associated with the fullerene, which were evident from δ 126.75-159.00.

^{13}C NMR of **2.14** ($\text{R} = \text{Cp}$) exhibited resonances of the cyclopentyl resonances at δ 22.40, 27.13, 27.18 and 27.46, corresponding to upfield shifts of 0.04, 0.07, 0.08 and 0.10 ppm, again associated with the deshielding effects associated with the close proximity to the carbon sphere.²⁰ Resonances of the pyrrolidine moiety were evident at δ 40.13 (NCH_3), 69.12 (CH) and 83.28 (CH), with the sp^3 carbon resonance again obscured by the CH_2O resonance at δ 70.13. The broadness of the aromatic resonances was again exhibited in the broad phenyl resonance at δ 115.10, with the remaining phenyl resonances obscured by the resonances of the fullerene, which were apparent from δ 126.75-159.00.

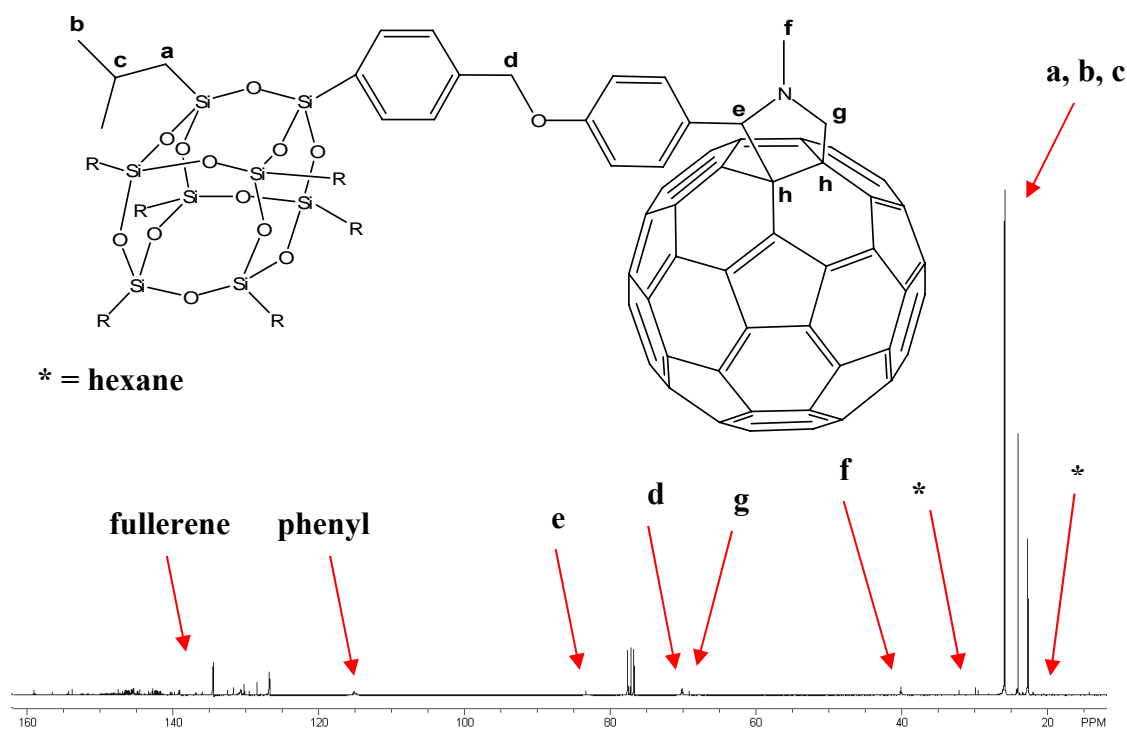


Figure 2.36. ^{13}C NMR of POSS fulleropyrrolidine **2.13** in CDCl_3

2.11.4 ^{29}Si NMR

^{29}Si NMR resonances of the POSS fulleropyrrolidines and precursor compounds are detailed in **Table 2.8**. All POSS compounds exhibited multiple peaks for the T type silicon atoms, indicative of mono-functionalisation.^{74,80}

Table 2.8. ^{29}Si NMR of POSS fulleropyrrolidines and precursor compounds
(synthetic pathway 2)

Compound	^{29}Si NMR
2.9	-67.97, -68.16, -68.29, -68.49
2.10	-67.81, -68.22, -79.61
2.11	-67.60, -68.23
2.12	-67.54, -68.19, -79.12
2.13	-67.65, -68.26
2.14	-66.22, -66.55

The ^{29}Si NMR spectrum of **2.13** exhibited resonances indicative of the monosubstituted POSS cage at δ -67.65 and -68.26 (**Figure 2.37**), with all other spectra comparable in appearance.

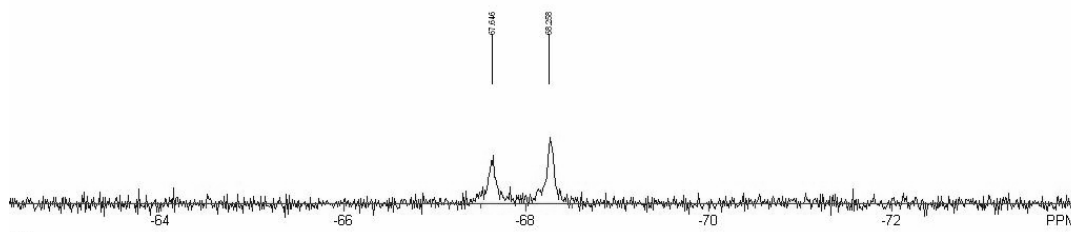


Figure 2.37. ^{29}Si NMR of POSS fulleropyrrolidine **2.12** in CDCl_3

2.11.5 High Resolution ESI Mass Spectrometry

The theoretical and experimental high resolution ESI mass spectrometry results are depicted in **Table 2.9**. The close correlation between the experimental and theoretical provided unequivocal evidence of the desired compounds.

Table 2.9. High resolution ESI mass spectrometry results of POSS fulleropyrrolidines and precursors (synthetic pathway 2)

Compound	Experimental	Theoretical
2.9	963.2536	963.2529
2.10	1047.2541	1047.2529
2.11	1049.3113	1049.3130
2.12	1133.3131	1133.3130
2.13	1774.3790	1774.3739
2.14	1880.3600	1880.3603

2.11.6 Elemental Analysis of POSS Fulleropyrrolidines

The theoretical and experimental elemental analysis results of POSS fulleropyrrolidines **2.13** and **2.14** are depicted in **Table 2.10**. The close correlation between the experimental and theoretical results offered further evidence of formation of the desired compounds.

Table 2.10. Elemental analysis results of POSS fulleropyrrolidines

Compound	Experimental (C, H, N)	Theoretical (C, H, N)
2.13	70.36, 4.48, 0.79	69.81, 5.01, 0.77
2.14	71.70, 4.28, 0.75	70.24, 4.82, 0.78

2.11.7 Optical Properties of POSS Fulleropyrrolidines

2.11.7.1 UV-Vis Spectra of POSS Fulleropyrrolidines

The absorption spectra of the fulleropyrrolidine derivative **2.13** (**Figure 2.38**) exhibited characteristic bands, as previously discussed in **Section 2.9.5.1**, at 432 and 706 nm, with molar extinction coefficients of 2695 and 214, respectively. Analogously, the UV-Vis spectra of **2.14** exhibited absorption maxima at 433 and 704 nm, with molar extinction coefficients of 3028 and 260, respectively.

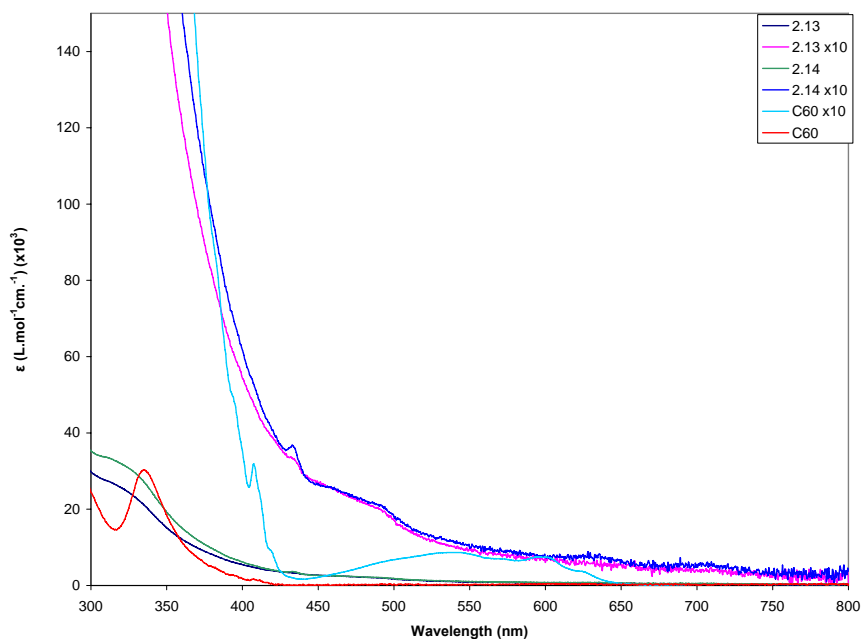


Figure 2.38. UV-Vis absorption spectra of POSS fulleropyrrolidines 2.13 and 2.14 in toluene

2.11.7.2 Steady State Spectrofluorometric Emission Studies of POSS Fulleropyrrolidines

Excitation of **2.13** and **2.14** ($\lambda_{\text{exc}} = 335\text{nm}$) yielded emission bands with maxima at 723 (**2.13**) and 721 nm (**2.14**) (**Figure 2.39**), which correspond to the fullerene excited singlet state emission ($^1\text{C}_{60}^*$), characteristic of a fullerene-based emission.^{68,86-89} The intensity of the emission in **2.13** was 3.5 times that of parent C_{60} , whilst the intensity of the emission in **2.14** was 4.6 times that of parent C_{60} . This was consistent with other fullerene derivatives, including **2.7** and **2.8**, as discussed previously in this chapter, which exhibited emissions ranging from 3 to 4 times the intensity of C_{60} .⁸¹

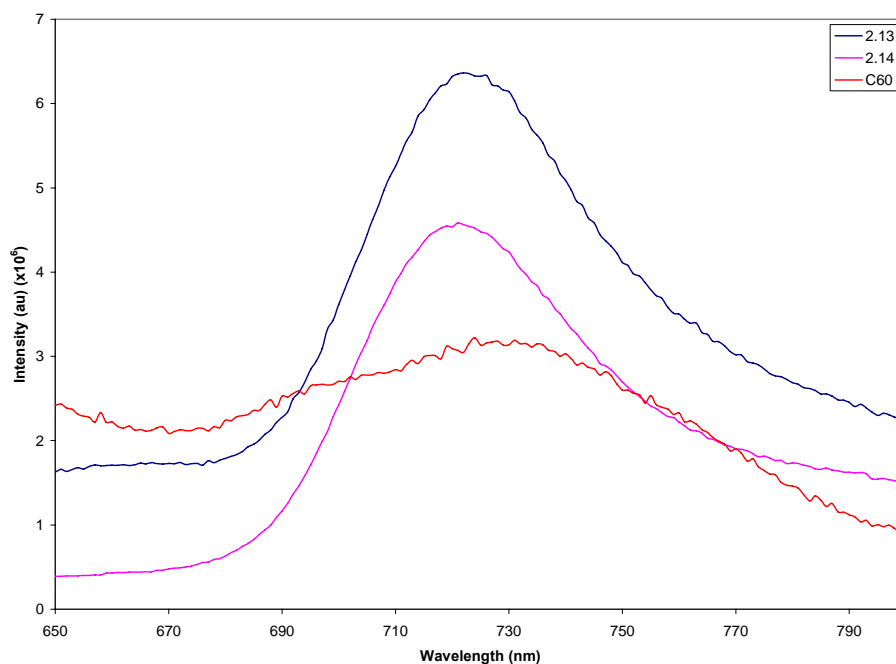


Figure 2.39. Emission spectra of POSS fulleropyrrolidines 2.13 and 2.14 in toluene ($\lambda_{\text{exc}} = 335\text{nm}$)

2.11.7.3 Power Limiting of POSS Fulleropyrrolidines

Figure 2.40 and **Figure 2.41** exhibit the power limiting results obtained for the two compounds. In the two cases examined; for solutions **2.13** and **2.14**, there was distinct power limiting of the transmission with the onset of approximately 200 mJ/cm^2 .

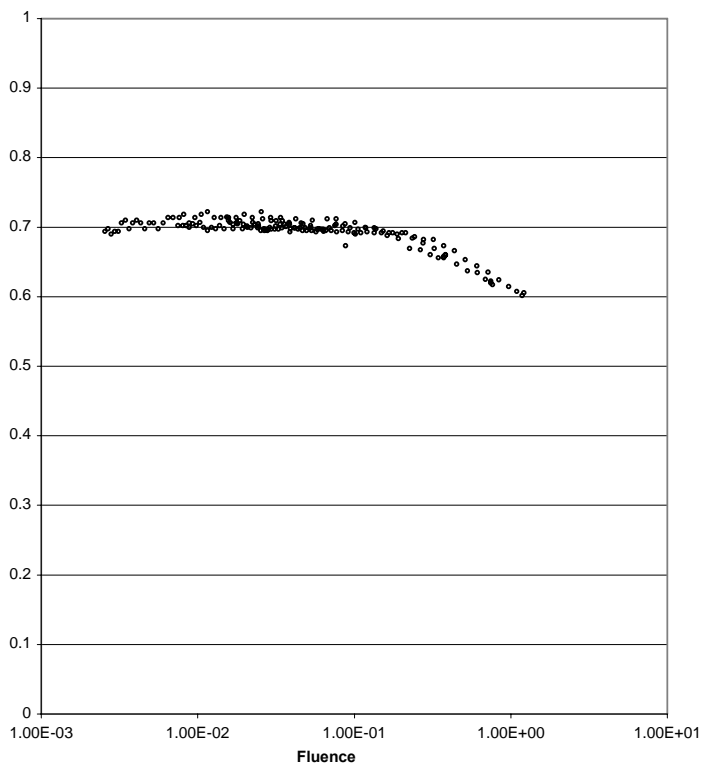


Figure 2.40. Power limiting plot of POSS fulleropyrrolidine 2.13

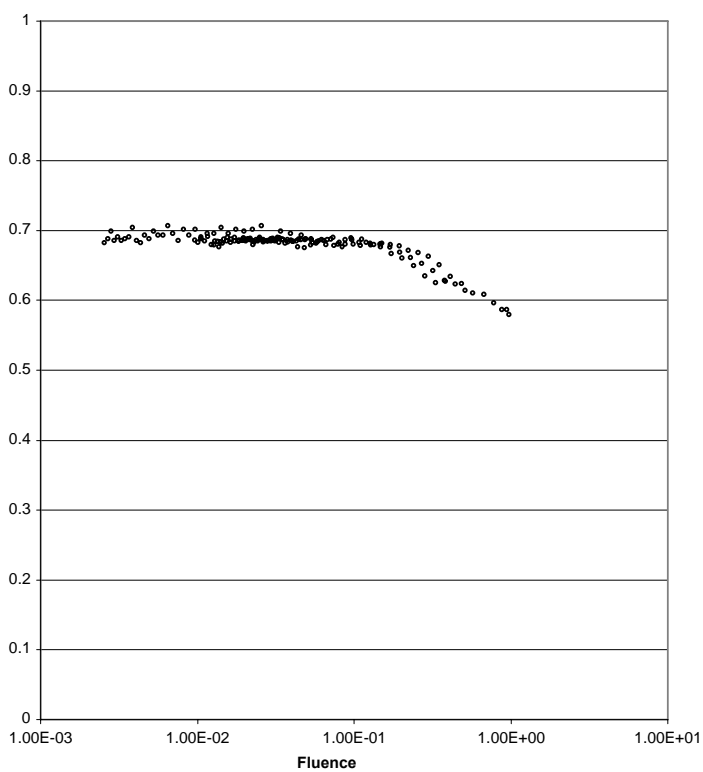


Figure 2.41. Power limiting plot of POSS fulleropyrrolidine 2.14

Strong thermal effects were again seen at fluences above ca 1 J/cm², evident from increased scattering which was contributed to the power limiting effect. The power limiting properties of 2.13 and 2.14 were essentially identical to those of C₆₀. While the results for 2.13 and 2.14 were obtained at higher concentrations by weight, the molar concentrations of C₆₀ and 2.13 and 2.14 were similar, thus leading to comparable number densities of the C₆₀ moieties.

2.12 Iminofullerenes

As discussed previously in **Section 2.3.1**, another widely accessible pathway to fullerene substitution was the generation of iminofullerenes through the addition of alkyl azides to C₆₀. The formation of POSS functionalised iminofullerenes would therefore be achievable through the reaction of POSS azides with C₆₀. POSS azides have been previously synthesised through the ring opening of epoxides by azides and nucleophilic substitution via azide/chloride exchange (**Figure 2.42**).¹⁰⁰

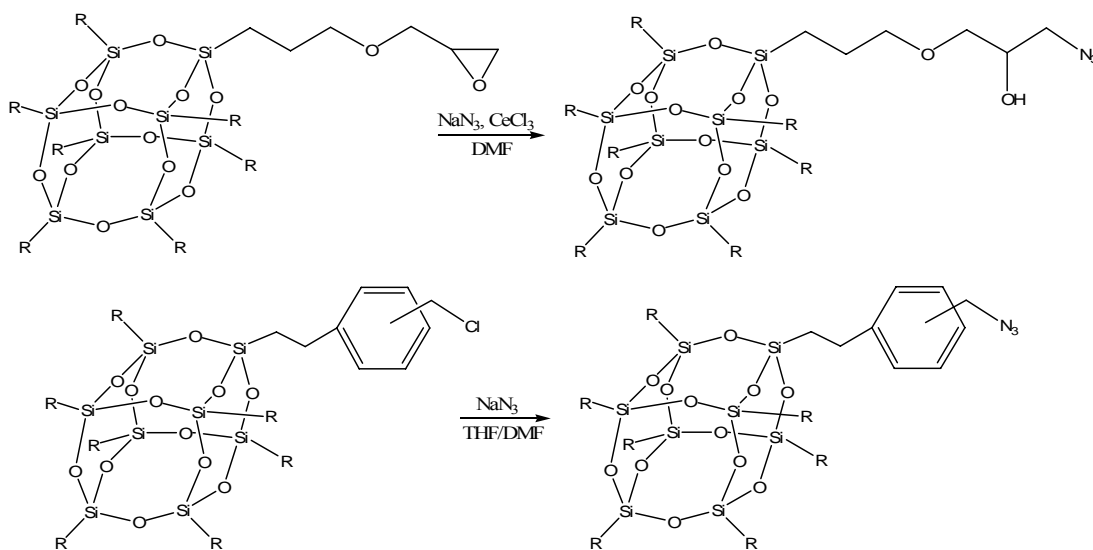


Figure 2.42. Synthesis of literature POSS azides¹⁰⁰

In order to synthesise a mono-functionalised POSS azide, chloride substituted POSS compounds was synthesised.¹⁰⁰ Nucleophilic substitution via halide/azide exchange was then performed by heating with sodium azide in dimethylformamide (**Figure 2.43**).¹⁰⁰

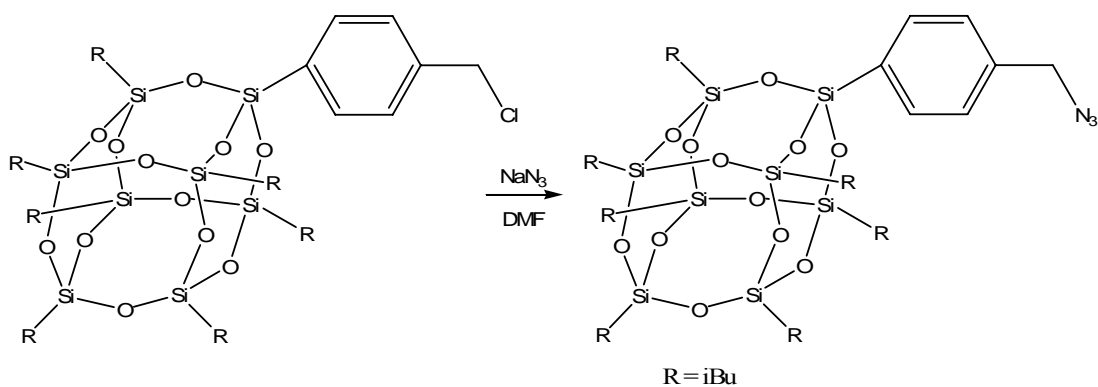


Figure 2.43. Synthesis of POSS azide (2.16)

2.13 Results & Discussion

2.13.1 FTIR

Following reaction with sodium azide, the presence of the azide group was confirmed by FTIR. The azido moiety exhibited a characteristic stretching band at 2099 cm^{-1} .^{100,101}

2.13.2 ^1H NMR

^1H NMR resonances of the POSS iminofullerenes and precursor compounds are detailed in **Table 2.11**.

Table 2.11. ^1H NMR of POSS iminofullerenes and precursor compounds

Compound	iBu	Spacer
2.9	0.58-0.62, 0.93-0.97, 1.85-1.91	4.59, 7.39 d (7.8 Hz), 7.64 d (7.8 Hz) ^a
2.15	0.57-0.67, 0.95-0.99, 1.85-1.93	4.36, 7.33 d (7.8 Hz), 7.69 d (7.8 Hz) ^a
2.16	0.63-0.68, 0.91-0.99, 1.85-1.93	4.98, 7.78-7.80

^a = $^3J_{\text{H-H}}$

2.13.2.1 Mono-benzyl Chloride POSS

As detailed previously in this chapter, ^1H NMR of benzyl chloride POSS (R = iBu, **2.9**) exhibited resonances at δ 0.58-0.62 (14H, CH_2), 0.93-0.97 (42H, CH_3), 1.85-1.91 (7H, CH), 4.59 (2H, CH_2Cl), 7.39 (d, $^3J_{\text{H-H}} = 7.50$ Hz, 2H, CH) and 7.64 (d, $^3J_{\text{H-H}} = 7.50$ Hz, 2H, CH). These resonances were consistent with those detailed in the literature.⁷¹

2.13.2.2 Mono-azide POSS

Mono-azide POSS was synthesised by reaction of **2.9** with sodium azide in dimethylformamide (**Figure 2.43**).¹⁰⁰ ^1H NMR of mono-azide POSS (**2.15**), exhibited resonances of the cage bound isobutyl chains at δ 0.57-0.67 (CH_2), 0.95-0.99 (CH_3) and 1.85-1.93 (CH). The benzyl resonance was displayed at δ 4.36 (CH_2N_3), resulting in an upfield shift of 0.23 ppm in the benzyl CH_2 resonance, relative to the corresponding resonance in **2.9**. This upfield shift occurred due to the increased deshielding effects associated with the higher electron density of the azido moiety, and was consistent with shifts observed in benzyl azide (0.26 ppm)¹⁰¹ and 4-methoxybenzyl azide (0.34 ppm),¹⁰² relative to the corresponding resonances of the chloride precursor. The aromatic resonances were apparent at δ 7.33 (d, $^3J_{\text{H-H}} = 7.8$ Hz, 2H, CH), 7.69 (d, $^3J_{\text{H-H}} = 7.8$ Hz, 2H).

2.13.2.3 POSS Iminofullerene

The reaction of **2.15** with C_{60} in dry, degassed chlorobenzene yielded the desired iminofullerene (**2.16**), following purification via flash chromatography (eluant hexane) (**Figure 2.44**).

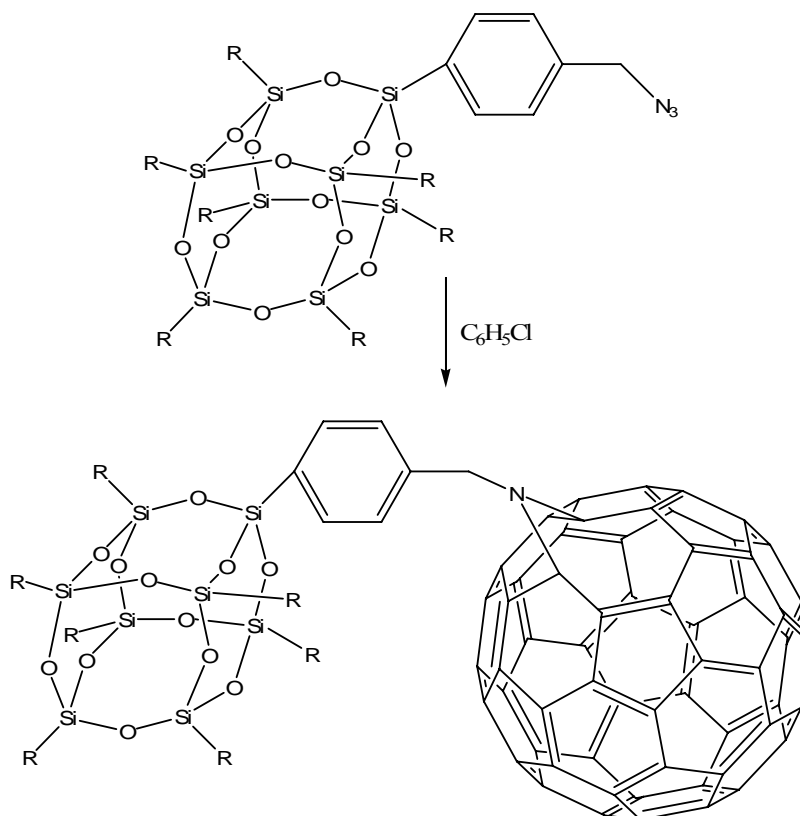


Figure 2.44. Synthesis of POSS iminofullerene (2.16)

¹H NMR of POSS iminofullerene (2.16) (Figure 2.45) exhibited little change in the resonances of the isobutyl chains of the POSS cage, with resonances apparent at δ 0.63-0.68 (CH₂), 0.91-0.99 (CH₃) and 1.85-1.93 (CH). The CH₂N resonance was observed at δ 4.98, resulting in a downfield shift of 0.62 ppm, relative to the corresponding resonance in 2.15. The resonance shift was again attributed to the increased deshielding associated with the presence of the carbon sphere.²⁰ The aromatic resonances were observed as a multiplet from δ 7.78-7.80.

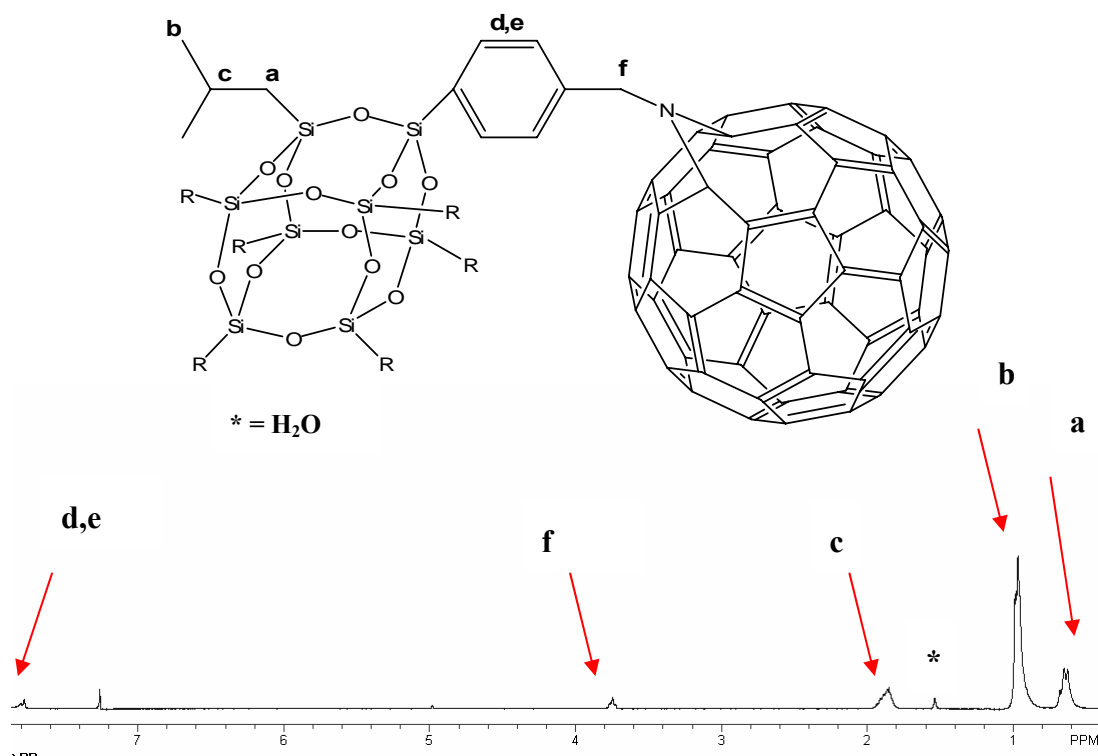


Figure 2.45. ^1H NMR of POSS iminofullerene 2.16 in CDCl_3

2.13.3 ^{13}C NMR

^{13}C NMR resonances of the POSS iminofullerene and precursor compounds are detailed in **Table 2.12**.

2.13.3.1 Mono-benzyl Chloride POSS

^{13}C NMR of **2.9** exhibited resonances at δ 22.37, 22.46, 23.85, 25.69, 46.09 (CH_2Cl), 127.68, 132.13, 134.44 and 139.28 (CH), with these resonances consistent with those evident in the literature.⁷¹

Table 2.12. ^{13}C NMR of POSS iminofullerenes and precursor compounds

Compound	POSS	Spacer	Fullerene
2.9	22.37, 22.46, 23.85, 25.69	46.09, 127.68, 132.13, 134.44, 139.28	-
2.15	22.59, 22.71, 23.28, 23.37, 24.05, 24.12	54.93, 127.48, 134.67, 134.74, 137.55	-
2.16	22.68, 22.74, 24.05, 25.88	68.12	128.52-152.74

2.13.3.2 Mono-azide POSS

^{13}C NMR of **2.15** exhibited the cage bound isobutyl resonances at δ 22.59, 22.71, 23.28, 23.37, 24.05 and 24.14. The benzyl resonance was apparent at δ 54.93, resulting in a downfield shift of 8.84 ppm, relative to the corresponding resonance in **2.9**. This shift was consistent with those exhibited in benzyl azide (8.61 ppm)¹⁰¹ and 4-methoxybenzyl azide (7.85 ppm).¹⁰² Shifts were also present in the aromatic resonances of 0.20 (upfield), 2.54 (downfield), 0.31 (downfield) and 2.27 ppm (upfield), with the resonances apparent at δ 127.48, 134.67, 134.74 and 137.55. Comparable resonance shifts were observed in benzyl azide (0.14, 0.25, 0.23 and 2.14 ppm).¹⁰¹

2.13.3.3 POSS Iminofullerenes

^{13}C NMR of the benzyl derivative (**2.16**) (**Figure 2.46**) exhibited isobutyl resonances at δ 22.68, 22.74, 24.05 and 25.88. The resonance at δ 25.88 (CH_3) was significantly shifted downfield compared to the azide precursor (1.74 ppm), relative to the corresponding resonance in **2.15**. A downfield shift of 13.09 ppm was apparent in the CH_2N resonance, with the resonance evident at δ 68.12. All resonance shifts were associated with the increased deshielding experienced due to the close proximity of the carbon sphere.²⁰

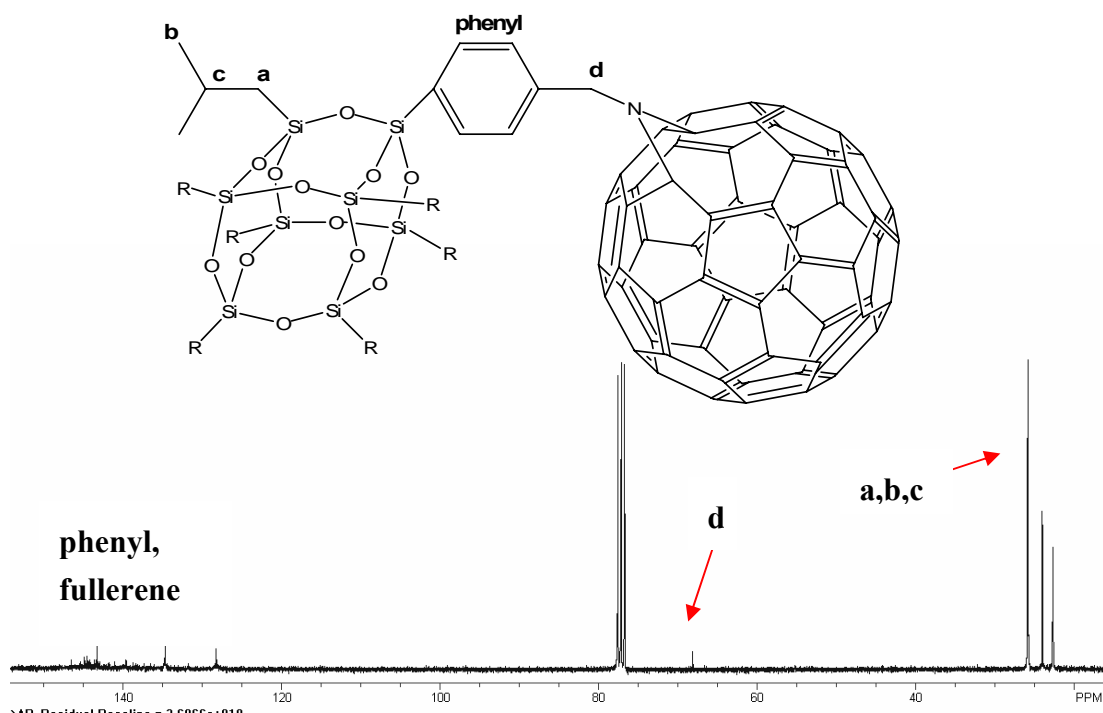


Figure 2.46. ^{13}C NMR of POSS iminofullerene 2.16 in CDCl_3

The iminofullerene structure can be quantified through ^{13}C NMR, as closed [6,6] fullerenes possess two sp^3 type carbons, whilst open [5,6] fullerenes contain only sp^2 type carbons (**Figure 2.47**). Therefore, closed [6,6] fullerenes exhibit a resonance at approximately δ 83 in the sp^3 region, whereas open [5,6] fullerenes exhibit no peaks in this region of the spectra, with all carbons apparent in the sp^2 range.^{20,103} All fullerene resonances were apparent from δ 128.25-152.74, indicating that the iminofullerene was of the open [5,6] type structure.

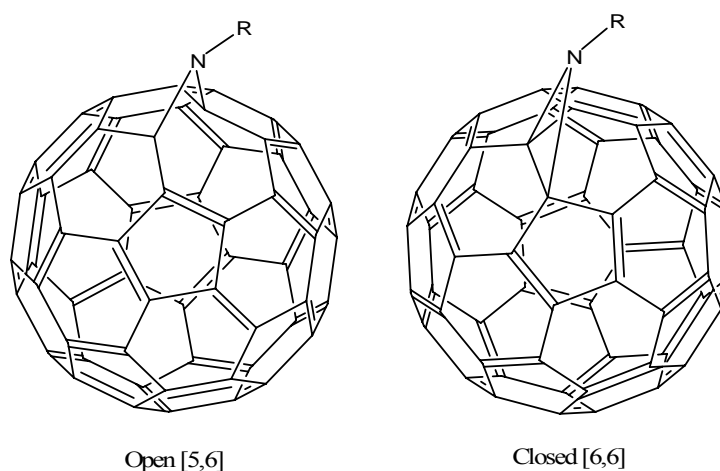


Figure 2.47. Open [5,6] and closed [6,6] iminofullerenes

2.13.4 ^{29}Si NMR

^{29}Si NMR resonances of the POSS iminofullerene and precursor compounds are detailed in **Table 2.13**. All POSS compounds exhibited multiple peaks for the T type silicon atoms, indicative of the mono-functionalisation and the retention of the cage structure during reaction.^{74,80}

Table 2.13. ^{29}Si NMR of POSS iminofullerenes and precursor compounds

Compound	^{29}Si NMR
2.9	-67.97, -68.26, -68.29, -68.49
2.15	-67.58, -68.24
2.16	-67.97, -68.25

The ^{29}Si NMR spectrum of 2.16 is depicted in **Figure 2.48**, with all other spectra being analogous in appearance.

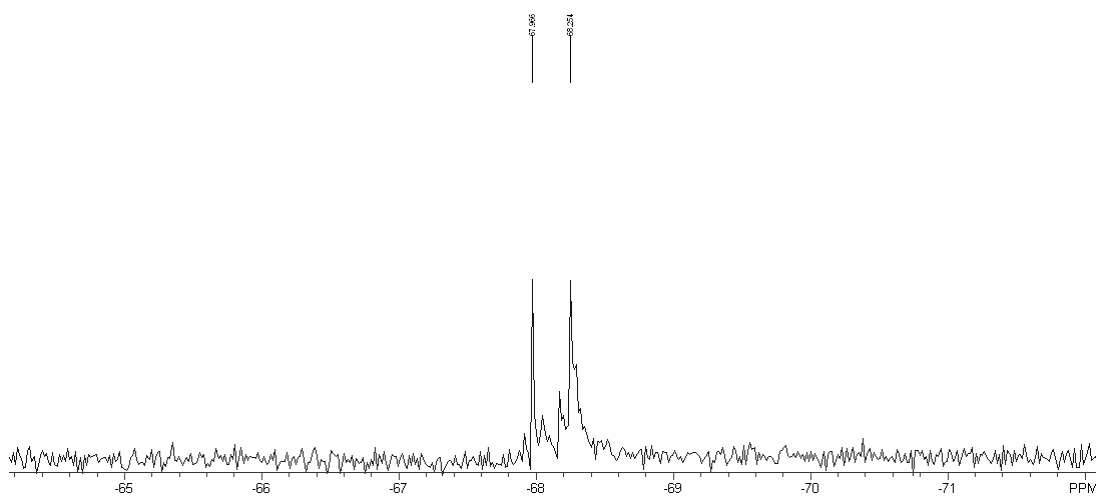


Figure 2.48. ^{29}Si NMR of POSS iminofullerene 2.16 in CDCl_3

2.13.5 High Resolution ESI Mass Spectrometry

The theoretical and experimental high resolution ESI mass spectrometry results are depicted in **Table 2.14**. The close correlation between the experimental and theoretical results offered unequivocal confirmation of the formation of the desired compounds.

Table 2.14. ESI mass spectrometry of POSS iminofullerenes and precursor compounds

Compound	Experimental [M+Na]⁺	Theory [M+Na]⁺
2.9	963.2536	963.2529
2.15	970.2937	970.2933
2.16	1779.0801	1779.0783

2.13.6 Elemental Analysis of POSS Fulleropyrrolidines

The close correlation between the experimental (69.29, 4.14, 0.75) and theoretical (70.78, 3.84, 0.74) elemental analysis results of **2.16** offered further evidence of formation of the desired compounds.

2.13.7 Optical Properties of POSS Iminofullerene

2.13.7.1 UV-Vis Spectrum of POSS Iminofullerene

The reaction of a carbon-carbon bond, located on a [5,6] junction implied that the 60π electron nature of the fullerene core was largely conserved in both open and closed isomers. The UV-Vis spectra of the open [5,6] iminofullerenes thus reveal strong resemblance to the isoelectronic core of C_{60} .¹⁰⁴ The most noticeable deviation of the iminofullerene spectra compared to that of C_{60} (**Figure 2.49**) resides in the low intensity maximum at approximately 698 nm, with a molar extinction coefficient of 138, which referred to the $S_0 \rightarrow {}^*S_1$ transition that characterised the energy of the singlet excited state.¹⁰⁴

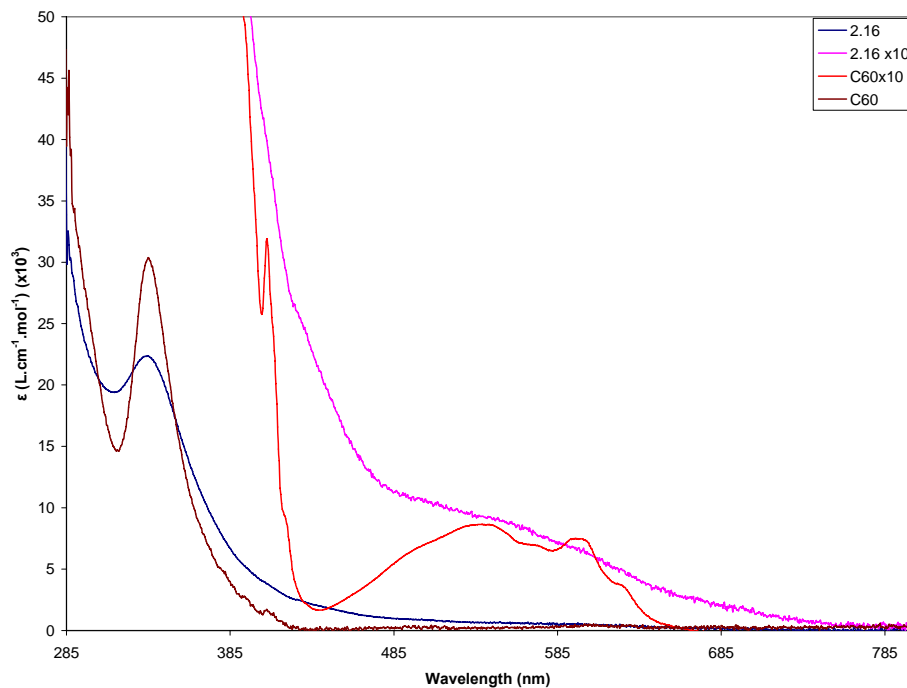


Figure 2.49. UV-Vis spectra of POSS iminofullerene 2.16 in toluene

2.13.7.2 Steady State Spectrofluorometric Emission Studies of POSS Iminofullerene

The fluorescence spectrum of **2.16** (**Figure 2.50**) exhibited an emission band at 726 nm. This broad, weak emission band is characteristic of the [5,6] open structure, whereas closed [6,6] iminofullerenes exhibited emission bands at approximately 680 nm, thus providing further confirmation of the [5,6] open structure.¹⁰⁴ The weakness of the emission, similar in intensity to that of C₆₀, is related to the combination of short singlet lifetime, quantitative intersystem crossing and the symmetry-forbidden nature of the lowest-energy transition.¹⁰⁴

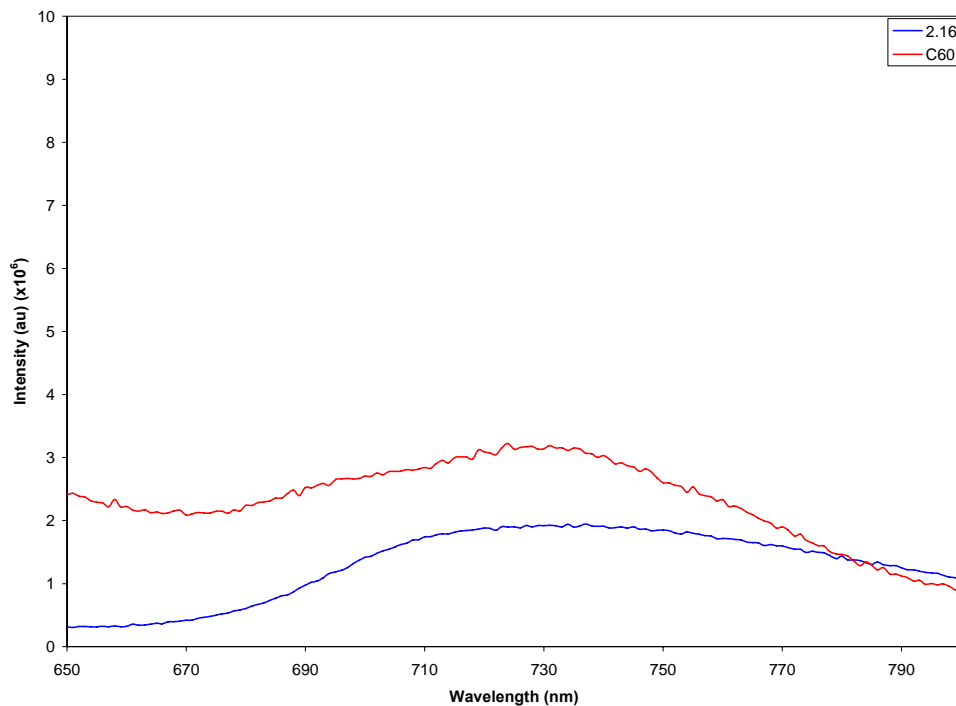


Figure 2.50. Fluorescence spectrum of POSS iminofullerene 2.16 in toluene
 $(\lambda_{\text{exc}} = 335 \text{ nm})$

2.13.7.3 Power Limiting of POSS Iminofullerene

Figure 2.51 exhibits the power limiting results obtained for the iminofullerene compound. A solution of **2.18** displayed distinct power limiting of the transmission with the onset at approximately 200 mJ/cm^2 . Strong thermal effects were again seen at fluences above ca 1 J/cm^2 , evident from increased scattering. The power limiting properties of **2.18** were thus essentially identical to those of C_{60} . While the results for **2.18** were obtained at higher concentrations by weight, the molar concentrations of C_{60} and **2.18** were similar, thus leading to comparable number densities of the C_{60} moieties.

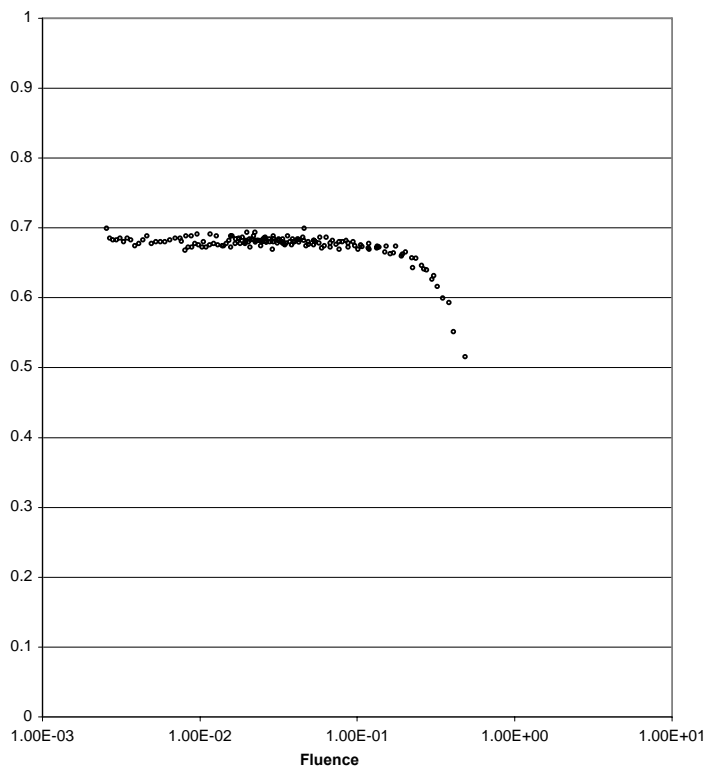


Figure 2.51. Power limiting plot of POSS iminofullerene 2.18

2.14 Conclusions and Future Work

A variety of POSS fullerene compounds have been synthesised through the employment of two synthetic pathways; the cycloaddition of azomethine ylides to C_{60} and the addition of alkyl azides to C_{60} , to generate [6,6] closed fulleropyrrolidines and a [5,6] open iminofullerene. The products were characterised by FTIR, 1H , ^{13}C and ^{29}Si NMR, ESI mass spectrometry and UV-Vis and fluorescence spectrophotometry. Power limiting measurements were performed on the POSS fullerene compounds, all of which exhibited essentially identical power limiting properties to that of C_{60} .

The use of N-functionalised amino acids in the synthesis of POSS fulleropyrrolidines allow for the further functionalisation of the compound with polymerisable functionalities. This would allow the covalent linkage of the POSS fulleropyrrolidine to a range of polymers, the physical and optical properties of which would be able to

be further investigated.

The synthesis of multi-functionalised POSS aldehydes, would allow for the synthesis of multi-fulleropyrrolidino POSS compounds. The use of octa-functionalised aldehydes was not investigated in this project, due to the large excess of aldehyde or azide required for the synthetic pathways of choice. This implied it was extremely unlikely that an octa-substituted product could be formed, with a range of substitutions that would be difficult to isolate the likely products. The use of bis- and tri-substituted POSS aldehydes would allow for the formation of the desired fulleropyrrolidines.

Alternatively, the investigation of different synthetic pathways, such as the addition of unsymmetrical protected malonates, would allow for selective deprotection of one site. DCC mediated coupling would allow for the covalently link the POSS moieties and subsequent deprotection of the other reactive site on the malonates would, in theory, allow for the synthesis of mono-, tri- and possibly octa-functionalised POSS fullerenes, with free reactive sites for the attachment of polymerisable functionalities.

Fullerenes in polymer films or solid matrices display significantly weaker optical limiting responses than in solution. Therefore, in order to maintain a high level of optical limiting response in cross-linked polymeric systems, the attachment of alternative optical limiting compounds to POSS is required.

2.15 References

- (1) H. W. Kroto; J. R. Heath; S. C. O'Brien; R. F. Curl; R. E. Smalley *Nature* **1985**, 318, 162.
- (2) W. Kratschmer; L. D. Lamb; K. Fostiropoulos; D. R. Huffman *Nature* **1990**, 347, 358.
- (3) A. Hirsch *Topics in Current Chemistry* **1999**, 199, 1.
- (4) N. Matsuzawa; D. A. Dixon; T. Fukunaga *J. Phys. Chem* **1992**, 96, 7594.
- (5) A. Alvarez; E. Ochoa; Y. Verdecia; M. Suarez; M. Sola; N. Martin *J. Org. Chem.* **2005**, 70, 3256.
- (6) R. C. Haddon *Science* **1993**, 261, 1545.
- (7) F. Wudl *Acc. Chem. Res.* **1992**, 25, 157.
- (8) F. Wudl; A. Hirsch; K. C. Khemani; T. Suzuki; P.-M. Allemand; A. Koch; H. Eckert; G. Srdanov; H. M. Webb In *Fullerenes: Synthesis, Properties and Chemistry ACS Symposium Series 481*; G. S. Hammond, V. J. Kuck, Eds.; American Chemical Society: Washington D.C., 1992, p 161.
- (9) T. Suzuki; Q. Li; K. C. Khemani; F. Wudl *J. Am. Chem. Soc.* **1992**, 114, 7301.
- (10) F. Diederich; L. Isaacs; D. Philp *Chem. Soc. Rev.* **1994**, 23, 243.
- (11) M. Prato; V. Lucchini; M. Maggini; E. Stimpfl; G. Scorrano; M. Eiermann; T. Suzuki; F. Wudl *J. Am. Chem. Soc.* **1993**, 115, 8479.
- (12) M. Eiermann; F. Wudl; M. Prato; M. Maggini *J. Am. Chem. Soc.* **1994**, 116, 8364.
- (13) R. A. J. Janssen; J. C. Hummelen; F. Wudl *J. Am. Chem. Soc.* **1995**, 117, 544.
- (14) R. Gonzalez; J. C. Hummelen; F. Wudl *J. Org. Chem.* **1995**, 60, 2618.
- (15) M. R. Banks; J. I. Cadogan; I. Gosney; P. K. Hodgson; P. R. R. Langford-Smith *Chem. Comm.* **1995**, 885.
- (16) G. Schick; T. Grosser; A. Hirsch *Chem. Comm.* **1995**, 2289.
- (17) A. B. Smith; H. Tokuyama *Tetrahedron* **1996**, 52, 5257.
- (18) P. P. Kanakamma; Huang, S.-L.; Juo, C.-G.; Her, G.-R.; Luh, T.-Y. *Chem. Eur. J.* **1998**, 4, 2037.
- (19) T. Grösser; Prato, M.; Lucchini, V.; Hirsch, A.; F. Wudl *Angew. Chem. Int. Ed.* **1995**, 34, 1343.
- (20) M. Prato; Q. C. Li; F. Wudl; V. Lucchini *J. Am. Chem. Soc.* **1993**, 115, 1148.
- (21) C. K.-F. Shen; H. Yu; C.-G. Juo; K. M. Chien; G.-R. Her; T.-Y. Kuh *Chem. Eur. J.* **1997**, 3, 744.
- (22) I. Lamparth; B. Nuber; G. Schick; A. Skiebe; T. Grösser; A. Hirsch *Angew. Chem. Int. Ed.* **1995**, 34, 2257.
- (23) G. Schick; A. Hirsch; H. Hauser; T. Clark *Chem. Eur. J.* **1996**, 34, 2257.
- (24) G. X. Dong; J. S. Li; T. H. Chan *Chem. Comm.* **1995**, 1725.
- (25) C. Bellavia-Lund; F. Wudl *J. Am. Chem. Soc.* **1997**, 119, 943.
- (26) J. Averdung; H. Luftmann; J. Mattay; K.-U. Claus; W. Abraham *Tet. Lett.* **1995**, 36, 2957.
- (27) J. C. Hummelen; M. Prato; F. Wudl *J. Am. Chem. Soc.* **1995**, 117, 7003.

- (28) C. K. F. Shen; K. M. Chien; C. G. Juo; G. R. Her; T. Y. Luh *J. Org. Chem.* **1996**, *61*, 9242.
- (29) B. Nuber; F. Hampel; A. Hirsch *Chem. Comm.* **1996**, 1799.
- (30) B. Nuber; A. Hirsch *Chem. Comm.* **1996**, 1421.
- (31) J. C. Hummelen; B. Knight; J. Pavlovich; R. Gonzalez; F. Wudl *Science* **1995**, *269*, 1554.
- (32) D. M. Guldi; S. Gonzalez; N. Martin; A. Anton; J. Garin; J. Orduna *J. Org. Chem.* **2000**, *65*, 1978.
- (33) M. Keshavarez; R. Gonzalez; R. Hicks; G. Srdanov; V. Srdanov; T. Collins; J. C. Hummelen; C. Bellavia-Lund; J. Pavlovich; F. Wudl *Nature* **1996**, *383*, 147.
- (34) M. Cases; M. Duran; J. Mestres; N. Martin; M. Sola *J. Org. Chem.* **2001**, *66*, 433.
- (35) A. Hirsch *Synthesis* **1995**, 895.
- (36) C. Bingel *Chem. Ber.* **1993**, *126*, 1957.
- (37) J.-F. Nierengarten; V. Gramlich; F. Cardullo; F. Diederich *Angew. Chem. Int. Ed.* **1996**, *35*, 2101.
- (38) X. Camps; A. Hirsch *J. Chem. Soc., Perkin Trans. 1* **1997**, 1595.
- (39) M. Maggini; G. Scorrano; M. Prato *J. Am. Chem. Soc.* **1993**, *115*, 9798.
- (40) O. Tsuge; S. Kanemasa *Adv. Het. Chem.* **1989**, *45*, 231.
- (41) M. Maggini; E. Menna In *Fullerenes: From Synthesis to Optoelectronic Properties*; D. M. Guldi, N. Martin, Eds.; Kluwer Academic Publishers: Dordrecht, 2002.
- (42) R. C. Hollins *Curr. Opin. Sol. State Mater. Sci.* **1999**, *4*, 189.
- (43) J. E. Riggs; Y.-P. Sun *J. Phys. Chem. A* **1999**, *103*, 485.
- (44) R. Signorini; R. Bozio; M. Prato In *Fullerenes: From Synthesis to Optoelectronic Properties*; D. M. Guldi, Martin, N., Eds.; Kluwer Academic Publishers: Netherlands, 2002, p 395.
- (45) G. J. Mains; J. M. White *J. Phys. Chem.* **1991**, *95*, 112.
- (46) D. M. Guldi; M. Prato *Acc. Chem. Res.* **2000**, *33*, 695.
- (47) L. Tutt; A. Kost *Nature* **1992**, *356*, 225.
- (48) D. G. McLean; M. C. Brant *Proc. SPIE-Int. Soc. Opt. Eng.* **1993**, *1856*, 162.
- (49) D. G. McLean; R. L. Sutherland; M. C. Bryant; D. M. Brandelik *Opt. Lett.* **1993**, *18*, 858.
- (50) M. I. Joshi; S. R. Mishra; H. S. Rawat; S. C. Mehendale; K. C. Rustagi *Appl. Phys. Lett.* **1993**, *62*, 1763.
- (51) S. R. Mishra; H. S. Rawat; M. P. Joshi; S. C. Mehendale *Appl. Phys. A: Mater. Sci. Process* **1996**, *A63*, 223.
- (52) R. C. Isaac; C. V. Bindhu; S. S. Harilal; G. K. Varier; V. P. N. Nampoore; C. P. G. Vallabhan *Mod. Phys. Lett. B* **1996**, *10*, 61.
- (53) R. C. Isaac; S. S. Harilal; G. K. Varier; C. V. Bindhu; V. P. N. Nampoore; C. P. G. Vallabhan *Opt. Eng.* **1997**, *36*, 332.
- (54) A. Kost; L. Tutt; M. Klein; T. K. Dougherty; W. E. Elias *Opt. Lett.* **1993**, *18*, 334.
- (55) M. Gevaert; P. V. Kamat *J. Phys. Chem.* **1992**, *96*, 9883.
- (56) A. Kost; L. Tutt; M. B. Klein; T. K. Dougherty; W. Elias *Opt. Lett.* **1993**, *18*, 334.
- (57) J. Schell; D. Ohlmann; D. Brinkmann; R. Lévy; M. Joucla; J. L.

- Rehspringer; B. Hönerlage *J. Chem. Phys.* **1999**, *111*, 5929.
- (58) F. Bentivegna; M. Canva; P. Georges; A. Brun; F. Chaput; L. Malier; J.-P. Boilet *Appl. Phys. Lett.* **1993**, *62*, 1721.
- (59) R. Signorini; M. Zerbetto; M. Meneghetti; R. Bozio; M. Maggini; C. De Faveri; M. Prato; G. Scorrano *Chem. Comm.* **1996**, 1891.
- (60) Y. Ba; J. A. Ripmeester *J. Chem. Phys.* **1998**, *108*, 8599.
- (61) A. Kraus; M. Schneider; A. Gügel; K. Müllen *J. Mater. Chem.* **1997**, *7*, 763.
- (62) M. Maggini; C. De Faveri; G. Scorrano; M. Prato; G. Brusatin; M. Guglielmi; M. Meneghetti; R. Signorini; R. Bozio *Chem. Eur. J.* **1999**, *5*, 2501.
- (63) R. Gvishi; J. D. Bhawalker; N. D. Kumar; G. Ruland; U. Narang; P. N. Prasad; B. A. Reinhardt *Chem. Mater.* **1995**, *7*, 2199.
- (64) J. Schell; Felder, D.; J.-F. Nierengarten; J.-L. Rehspringer; R. Levy; B. Honerlage *J. Sol-Gel Sci. Tech.* **2001**, *22*, 225.
- (65) A. Reissova; M. Capka *Synth. React. Inorg. Met. Org. Chem.* **1986**, *16*, 707.
- (66) E. Ntararas; H. Matralisa; G. M. Tsivgoulis *Tet. Lett.* **2004**, *45*, 4389.
- (67) K. Kordatos; M. Prato; E. Menna; G. Scorrano; M. Maggini *J. Sol-Gel Sci. Tech.* **2001**, *22*, 237.
- (68) S. Cattarin; P. Ceroni; D. M. Guldi; M. Maggini; E. Menna; F. Paolucci; S. Roffia; G. Scorrano *J. Mater. Chem.* **1999**, *9*, 2743.
- (69) D. M. Guldi; M. Maggini; S. Mondini; F. Guerin; J. H. Fendler *Langmuir* **2000**, *16*, 1311.
- (70) A. Bianco; F. Gasparri; M. Maggini; D. Misiti; A. Polese; M. Prato; G. Scorrano; C. Toniolo; C. Villani *J. Am. Chem. Soc.* **1997**, *119*, 7550.
- (71) C. M. Leu; Y. T. Chang; K. H. Wei *Macro.* **2003**, *36*, 9122.
- (72) B. W. Manson; J. J. Morrison; P. I. Coupar; P.-A. Jarès; R. E. Morris *J. Chem. Soc., Dalton Trans.* **2001**, 1123.
- (73) Y. Lee; R. B. Silverman *Org. Lett.* **2000**, *2*, 303.
- (74) E. G. Shockey; A. G. Bolf; P. F. Jones; J. J. Schwab; K. P. Chaffee; T. S. Haddad; J. D. Lichtenhan *Appl. Organomet. Chem.* **1999**, *13*, 311.
- (75) Y. Morimoto; K. Ito; M. Yamahiro; K. Watanabe; N. Ootake USA, 2004.
- (76) D. Zhou; L. Gan; H. S. Tan; C. P. Luo; C. H. Huang; J. Q. Pan; M. J. Lu; Y. Wu *Chi. J. Chem.* **1995**, *6*, 1033.
- (77) C. M. Cardona; A. Kitaygorodskiy; A. Ortiz; M. A. Herranz; L. Echegoyen *J. Org. Chem.* **2005**, *70*, 5092.
- (78) Y. Rio; G. Accorsi; H. Nierengarten; J.-L. Rehspringer; B. Hönerlage; G. Kopitkovas; A. Chugreev; A. Van Dorselaer; N. Armaroli; Nierengarten, J.-F. *New J. Chem.* **2002**, *26*, 1146.
- (79) B.-H. Ye; Y. Narutaa *Tetrahedron* **2003**, *59*, 3593.
- (80) C. Marcolli; G. Calzaferri *Appl. Organometal. Chem.* **1999**, *13*, 213.
- (81) S. K. Lin; L. L. Shiu; K. M. Chien; T. Y. Luh; T. I. Lin *J. Phys. Chem.* **1995**, *99*, 105.
- (82) D. Kim; M. Lee; Y. D. Suh; S. K. Kim *J. Am. Chem. Soc.* **1992**, *114*, 4429.
- (83) R. V. Bensasson; E. Bienvenüe; C. Fabre; J.-M. Janot; E. J. Land; S. Leach; V. Leboulle; A. Rassat; S. Roux; P. Seta *Chem. Eur. J.* **1998**, *4*, 270.
- (84) S. Leach; M. Vervloet; A. Despres; E. Breheret; J. P. Hare; T. J. Dennis; H. W. Kroto; R. Taylor; D. R. M. Walton *Chem. Phys.* **1992**, *160*, 451.

- (85) M. Meneghetti; R. Signorini; M. Zerbetto; R. Bozio; M. Maggini; G. Scorrano; M. Prato; G. Brusatin; E. Menegazzo; M. Guglielmi *Synth. Met.* **1997**, *86*, 2353.
- (86) D. M. Guldi; Asmus, K. D. *J. Phys. Chem. A* **1997**, *101*, 1472.
- (87) Y. Zhao; Y. Fang; Y. Jang *Spectrochim. Acta A* **2006**, *64*, 564.
- (88) R. M. Williams; J. M. Zwier; J. W. Verhoeven *J. Am. Chem. Soc.* **1995**, *117*, 4093.
- (89) R. M. Williams; M. Koeberg; J. M. Lawson; Y. Z. An; Y. Rubin; M. N. Paddon-Row; J. W. Verhoeven *J. Org. Chem.* **1996**, *61*, 5055.
- (90) Y. Zhao; Y. Fang *J. Phys. Chem. B* **2004**, *108*, 13586.
- (91) D. H. Williams; I. Fleming *Spectroscopic Methods in Organic Chemistry*; Fifth ed.; McGraw-Hill: Berkshired, 1995.
- (92) J.-F. Nierengarten; T. Gu; G. Hadziioannou; D. Tsamouras; V. Krasnikov *Helv. Chim. Acta* **2004**, *87*, 2948.
- (93) J.-F. Eckert; J.-F. Nicoud; J.-F. Nierengarten; S. G. Liu; L. Echegoyen; F. Barigelletti; N. Armaroli; L. Ouali; V. Krasnikov; G. Hadziioannou *J. Am. Chem. Soc.* **2000**, *122*, 7467.
- (94) T. Gu; C. Bourgogne; J.-F. Nierengarten *Tet. Lett.* **2001**, *42*, 7249.
- (95) P. de la Cruz; A. de la Hoz; L. M. Font; F. Langa; M. C. Perez-Rodriguez *Tet. Lett.* **1998**, *39*, 6053.
- (96) B. Illescas; M. A. Martinez-Grau; M. I. Torres; J. Fernandez-Gadea; N. Martin *Tet. Lett.* **2002**, *43*, 4133.
- (97) M. D. L. de la Torre; G. L. Marcorin; G. Pirri; A. C. Tome; A. M. S. Silva; J. A. S. Cavaleiro *Tet. Lett.* **2002**, *43*, 1689.
- (98) M. Suarez; Y. Verdecia; B. Illescas; R. Martinez-Alvarez; A. Alvarez; E. Ochoa; C. Seoane; N. Kayali; N. Martin *Tetrahedron* **2003**, *59*, 9179.
- (99) F. Ajamaa; T. M. F. Duarte; C. Bourgogne; M. Holler; P. W. Fowler; J.-F. Nierengarten *Eur. J. Org. Chem.* **2005**, *17*, 3766.
- (100) L. Petraru; W. H. Binder *Polym. Prepr.* **2005**, *46*, 841.
- (101) Y. Ju; D. Kumar; R. S. Varma *J. Org. Chem.* **2006**, *71*, 6697.
- (102) U. Sirion; H. J. Kim; J. H. Lee; J. W. Seo; B. S. Lee; S. J. Lee; S. J. Oh; D. Y. Chi *Tet. Lett.* **2007**, *48*, 3953.
- (103) S. Xiao; Y. Li; H. Fang; H. Li; H. Liu; L. Jiang; D. Zhu *Synth. Met.* **2003**, *135*, 839-840.
- (104) D. M. Guldi; H. Hungerbuhler; I. Carmichael; K. D. Asmus; M. Maggini *J. Phys. Chem. A* **2000**, *104*, 8601.

3 POSS IMIDES

3.1 Outline

This chapter describes the synthetic routes for the covalent attachment of a range of UV and fluorescent aromatic moieties to the periphery of POSS cages. Functionalities of interest included benzene (phthalic), naphthalene, biphenyl and perylene (**Figure 3.1**). These particular groups were chosen as a result of the synthetic method of choice involving tetracarboxylic dianhydrides, and also to encompass a range of both absorptive and fluorescent functional groups.

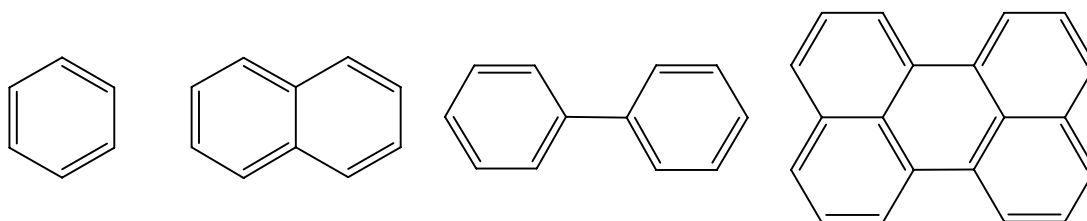


Figure 3.1. Benzene, naphthalene, biphenyl and perylene functional groups

This chapter details a review of the properties and functionalisation of perylene and the other functional groups, benzene, naphthalene and biphenyl. The synthesis and characterisation of phthalic, naphthalic, biphenyl and perylene functionalised POSS imides is detailed, followed by discussion of the single crystal x-ray crystal structure of the perylene derivative. Full experimental conditions and general characterisation techniques used and sample data are detailed in **Chapter 6**.

3.2 Perylenes

Perylenes are colourants which have recently received considerable attention in both academic and industrial dye and pigment research.^{1,2} In the 1950's several perylene compounds were used as pigments in products such as automotive finishes, due to their insolubility, migrational stability, light- and weather- fastness, thermal stability, chemical strength and high tinctorial strength, with hues ranging from red to black.² More recently, perylenes have been used in electronic applications where they are

among the best available *n*-type semiconductors.^{3,4} The *n*-type semi-conductivity is related to the high electron affinity of the rylene bis-imide dyes,⁵ making the rylene bis-imide family promising for use as organic field transistors.⁶ Perylene bis-imides also possess a unique combination of optical, redox and stability properties, which have led to them being investigated in electrophotography⁷ and photovoltaics.⁸

Perylene bis-imides are intrinsically insoluble, therefore their potential as fluorescent dyes was only uncovered in 1959, with the study detailing their high fluorescence quantum yields and photostability.⁹ As a result of these properties, perylene monoamide and bis-imide dyes have proved to be among the best fluorophores available for single molecule spectroscopy.¹⁰

3.2.1 Perylenes Incorporated into Sol-gel Matrices

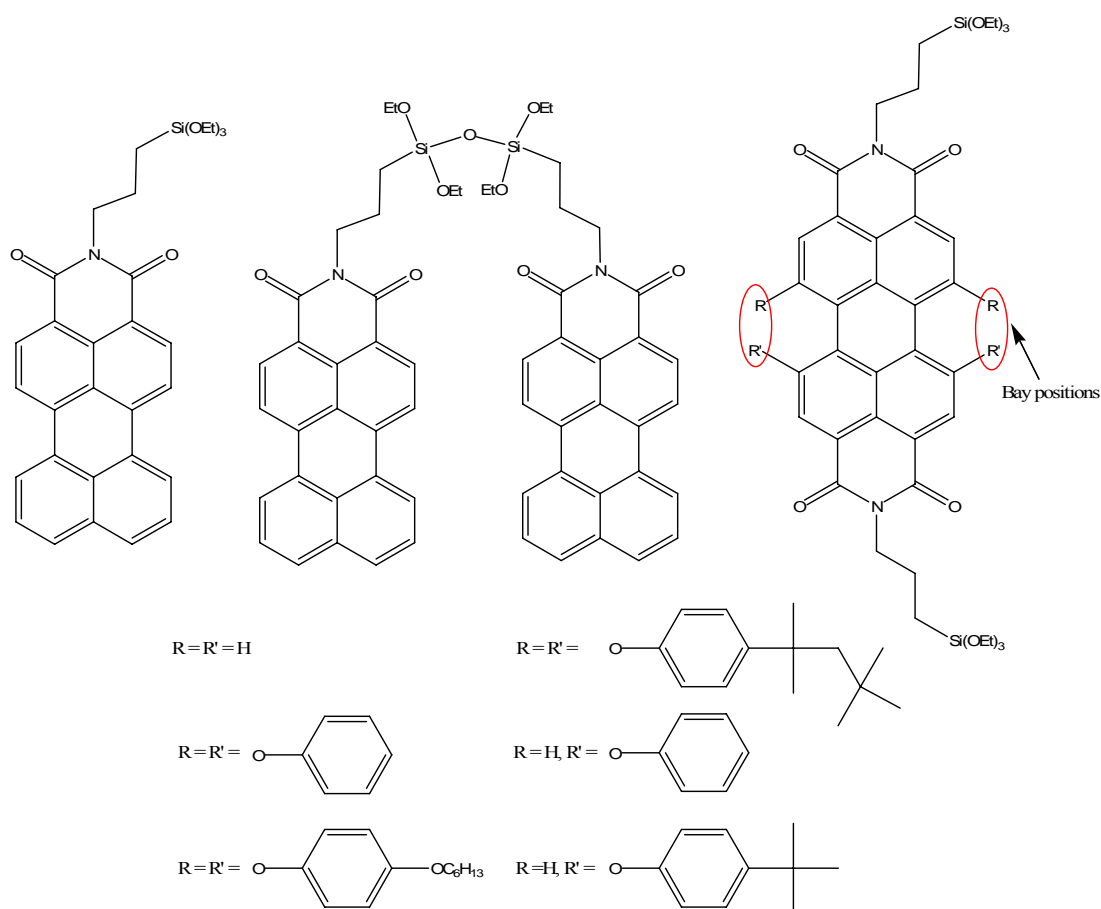


Figure 3.2. Ethoxysilane substituted perylene derivatives¹¹

A range of mono- and bis-imide perylenes have previously been incorporated into sol-gel matrices through the covalent attachment of trimethoxysilane moieties (**Figure 3.2**).¹¹ Substitution in the bay positions, i.e. the 1, 6, 7 and 12 positions of perylenetetracarboxy diimides led to an increase in dye concentration in the sol-gel matrix, due to the increased solubility of the perylene.

Thin sol-gel films, doped with Perylene Orange (**Figure 3.3**) have also been prepared.^{12,13} Perylene Orange was primarily used as a structural probe in order for obtaining a better understanding of the properties of the sol-gel films, such as porosity and structural characteristics.

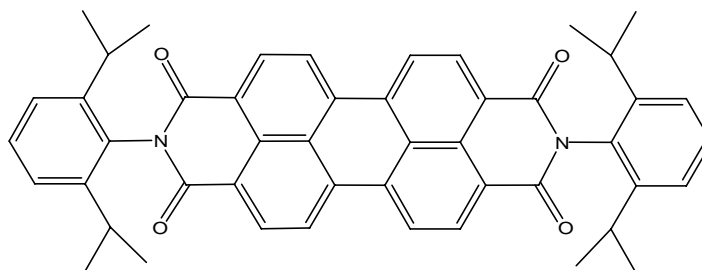


Figure 3.3. Structure of Perylene Orange^{12,13}

The reaction of 3-aminopropyltriethoxysilane with perylenetetracarboxylic dianhydride yielded the diimide-bridged silsesquioxane (**Figure 3.4**), which self-assembled into a superlong tubular structure, with highly ordered lamellar mesostructure in the tube walls, upon crystallisation from acetone.¹⁴

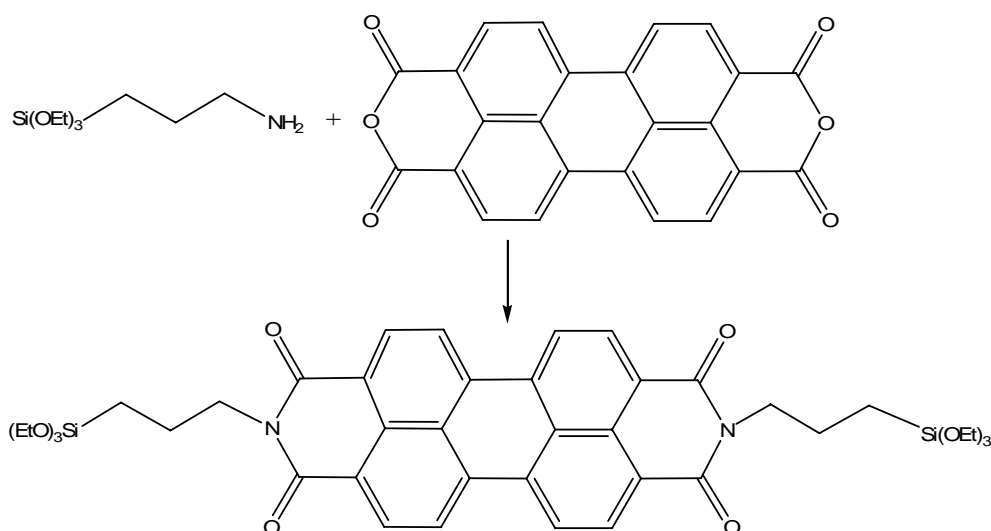


Figure 3.4. Synthesis of bis-(propyltriethoxysilyl)perylene diimide¹⁴

Self assembly occurred due to the combination of π - π interactions between the perylene diimide cores and the solvophilic interactions of the triethoxysilane moiety (**Figure 3.5**).

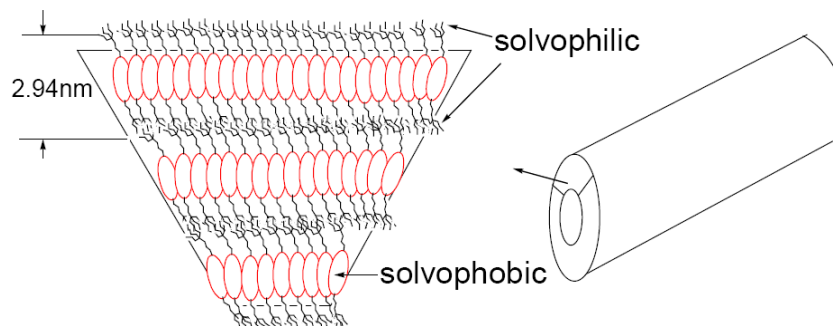


Figure 3.5. Self-assembly of bis(propyltriethoxysilyl)perylene diimide¹⁴

3.2.2 Other Anhydrides

A variety of other anhydrides have also been functionalised with triethoxysilane moieties for incorporation into sol-gel matrices. Condensation of allylamine with benzene-1,2,4,5-tetracarboxylic dianhydride was used by Rousseau *et. al.*¹⁵ to synthesise the bis-allyl derivative. Subsequent hydrosilylation with trimethoxysilane, in the presence of a platinum catalyst, yielded the bis-triethoxysilane compound (**Figure 3.6**). Similar reactions have been reported for other anhydrides, such as phthalic anhydride and naphthalic anhydride.¹⁶

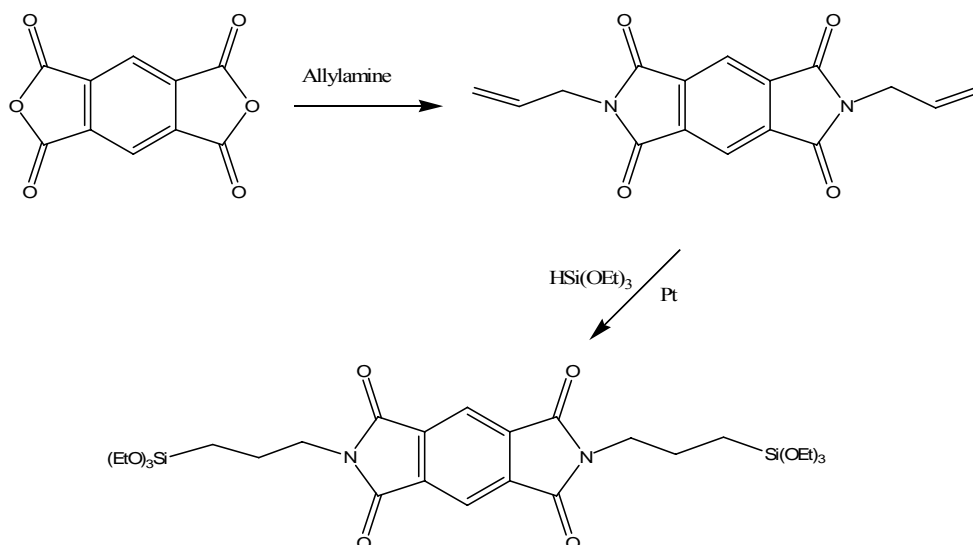


Figure 3.6. Synthesis of bis(propyltriethoxysilyl)phthalic diimide¹⁵

The smallest representatives of the conjugated aromatic dyes, naphthalene bis-imides, generally exhibit a colourless, nonfluorescent π system, which has been extensively applied in supramolecular chemistry,^{17,18} DNA intercalation,¹⁹ electrically conductive aggregates²⁰ and as the active layer in organic field effect transistors.²¹ Naphthalene bis-imides also possess high thermal and photostability.²²

Biphenyl dianhydrides are widely employed to increase the solubility of polyimides without sacrificing the excellent polyimide mechanical properties. Biphenyl dianhydrides also exhibit strong absorption in the UV.²³

3.3 POSS Imides

A significant drawback for perylene dyes was the tendency for formation of dye aggregates due to the presence of the extended π systems.^{24,25} The prevention of aggregation in conjugated chromophores and polymers, such as carbazole,²⁶ terfluorene²⁷ and polyfluorenes²⁷⁻³¹ through the incorporation of POSS cages has previously been investigated. An analogous study of the aggregation of POSS bound perylene moieties in the solid state was therefore of interest.

POSS polyimides exhibit enhanced thermal stability and improved mechanical properties.^{32,33} It was envisaged that the anhydrides investigated in this chapter could, in future work, be condensed with multi-amino POSS systems combined with additional anhydride or amino systems to synthesise a range of optically active polyimides.

The ready availability of functionalised anhydrides, which are able to undergo condensation with amines to form imides, implied that the easiest route to POSS imides required an amino functionality on the periphery of the POSS cage. The formation of monosubstituted POSS amines has previously been achieved through the condensation of 3-aminopropyltriethoxysilane with $i\text{Bu}_7\text{Si}_7\text{O}_9(\text{OH})_3$ in the presence of tetrabutylammonium hydroxide as a catalyst, to yield $i\text{Bu}_7\text{Si}_7\text{O}_{12}(\text{CH}_2\text{CH}_2\text{CH}_2\text{NH}_2)$ [mono(3-aminopropyl)POSS] (**Figure 3.7**).³⁴

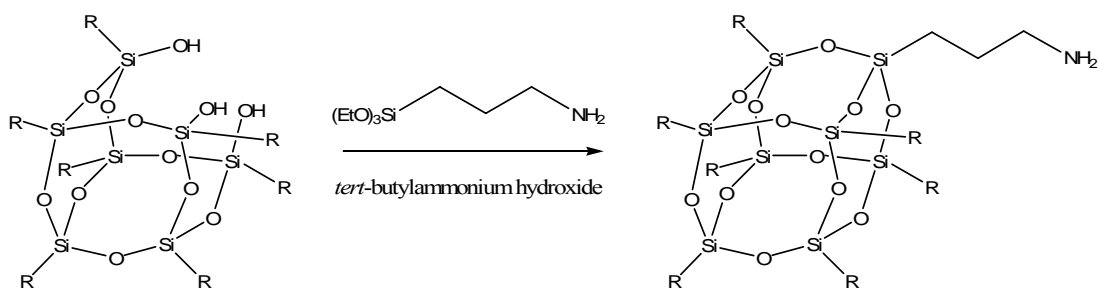


Figure 3.7. Synthesis of mono(3-aminopropyl)POSS³⁴

Octa(chloroammoniumpropyl)POSS has also been previously synthesised through the hydrolytic condensation of (3-aminopropyl)triethoxysilane in methanol and hydrochloric acid, and exists as the octa-hydrochloride salt (**Figure 3.8**).³⁵⁻³⁷

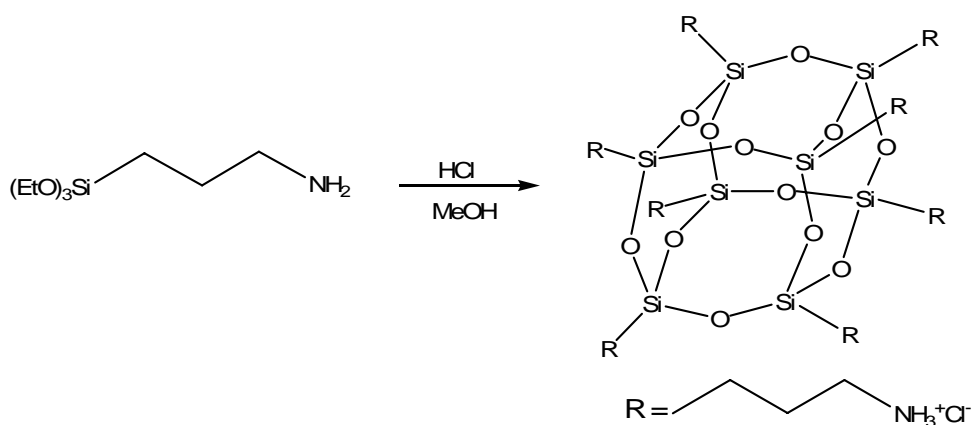


Figure 3.8. Synthesis of octa(chloroammoniumpropyl)POSS³⁵⁻³⁷

The reaction of POSS amines with a variety of mono- and bis-anhydrides, including succinic anhydride (**Figure 3.9**),³⁶ maleic anhydride,^{38,39} phthalic anhydride, benzene-1,2,4,5-tetracarboxylic dianhydride,^{32,33,40,41} naphthalenetetracarboxylic dianhydride⁴² and perylenetetracarboxylic dianhydride⁴² have previously been reported. A variety of POSS amines have been employed, including octa(aminopropyl)POSS,³⁶ octa(aminophenyl) POSS,^{32,33,38,41} mono-(3-aminopropyl)POSS,⁴² $\text{Cp}_7\text{Si}_8\text{O}_{12}(\text{C}_6\text{H}_4\text{CH}_2\text{OC}_6\text{H}_4\text{NH}_2)$ ⁴⁰ and $\text{Cp}_7\text{Si}_8\text{O}_{12}[\text{C}_6\text{H}_4\text{CH}_2\text{OC}_6\text{H}_4\text{CH}(p\text{-NH}_2\text{C}_6\text{H}_4)_2]$.⁴³ Polyimides have also been synthesised through the reaction of octa(aminophenyl)POSS with bis-anhydrides, such as benzenetetracarboxylic dianhydride⁴⁰ and 3,3',4,4'-benzophenonetetracarboxylic dianhydride.^{32,44}

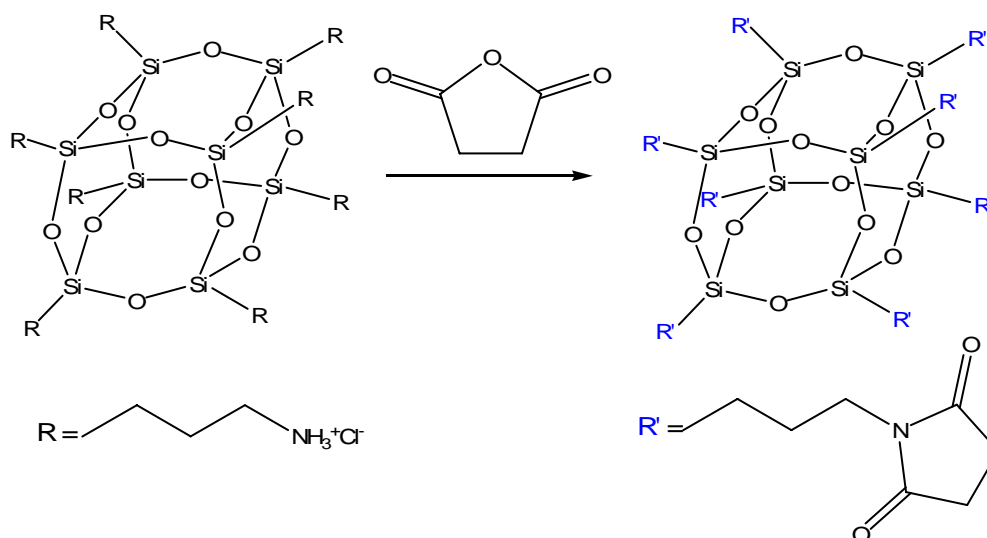


Figure 3.9. Synthesis of octa(propylsuccinimide) POSS³⁶

3.4 Synthesis

The reactions of a variety of mono- and bis- anhydrides with mono- and octa-substituted POSS amines are discussed herein. The condensation of the desired anhydrides with a large stoichiometric excess (approximately 4 fold) of mono-amino POSS was performed with the use of microwave radiation^{45,46} in imidazole.⁴⁷ Thermal condensation of amino POSS with a range of bis-anhydrides, including perylene, naphthalene and biphenyl have recently been reported,⁴² however the use of microwave radiation enabled the synthesis of the desired POSS imides to be achieved in a greatly reduced timeframe. Purification was achieved by washing with dilute hydrochloric acid and water, followed by column chromatography (eluant hexane/chloroform), to yield the desired POSS imide. Anhydrides reacted with the amino-POSS derivatives included phthalic anhydride, benzene-1,2,4,5-tetracarboxylic dianhydride, 1,8-naphthalic anhydride, naphthalic-1,4,5,8-tetracarboxylic dianhydride, 3,3',4,4'-biphenyl tetracarboxylic dianhydride and perylene-3,4,9,10-tetracarboxylic dianhydride.

3.5 Characterisation

Characterisation was performed by FTIR, ^1H , ^{13}C and ^{29}Si NMR, UV-VIS and fluorescence spectrophotometry, ESI mass spectrometry and single crystal x-ray crystallography, the details of which are discussed in **Chapter 6**.

3.6 Results & Discussion

3.6.1 FTIR

FTIR spectra of the POSS imides exhibited a new band at approximately 1465 cm^{-1} for the mono and bis- POSS derivatives, and 1410 cm^{-1} for the octa-phthalic POSS imide (**3.5**), assigned to the stretching mode of the C-N bond in the imide functionality.^{14,48} The POSS imides exhibited a carbonyl stretching band from 1700 to 1727 cm^{-1} , with the second carbonyl stretching band only present in the bis-naphthalic (**3.7**) and perylene (**3.9**) imides at 1672 and 1663 cm^{-1} .⁴⁹ The FTIR bands of interest of the POSS imides are detailed in **Table 3.1**.

Table 3.1. FTIR of POSS Imides

Compound	$\nu(\text{C=O})^{50}$	$\nu(\text{C-N})^{50}$
3.2 (mono-phthalic)	1719	1465
3.3 (bis-phthalic)	1727	1465
3.5 (octa-phthalic)	1713	1415
3.6 (mono-naphthalic)	1703	1465
3.7 (bis-naphthalic)	1709, 1672	1465
3.8 (bis-biphenyl)	1706	1465
3.9 (bis-perylene)	1700, 1663	1465

3.6.2 ^1H NMR

The ^1H NMR resonances of all the POSS imide compounds are summarised in **Table 3.2**.

Table 3.2. ¹H NMR of POSS imides

Compound	iBu CH ₂	iBu CH ₃	iBu CH	SiCH ₂	CH ₂	CH ₂ N	Aromatic
3.1	0.58-0.61	0.95 d (6.6 Hz) ^a	1.80-1.92	Obs.	1.50-1.58	2.67 t (7.2 Hz) ^a	
3.2	0.57-0.65	0.92-0.96	1.78-1.87	Obs.	Obs.	3.67 t (7.2 Hz) ^a	7.69-7.72, 7.84-7.86
3.3	0.57-0.65	0.92-0.96	1.80-1.90	Obs.	Obs.	3.72 m	8.27
3.4	-	-	-	0.80 t (7.2 Hz) ^a	1.77 p (7.2 Hz) ^a	2.99 t (7.2 Hz) ^a	
3.5	-	-	-	0.62-0.68	1.69-1.80	3.59-3.64	7.57-7.61, 7.64 - 7.68
3.6	0.57-0.61	0.93-0.96	1.79-1.90	0.70-0.76	Obs.	4.15 t (6.6 Hz) ^a	7.73 t (7.8 Hz) ^a , 8.18 dd (8.4 Hz) ^a (0.9 Hz) ^b , 8.58 dd (7.8 Hz) ^a (0.9 Hz) ^b
3.7	0.57-0.61	0.92-0.96	1.84 n (6.3 Hz) ^a	0.69-0.75	Obs.	3.67 t (7.2 Hz) ^a	8.76
3.8	0.57-0.61	0.93-0.96	1.85 n (6.3 Hz) ^a	Obs.	Obs.	3.70 t (7.2 Hz) ^a	7.97, 8.10
3.9	0.54-0.59	0.93	1.83-1.90	Obs.	Obs.	4.20 m	8.60

^a = ³J_{H-H}, ^b = ²J_{H-H}

3.6.2.1 Mono-(3-aminopropyl) POSS

Mono-(3-aminopropyl) POSS (**3.1**) was synthesised according to the procedure detailed by Carsten and Adolf.³⁴ The ¹H NMR spectrum exhibited resonances of the cage bound isobutyl groups at δ 0.58-0.61 (16H, SiCH₂/iBu CH₂), 0.95 (42H, iBu CH₃) and 1.80-1.92 (7H, iBu CH). The propyl chain SiCH₂ resonance was obscured, with the remaining propyl resonances evident at δ 1.50-1.58 (2H, CH₂) and 2.67 (t, ³J_{H-H} = 7.2 Hz, 2H, CH₂N). The resonances were consistent with those reported in the literature.³⁴

3.6.2.2 Mono-phthalic POSS Imide

The synthesis of mono-phthalic POSS imide (**3.2**) is depicted in **Figure 3.10**.

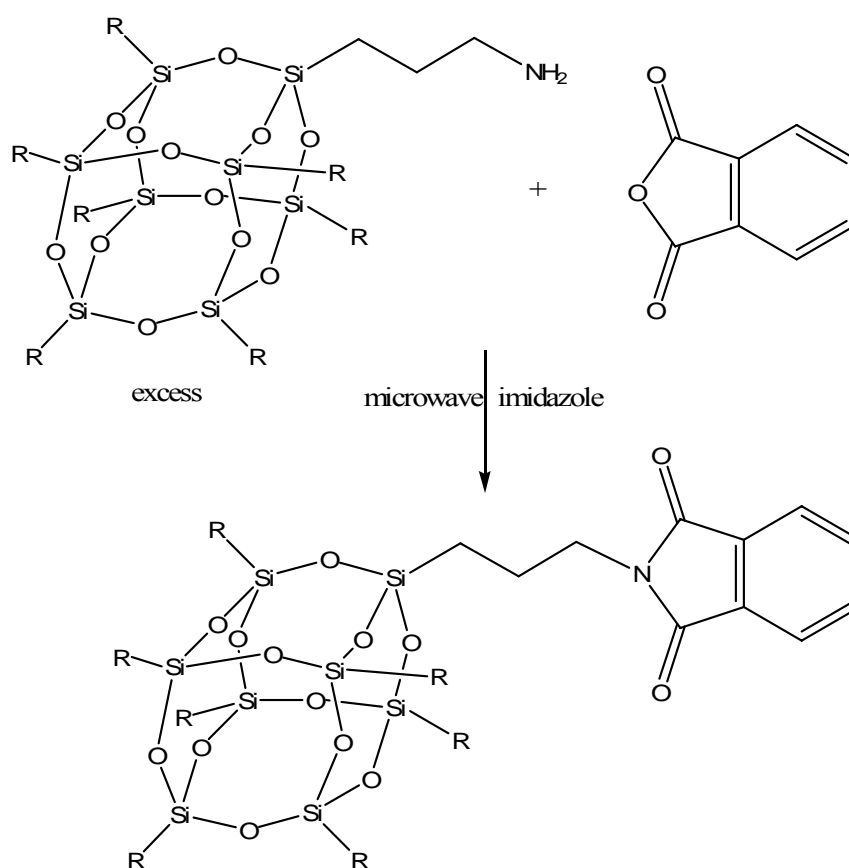


Figure 3.10. Synthesis of mono-phthalic POSS imide (**3.2**)

The ^1H NMR spectrum displayed little change in the resonances of the isobutyl chains of the POSS cage with resonances apparent at δ 0.57-0.65 (16H, $\text{SiCH}_2/\text{iBu CH}_2$), 0.92-0.96 (42H, iBu CH_3) and 1.78-1.87 (9H, $\text{CH}_2/\text{iBu CH}$). Resonances of the propyl chain were obscured, with the exception of the CH_2N resonance, which was shifted downfield by 1 ppm to δ 3.67, relative to the corresponding resonance in mono-(3-aminopropyl)POSS. The aromatic resonances were evident as multiplets at δ 7.69-7.72 (2H, CH) and 7.84-7.86 (2H, CH).

Comparable resonance shifts in similar compounds have been reported in the literature. One such example is N-[3-(isobutylPOSS)propyl]bis(benzyloxybenzamide) (**Figure 3.11**),⁵¹ which exhibited a downfield shift in the CH_2N resonance of 0.75 ppm, relative to mono(3-aminopropyl)POSS.

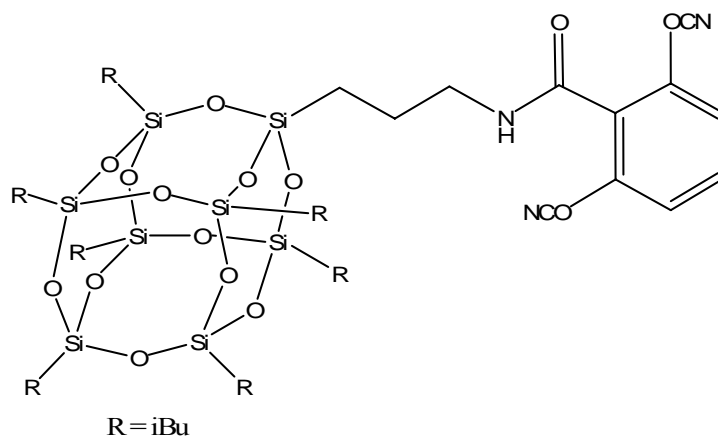


Figure 3.11. Structure of N-[3-(isobutylPOSS)propyl]bis(benzyloxybenzamide)⁵¹

A comparable shift in the CH_2N resonance (0.92 ppm) was exhibited in the ^1H NMR of the bis-phthalic propyltriethoxysilane derivative, the synthesis of which was detailed in **Section 3.2.1**, relative to (3-aminopropyl)triethoxysilane.¹⁵ The ^1H NMR spectrum of **3.2** is depicted in **Figure 3.12**, with the ^1H NMR spectra of all other POSS imide derivatives being analogous in appearance.

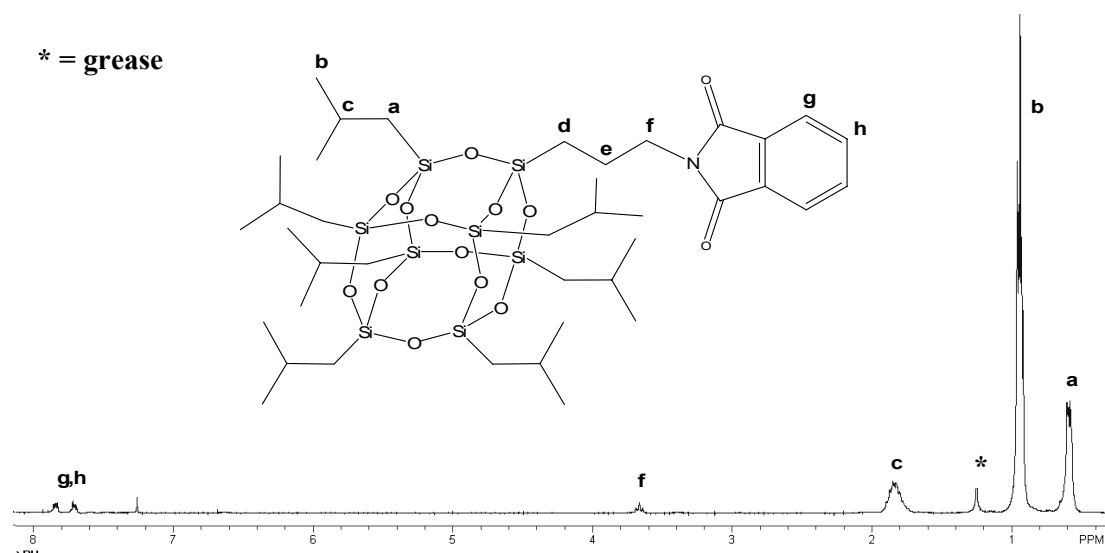


Figure 3.12. ¹H NMR of mono-phthalic POSS imide 3.2 in CDCl₃

3.6.2.3 Bis-phthalic POSS Imide

The synthesis of bis-phthalic POSS imide (**3.3**) is depicted in **Figure 3.13**. ¹H NMR of this compound exhibited a singlet at δ 8.27 (2H, CH), with the aromatic protons being equivalent due to molecular symmetry. No change was evident in the resonances of the isobutyl chains of the POSS cage, which were apparent at δ 0.57-0.65 (32H, CH₂/iBu CH₂), 0.92-0.96 (84H, iBu CH₃) and 1.80-1.90 (18H, CH₂/iBu CH). Resonances of the propyl chain were obscured, with the exception of the CH₂N resonance, which was apparent at δ 3.72 (4H). The CH₂N resonance was significantly shifted downfield by 1.05 ppm, relative to the corresponding resonance in mono-(3-aminopropyl)POSS, to. Comparable resonance shifts were also apparent in similar compounds in the literature for the benzamide derivative (0.75 ppm) and **3.2** (0.92 ppm), as discussed previously in **Section 3.6.2.2**.^{51,52}

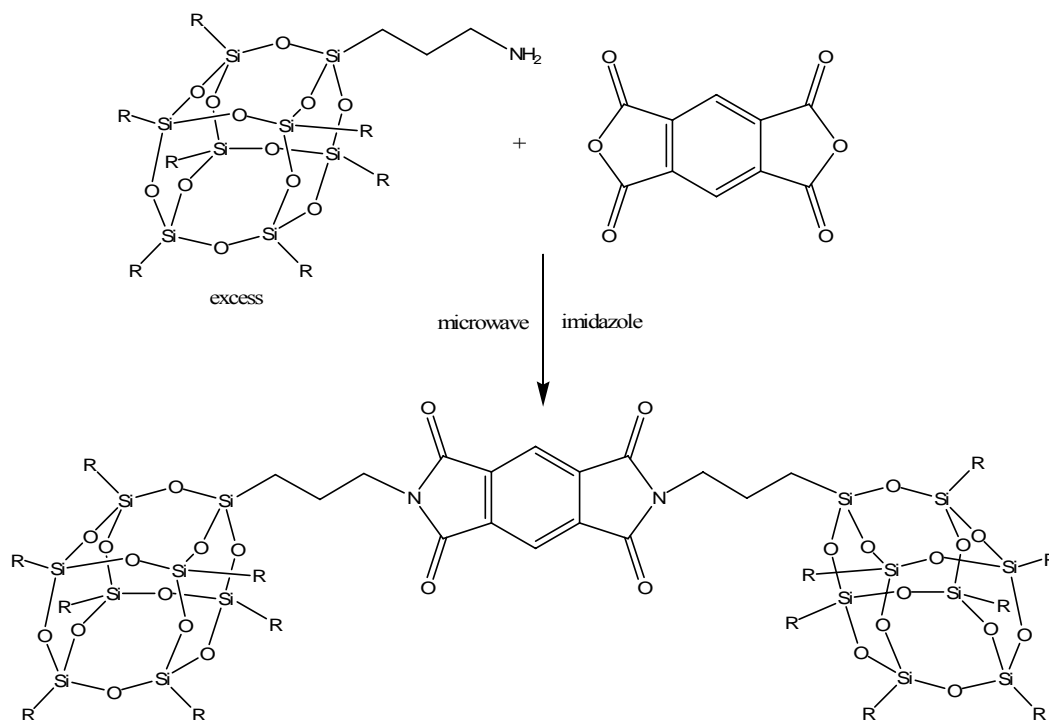


Figure 3.13. Synthesis of bis-phthalic POSS imide (3.3)

3.6.2.4 Octa-(3-chloroammoniumpropyl)POSS

Octa-(3-chloroammoniumpropyl) POSS (**3.4**) was synthesised according to the literature procedure (**Figure 3.8**).³⁵⁻³⁷ The ^1H NMR spectrum (D_2O) exhibited resonances at δ 0.80 (t, $^3J_{\text{H-H}} = 7.2$ Hz, SiCH_2), 1.77 (p, $^3J_{\text{H-H}} = 7.2$ Hz, CH_2) and 2.99 (t, $^3J_{\text{H-H}} = 7.2$ Hz, CH_2N), with these resonances consistent with those detailed in the literature.³⁵⁻³⁷

3.6.2.5 Octa-phthalic POSS Imide

The synthesis of octa-phthalic POSS imide (**3.5**) is depicted in **Figure 3.14**. ^1H NMR exhibited resonances associated with the propyl chain at δ 0.62-0.68 (16H, SiCH_2), 1.69-1.80 (16H, CH_2) and 3.59-3.64 (16H, CH_2N). Comparison of the resonances with those observed for the octa-amino derivative, indicated an upfield shift in the SiCH_2 resonance, with a slight downfield shift apparent in the CH_2 resonance, relative to (3-chloroammoniumpropyl)POSS. The significance of this resonance shift was not quantifiable due to the change in solvent required to perform the spectra. Similar resonance positions have been reported for other octa-(propylimide) POSS

compounds in the literature, such as octa-succinimide (δ 0.58, 1.43 and 3.01) and octa-maleic imide (δ 0.65, 1.54 and 3.15) in d_6 -DMSO.³⁹ The increased downfield position of the CH_2N resonance in **3.5** was attributed to the increased electron density, and subsequently enhanced deshielding experienced by the propyl chain protons, associated with the phenyl ring present in the substituent. Resonances of the aromatic protons were evident as multiplets from δ 7.57-7.61 (16H, CH) and 7.64-7.68 (16H, CH).

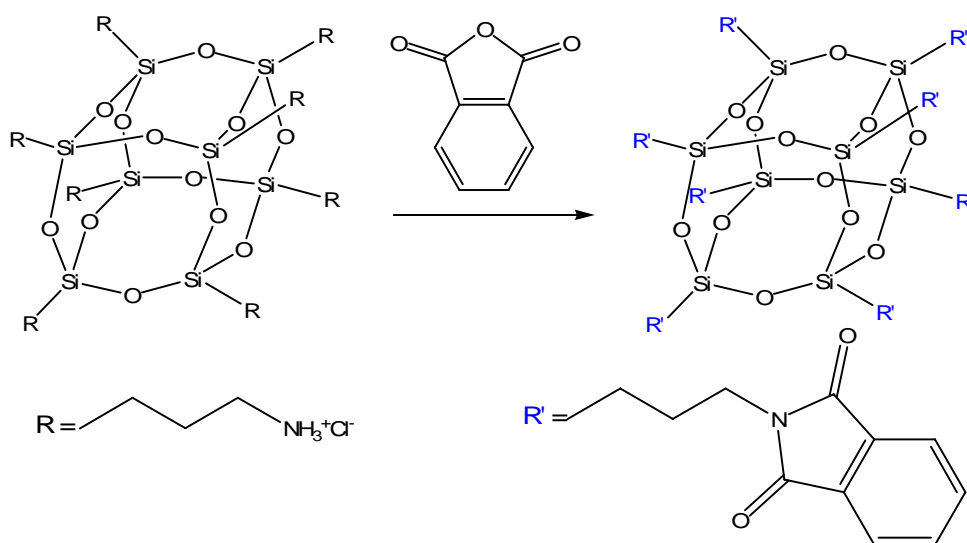


Figure 3.14. Synthesis of octa-phthalic POSS imide (3.5)

3.6.2.6 Mono-naphthalic POSS Imide

The synthesis of mono-naphthalic POSS imide (**3.6**) is depicted in **Figure 3.15**. ^1H NMR exhibited resonances of the aromatic protons at δ 7.73 (t, $^3J_{\text{H-H}} = 7.8$ Hz, 2H), 8.18 (dd, $^3J_{\text{H-H}} = 8.40$, $^2J_{\text{H-H}} = 0.9$ Hz, 2H) and 8.58 (dd, $^3J_{\text{H-H}} = 7.8$ Hz, $^2J_{\text{H-H}} = 0.9$ Hz, 2H). Analogously to the phthalic examples, the resonances of the isobutyl chains of the POSS moiety exhibited little change upon reaction, with resonances evident at δ 0.57-0.61 (14H, iBu CH_2), 0.93-0.96 (42H, iBu CH_3) and 1.79-1.90 (9H, CH_2/iBu CH). A significant downfield shift (1.48 ppm) was again evident in the CH_2N resonance, relative to mono-(3-aminopropyl)POSS, with the resonance apparent at δ 4.15 (2H, CH_2N). The increased downfield shift evident in **3.6** (1.48 ppm), compared with that observed in the corresponding resonance in **3.2** (1.00 ppm), was attributed to the increased electron density of the asymmetrical naphthalene moiety.

The SiCH₂ resonance was evident at δ 0.70-0.76 (2H, SiCH₂), with the remaining propyl resonance obscured.

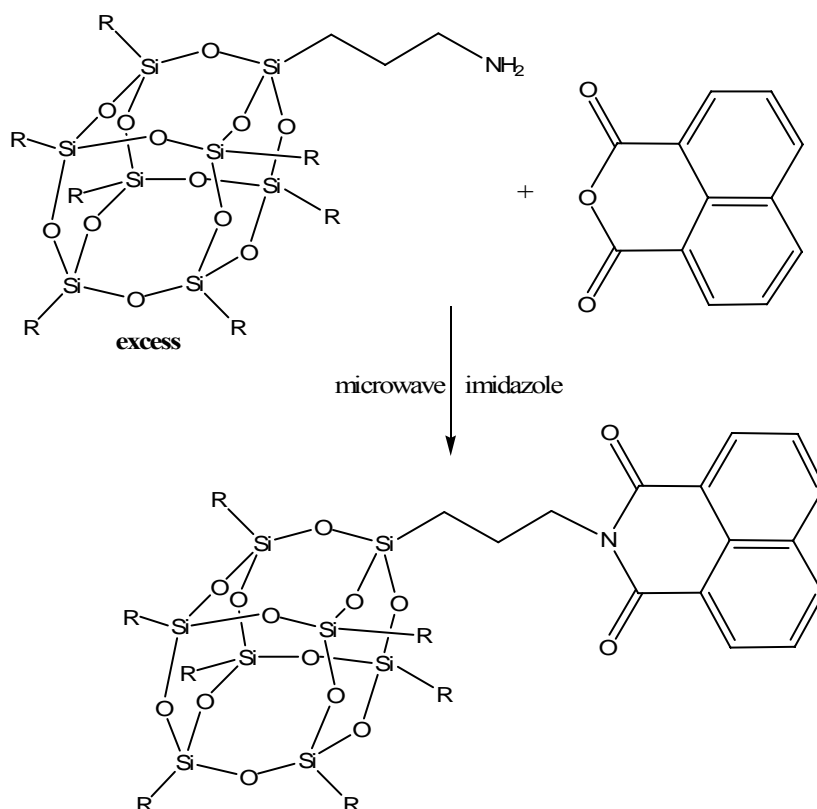


Figure 3.15. Synthesis of mono-naphthalic POSS imide (3.6)

3.6.2.7 Bis-naphthalic POSS Imide

The synthesis of bis-naphthalic POSS imide (3.7) is depicted in **Figure 3.16**. ¹H NMR displayed a singlet resonance of the aromatic protons at δ 8.76 (4H, CH) due to molecular symmetry. The isobutyl resonances exhibited little change upon reaction, with resonances apparent at δ 0.57-0.61 (28H, iBu CH₂), 0.92-0.96 (84H, iBu CH₃) and 1.84 (n, ³J_{H-H} = 6.3 Hz, 18H, CH₂/iBu CH). The SiCH₂ and CH₂N resonances of the propyl chain were observed at δ 0.69-0.75 (4H, SiCH₂) and 3.67 (t, ³J_{H-H} = 7.2 Hz, 4H, CH₂N), whilst the central CH₂ resonance was obscured. A downfield shifts of 1.00 ppm was evident in the CH₂N resonance, relative to the corresponding resonance in mono-(3-aminopropyl)POSS, analogous to that detailed for bis-imides **3.2** (0.92 ppm) and **3.3** (1.05 ppm). The reduced downfield shift evident in **3.7** in comparison to **3.6** (1.48 ppm) was associated with the presence of the bis-substituted naphthalene core. Subsequently, the electronic effects experienced by the CH₂N

protons of the two POSS substituents were reduced, causing a decrease in deshielding experienced by the propyl chain protons and subsequent reduction in the downfield shift of the CH₂N resonance.

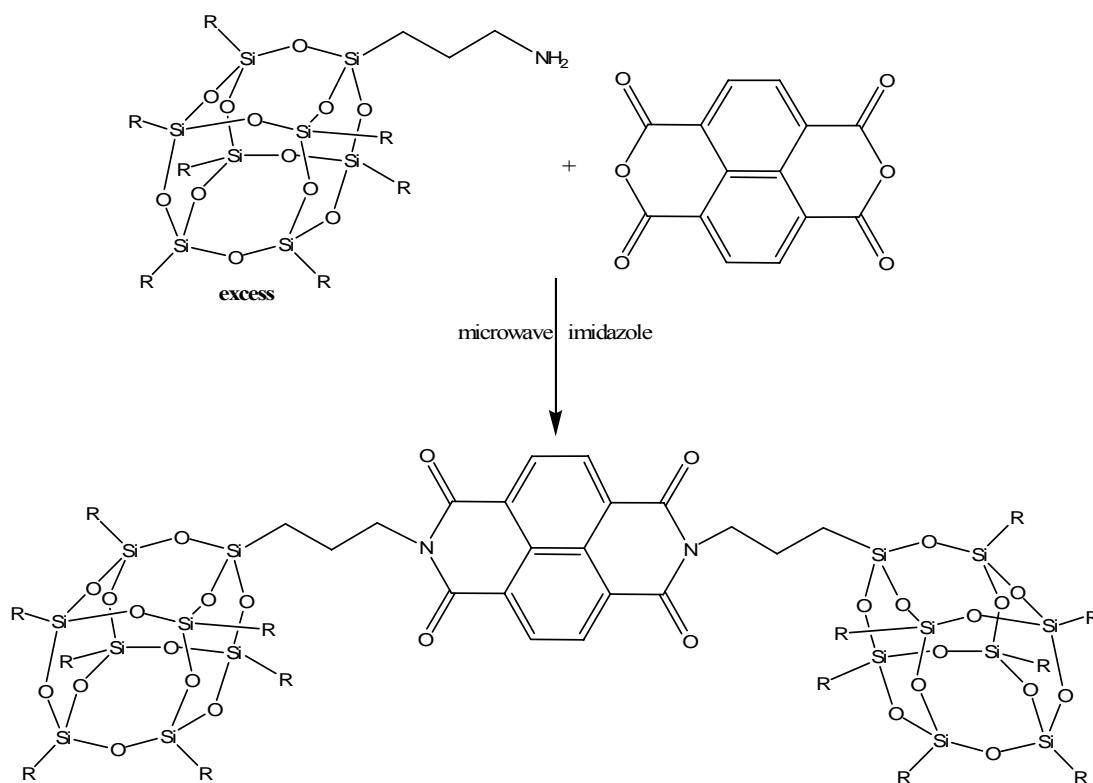


Figure 3.16. Synthesis of bis-naphthalic POSS imide (3.7)

3.6.2.8 Biphenyl POSS Imide

The synthesis of biphenyl POSS imide (**3.8**) is shown in **Figure 3.17**. ¹H NMR exhibited resonances associated with the aromatic protons as singlets at δ 7.97 (4H, CH) and 8.10 (4H, CH). The resonances associated with the isobutyl chains of the POSS moiety exhibited no change, with resonances apparent at δ 0.57-0.61 (32H, SiCH₂/iBu CH₂), 0.93-0.96 (84H, iBu CH₃) and 1.80-1.90 (n, ³J_{H-H} = 6.3 Hz, 18H, CH₂/iBu CH). The propyl chain resonances were obscured, with the exception of the CH₂N resonance, which was present at δ 3.70 (t, ³J_{H-H} = 7.20 Hz, 4H, CH₂N), resulting in a downfield shift of 1.03 ppm, relative to the corresponding resonance in mono-(3-aminopropyl)POSS. The shift magnitude (1.03 ppm) was analogous to those detailed previously for bis-imides **3.2** (0.92 ppm), **3.3** (1.05 ppm) and **3.6** (1.00 ppm).

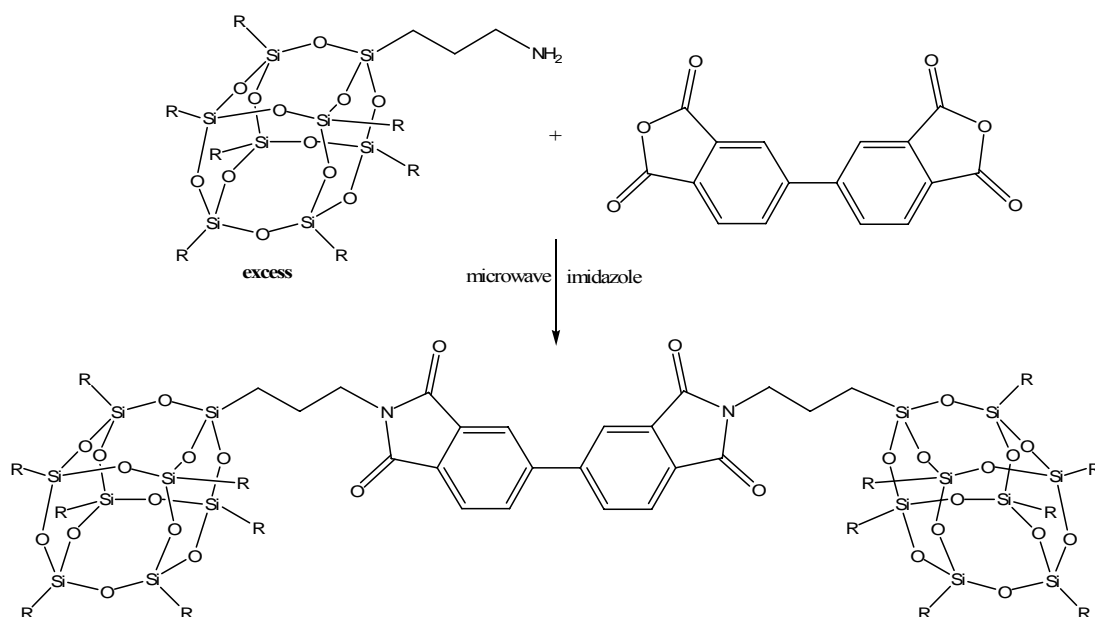


Figure 3.17. Synthesis of biphenyl POSS bis-imide (**3.8**)

3.6.2.9 Perylene POSS Imide

The synthesis of the perylene POSS imide (**3.9**) is detailed in **Figure 3.18**. ¹H NMR exhibited a resonance associated with the chemically equivalent aromatic protons as a broad multiplet at δ 8.60 (8H, CH). The resonances of the isobutyl chain protons of the POSS moiety exhibited no change, with resonances apparent at δ 0.54-0.59 (32H, SiCH₂/iBu CH₂), 0.93 (84H, iBu CH₃) and 1.83-1.90 (18H, CH₂/iBu CH). The propyl chain resonances were obscured, with the exception of the CH₂N resonance at δ 4.20 (4H, CH₂N), which was shifted downfield by 1.53 ppm, relative to the corresponding resonance in mono-(3-aminopropyl)POSS. The magnitude of the downfield shift was comparable to that displayed in **3.6** (1.48 ppm), as perylene bis-imides are generally regarded as two naphthalene half units connected to the other naphthalene by two C sp²-C sp² single bonds.⁵³ The naphthalene half unit of **3.9** was therefore essentially identical to the structure of **3.6** and consequently, similar resonance shifts were present in the NMR spectra of these two derivatives. The downfield shift was greater in magnitude than those observed for the remaining POSS imides **3.2** (0.92 ppm), **3.3** (1.05 ppm), **3.6** (1.00 ppm) and **3.8** (1.00 ppm), attributed to the increased electron density of the perylene core, and subsequent increase in deshielding experienced by the adjacent propyl chain protons.

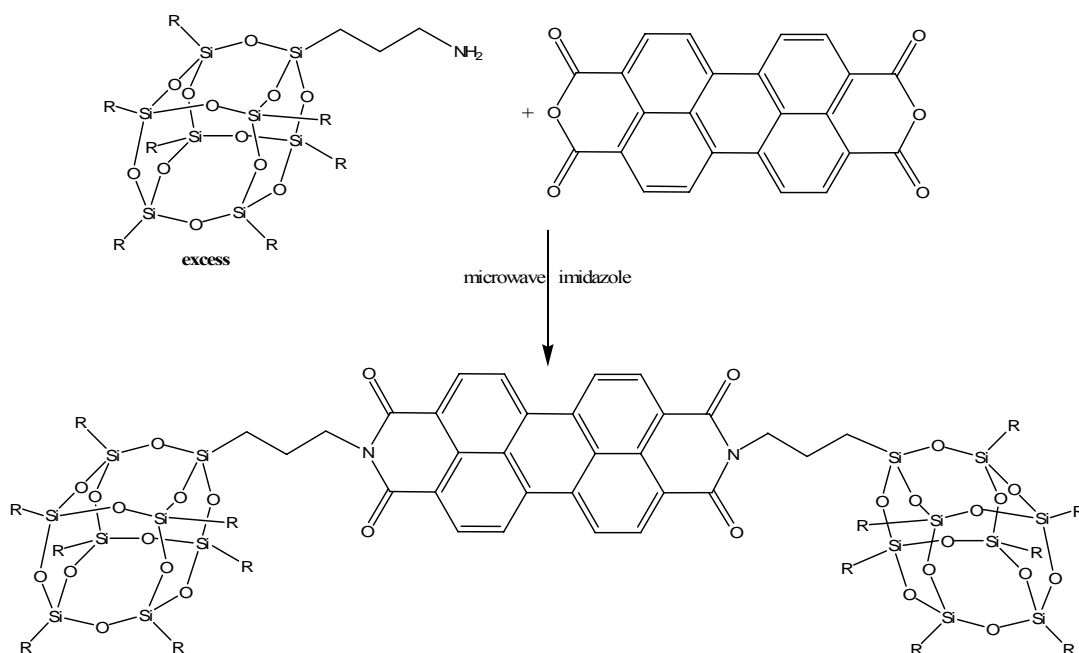


Figure 3.18. Synthesis of POSS perylene bis-imide (3.9)

3.6.3 ^{13}C NMR

3.6.3.1 *Mono-(3-aminopropyl)POSS*

^{13}C NMR of **3.1** exhibited resonances of the isobutyl carbons at δ 24.01, 25.84 and 27.23, with resonances of the propyl carbons apparent at δ 9.36 (SiCH_2), 22.65 (CH_2) and 44.90 (CH_2N). The resonances were consistent with those reported in the literature.³⁴

3.6.3.2 *Mono-phthalic POSS Imide*

^{13}C NMR of **3.2** exhibited upfield shifts in the resonances of the isobutyl chains of the POSS moiety, with the resonances evident at approximately δ 22.47, 23.85 and 25.69 compared to 24.01, 25.84 and 27.23 in the amine, giving rise to upfield shifts in the resonances of 1.54, 1.99 and 1.54 ppm. Similar shifts in the resonances of the isobutyl carbons were also apparent in the benzamide derivative, as detailed

Table 3.3. ¹³C NMR of POSS imides

Compound	iBu	SiCH₂	CH₂	CH₂N	Aromatic	C=O
3.1	24.01, 25.84, 27.23	9.36	22.65	44.90	-	-
3.2	22.47, 23.85, 25.69	9.56	22.14	40.48	123.13, 132.20, 133.80	168.33
3.3	22.47, 23.85, 25.68	9.56	22.04	41.09	118.06, 137.23	166.18
3.4	-	8.08	20.60	41.68	-	-
3.5	-	8.97	21.85	40.16	122.97, 132.25, 133.46	168.17
3.6	22.39, 22.50, 23.84, 25.68	9.72	21.55	42.69	122.81, 126.85, 128.15, 131.04, 131.55, 133.68	163.98
3.7	22.47, 23.85, 25.68	9.72	21.55	43.16	126.68, 126.70, 130.86	162.71
3.8	22.37, 23.86, 25.69	9.58	22.12	40.71	121.99, 123.97, 131.94, 132.74, 133.38, 145.07	167.74
3.9	22.49, 23.93, 25.69	9.78	21.57	42.94	123.08, 123.30, 126.27, 129.23, 131.29, 134.38	163.11

previously in the ^1H NMR discussion (Section 3.6.2.2) (1.0, 2.0/2.0 and 1.5 ppm).⁵⁴

Resonances of the propyl chain were observed at δ 9.56 (SiCH₂), 22.14 (CH₂) and 40.48 (CH₂N). A downfield shift of the SiCH₂ resonance of 0.20 ppm, and upfield shifts of the CH₂ and CH₂N resonance of 0.41 and 3.42 ppm, relative to mono-(3-aminopropyl)POSS, were evident. Comparable shifting patterns were apparent in the bis-propyl triethoxysilane phthalic derivative (0.1, 5.4 and 4.2 ppm), relative to (3-aminopropyl)triethoxysilane.⁵² The electron-withdrawing properties of a POSS cage were comparable to those associated with a trifluoromethyl (CF₃) group,^{55,56} therefore, the adjacent propyl chain carbons experienced increased deshielding, with a reduced upfield shifts of the propyl chain resonances of phthalic POSS imides observed.⁵⁷ Resonances of the aromatic moiety were evident at δ 123.13, 132.20 and 133.80, with the carbonyl resonance visible at δ 168.33. The ^{13}C NMR spectrum of **3.2** is depicted in Figure 3.19, with the spectra of all other POSS imide derivatives being analogous in appearance.

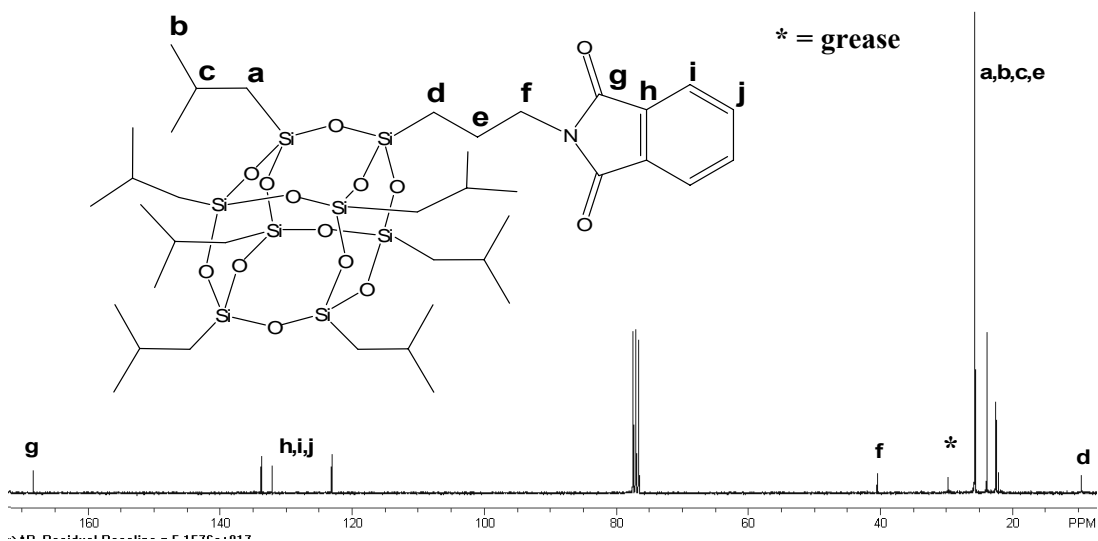


Figure 3.19. ^{13}C NMR of mono-phthalic POSS imide **3.2** in CDCl_3

3.6.3.3 Bis-phthalic POSS Imide

^{13}C NMR of **3.3** exhibited resonances of the cage bound isobutyl groups at δ 22.47, 23.85 and 25.68, corresponding to upfield shifts in the resonances of 1.54, 1.99 and 1.55 ppm. Similar upfield shifts were observed in **3.2** (1.54, 1.99 and 1.54 ppm) and

the benzamide derivative (1.0, 2.0 and 1.5 ppm).⁵¹ Resonances of the propyl chain were evident at δ 9.56 (SiCH₂), 22.04 (CH₂) and 41.09 (CH₂N), resulting in a downfield shift of 0.2 ppm in the SiCH₂ resonance, and upfield shifts of 0.61 and 3.81 ppm in the resonances of the central CH₂ and SiCH₂ resonances, relative to the corresponding resonances in mono-(3-aminopropyl)POSS. A comparable shifting pattern was observed in **3.2** (0.2, 0.4 and 3.42 ppm).⁵² Resonances of the aromatic moiety were evident at δ 118.06 and 137.23, with the carbonyl resonance observed at δ 166.18.

3.6.3.4 *Octa-(3-chloroammoniumpropyl) POSS*

The octa-amino precursor **3.4** exhibited resonances at δ 8.08 (SiCH₂), 20.60 (CH₂) and 41.68 (CH₂N) in D₂O. These resonances were consistent with those detailed in the literature.³⁵⁻³⁷

3.6.3.5 *Octa-phthalic POSS Imide*

The ¹³C NMR spectrum of **3.5** exhibited propyl chain resonances at δ 8.97 (SiCH₂), 21.85 (CH₂) and 40.16 (CH₂N), with aromatic resonances apparent at δ 122.97, 132.25 and 133.46 and the carbonyl resonance observed at δ 168.17. The resonance positions were consistent with those of the octa-succinic (δ 8.75, 22.49 and 41.01) and maleic derivatives (8.61, 21.82 and 41.41).³⁷ The downfield position of the SiCH₂ resonance, relative to the corresponding resonance in the octa-maleic and succinic derivatives, coupled with the upfield appearance of the CH₂ and CH₂N resonances, were attributed to the increased electron density associated with the phthalic substituent compared with the maleic and succinic functional groups, and subsequent enhancement in deshielding experienced by the propyl chain protons (**Figure 3.20**).³⁷

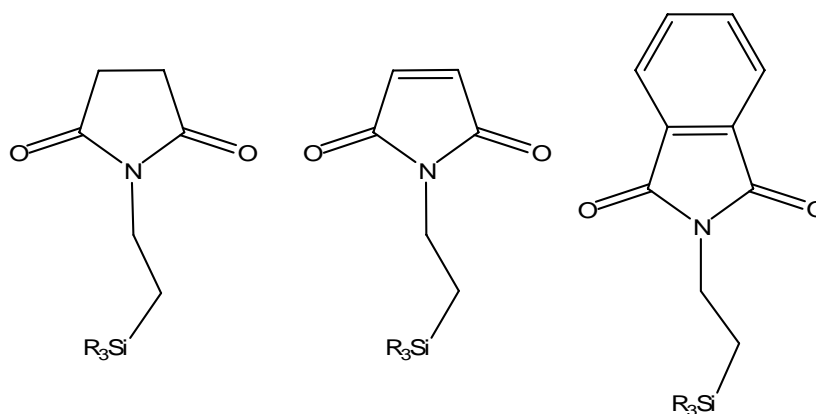


Figure 3.20. Succinimide, maleimide and phthalic imide functional groups

3.6.3.6 *Mono-naphthalic POSS Imide*

The ¹³C NMR spectrum of **3.6** displayed cage bound isobutyl resonances at δ 22.39, 22.50, 23.84 and 25.68, corresponding to upfield shifts of 1.62, 1.51, 2.00 and 1.55 ppm. These upfield shifts were comparable to those detailed previously for **3.2** (1.54, 1.99, 1.54 ppm) and **3.3** (1.54, 1.99, 1.55 ppm). Propyl chain resonances were evident at 9.72 (SiCH₂), 21.55 (CH₂) and 42.69 (CH₂N), with downfield shifting of the SiCH₂ resonance of 0.36 ppm and upfield shifting of the CH₂ and CH₂N resonances by 1.10 (CH₂) and 2.21 ppm (CH₂N) apparent, relative to mono-(3-aminopropyl)POSS. The increased downfield shift observed in the CH₂ resonance (1.10 ppm), coupled with the reduced upfield shift in the CH₂N resonance (2.21 ppm), in contrast with the shifts observed for the corresponding resonances in **3.2** (0.40 and 3.42 ppm) and **3.3** (0.60, 3.81 ppm), was attributed to the increased electron density associated with the naphthalene substituent compared to the phthalic functionality, and subsequent increased deshielding experienced by the propyl chain carbons. Resonances of the aromatic moiety were evident at δ 122.81, 126.85, 128.15, 131.04, 131.55 and 133.68, along with the carbonyl resonance at δ 163.98.

3.6.3.7 *Bis-naphthalic POSS Imide*

The ¹³C NMR spectrum of **3.7** displayed cage bound isobutyl resonances at δ 22.47, 23.85 and 25.68. Upfield shifts in the resonances of the isobutyl chains of the POSS moiety were again present, with shifts of 1.54, 2.01 and 1.55 ppm evident, similar to

the shifts observed for **3.2** (1.54, 1.99 and 1.54 ppm), **3.3** (1.54, 1.99 and 1.55 ppm) and **3.6** (1.62, 1.51, 2.00 and 1.55 ppm), as previously detailed within this chapter. Propyl chain resonances were apparent at δ 9.72 (SiCH₂), 21.55 (CH₂) and 43.16 (CH₂N), resulting in a downfield shift of the resonance of the SiCH₂ resonance of 0.36 ppm, coupled with upfield shifting of the CH₂ and CH₂N resonances by 1.10 (CH₂) and 1.74 ppm (CH₂N), relative to the corresponding resonances in mono-(3-aminopropyl)POSS. The reduced upfield shift of the CH₂N resonance, in comparison with **3.6** (2.21 ppm), occurred due to the reduction in electron density, associated with the molecular symmetry of the bis-imide. Resonances of the naphthalene core were evident at δ 126.68 (CC), 126.70 (CC), 130.86 (CH) and 162.71 (C=O).

3.6.3.8 *Biphenyl POSS Imide*

The ¹³C NMR spectrum of **3.8** exhibited cage bound isobutyl resonances at δ 22.37, 23.86 and 25.69, resulting in upfield shifts of 1.64, 2.02 and 1.54 ppm, relative to the corresponding resonances in mono-(3-aminopropyl)POSS. The isobutyl resonance shifts were analogous to those observed for **3.2** (1.54, 1.99 and 1.54 ppm), **3.3** (1.54, 1.99 and 1.55 ppm), **3.6** (1.62, 1.51, 2.00 and 1.55 ppm) and **3.7** (1.54, 2.01 and 1.55 ppm), as detailed earlier within this chapter. Propyl chain resonances were exhibited at δ 9.58 (SiCH₂), 22.12 (CH₂) and 40.71 (NCH₂). A downfield shift in the SiCH₂ resonance of 0.22 ppm was evident, along with upfield shifts in the CH₂ and CH₂N resonances of 0.53 and 4.19 ppm, respectively, relative to the corresponding resonances in mono-(3-aminopropyl)POSS. The resonance shifts were similar to those observed for **3.2** (0.20, 0.42 and 3.42 ppm) and **3.3** (0.20, 0.61, 3.81 ppm), as detailed earlier in this chapter, with the increased upfield shift of the CH₂N resonance indicative of the low degree of conjugation in the biphenyl moiety.⁵⁸ Aromatic resonances were observed at δ 121.99, 123.97, 131.94, 132.74, 133.38 and 145.07, whilst the carbonyl group exhibited a resonance at δ 167.74.

3.6.3.9 *Perylene POSS Imide*

The ¹³C NMR spectrum of **3.9** displayed cage bound isobutyl resonances at δ 22.49, 23.93 and 25.69, with the resonances being shifted upfield by 1.52, 1.91 and 1.54

ppm, similar to the shifts observed for **3.2** (1.54, 1.99 and 1.54 ppm), **3.3** (1.54, 1.99 and 1.55 ppm), **3.6** (1.62, 1.51, 2.00 and 1.55 ppm), **3.7** (1.54, 2.01 and 1.55 ppm) and **3.8** (1.64, 2.02 and 1.54 ppm) previously detailed within this chapter. Propyl chain resonances were observed at δ 9.78 (SiCH₂), 21.57 (CH₂) and 42.94 (NCH₂), resulting in a downfield shift in the SiCH₂ resonance of 0.42 ppm, coupled with upfield shifts in the CH₂ and CH₂N resonances of 1.08 and 1.96 ppm, relative to mono-(3-aminopropyl)POSS. The reduced upfield shift in the CH₂N resonance (1.96 ppm), compared to **3.2** (3.42 ppm), **3.3** (3.81 ppm), **3.6** (2.21 ppm) and **3.8** (4.19 ppm) was attributed to the increased electron density associated with the perylene substituent. The magnitude of the resonance shift was comparable to that observed in **3.6** (1.74 ppm) due to the structural similarity of the naphthalene half unit of **3.9** to the structure of **3.6**, associated with molecular symmetry, as discussed in **Section 3.6.2.9**. Resonances of the central perylene moiety were evident at δ 123.08, 123.30, 126.27, 129.23, 131.29 and 134.38, with the carbonyl resonance observed at δ 163.11.

3.6.4 ²⁹Si NMR

The ²⁹Si NMR resonances of the POSS amines and imides are detailed in **Table 3.4**. All POSS imides exhibited resonances characteristic of the monosubstituted POSS cage, indicating that the cage structure remained intact during reaction, with upfield shifts of approximately 0.3 ppm present in resonances of all mono- and bis-imides following reaction of the amino group.

Table 3.4. ²⁹Si NMR of POSS imides

Compound	²⁹ Si NMR
3.1	-67.64, -68.06, -68.26
3.2	-68.02, -68.36, -68.56
3.3	-68.01, -68.30, -68.51
3.4	-66.65 ^a
3.5	-67.61
3.6	-68.05, -68.30, -68.40
3.7	-68.03, -68.34, -68.54
3.8	-68.06, -68.34, -68.44
3.9	-68.05, -68.14, -68.38

^a = D₂O

The ^{29}Si NMR spectrum of the octa-amino precursor **3.4** exhibited a single resonance at δ -66.65 (D_2O).³⁵⁻³⁷ An upfield shift in the resonance was apparent upon reaction of the amino functionality in **3.5**. The resonance shift was not quantifiable due to the different solvents required for the spectra. Similar resonance positions were evident for the octa-succinimide and maleic derivatives, at δ -66.17 and -66.17, respectively, in d_6 -DMSO.³⁹

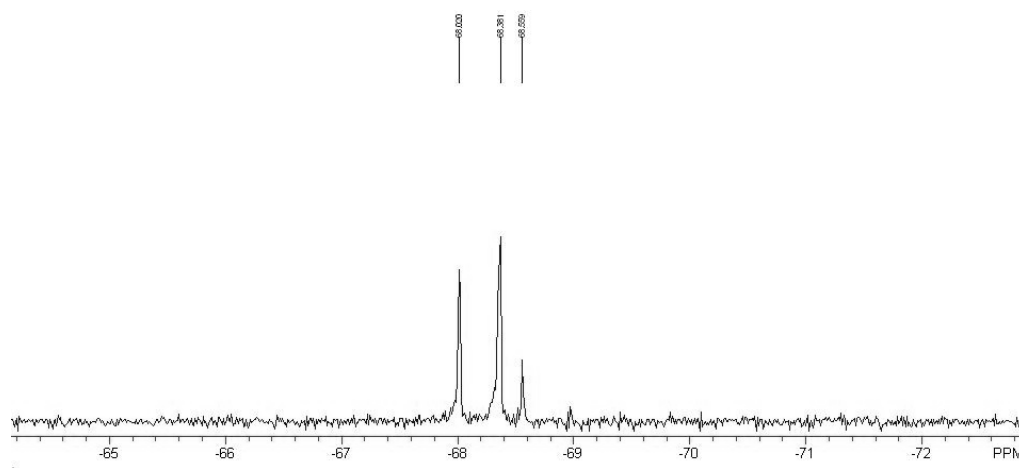


Figure 3.21. ^{29}Si NMR of mono-phthalic POSS imide **3.2** in CDCl_3

The ^{29}Si NMR spectrum of **3.1** is depicted in **Figure 3.21**, with the spectra of all other POSS imide derivatives being analogous in appearance.

3.6.5 High Resolution ESI Mass Spectrometry

The theoretical and experimental high resolution ESI mass spectrometry results are depicted in **Table 3.5**. The close correlation between the experimental and theoretical results gave indisputable verification of the formation of the desired POSS imides.

Table 3.5. High resolution ESI mass spectrometry of POSS imides

POSS Imide	Experimental $[\text{M}+\text{Na}]^+$	Theoretical $[\text{M}+\text{Na}]^+$
3.1	874.3202	874.3126
3.2	1026.3072	1026.3083
3.3	1951.5289	1951.5799
3.5	983.1506	983.1516
3.6	1076.3229	1076.3239
3.7	2001.5946	2001.5955
3.8	2027.6108	2027.6112
3.9	2125.6260	2158.6268

3.6.6 Elemental Analysis of POSS Imides

The theoretical and experimental elemental analysis results are depicted in **Table 3.6**. The close correlation between the experimental and theoretical results gave further confirmation of the formation of the desired POSS imides.

Table 3.6. Elemental Analysis of POSS imides

POSS Imide	Experimental (C, H, N)	Theoretical (C, H, N)
3.2	46.38, 8.13, 1.06	46.62, 7.32, 1.39
3.3	45.02, 7.45, 1.39	44.78, 7.31, 1.45
3.6	48.31, 7.42, 1.43	48.97, 7.17, 1.33
3.7	46.31, 7.42, 1.43	46.02, 7.32, 1.41
3.8	45.76, 7.55, 1.04	46.67, 7.23, 1.40
3.9	49.10, 7.05, 1.53	49.06, 6.99, 1.33

3.6.7 UV-Vis Spectra of POSS Imides

3.6.7.1 UV-Vis Spectra of Phthalic POSS Imides

The UV-Vis spectra of **3.2**, **3.3** and **3.5** are depicted in **Figure 3.22**. The absorption maxima of **3.2**, **3.3** and **3.5** were apparent at 294, 309 and 319 nm exhibiting molar extinction coefficients of 1078, 2356 and 2154, respectively. The molar extinction coefficient of **3.5** was a factor of 7.96 greater than that observed for **3.2**, indicative of the octa-functionality of the molecule. The maxima position in **3.3** was similar to other bis-imide examples in the literature, such as N',N'-dicyclohexylpyromellitimide (310 and 320 nm).⁵⁹

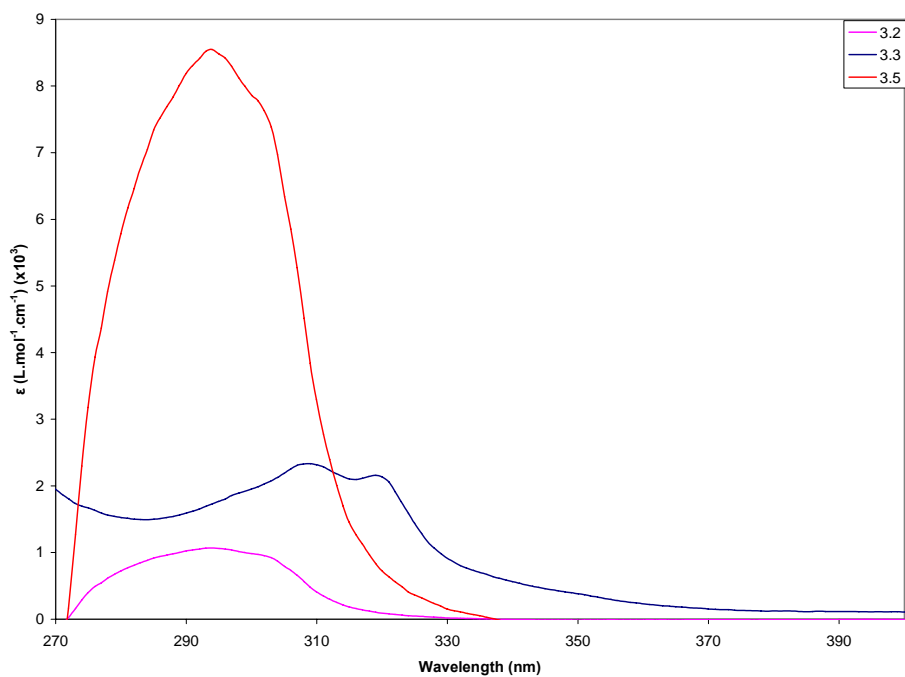


Figure 3.22. UV-Vis spectra of phthalic POSS imides 3.2, 3.3 and 3.5 in toluene

3.6.7.2 UV-Vis Spectrum of Mono-naphthalic POSS Imide

The absorption spectra of **3.6** (**Figure 3.23**) exhibited absorption maxima at 335 and 350 nm, with molar extinction coefficients of 15022 and 13846, respectively.

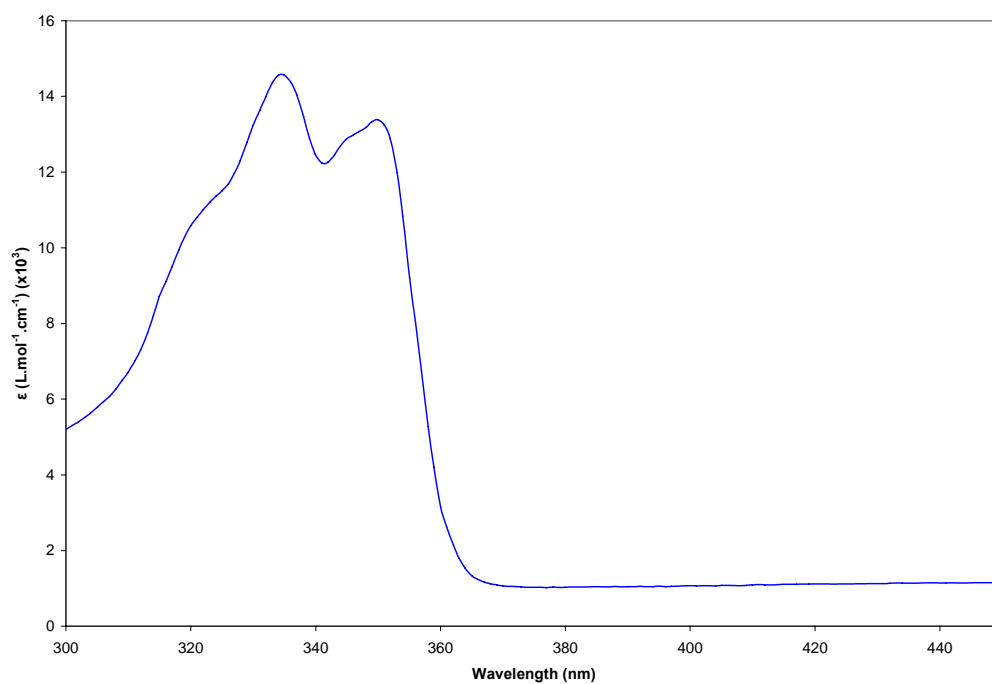


Figure 3.23. UV-Vis spectrum of mono-naphtha POSS imide 3.6 in toluene

Literature examples of mono-naphthalimides (**Figure 3.24**) exhibited absorption maxima at approximately 330 nm and 345 nm, with the exact position of the maxima being solvent dependent.⁶⁰ The solvent polarity had a minimal influence on the position of the absorption maxima, however some changes were evident in the molar extinction coefficients in methanol due to hydrogen bonding of the imide with the solvent molecules.⁶⁰

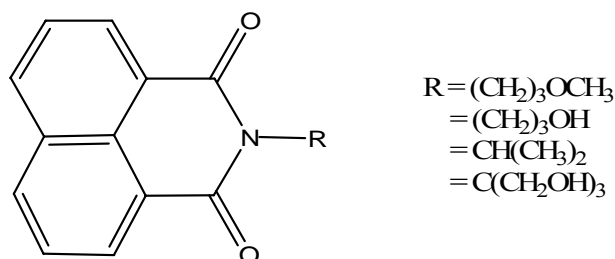


Figure 3.24. Literature examples of mono-naphthalimides⁶⁰

Calculated absorption spectra (performed by modification of the INDO/S method)⁶¹⁻⁶⁴ of the naphthalic imide (**Figure 3.25**) exhibited two $\pi\text{-}\pi^*$ transitions, one of high intensity at 328 nm and the other, of low intensity, at 323 nm. The observed absorption maxima were apparent at 331 and 342 nm, similar to the absorption maxima displayed in **3.6** (335 and 350 nm).⁶⁵

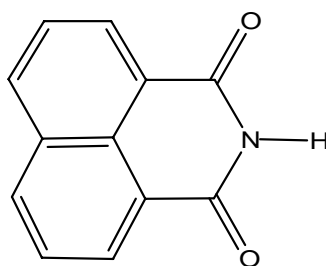


Figure 3.25. Naphthalic imide used for absorption calculations⁶⁵

3.6.7.3 UV-Vis Spectrum of Bis-naphthalic POSS Imide

The absorption spectrum of **3.7** (**Figure 3.26**) was analogous to literature bis-naphthalic derivatives.⁶⁶⁻⁶⁸ The absorption maxima were apparent at 342, 360 and 381 nm, with molar extinction coefficients of 10084, 15864 and 19153, respectively.

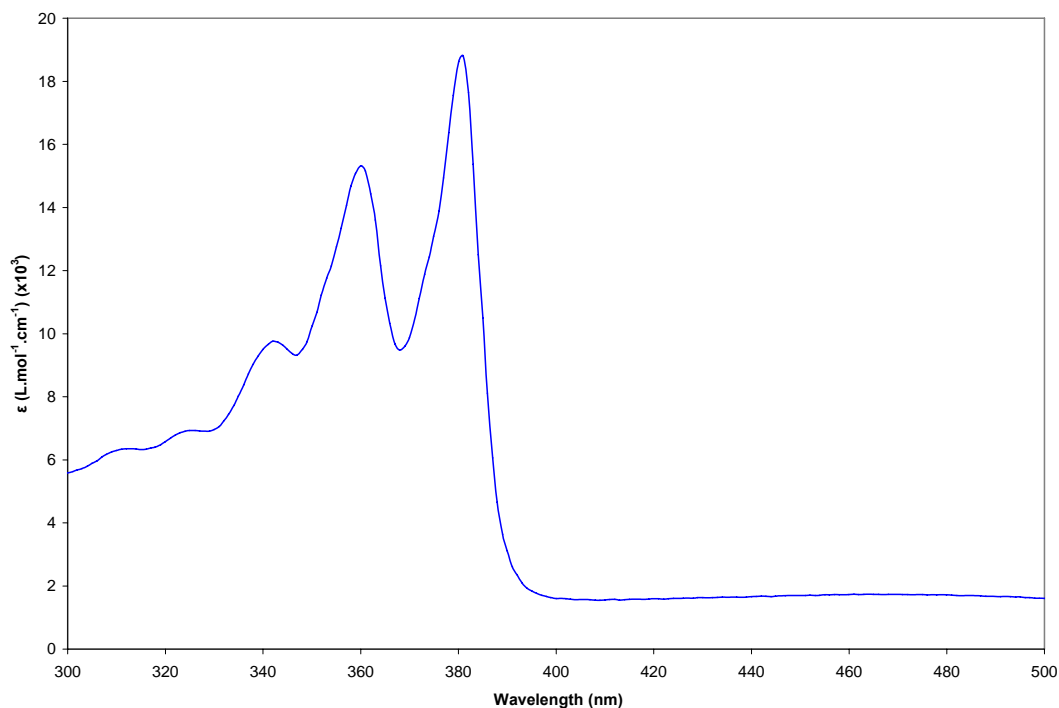
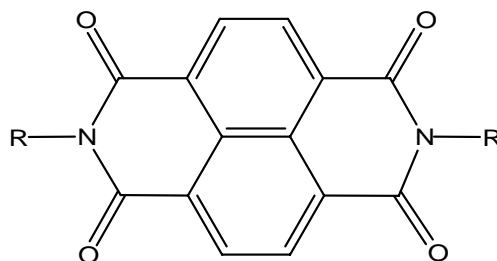


Figure 3.26. UV-Vis spectrum of bis-naphtha POSS imide 3.7 in toluene

The absorption maxima positions were similar to those detailed in the literature for naphthalene bis-imides (**Figure 3.27**), which exhibited absorption maxima at 342, 360 and 380 nm.⁶⁶⁻⁶⁸ The similarity in absorbance maxima position over a range of N-substituents confirmed that the nature of the substituent bound to the nitrogen had little or no effect on the wavelength of the absorption bands.^{60,69} Gaussian analysis of the absorption spectrum of bis(ethylamine)naphthalene imide indicated that a vibronic pattern similar to that observed in perylene dyes, was present.^{66,70}



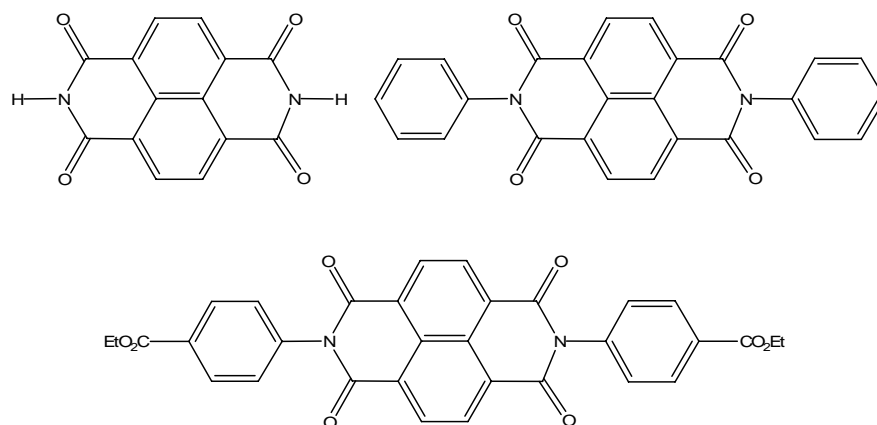
R= *s*-butyl, *n*-butyl, *n*-dodecyl, isoamyl, 2-ethylmorpholine, cyclohexyl, dehydroabietyl, phenyl, *p*-nitrophenyl, *p*-chlorophenyl, *o*-chlorophenyl, *p*-bromophenyl, *p*-tolyl, α -naphthyl, benzyl

Figure 3.27. Bis-naphtha diimide examples⁶⁶⁻⁶⁸

Table 3.7. UV-Vis data of bis-naphthalic imides⁶⁸

R	λ_1	ϵ_1	λ_2	ϵ_2	λ_3	ϵ_3	Conc. (x 10 ⁻⁵ M)
<i>n</i> -butyl	342	18,000	358	25,800	379	31,600	4.56
<i>n</i> -dodecyl	342	7352	359	12,151	380	13,373	1.93
isoamyl	342	7858	358	12,692	379	13,174	1.90
2-ethylmorpholine	342	8422	359	14,049	380	15,714	2.27
cyclohexyl	343	18,570	360	29,552	380	33,159	4.79
dehydroabietyl	343	30,210	359	45,667	380	49,229	7.10
phenyl	342	15,106	358	24,058	379	24,604	3.55
<i>p</i> -chlorophenyl	342	9037	358	14,084	379	14,088	2.03
<i>o</i> -chlorophenyl	341	8234	358	13,114	378	13,720	1.98
<i>p</i> -bromophenyl	342	6169	359	9781	379	10,136	1.46
<i>p</i> -tolyl	342	14,784	359	24,719	379	26,483	3.82
α -naphthyl	341	19,397	358	32,712	379	36,923	5.33
2.7	342	10,084	360	15,864	381	19,153	4.00

The magnitude of the molar extinction coefficient was found to be strongly dependent on the nature of the N-substituent, due to a combination of electronic and steric effects, with no discernable trend evident in the results of a range of substituents (**Table 3.7**). Absorption calculations (performed by modification of the INDO/S method)⁶¹⁻⁶⁴ have previously been performed for a range of bis-naphthalic imides (**Figure 3.28**), with absorption bands calculated to occur between 336 and 345 nm and 334 and 338 nm.

**Figure 3.28. Literature examples of bis-naphthalic imides⁶⁵**

The absorption bands were experimentally observed at 344, 361 and 382 nm, corresponding to the calculated electronic transitions at 337 and 336 nm and one of their vibronic progressions.⁶⁵ The position of the absorption maxima in the literature examples, were comparable to those observed in **3.7** (342, 360 and 381 nm).

3.6.7.4 UV-Vis Spectrum of Biphenyl POSS Imide

Biphenyl compounds possess strong absorption in the visible spectrum, with $\pi\text{-}\pi^*$ absorption bands generally observed at 320 nm.^{58,71} The UV-VIS spectrum of **3.8** (**Figure 3.29**) exhibited an absorption band at 322 nm, with a molar extinction coefficient of 7358.

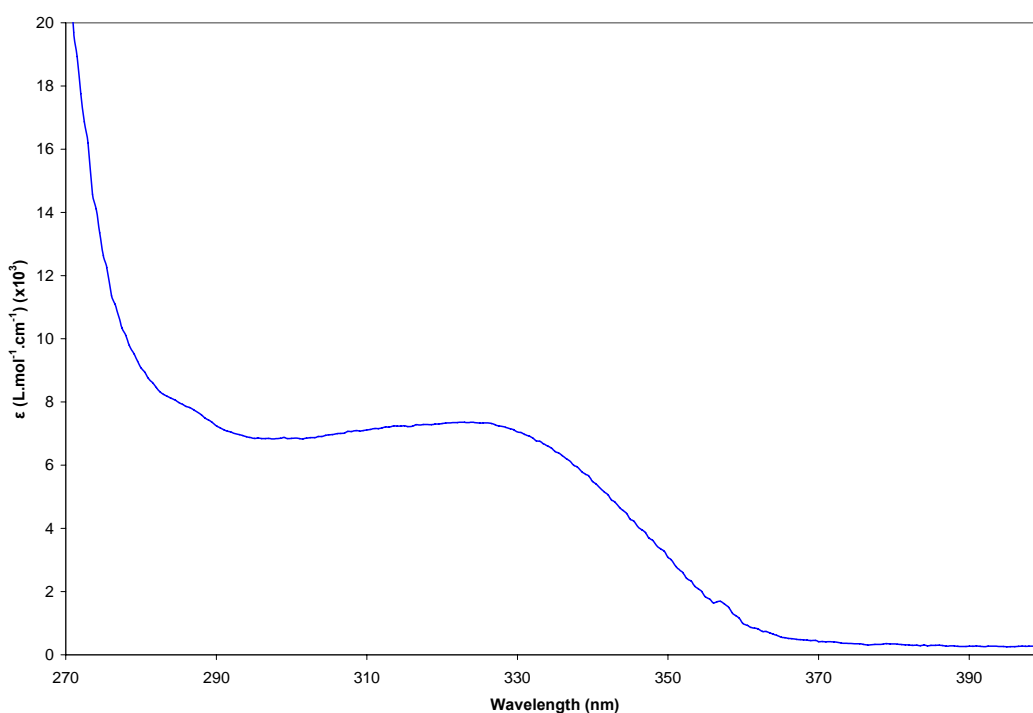


Figure 3.29. UV-Vis spectrum of biphenyl POSS imide **3.8** in toluene

The position of the absorption maxima of **3.8** (320 nm) was analogous to that reported for other biphenyl imides in the literature (320 nm) (**Figure 3.30**).⁷¹

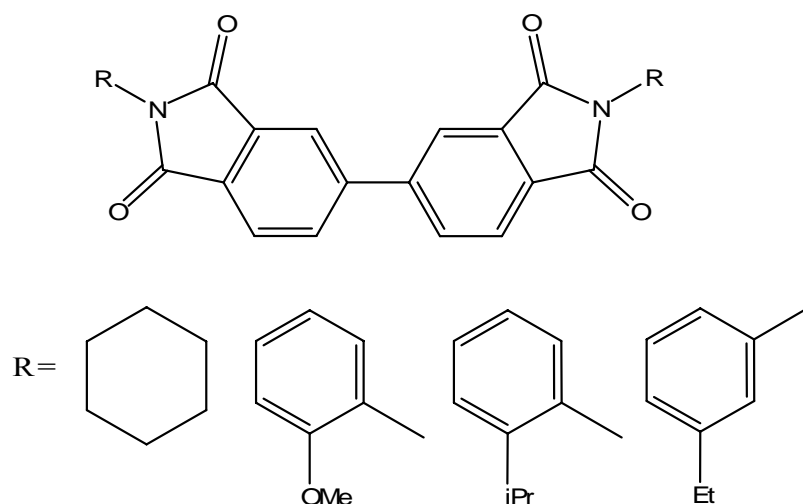


Figure 3.30. Literature biphenyl bis-imides⁷¹

3.6.7.5 UV-Vis Spectrum of Perylene POSS Imide

The UV-Vis spectrum of **3.9** (**Figure 3.31**) displayed three characteristic absorption bands at 459, 490 and 526 nm, with molar extinction coefficients of 17157, 48730 and 80877 respectively.^{48,49,72} The band at 526 nm represented a lowest energy transition from the ground state (zero vibrational level) to the first excited state, whilst the subsequent maxima at 490 and 459 nm corresponded to transitions to the various excited vibrational levels of the first electronic excited state.⁷³

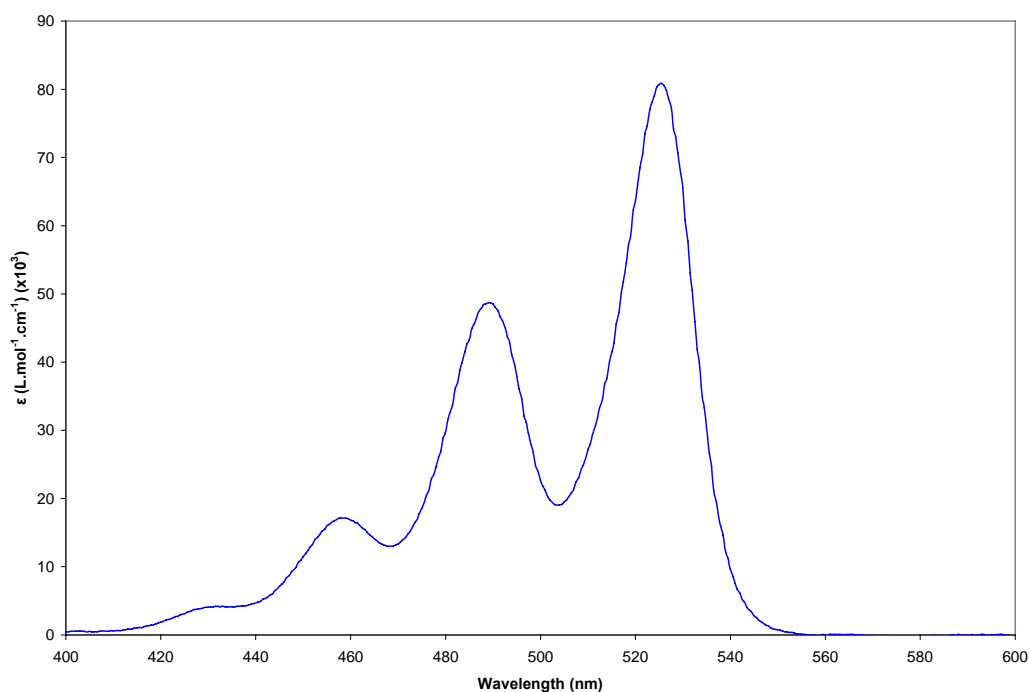


Figure 3.31. UV-Vis spectrum of perylene POSS imide 3.9 in toluene

The absorption maxima positions were established to be impervious to substituent type, however the extinction coefficients, stability and aggregation were strongly dependent on the nature of the N-substituent.⁴⁸ The imide substituent exhibited a negligible effect on the absorption and emission properties due to the presence of nodes in both the Highest Occupied Molecular Orbital (HOMO) and Lowest Unoccupied Molecular Orbital (LUMO) orbitals at the imide nitrogen atoms (**Figure 3.32**).⁵³ Therefore, perylene bis-imides can be regarded as a closed chromophoric system, with a ground-state to first excited state singlet ($S_0 \rightarrow S_1$) transition, polarised along the extended molecular axis. The intensity and position of the transition remained unchanged by the nature of the imide substituent. Also, little solvatochromism, defined as the changing of the position of the absorption maxima in diverse solvents, was observed for the perylene dyes.⁵³

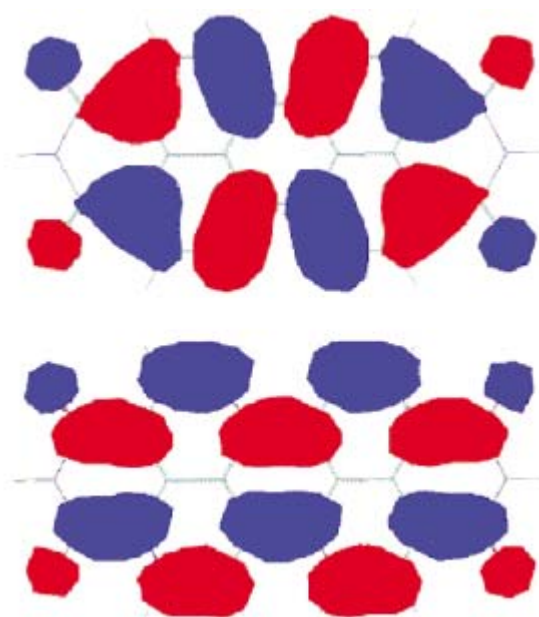


Figure 3.32. HOMO (top) and LUMO (bottom) of perylene bisimides⁵³

Absorption spectra have previously been calculated (by modification of the INDO/S method),⁶¹⁻⁶⁴ for the case where R = Ph. The calculated absorption maxima occurred at 441 nm, whereas the experimentally determined absorption spectra exhibited bands at 458, 489 and 525 nm. These three bands were assigned to one electronic transition (525 nm) and its vibronic progressions (489 and 458 nm).⁶⁵ The position of these bands was similar to the absorption maxima displayed in **3.9** (459, 490 and 526 nm). In the literature examples where R = *p*-cyanophenyl,⁷⁴ *p*-hydroxyphenyl⁷⁵ and

(CH₂)₁₇CH₃,⁷⁵ absorption bands were also present at 579, 564 and 582 nm respectively, attributed to aggregation within the solution phase.

As previously noted, the imide substituent had a negligible effect on the position of the absorption maxima. This was confirmed by comparison between the observed absorption maxima and those reported in the literature (**Table 3.8**).⁵³ Little change in the position of the absorption band is evident upon the variation of the N-bound substituent; however comparison between the molar absorption coefficients of the various R groups confirmed that the nature of the substituent had a significant effect on the intensity, with no discernable trend evident.

Table 3.8. UV-Vis data of various N-substituted perylenes in CHCl₃

N substituent	λ_{\max} (ϵ , L.mol ⁻¹ .cm ⁻¹)
(CH ₂) ₁₂ NH ₂ (CHCl ₃) ⁴⁸	458 (6500), 489 (17875), 525 (28500)
<i>p</i> -hydroxyphenyl (DMF) ⁷⁵	454 (14450), 486 (28500), 522 (40240), 582
<i>p</i> -chlorophenyl (DMF) ^{48,75}	458 (37000), 489 (65000), 525 (90156)
(CH ₂) ₁₁ CH ₃ (CHCl ₃) ⁷⁶	460 (17400), 490 (47400), 526 (76200)
(CH ₂) ₃ Si ₈ O ₁₂ iBu ₇ (CHCl ₃)	459 (17157), 490 (48730), 526 (80877)
(CH ₂) ₁₇ CH ₃ (DMF) ⁷⁵	458(18580), 489 (52850), 525 (86100), 582
(CH ₂) ₁₁ CH ₃ (DMF) ⁷⁵	454 (18580), 487 (52850), 523 (87630)
CH(C ₆ H ₁₃) ₂ (CHCl ₃) ⁷⁷	524 (88700)
N-N'-di(1-dehydroabietyl) (CHCl ₃) ⁷⁶	458 (25800), 490 (58950), 526 (93200)
(3,5-C(CH ₃) ₃)C ₆ H ₃ (CHCl ₃) ⁷⁸⁻⁸¹	526 (95000)
CH ₂ (CH ₃) ₃ ⁸²	456, 486, 522 (99000)
Ph ⁸²	525
<i>p</i> -cyanophenyl ⁷⁵	462, 490, 526, 579
3.9	459 (17157), 490 (48730), 526 (80877)

3.6.8 Steady State Spectrofluorometric Emission Studies of POSS Imides

3.6.8.1 Emission Spectrum of Mono-naphtha POSS Imide

Excitation of **3.6** ($\lambda_{\text{exc}} = 335\text{nm}$) yielded emission bands with a maximum at 380 nm and shoulder bands at 362 and 398 nm (**Figure 3.33**). The fluorescence observed was extremely weak compared to that of perylenes, with a quantum yield (Φ_{F}) of 0.02 (N,N'-Bis(2,6-dimethylphenyl)perylene-3,4,9,10-tetracarboxylic diimide reference) observed. Two overlapping electronic levels of the naphthalene structure were postulated as being responsible for the fluorescence deactivation.⁶⁵

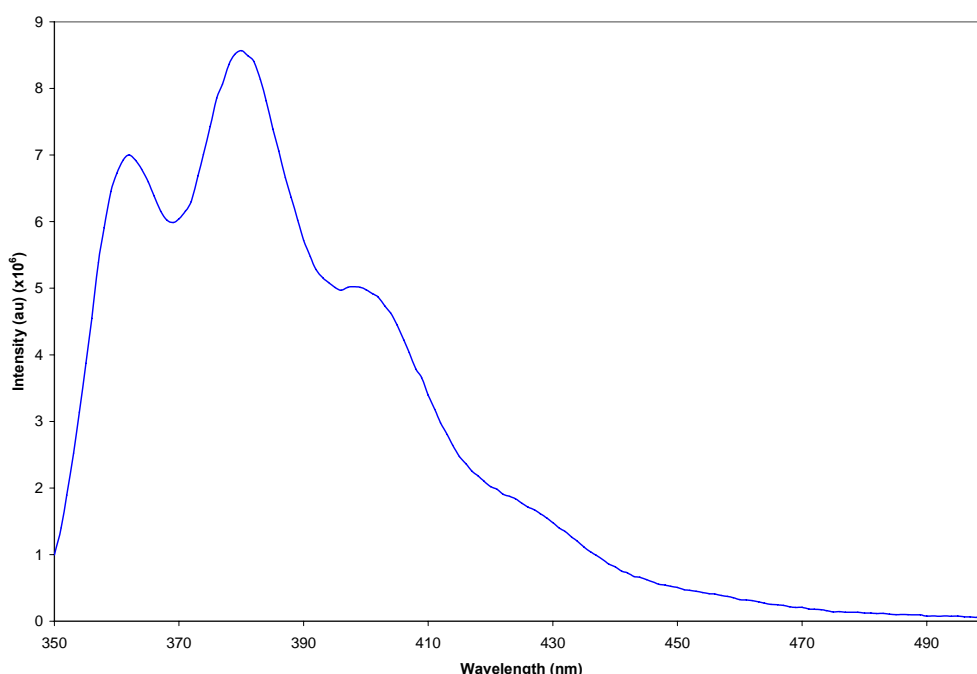


Figure 3.33. Emission spectrum of mono-naphtha POSS imide 3.6 in toluene ($\lambda_{\text{exc}} = 335\text{nm}$)

The weak fluorescence of **3.6** was similar to that of other mono-naphtha imides (**Figure 3.33**), which exhibited solvent dependant fluorescence maxima. Chloroform was not detailed in this particular literature study; however spectra acquired in solvents of comparable dielectric constants (κ), such as toluene ($\kappa = 2.236$) and 1-chlorobutane ($\kappa = 7.147$) exhibited fluorescence maxima ranging from 367 to 391 nm for a range of R groups, where R = *i*Pr, C₂H₅OH and CH(CH₂OH)₃.⁶⁰ Quantum yields of various naphthalene imides were 0.01 (toluene, R = *i*Pr), 0.01 (1-

chlorobutane, R = *i*Pr), 0.05 (toluene, R = C₂H₅OH), 0.01 (1-chlorobutane, R = C₂H₅OH), 0.09 (toluene, R = CH(CH₂OH)₃) and 0.16 (1-chlorobutane R = CH(CH₂OH)₃), relative to 2-aminopyridine as a standard.⁶⁰ The fluorescence quantum yields are able to be compared due to the use of absolute values for the quantum yield determinations. The quantum yield of the literature mono-naphthalimides were determined relative to 2-aminopyridine, which exhibited an absolute quantum yield of 0.68, determined by the use of a fully corrected integrating sphere spectrofluorometer, calibrated with quinine bisulfate.⁸³ The perylene standard used in this work, N,N'-Bis(2,6-dimethylphenyl)perylene-3,4,9,10-tetracarboxylic diimide, exhibited a quantum yield of 0.98 relative to rhodamine,⁸² which itself possessed a quantum yield of 1.0.⁸⁴

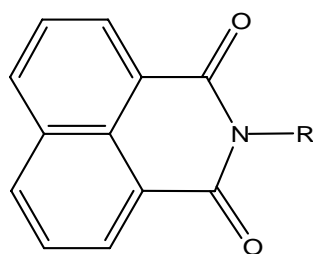


Figure 3.34. Examples of mono-naphthalimides⁶⁰

3.6.8.2 Emission Spectrum of Bis-naphthalimide

Excitation of **3.7** ($\lambda_{\text{exc}} = 350$ nm) yielded emission bands with maxima at 386 and 404 nm (**Figure 3.35**). The resultant weak fluorescence ($\Phi_{\text{F}} = 0.05$) is similar to that present in other bis-naphthalimides, such as bis(1-methylpropyl)naphthalene diimide, which displayed a weak fluorescence band at approximately 420 nm (no Φ_{F} reported),⁶⁶ and bis-(cyanophenyl)naphthalene diimide, which displayed a fluorescence maxima at 403 nm in DMF ($\Phi_{\text{F}} = 0.003$).⁷⁴ As noted for the mono-naphthalimides, two overlapping electronic levels of the naphthalene structure were postulated as being responsible for the fluorescence deactivation.⁶⁵

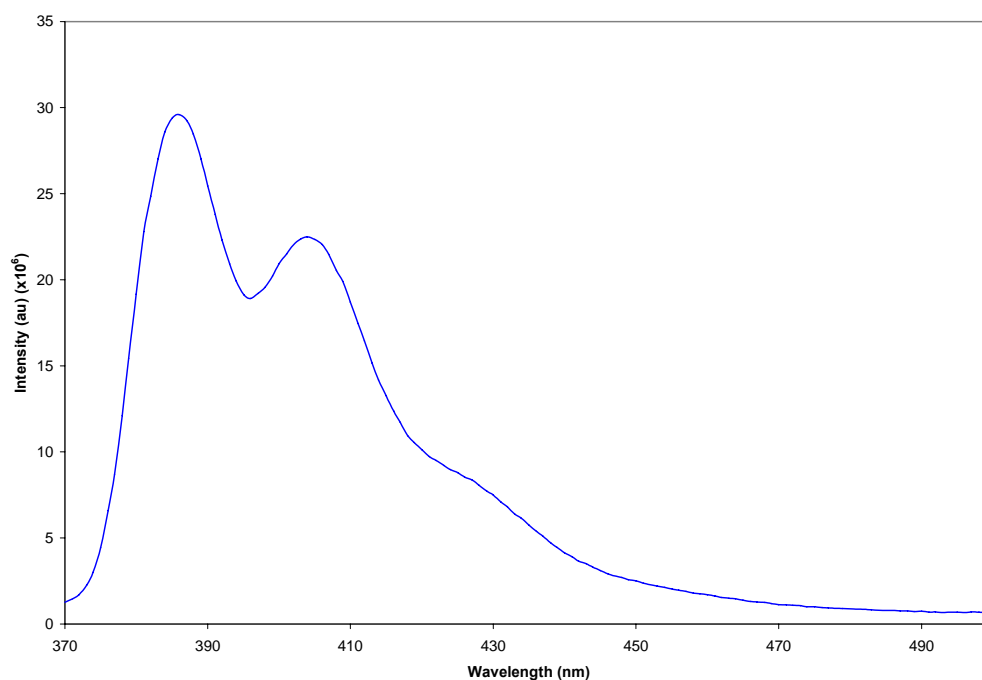


Figure 3.35. Emission spectrum of bis-naphtha POSS imide 3.7 in toluene
($\lambda_{\text{exc}} = 350 \text{ nm}$)

3.6.8.3 Emission Spectrum of Biphenyl POSS Imide

The fluorescence spectrum of **3.8** ($\lambda_{\text{exc}} = 320 \text{ nm}$) (**Figure 3.36**) contained a $\pi\text{-}\pi^*$ fluorescence band at 389 nm ($\Phi_{\text{F}} = 0.07$, N,N'-Bis(2,6-dimethylphenyl)perylene-3,4,9,10-tetracarboxylic diimide). The position of the fluorescence band was similar to that of comparable structures described in the literature, such as bis(butyl)biphenyldiimide, which exhibited a fluorescence maximum at 380 nm (no Φ_{F} reported)⁸⁵ and bis(cyclohexyl)biphenyldiimide, which exhibited a fluorescence maximum at 385nm, ($\Phi_{\text{F}} = 0.04$).⁷¹

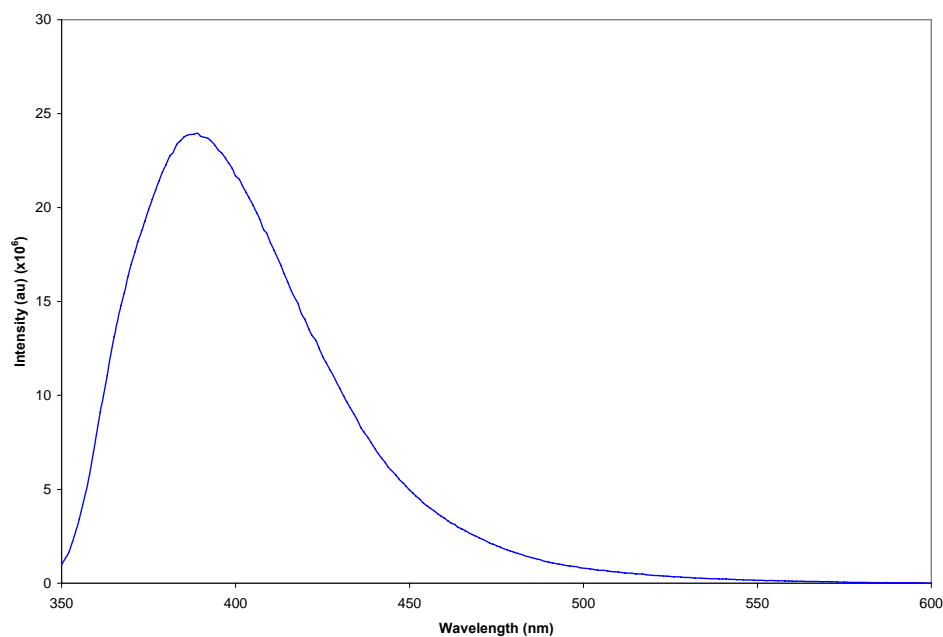


Figure 3.36. Emission spectrum of biphenyl POSS imide 3.8 in toluene
 $(\lambda_{\text{exc}} = 320 \text{ nm})$

3.6.8.4 Emission Spectrum of Perylene POSS Imide

Excitation of **3.9** ($\lambda_{\text{exc}} = 450\text{nm}$) resulted in an emission maximum at 533 nm, with the first and second red-shifted vibrational satellites at 575 and 620 nm ($\Phi_{\text{F}} = 1.0$) (**Figure 3.37**).

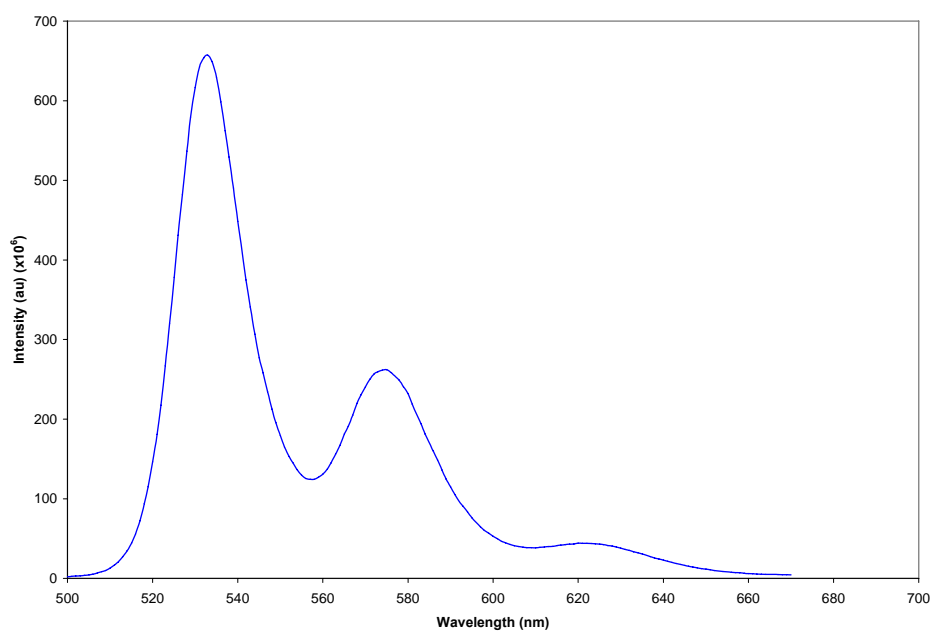


Figure 3.37. Emission spectrum of perylene POSS imide 3.9 in toluene
 $(\lambda_{\text{exc}} = 450\text{nm})$

This quantum yield was comparable to values reported for a range of perylene derivatives in the literature, from 0.70 to 1 (**Table 3.9**). Perylene bis-imides, where R = *p*-cyanophenyl⁷⁴ and *p*-hydroxyphenyl,⁷⁵ exhibited much lower quantum yields of 0.14 and 0.20, due to molecular aggregation in solution. The perylene bis-imide where R = Ph also displayed a lower quantum yield of 0.70, due to a lower degree of twisting freedom relative to the perpendicular orientation, and reduced solubility, as the external phenyl groups were able to twist into near co-planarity with the perylene core.⁸²

Table 3.9. Fluorescence data of various N-substituted perylenes in chloroform

N substituent	λ_F (nm)	Φ_F
(CH ₂) ₁₂ NH ₂ (CHCl ₃) ⁴⁸	537	0.83
<i>p</i> -hydroxyphenyl (DMF) ⁷⁵	534	0.20
<i>p</i> -chlorophenyl (DMF) ^{48,75}	534	0.84
(CH ₂) ₁₁ CH ₃ (CHCl ₃) ⁷⁶	533	1
(CH ₂) ₁₇ CH ₃ (DMF) ⁷⁵	535	0.80
(CH ₂) ₁₁ CH ₃ (DMF) ⁷⁵	536	1
CH(C ₆ H ₁₃) ₂ (CHCl ₃) ⁷⁷	534	1
N-N'-di(1-dehydroabietyl) (CHCl ₃) ⁷⁶	536	1
(3,5-C(CH ₃) ₃)C ₆ H ₃ (CHCl ₃) ⁷⁸⁻⁸¹	540	1
CH ₂ (CH ₃) ₃ ⁸²	538	0.99
Ph ⁸²	-	0.70
<i>p</i> -cyanophenyl ⁷⁵	537	0.136
3.9	533	1.0

3.6.9 Single Crystal X-ray Structure of Perylene POSS Imide

Crystallisation of the POSS imides was attempted with **3.2** and **3.3**; however the compounds remained amorphous despite the use of a wide range of solvents and conditions. Therefore, more conjugated systems, such as naphthalic and biphenyl POSS imides were synthesised. However, once again the compounds remained amorphous in nature. The self-assembly of triethoxysilane functionalised perylenes

through π - π interactions of the aromatic perylene cores had previously been reported in the literature, and it was postulated that the extended conjugation of the perylene moiety and increased separation of the POSS moieties, due to the larger size of the perylene group, would aid in crystallisation. Single crystals suitable for x-ray crystallography were grown from the vapour diffusion of methanol into a chloroform solution of **3.9**.

Table 3.10. X-ray parameters

Molecular formula	$C_{86}H_{146}N_2O_{28}Si_{16}$
Formula weight	2105.44
Crystal description	Plate
Crystal colour	Red
Crystal dimensions (mm)	0.33 x 0.07 x 0.011
Crystal system	Triclinic
Space group	P-1
a [Å]	11.464(3)
b [Å]	20.859(7)
c [Å]	23.103(2)
α [°]	89.46(2)
β [°]	81.78(2)
γ [°]	81.96(2)
V [Å ³]	5414(2)
Z	2
D _{calc} [g/cm ³]	1.292
F(000)	2248
Temperature (K)	100(2)
λ (CuK α) [Å]	1.5418
Range in Θ [°]	2.8654 - 65.7028
<i>hkl</i> range	-13 to 13, -24 to 24, -27 to 26
Reflections collected	18388
Unique data	5745
$I_0 > 2\sigma$	6576
Parameters refined	1217
R(gt)	0.1774
R _w (gt)	0.067
Goodness of Fit	0.0849

The molecular structure of **3.9** is depicted in **Figure 3.38**. A summary of crystallographic data is given in **Table 3.10**, with interatomic parameters detailed in **Table 3.11** and **Table 3.12**.

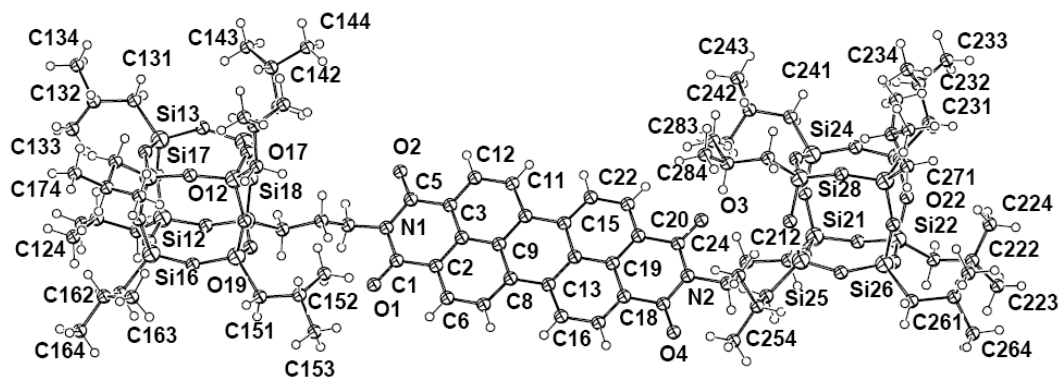


Figure 3.38. Single crystal x-ray structure of perylene POSS imide **3.9**

The POSS perylene molecules crystallised in the triclinic space group P-1. The central perylene core was essentially flat in nature, with a C4-C3-C9-C8 torsional angle of 1.861 °. The nitrogen bound POSS cages essentially adopted a *cis*-like conformation. This allowed for optimum packing of the molecule within the unit cell (**Figure 3.39**), as a POSS cage of an adjacent molecule was able to slot within the cavity between two POSS cages of one molecule of **3.9**, thus allowing for the π - π stacking of adjacent perylene cores on the neighbouring surface of the molecule.

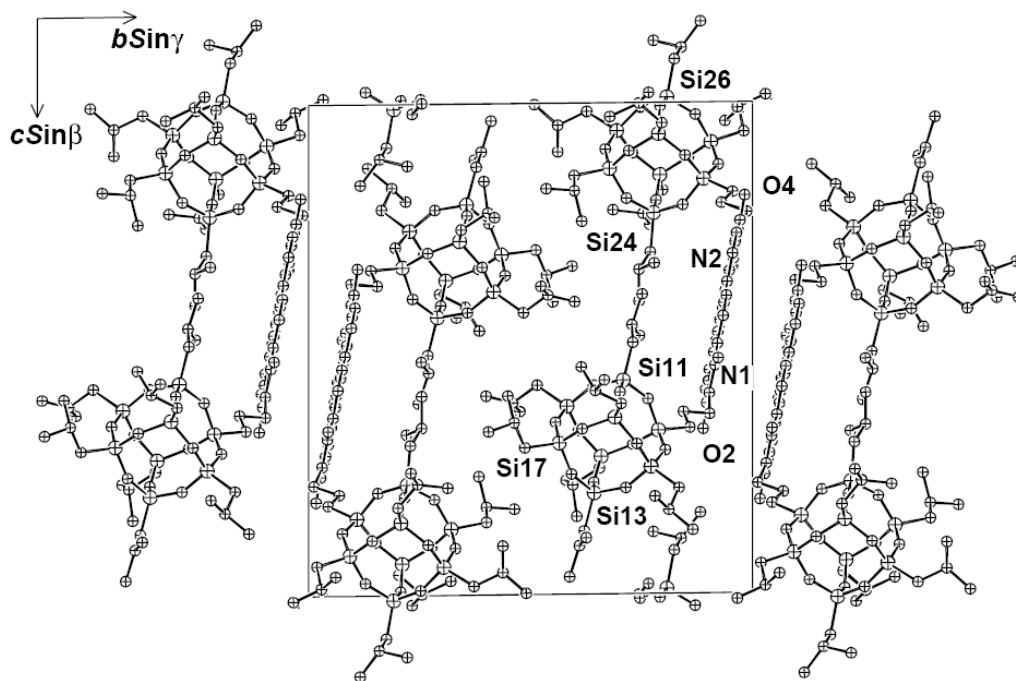


Figure 3.39. Unit cell diagram of perylene POSS imide 3.9

X-ray diffraction of several single crystal structures has shown that parent perylene bis-imides exhibit flat π -systems.^{53,86-90} The numbering scheme used to describe the POSS perylene bis-imide core used in the structural description of **3.9** is shown in **Figure 3.40**.

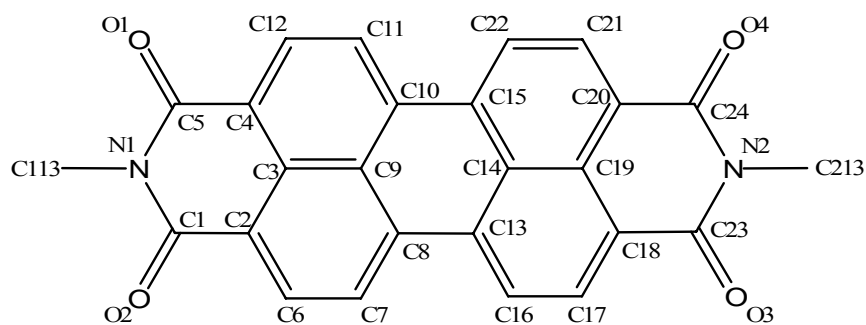


Figure 3.40. Numbering scheme used for perylene POSS imide 3.9

Table 3.11. Bond distances of perylene POSS imide (3.9) and literature perylene bis-imides⁵³

Bond	POSS Distance (Å)	Bond	POSS Distance (Å)	Avg. Distance (Å)
C1-N1	1.3639 (.0099)	C23-N2	1.3969 (.0087)	1.38
C1-C2	1.4957 (.0087)	C18-C23	1.4879 (.0088)	1.47
C2-C3	1.4171 (.0088)	C18-C19	1.3978 (.0099)	1.41
C2-C6	1.3532 (.0099)	C17-C18	1.3760 (.0096)	1.36
C3-C4	1.3819 (.0099)	C19-C20	1.4102 (.0088)	1.43
C3-C9	1.4130 (.0083)	C14-C19	1.4269 (.0083)	1.41
C4-C5	1.4987 (.0092)	C20-C24	1.4924 (.0088)	1.47
C4-C12	1.3761 (.0095)	C20-C21	1.3451 (.0099)	1.37
C5-N1	1.4050 (.0090)	C24-N2	1.3583 (.0085)	1.41
C6-C7	1.3851 (.0092)	C16-C17	1.4083 (.0092)	1.39
C7-C8	1.3862 (.0101)	C13-C16	1.3681 (.0099)	1.40
C8-C9	1.4346 (.0099)	C13-C14	1.4300 (.0088)	1.42
C8-C13	1.4464 (.0088)	C10-C15	1.4736 (.0084)	1.46
C9-C10	1.4412 (.0088)	C14-C15	1.4179 (.0099)	1.43
C10-C11	1.3811 (.0098)	C15-C22	1.3827 (.0088)	1.37
C11-C12	1.4120 (.0083)	C21-C22	1.4014 (.0088)	1.40
C113-N1	1.4775 (.0077)	C213-N2	1.4776 (.0076)	1.51
C111-C112	1.5434 (.0078)	C211-C212	1.5486 (.0085)	-
C112-C113	1.5014 (.0092)	C212-C213	1.5220 (.0078)	-
C113-N1	1.4775 (.0097)	C213-N2	1.4776 (.0076)	-
C113-Si1	1.8431 (.0068)	C213-Si2	1.8504 (.0057)	-

The average bond distances observed in a range of perylene bis-imide crystal structures together with the bond distances observed in the POSS perylene bis-imide synthesised in the present work are detailed in **Table 3.11**.⁵³ It was evident from the bond distances of the perylene POSS that the two naphthalene half units exhibited similar bond distances and, in the majority of instances, there was close correlation between the literature bond distances and those observed in the perylene-POSS structure. Thus the perylene core of the molecule was consistent with other perylene crystal structures described in the literature.

The bond angles associated with the perylene moiety are detailed in **Table 3.12**. The bond angles associated with the imide ring were 123.84 and 125.14 ° for C-N-C and

115.39 to 118.78 ° for N-C-C, with these values falling within the range reported in the literature (121.9 to 124.9 ° and 116.6 to 118.4 °).^{88,90,91} The bond angles of the perylene core ranged from 118.70 to 121.79 ° with a mean of 119.46 ° for C-C-C, with these values within the range reported in the literature (118.5 to 120.7 °).⁹²

Table 3.12. Bond Angles of perylene POSS imide (3.9)

Bonds	Angle (°)	Bonds	Angle (°)
Si11-C111-C112	113.57 (.42)	Si21-C211-C212	113.69 (.42)
C111-C112-C113	108.67 (.48)	C211-C212-C213	109.82 (.50)
N1-C113-C112	113.21 (.52)	N2-C213-C212	113.19 (.52)
C1-N1-C5	123.84 (.55)	C23-N2-C24	125.14 (.52)
N1-C1-C2	118.77 (.59)	N2-C23-C18	115.59 (.57)
C1-C2-C3	119.61 (.61)	C23-C18-C19	121.60 (.57)
C2-C3-C4	119.54 (.56)	C18-C19-C20	120.13 (.55)
C3-C4-C5	121.79 (.62)	C19-C20-C24	118.70 (.61)
C4-C5-N1	116.37 (.60)	C20-C24-N2	118.78 (.60)
C-C-C perylene	120.02		

The bond angles associated with the propyl chains of the POSS cages were 113.57 and 113.69 ° for the Si-C-C bond angle, with these values falling within the range reported in the literature.⁹³⁻⁹⁶ The C-C-C bond angles were 108.67 and 109.82 °, with these values falling within the range reported in the literature (109.907 to 114.623 °).⁹³ The N-C-C bond angles were 113.21 and 113.19 °, with these values falling within the range reported in the literature (111.246 to 113.70°).^{90,91,96}

Table 3.13 details the variation of bond distances and angles of a variety of octasubstituted POSS crystal structures from the literature together with the perylene POSS structure in the present work. Despite the wide variety in size of the carbon-bound pendant groups, only slight variations in the cage geometry were detected. This resulted from the primary factor influencing the cage geometry in the solid state being the molecule's crystal lattice; with the influence of the carbon-bound pendant group on the geometry of the silicon atom to which it is attached being relatively minor.⁹⁴

Table 3.13. Bond distances and angles of POSS containing crystal structures

R group	Mean Si-O (Å)	Mean Si-O-Si (°)	Mean O-Si-O (°)	Ortho Si-Si (Å)	Meta Si-Si (Å)	Para Si-Si (Å)
Allyl ⁹⁷	1.62	150.7	108.2	3.13	4.43	5.42
CH ₂ CH ₂ Si(CH=CH ₂) ₃ ⁹⁸	1.60	150.3	108.4	3.10	4.38	5.37
Vinyl ⁹⁹	1.61	150.3	108.5	3.10	4.39	5.37
Cyclohexyl ⁹⁴	1.61	150.1	108.6	3.10	4.39	5.38
Cyclohexyl ⁹⁴	1.61	149.4	108.8	3.11	4.39	5.38
Cyclohexyl ⁹⁴	1.62	149.3	109.0	3.12	4.41	5.40
<i>i</i> -Butyl ⁹⁹	1.62	149.8	108.7	3.12	4.41	5.40
<i>p</i> -Methoxyphenylpropyl ⁹⁴	1.62	149.5	108.8	3.12	4.41	5.40
CH ₂ CH ₂ CMe ₂ CO ₂ Me ¹⁰⁰	1.62	149.2	108.8	3.12	4.41	5.40
<i>n</i> -Octyl ⁹⁴	1.62	149.2	108.8	3.12	4.41	5.40
Me-piperidone ¹⁰¹	1.61	148.8	108.9	3.11	4.40	5.38
Cyclopentyl ¹⁰⁰	1.62	148.6	108.9	3.12	4.41	5.40
3-Iodopropyl ⁹⁵	1.62	149.3	109.0	3.11	4.40	5.39
Benzyl ⁵⁶	1.62	148.9	109.0	3.11	4.40	5.39
Ethyl ¹⁰²	1.61	149.3	109.0	3.10	4.39	5.37
Phenyl ¹⁰³	1.61	149.2	109.1	3.10	4.39	5.38
CH ₂ CH ₂ OCH ₂ CH ₂ Cl ¹⁰⁴	1.62	-	108.9	-	-	-
3.9	1.62	149.4	108.7	3.12	4.42	5.41

The Si-O bonds ranged from 1.5934 to 1.6385 Å, with a mean bond distance of 1.6188 Å, with these values falling within the range of those reported in the literature (1.60 to 1.62 Å).^{56,94,95,97-103} The Si-C bond distances range from 1.8182 to 1.8524 Å, with a mean bond distance of 1.8390 Å, with these values falling within the range of those reported in the literature (1.71 to 1.97 Å).^{95-97,101} The Si-O-Si angles ranged from 140.29 to 160.16 ° with a mean bond angle of 149.38 °, with these values falling within the range of those reported in the literature (148.6 to 150.7 °).^{56,94,95,97-103} The O-Si-O bond angles ranged from 107.21 to 110.18° with a mean bond angle of 108.71° with these values falling within the range of those reported in the literature (108.2 to 109.1 °). The O-Si-C bond angles in the POSS perylene ranged from 107.87 to 112.97 °, with these values falling within the range of those reported in the literature (107.63 to 113.10 °) for octa-(isobutyl)POSS.¹⁰⁰ The cage geometry contained within the POSS-perylene molecule agreed with other POSS containing crystal structures detailed within the literature, thus there was little distortion of the

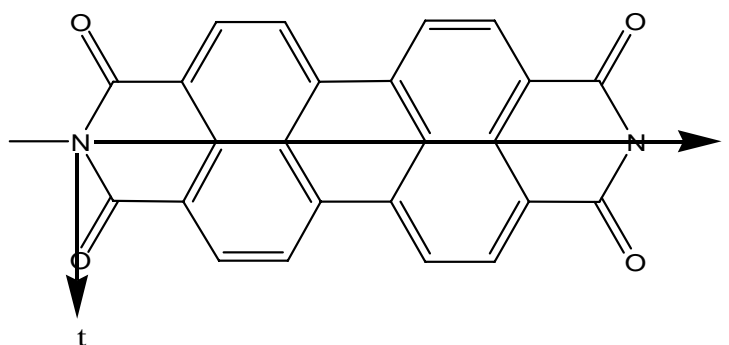
cage structure through the attachment of the perylene group.

The *ortho* Si-Si distances ranged from 3.0553 to 3.1874 Å, with a mean value of 3.12 Å, with the mean value falling within the range of those reported in the literature (3.10 to 3.13 Å).^{56,94,95,97-103} The *meta* Si-Si distances ranged from 4.3653 to 4.4421 Å, with a mean value of 4.42 Å, with the mean value falling within the range of those reported in the literature (4.38 to 4.43 Å).^{56,94,95,97-103} The *para* Si-Si distances ranged from 5.3743 to 5.5737 Å, with a mean value of 5.41 Å, with the mean value falling within the range of those reported in the literature (5.37 to 5.42 Å).^{56,94,95,97-103} Thus, the silicon-silicon distances contained within the cage geometry were in agreement with a range of other POSS crystal structures in the literature.

Sterical strain in the bay region of the perylene moiety can lead to propeller-like twisting of the two naphthalene sub units, examples of which have been seen crystallographically for a tetrachloro-¹⁰⁵ and tetraphenoxy-substituted¹⁰⁶ perylene bis-imides, with torsional angles of 37 and 25 °, respectively. This distortion from planarity imposed considerable distortion in the solid state packing and molecular aggregation of these dye molecules. The solubility was enhanced, especially for the tetraphenoxy- derivative, due to the motional freedom of the substituents. The lack of substitution in the bay region of the perylene POSS bis-imide implied that the perylene units, similar to other previously investigated perylene bis-imides; exhibited an essentially planar geometry, confirmed by the C4-C3-C9-C8 torsional angle of 1.861 °. The parallel separation distance of **3.9** (3.496 Å), was comparable to other perylene bis-imides in the literature, which exhibited parallel separation distances ranging from 3.34-3.55 Å.^{53,86-89}

A remarkable feature of perylene bis-imides is their crystallochromy, defined as colour changes resulting from interaction of the π systems in the crystal lattice.⁵³ Whilst all perylene dyes exhibit an orange colour in solution, vastly different colours are present in the solid state, including red, maroon, red-violet and black.² An empirical relationship (**Figure 3.41**), has previously been postulated for the dependence of crystal colour upon the longitudinal and transverse offsets of the dye, relating the bathochromic shift and band broadening to the extent of the π - π contact

area between the stacked chromophores.^{86-89,107}



$$\lambda_{\max} = 9.78t^2 - 82.009t - 21.888l + 735.329$$

Figure 3.41. Empirical variation of perylene absorption maximum¹⁰⁸

Relatively large transverse offsets result in minimum π - π interactions, leading to pigments with small crystallochromic shifts compared with their solution spectra. An example of this is PR 178 (**Figure 3.42**), which exhibits a brilliant red shade. For smaller transverse offsets, more perturbation occurred and maroon pigments were apparent, such as PR 179 (**Figure 3.42**). The extended chromophoric system in the longitudinal direction implied that shifting in this direction was less effective at reducing the coupling between neighbouring π systems. Therefore pigments with even further reduced transverse offset, such as PBI 32 (**Figure 3.42**), were often black due to the strong electronic interactions between neighbouring dyes.¹⁰⁶

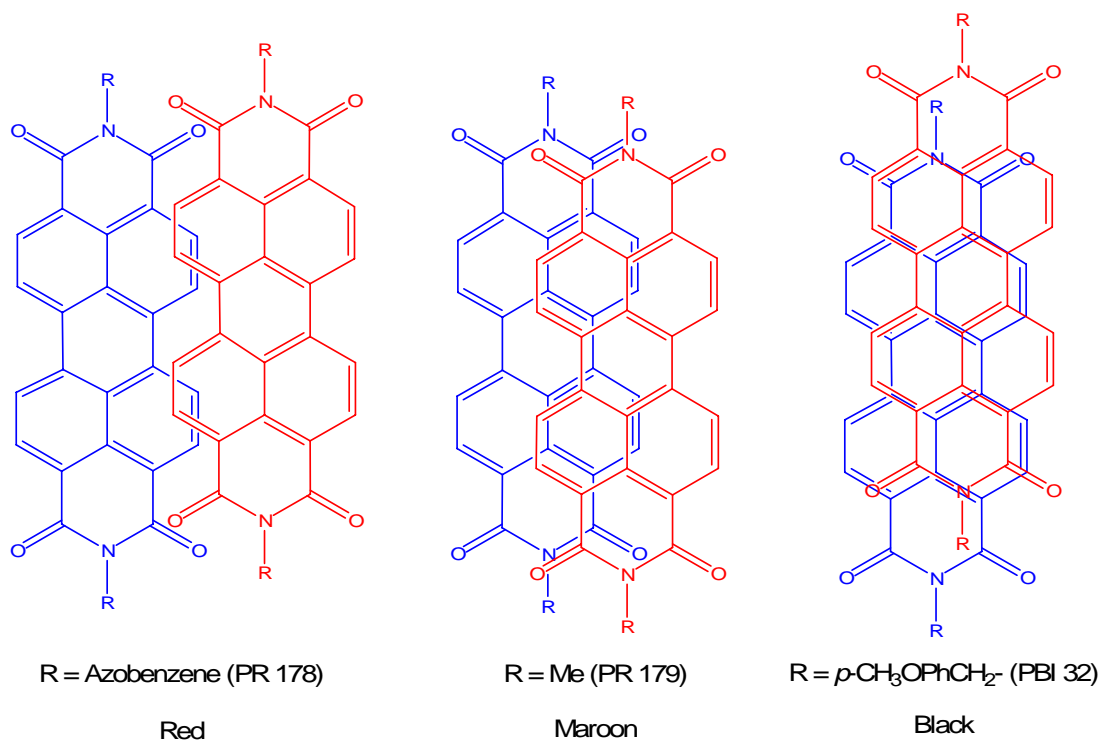


Figure 3.42. Transverse and longitudinal displacements of perylenes¹⁰⁶

3.9 exhibited transverse and longitudinal offsets of 3.0 and 1.5 Å (**Figure 3.43**), with a red pigment observed.

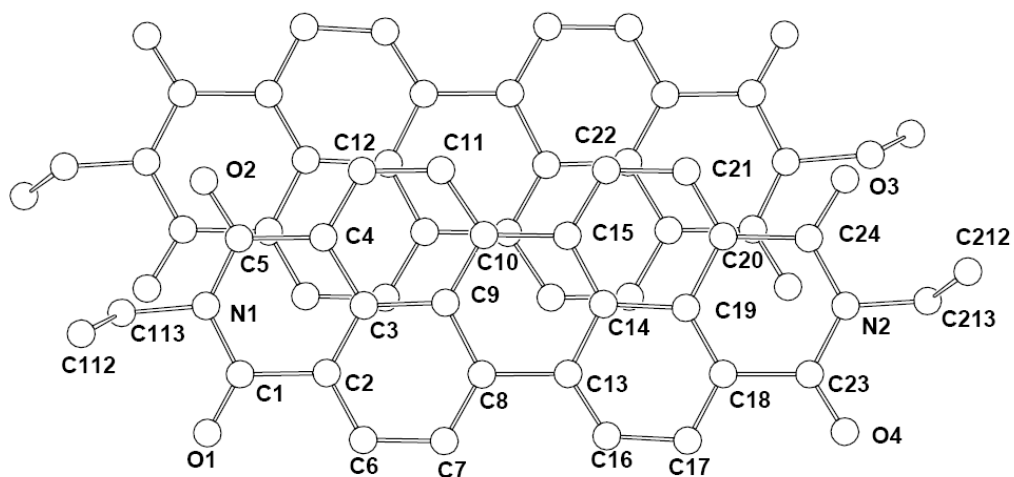


Figure 3.43. Overlay of perylene regions

Crystallochromic effects have also been studied via the use of extended Hückel calculations on one-dimensional infinite stacks of dyes as a function of the two offset parameters. The results indicated that the crystallochromic effect was a product of

not only the degree of overlap of adjacent perylene moieties but also the nodal characteristics of the HOMO and LUMO orbitals of the individual perylenes.¹⁰⁸

The steric requirement of the imide substituent dictates the stacking distance and longitudinal and transverse offset of the perylene bisimides.^{86-89,107} The unit cell, (**Figure 3.39**), showed the bulky POSS groups being present in a *cis*-like coordination, with the central perylene core interacting with an adjacent perylene moiety through π - π interactions. The incorporation of π -electron perylenes onto the periphery of the POSS cage effectively isolated the chromophores from each other by both steric and electronic effects, due to the rigid and bulky core and the non-conjugated nature of the siloxane bond.²⁶

3.7 Conclusions and Future Work

A range of POSS imides have been synthesised through the condensation of POSS amines with a variety of mono and bis-anhydrides. The POSS imides were characterised by ¹H, ¹³C and ²⁹Si NMR, FTIR, elemental analysis, UV-VIS and fluorescence spectrophotometry and ESI mass spectrometry. The bis-POSS perylene diimide was also characterised by single crystal x-ray crystallography. The various methods of characterisation confirmed the formation of the desired POSS imides.

The x-ray crystal structure of the perylene diimide confirmed that the incorporation of perylene functionality onto the periphery of the bulky POSS molecule partially isolated the perylene moieties and thus reduced the aggregation of the aromatic perylene cores in the solid state.

The formation of POSS polyimide hybrid materials has previously been investigated. The incorporation of the anhydrides used to synthesise mono-functional imides in this chapter could be applied on a multi-functional scale and the mechanical and physical properties examined. This would likely involve the use of another bis-anhydride, in conjunction with a small amount of the perylene bis-anhydride to form the POSS imide product. It is expected that a reduction in the dielectric constant

would occur, due to the presence of the porous POSS cages and the increase in free volume from the presence of the large, rigid POSS structure.¹⁰⁹

Incorporation of bay functionalised perylenes would allow for the formation of a variety of pigments, due to the disruption of the planarity and solid state packing of the perylene moieties.

Synthesis of a monosubstituted perylene anhydride and subsequent reaction with octa-aminopropyl POSS would enable the synthesis of octa-perylene functionalised POSS. This could be done in a variety of ways, through decarboxylation of one of the anhydride functionalities to form a perylene mono anhydride, or the reaction of one anhydride with a long chain amine, to increase the solubility of the desired product.

3.8 References:

- (1) H. Zollinger *Color Chemistry*; VCH: Weinheim, 2003; Vol. 3rd Edn.
- (2) W. Herbst; K. Hunger *Industrial Organic Pigments: Production Properties, Applications*; 2nd Edn. ed.; Wiley-VCH: Weinheim, 1997.
- (3) C. W. Struijk; A. B. Sieval; J. E. J. Dakhorst; M. van Dijk; P. Kimkes; R. B. M. Koehorst; H. Donker; T. J. Schaafsma; S. J. Picken; A. M. van de Craats; J. M. Warman; H. Zuilhof; E. J. R. Sudholter *J. Am. Chem. Soc.* **2000**, *122*, 11057.
- (4) C. D. Dimitrakopoulos; P. R. L. Malenfant *Adv. Mater.* **2002**, *14*, 99.
- (5) S. K. Lee; Y. Zu; A. Herrmann; Y. Geerts; K. Mullen; A. J. Bard *J. Am. Chem. Soc.* **1999**, *121*, 3513.
- (6) F. Wuerthner *Angew. Chem. Int. Ed.* **2001**, *40*, 1037.
- (7) K. Y. Law *Chem. Rev.* **1993**, *93*, 449.
- (8) A. Yakimov; S. R. Forrest *Appl. Phys. Lett.* **2002**, *80*, 1667.
- (9) G. Geissler; H. Remy; Hoechst AG: DE, 1959.
- (10) S. Mais; J. Tittel; T. Basche; C. Brauchle; W. Gohde; H. Fuchs; G. Muller; K. Mullen *J. Phys. Chem. A* **1997**, *101*, 8435.
- (11) M. Schneider; K. Mullen *Chem. Mater.* **2000**, *12*, 352.
- (12) C. Julien; A. Debarre; D. Nutarelli; A. Richard; P. Tchenio *J. Phys. Chem. B* **2006**, *110*, 3902.
- (13) C. Julien; A. Debarre; D. Nutarelli; A. Richard; P. Tchenio *J. Phys. Chem. B* **2005**, *109*, 23145.
- (14) Y. Luo; J. Lin; H. Duan; J. Zhang; C. Lin *Chem. Mater.* **2005**, *17*, 2234.
- (15) L. Bes; A. Rousseau; B. Boutevin; R. Mercier; B. Sillion *Macromol. Chem. Phys.* **2001**, *202*, 933.
- (16) S. Duda-Johner; J. O. Dai; K. Mohr; R. Tacke *J. Organomet. Chem.* **2003**, *686*, 75.
- (17) N. Kimizuka; T. Kawasaki; K. Hirata; T. Kunitake *J. Am. Chem. Soc.* **1995**, *117*, 6360.
- (18) G. Chen; J. T. Lean; M. Alcalá; T. E. Mallouk *J. Org. Chem.* **2001**, *66*, 3027.
- (19) S. Bevers; S. Schutte; L. W. McLaughlin *J. Am. Chem. Soc.* **2000**, *122*, 5905.
- (20) L. L. Miller; K. R. Mann *Acc. Chem. Res.* **1996**, *29*, 417.
- (21) F. Würthner *Angew. Chem. Int. Ed.* **2001**, *40*, 1037.
- (22) S. Erten; S. Alp; S. Icli *J. Photochem. Photobiol. A: Chem.* **2005**, *175*, 214.
- (23) Z. Qiu; S. Zhang *Polymer* **2005**, *46*, 1693.
- (24) F. Wuerthner; C. Thalacker; S. Diele; C. Tschierske *Chem. Eur. J.* **2001**, *7*, 2245.
- (25) F. Wuerthner; C. Thalacker; A. Sautter; W. Scharlt; W. Ibach; O. Hollricher *Chem. Eur. J.* **2000**, *6*, 3871.
- (26) I. Imae; Y. Kawakami *J. Mater. Chem.* **2005**, *15*, 4581.
- (27) H. J. Cho; D. H. Hwang; J. I. Lee; Y. K. Jung; J. H. Park; J. Lee; S. K. Lee; H. K. Shim *Chem. Mater.* **2006**, *18*, 3780.
- (28) Y. Xiao; L. Liu; C. He; W. S. Chin; T. Lin; K. Y. Mya; J. Huang; Lu, X. *J. Mater. Chem.* **2006**, *16*, 829.

- (29) J. Lee; H.-J. Cho; N. S. Cho; D.-H. Hwang; J.-M. Kang; E. L.; J.-I. Lee; H.-K. Shim *J. Polym. Sci. A. Polym. Chem.* **2006**, *44*, 2943.
- (30) K. Takagi; S. Kunii; Y. Yuki *J. Appl. Polym. Sci.* **2005**, *43*, 2119.
- (31) W.-J. Lin; W.-C. Chen; W.-C. Wu; Y.-H. Niu; Jen, A. K.-Y. *Macro.* **2004**, *37*, 2335.
- (32) J.-C. Huang; C.-B. He; Y. Xiao; K. Y. Mya; J. Dai; Y. P. Siow *Polymer* **2003**, *44*, 4491.
- (33) R. Tamaki; J. Choi; R. M. Laine *Chem. Mater.* **2003**, *15*, 793.
- (34) J. Carsten; K. Adolf **2003**, WO03042223.
- (35) H. Liu; W. Zhang; S. Zheng *Polymer* **2005**, *46*, 157.
- (36) M.-C. Gravel; C. Zhang; M. Dinderman; R. M. Laine *Appl. Organometal. Chem.* **1999**, *13*, 329.
- (37) F. J. Feher; Kevin D. Wyndham *Chem. Comm.* **1998**, 323.
- (38) S. Jothibas; S. Premkumar; M. Alagar; I. Hamerton *High Perf. Polym.* **2008**, *20*, 67.
- (39) F. J. Feher; K. D. Wyndham; D. Soulivong; F. Nguyen *J. Chem. Soc., Dalton Trans.* **1999**, *9*, 1491.
- (40) C.-M. Leu; G. M. Reddy; K.-H. Wei; C.-F. Shu *Chem. Mater.* **2003**, *15*, 2261.
- (41) R. Tamaki; Y. Tanaka; M. Z. Asuncion; J. Choi; R. M. Laine *J. Am. Chem. Soc.* **2001**, *123*, 12416.
- (42) S. G. Jegenathan; G. Suruliappa; D. Bramer; R. Kote; G. J. Maladkar; Corporation, C. S. C., Ed. USA, 2008.
- (43) C. M. Leu; Y. T. Chang; K. H. Wei *Macro.* **2003**, *36*, 9122.
- (44) K. H. Wei; C. M. Leu; National Chiao Tung University: USA, 2005.
- (45) K. Kacprzak *Synth. Comm.* **2003**, *33*, 1499.
- (46) M. O. Liu; C.-H. Tai; C.-W. Chen; W.-C. Chang; A. T. Hu *J. Photochem. Photobiol. A: Chem.* **2004**, *163*, 259.
- (47) N. B. Bowden; K. A. Willets; W. E. Moerner; R. M. Waymouth *Macro.* **2002**, *35*, 8122.
- (48) H. Icil; E. Arslan *Spec. Lett.* **2001**, *34*, 355.
- (49) L. Feiler; H. Langhals; K. Polborn *Lieb. Annal.* **1995**, 1225.
- (50) D. H. Williams; I. Fleming *Spectroscopic Methods in Organic Chemistry*; Fifth ed.; McGraw-Hill: Berkshired, 1995.
- (51) M. E. Wright; B. J. Petteys; A. J. Guenther; G. R. Yandek; L. C. Baldwin; C. Jones; M. J. Roberts *Macro.* **2007**, *40*, 3891.
- (52) Laurence Bes, A. R. B. B. R. M. B. S. *Macromolecular Chemistry and Physics* **2001**, *202*, 933-942.
- (53) F. Würthner *Chem. Comm.* **2004**, 1564.
- (54) P. A. Wheeler; B. X. Fu; J. D. Lichtenhan; J. Weitao; L. J. Mathias *J. Appl. Polym. Sci.* **2006**, *102*, 2856.
- (55) F. J. Feher; T. A. Budzichowski; R. L. Blanski; K. J. Weller; J. W. Ziller *Organomet.* **1991**, *10*, 2526.
- (56) F. J. Feher; T. A. Budzichowski *J. Organomet. Chem.* **1989**, *373*, 153.
- (57) C. Thieuleux; E. Alessandra Quadrelli; J.-M. Basset; J. Döbler; J. Sauer *Chem. Comm.* **2004**, 1729.
- (58) I. Rozhanskii; K. Okuyama; K. Goto *Polymer* **2000**, *41*, 7057.
- (59) H. Ishida; S. T. Wellinghoff; E. Baer; J. L. Koenig *Macro.* **1980**, *13*, 826.

- (60) O. V. Prezhdo; B. V. Uspenskii; V. V. Prezhdo; W. Boszczyk; Distanov, V. B. *Dyes and Pigments* **2007**, *72*, 42.
- (61) J. E. Ridley; M. C. Zerner *Theor. Chim. Acta* **1973**, *32*, 111.
- (62) J. E. Ridley; M. C. Zerner *J. Mol. Spectroscopy* **1974**, *50*, 457.
- (63) A. D. Bacon; M. C. Zerner *Theor. Chim. Acta* **1979**, *53*, 21.
- (64) M. C. Zerner; G. H. Loew; R. F. Kirchner; U. T. Mueller-Westerhoff *J. Am. Chem. Soc.* **1980**, *102*, 589.
- (65) M. Adachi; Y. Murata; S. Nakamura *J. Phys. Chem.* **1995**, *99*, 14240.
- (66) H. Langhals; H. Jaschke *Chem. Eur. J.* **2006**, *12*, 2815.
- (67) Y. L. Lee; H. L. Hsu; S. Y. Chen; T. R. Yew *J. Phys. Chem. C* **2008**, *112*, 1694.
- (68) S. Erten; Y. Posokhov; S. Alp; S. Icli *Dyes and Pigments* **2005**, *64*, 171.
- (69) A. Blaszczyk; Fischer, M.; von Hänisch, C.; M. Mayor *Helv. Chim. Acta* **2006**, *89*, 1986.
- (70) H. Langhals *Spectrochim. Acta Part A* **2000**, *56*, 2207.
- (71) M. Hasegawa; Y. Shindo; T. Sugimura ; S. Ohshima; K. Horie; M. Kochi; R. Yokota; I. Mita *J. Polym. Sci. B. Polym. Phys.* **1993**, *31*, 1617.
- (72) K. Balakrishnan; A. Datar; Oitker., R.; H. Chen; J. Zuo; L. Zang *J. Am. Chem. Soc.* **2005**, *127*, 10496.
- (73) V. J. Sapagovas; V. Gaidelis; V. Kovalevskij; Undzenas, A. *Dyes and Pigments* **2006**, *71*, 178.
- (74) D. Uzun; M. E. Ozser; K. Yuney; H. Icil; M. Demuth *J. Photochem. Photobiol. A: Chem.* **2003**, *156*, 45.
- (75) N. Pasaogullari; H. Icil; M. Demuth *Dyes and Pigments* **2006**, *69*, 118.
- (76) C. Karapire; C. Timur; S. Icli *Dyes and Pigments* **2003**, *56*, 135.
- (77) H. Langhals; J. Karolin; L. Johansson *J. Chem. Soc., Faraday Trans.* **1998**, *94*, 2919.
- (78) M. Sadrai; G. R. Bird *Opt. Comm.* **1984**, *51*, 62.
- (79) H.-G. Lohmannsroben; H. Langhals *Appl. Phys. B* **1989**, *48*, 449.
- (80) R. Reisfeld; G. Seybold *Chimia* **1990**, *44*, 295.
- (81) W. E. Ford; P. V. Kamat *J. Phys. Chem* **1987**, *91*, 6373.
- (82) M. Sadrai; L. Hadel; R. R. Sauers; S. Husain; K. Krogh-Jespersen; J. D. Westbrook; G. R. Bird *J. Phys. Chem.* **1992**, *96*, 7988.
- (83) S. R. Meech; D. Phillips *J. Photochem.* **1983**, *23*, 193.
- (84) T. Karstens; K. Kobs *J. Phys. Chem.* **1980**, *84*, 1871.
- (85) S. Mayaki; J. Kato; Y. Muroya; Y. Katsumura; T. Yamashita *J. Photopolym. Sci. Tech.* **2003**, *16*, 255.
- (86) F. Graser; E. Hadicke *Lieb. Annal. Chem.* **1980**, 1994.
- (87) F. Graser; Hadicke., E. *Lieb. Annal. Chem.* **1984**, 483.
- (88) E. Hadicke; F. Graser *Acta Cryst. Sect. C* **1986**, *42*, 189.
- (89) G. Klebe; F. Graser; E. Hadicke; J. Berndt *A. Cryst. Sect. B* **1989**, *45*, 69.
- (90) E. Hadicke; F. Graser *Acta Cryst. Sect. C* **1986**, *42*, 195.
- (91) J. Mizuguchi *Acta Cryst. C* **1998**, *C54*, 1479.
- (92) C. Nather; H. Bock; Z. Havlas; T. Hauck *Organomet.* **1998**, *17*, 4707.
- (93) G. Calzaferri; R. Imhof; K. W. Törnroos *J. Chem. Soc., Dalton Trans.* **1994**, 3123.

- (94) A. R. Bassindale; H. Chen; Z. Liu; I. A. MacKinnon; D. J. Parker; P. G. Taylor; Y. Yang; M. E. Light; P. N. Horton; M. B. Hursthouse *J. Organomet. Chem.* **2004**, 689, 3287.
- (95) U. Dittmar; B. J. Hendan; U. Florke; C. Heinrich; C. Marsmann *J. Organomet. Chem.* **1995**, 489, 185.
- (96) S. Lucke; K. Stoppeck-Langner; B. Krebs; Lage, M. *Z. Anorg. Allg. Chem.* **1997**, 623, 1243.
- (97) N. V. Podberezskaya; I. A. Baidina; V. I. Alekseev; S. V. Borisov; T. N. Martynova *J. Struct. Chem. (Engl. Transl.)* **1981**, 22, 737.
- (98) P.-A. Jaffrès; R. E. Morris *J. Chem. Soc., Dalton Trans.* **1998**, 2767.
- (99) C. Bonhomme; P. Toledano; J. Maquet; J. Livage; L. Bonhomme-Coury *J. Chem. Soc., Dalton Trans.* **1997**, 1617.
- (100) A. R. Bassindale; Z. Liu; I. A. MacKinnon; P. G. Taylor; Y. Yang; M. E. Light; P. N. Horton; M. B. Hursthouse *J. Chem. Soc., Dalton Trans.* **2003**, 2945.
- (101) I. Richter; C. Burschka; R. Tacke *J. Organomet. Chem.* **2002**, 646, 200.
- (102) N. V. Podberezskaya; S. A. Magarill; I. A. Baidina; S. V. Borisov; L. E. Gorsh; A. N. Kanev; T. N. Martynova *J. Struct. Chem. (Engl. Transl.)* **1982**, 23, 422.
- (103) M. A. Hossain; M. B. Hursthouse; K. M. A. Malik *Acta Cryst. B* **1979**, 35, 2258.
- (104) E. O. Dare; H. A. Olatunji; D. S. Ogunniyi *J. Appl. Polym. Sci.* **2004**, 93.
- (105) Z. Chen; G. Deibje; T. Debaerdemaeker; P. Osswald; F. Wuerthner *Chem. Phys. Chem.* **2004**, 5, 137.
- (106) F. Wuerthner; A. Sautter; J. Schilling *J. Org. Chem.* **2002**, 67, 3037.
- (107) E. Hadicke; Graser, F. *Acta Crystallographica, Section C* **1986**, 42, 189.
- (108) P. M. Kazmaier; R. Hoffmann *J. Am. Chem. Soc.* **1994**, 116, 9684.
- (109) Y. J. Lee; J. M. Huang; S. W. Kuo; J. S. Lu; F. C. Chang *Polymer* **2005**, 46, 173.

4 POSS BOUND PORPHYRIN

4.1 Outline

This chapter details a review of the properties and functionalisation of porphyrins, followed by the synthesis and characterisation of the POSS porphyrin derivative. Full experimental conditions, general characterisation techniques and sample data are detailed in **Chapter 6**.

4.2 Porphyrins

Porphyrins are defined as a large class of fluorescent crystalline pigments, having in common a substituted aromatic macrocyclic ring, consisting of four pyrrole-type units, linked by four methylene bridging units (**Figure 4.1**). The macrocyclic structure of porphyrin (derived from the Greek word for purple) was first proposed in 1912 by Kuster, however it was not until 1929 that the synthesis of heme, the iron porphyrin in hemoproteins, was first reported.¹

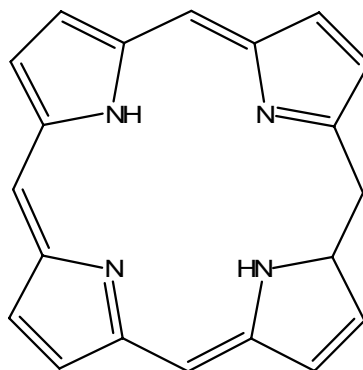


Figure 4.1. The unsubstituted porphyrin macrocycle¹

X-ray crystallography of octaethylporphyrin (OEP) confirmed that porphyrins were essentially flat molecules; however, the shape can become majorly distorted from planarity when binding to metal atoms occurred.¹ Distortion also occurred when the unprotonated central nitrogen's were protonated, combined with the employment of bulky substituents. Oxidation of the porphyrin, removing aromaticity and substitution of groups on the central nitrogen atoms have also been shown to lead to major distortions in the planarity molecule.¹

Porphyrins are traditionally synthesised via the condensation of aldehydes and pyrrole (**Figure 4.2**).²⁻⁴ The scope of this reaction is generally limited to porphyrins with a symmetrical arrangement of peripheral substituents, such as tetraphenylporphyrin (TPP) and OEP. Mixed aldehyde condensations, involving the use of more than one aldehyde have been previously employed in order to synthesis porphyrins containing more than one type of *meso* substituent; however the resultant statistical distribution of products was generally difficult to separate via chromatography.⁵ Porphyrins of more complicated structure have been synthesised through a range of synthetic routes, such as dipyrrolic precursors and open chain tetrapyrrolic intermediates,¹ however the porphyrin of interest within this thesis was TPP and such synthetic procedures will not be further discussed.

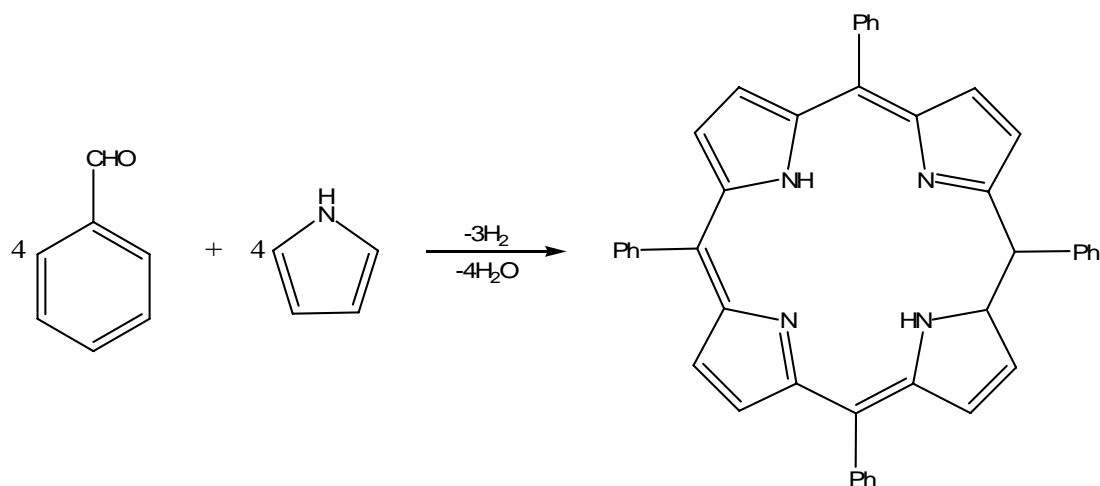


Figure 4.2. Synthesis of TPP²⁻⁴

Porphyrins have been investigated for a range of molecular electronic applications, such as thermochromism, where the absorption properties of a zinc porphyrin complex exhibited significant variation upon heating.⁶ The complexation of porphyrins with fullerenes has been investigated for use in photoinduced electron-transfer (PET) systems.⁷⁻¹² Organic photovoltaic cells containing supramolecular complexes of porphyrin-peptide oligomers with fullerene exhibited enhanced photoelectrochemical performance and high power conversion efficiency, with possible application in solar energy conversion.¹³ The use of a ruthenium porphyrin as a photosensitiser, in conjunction with a suitable electron acceptor and an alkene, induced selective epoxidation of the alkene, whilst concurrently exhibiting oxidation of a water molecule, thus offering a potential route for photochemical water splitting.^{14,15}

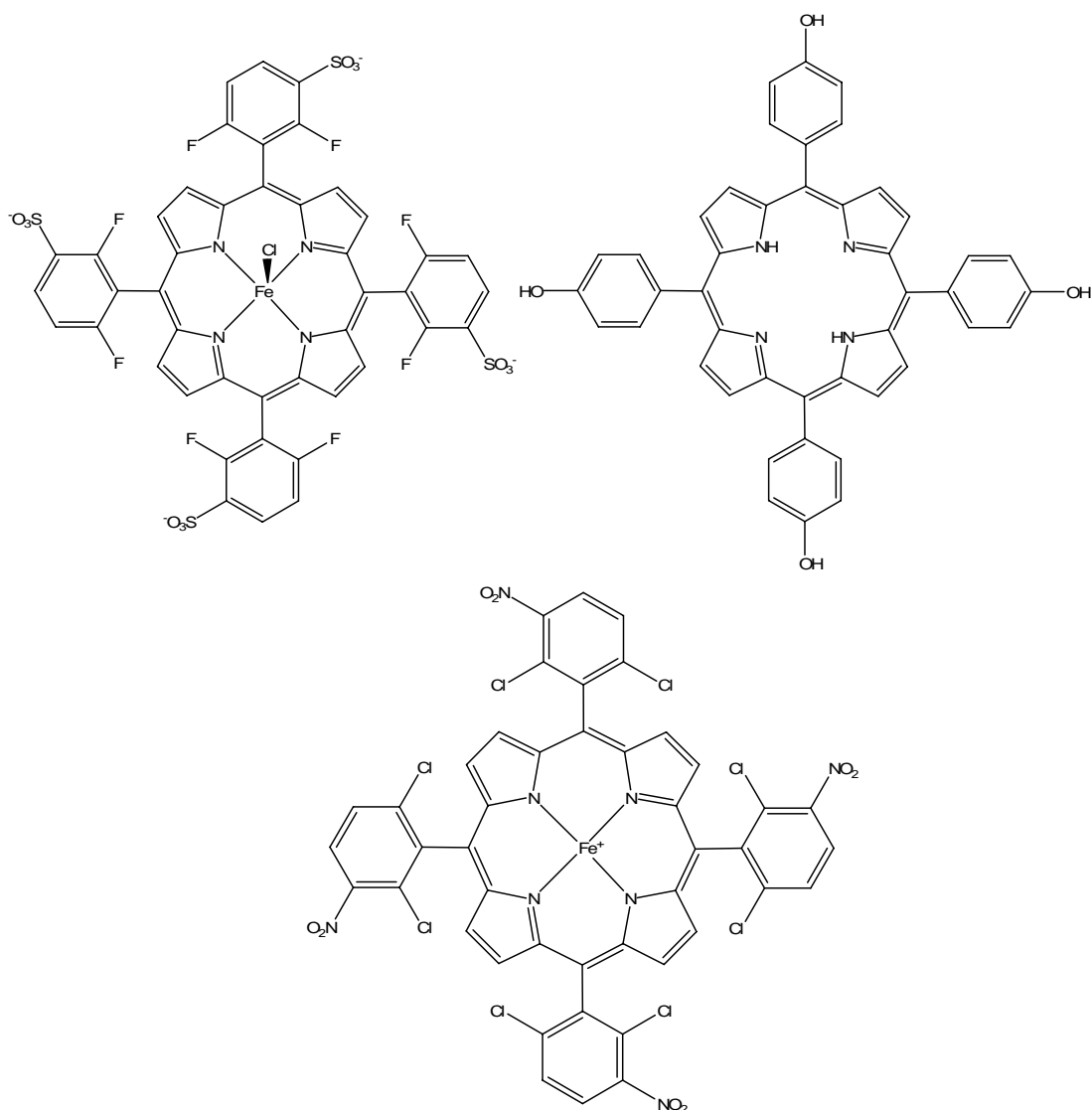


Figure 4.3. Porphyrins employed in solid matrices¹⁶⁻¹⁸

A range of porphyrins have been immobilised in a variety of inorganic matrices (**Figure 4.3**), such as zeolites, clays and silica, to electrocatalyse the electrooxidation of hydrazine.¹⁶ Porphyrins have also been dispersed in polymer composite films as an optical sensor of hydrogen chloride.¹⁷ The dispersion of porphyrins within sol-gel matrices has previously been investigated in order to construct optical components with good thermal and chemical stabilities.¹⁸

4.3 POSS Ligands

In order to covalently link metalloporphyrins to POSS cages, a suitable coordination ligand was required. A variety of ligands have previously been incorporated on the

periphery of POSS cages, such as diphenylphosphine (**Figure 4.4**),¹⁹ which has been used to coordinate ruthenium complexes.

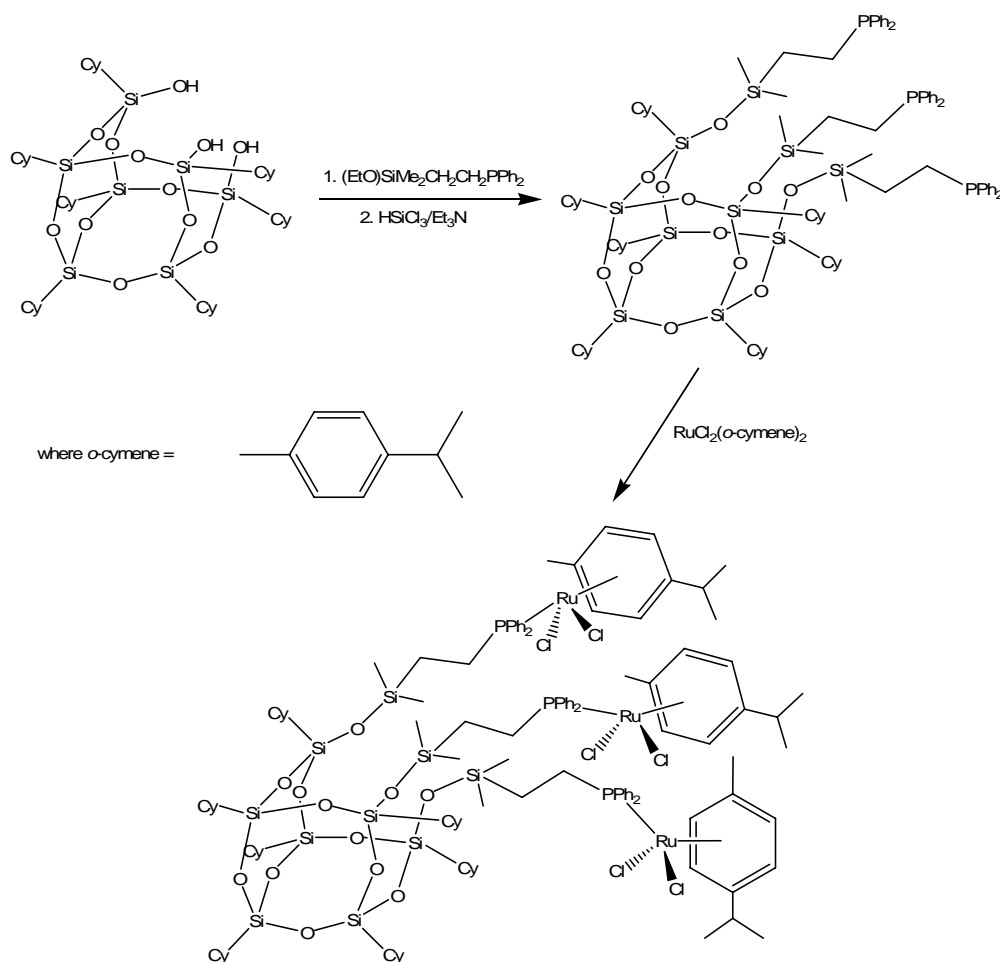


Figure 4.4. Synthesis of ruthenium functionalised POSS¹⁹

The silanol groups of incompletely condensed POSS cages have also been used as coordinating ligands for the coordination of platinum complexes (**Figure 4.5**).²⁰

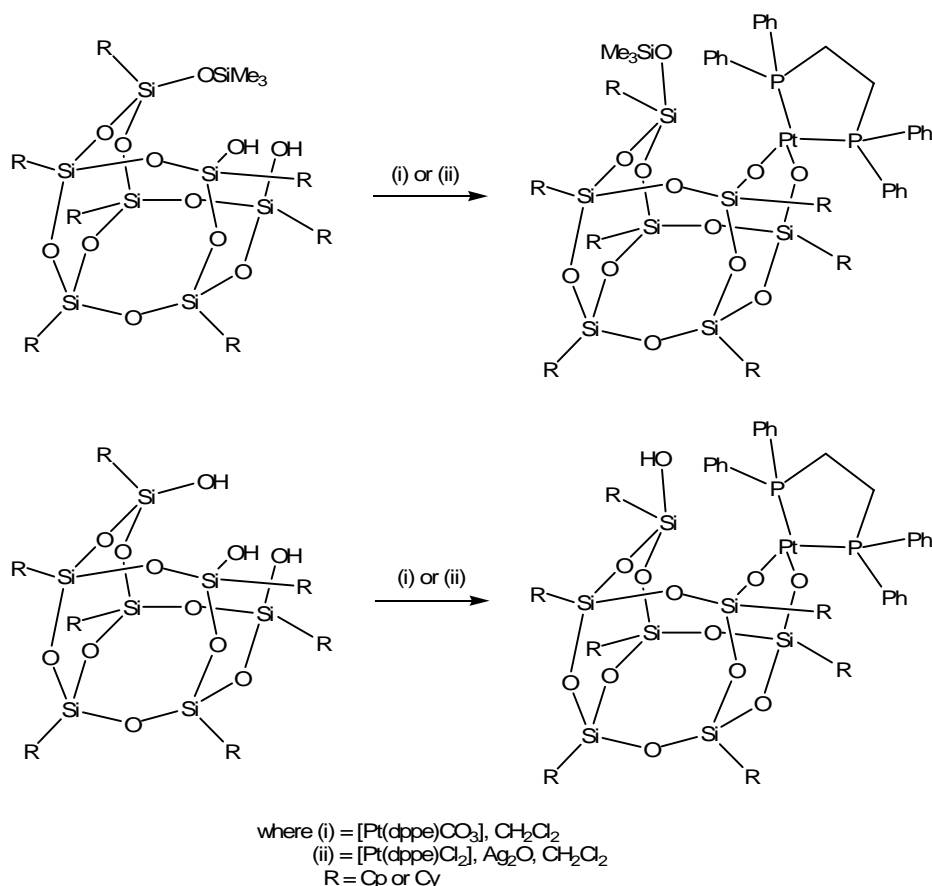


Figure 4.5. Synthesis of platinum functionalised POSS²⁰

Other examples of ligands incorporated onto the periphery of POSS cages include thiol,²¹ bipyridyl²² and terpyridyl,^{23,24} which have been used to enable the coordination of transition metal ions. Terpyridyl groups have been employed in the formation of metallodendrimers (**Figure 4.6**) with octa-phosphino POSS used as a building core for the dendrimer. The phosphine was then reacted with 4'-(*p*-bromomethylphenyl)-2,2':6',2''-terpyridine to covalently attach terminal terpyridyl units.^{23,24}

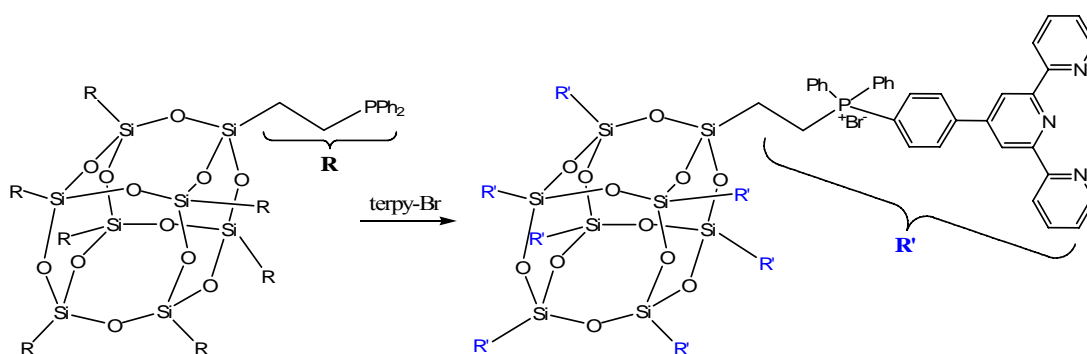


Figure 4.6. Synthesis of octa-terpyridyl functionalised POSS^{23,24}

The terpyridyl functionality allowed for easy complexation of transition metal complexes, such as $\text{Ru}(\text{bipy})\text{Cl}_2$, in order to form generation 1 metallodendrimers (**Figure 4.7**).^{23,24} Similar synthetic pathways have also been followed to obtain generation 2 and 3 metallodendrimers, containing 16 and 64 ruthenium terpyridyl functionalities on the periphery of the POSS cage, respectively.^{23,24}

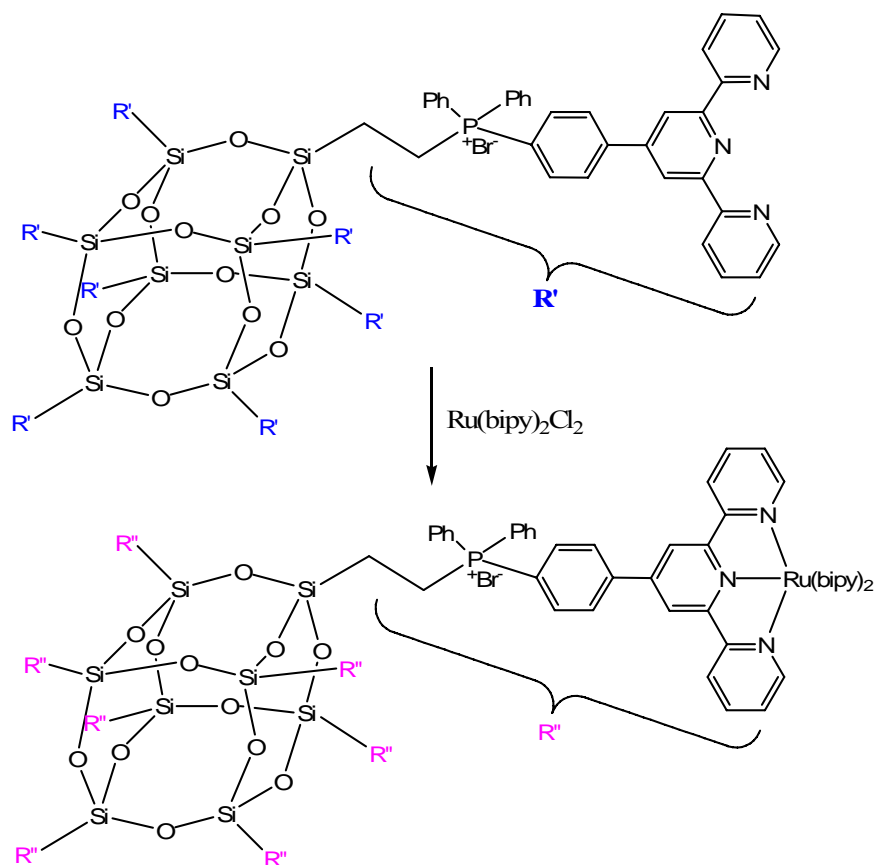


Figure 4.7. Synthesis of POSS based ruthenium metallodendrimers^{23,24}

One of the simplest and easy to synthesise ligands used for the coordination of ruthenium porphyrin complexes is the pyridyl ligand. Since the Ru^{II} cation was d^6 and low spin, exchange processes at the metal centre were slow, unless the axial positions were labilised by the presence of a π -acid, such as a carbonyl (CO). Carbonyl complexes readily exchange ligands at the position *trans* to the CO.

One such complex was the commercially available ruthenium tetraphenylporphyrin $[\text{Ru}(\text{TPP})(\text{CO})\text{ROH}]$, which has one alcohol molecule bound weakly to the metal which, in the presence of a stronger ligand, such as pyridyl, was easily displaced.²⁵ $[\text{Ru}(\text{TPP})(\text{CO})\text{ROH}]$ has previously been reacted with pyridyls, such as pyridine

(py)²⁶ and pyridylfulleropyrrolidine (py-fp),²⁷ at room temperature to form metalloporphyrin complexes (**Figure 4.8**).

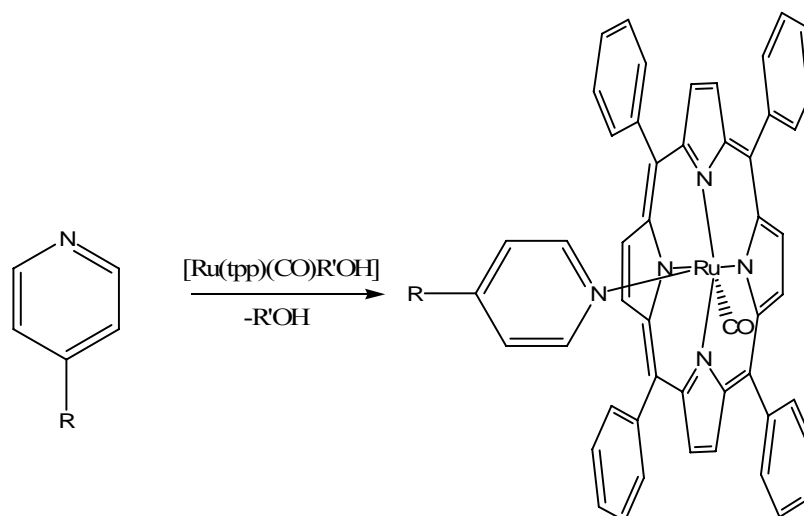


Figure 4.8. Synthesis of Ru(TPP)(CO)(Rpy)²⁶⁻²⁸

4.4 Synthesis

In order to take advantage of the easy complexation of ruthenium complexes to pyridyls, a pyridyl ligand on the periphery of the POSS cage was required. The reaction of octa-aminopropyl POSS with benzoyl chloride to yield the corresponding octa-amide had been previously achieved (**Figure 4.9**).²⁹ In order to obtain the desired pyridyl functionality, the reaction of a mono-amino POSS compound with a pyridyl acid chloride was performed, in order to obtain the desired pyridyl functionalised POSS product, which was subsequently reacted with [Ru(TPP)(CO)(EtOH)] to yield the desired POSS porphyrin product.

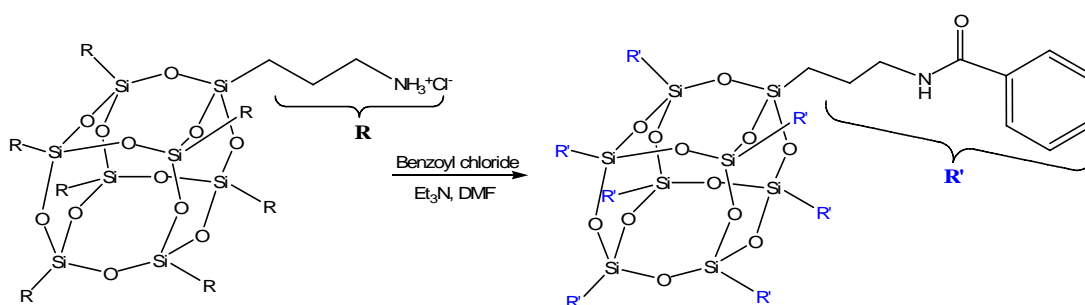


Figure 4.9. Synthesis of octa-(phenyl amide) POSS²⁹

4.5 Characterisation

Characterisation was performed by FTIR, ^1H , ^{13}C and ^{29}Si NMR, UV-VIS and fluorescence spectrophotometry and ESI mass spectrometry, the details of which are discussed in **Chapter 6**.

4.6 Results & Discussion

The reaction of (3-aminopropyl)POSS with benzoyl and isonicotinic acid chloride, and subsequent reaction of the pyridyl functionalised POSS with $[\text{Ru}(\text{TPP})(\text{CO})(\text{EtOH})]$ to enable formation of the desired POSS porphyrin compound is described herein.

4.6.1 FTIR

The presence of the amide functionality was confirmed by FTIR, with amide band I (C=O stretching) apparent at 1637 cm^{-1} (**4.1**) and 1677 cm^{-1} (**4.3**), and amide band II (N-H deformation) displayed at 1544 cm^{-1} (**4.1**) and 1545 cm^{-1} (**4.3**).³⁰ FTIR also confirmed the covalent attachment of the metalloporphyrin, with the ruthenium bound carbonyl stretching band observed at 1972 cm^{-1} .^{27,28,31}

4.6.2 ^1H NMR

The ^1H NMR resonances of all functionalised POSS compounds are summarised in **Table 4.1**.

4.6.2.1 (3-aminopropyl)POSS

As detailed previously in **Section 3.6.2.1**, ^1H NMR of (3-aminopropyl)POSS (**3.1**) exhibited resonances associated with the isobutyl chains of the POSS cage at δ 0.58-

Table 4.1. ¹H NMR of POSS porphyrin and precursor compounds

Compound	iBu	iBu CH ₃	iBu CH	SiCH ₂	CH ₂	CH ₂ N	NH	Ph/Py	Porphyrin
3.1	0.58-0.61	0.95 d (6.6 Hz) ^a	1.80-.92	-	1.50-1.58	2.67 t (7.2 Hz) ^a	-	-	-
4.1	0.59-0.61	0.94-0.96	1.81-1.90	0.65-0.71	1.69-1.79	3.43-3.49	6.11	7.43-7.47, 7.74-7.83	-
4.2	-	-	-	-	-	-	-	8.32 d (5.7 Hz), 9.07 d (5.7 Hz)	-
4.3	0.60 d (6.6 Hz) ^a	0.92-0.96	1.80-1.89	0.68-0.75	1.67-1.78	3.45 t (6.6 Hz) ^a	6.24	7.58-7.60, 8.72-8.74	-
4.4	0.45 d (6.9 Hz), ^a 0.55 d (6.9 Hz), ^a 0.58-0.62	0.80 d (6.6 Hz), ^a 0.91-0.97	1.62-1.89	0.22-0.27	-	2.41-2.45	-	5.48-5.50	7.64-7.74, 8.04-8.06, 8.20-8.23, 8.62

^a = ³J_{H-H}

0.61 (16H, SiCH₂/iBu CH₂), 0.95 (42H, iBu CH₃) and 1.80-1.92 (7H, iBu CH), and propyl chain resonances at δ 1.50-1.58 (2H, CH₂) and 2.67 (2H, CH₂N). The remaining propyl resonance (SiCH₂) was obscured by the broad isobutyl resonance. These resonances were consistent with those detailed in the literature.³²

4.6.2.2 Mono-phenyl POSS

In order to verify the synthetic methodology, the reaction of benzoyl chloride with **3.1** was undertaken (**Figure 4.10**).

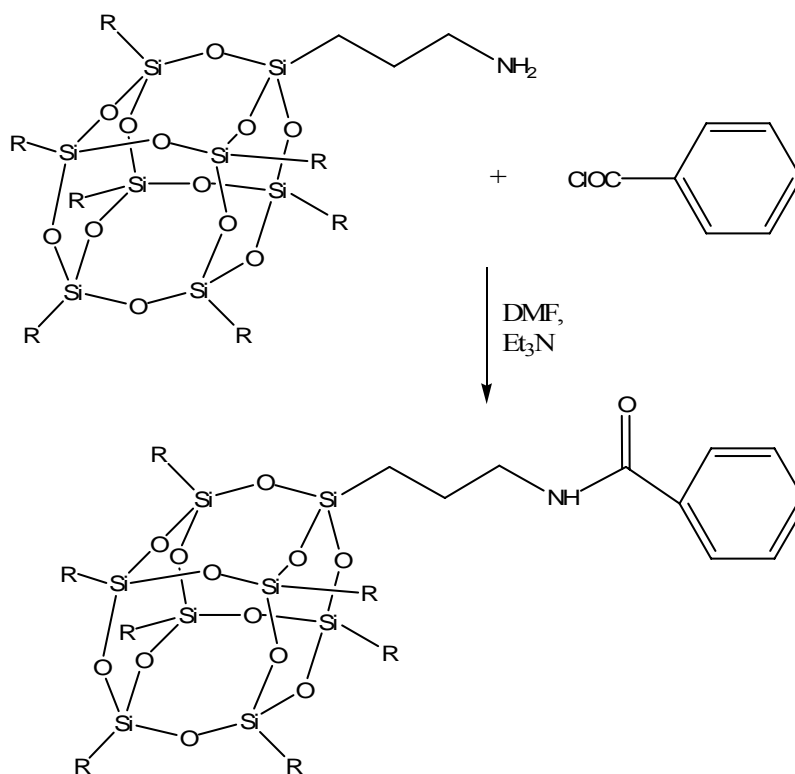


Figure 4.10. Synthesis of mono-phenyl POSS amide (4.1)

¹H NMR of mono-phenyl POSS amide (**4.1**) exhibited isobutyl resonances at δ 0.59-0.61 (14H, iBu CH₂), 0.94-0.96 (42H, iBu CH₃) and 1.81-1.90 (7H, iBu CH). Propyl chain resonances were apparent at δ 0.65-0.71 (2H, SiCH₂), 1.69-1.79 (2H, CH₂) and 3.43-3.49 (2H, CH₂N), resulting in downfield shifts of 0.19 and 0.76 ppm in the CH₂ and CH₂N resonances, relative to the corresponding resonances of mono-(3-aminopropyl)POSS. Comparable resonance shifts were also apparent in the equivalent CH₂N resonance of similar compounds in the literature, such as N-[3-

(isobutylPOSS)propyl]-bis(benzyloxybenzamide)³³ (**Figure 4.11**) (0.12 and 0.85 ppm). The downfield shifts resulted from the covalent attachment linkage of the relatively electron dense phenyl ring, ensuring the propyl chain protons experienced increased deshielding. The phenyl ring exhibited broad resonances at δ 7.43-7.47 (3H, *m/p* CH) and 7.74-7.63 (2H, *o* CH), with the NH resonance evident at δ 6.11 (1H).

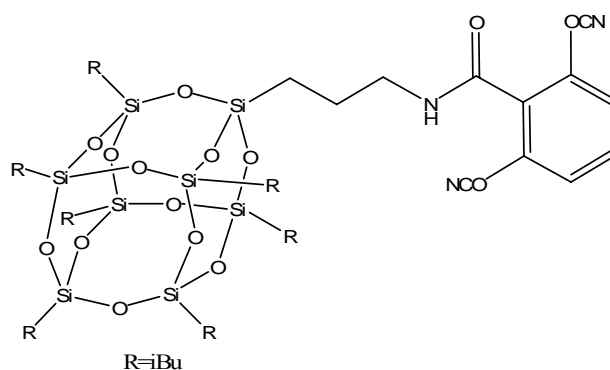


Figure 4.11. Structure of N-[3-(isobutylPOSS)propyl]bis(benzyloxybenzamide)³³

4.6.2.3 Isonicotinic Acid Chloride

The synthesis of acid chlorides from corresponding pyridine carboxylic acids has been well established, however the reflux of pyridyl carboxylic acids with thionyl chloride generally led to formation of pyridinecarboxylic acid chloride hydrochlorides, with a chloride anion bonded to the protonated nitrogen on the pyridine ring.³⁴ In order to avoid this, oxalyl chloride was used in the synthesis of isonicotinic acid chloride (**4.2**) (**Figure 4.12**).³⁵ ¹H NMR exhibited resonances at δ 8.32 (d, ³J_{H-H} = 5.7 Hz) and 9.07 (d, ³J_{H-H} = 5.7 Hz). These resonances were consistent with those detailed in the literature.³⁵

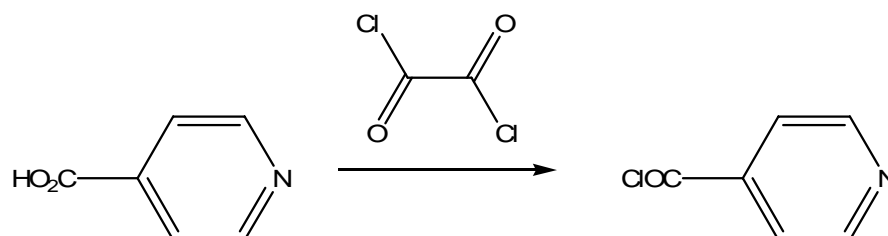


Figure 4.12. Synthesis of isonicotinic acid chloride (**4.2**)

4.6.2.4 Mono-pyridyl POSS

The desired pyridyl functionality was obtained through the reaction of **4.2** with **3.1** (**Figure 4.13**).

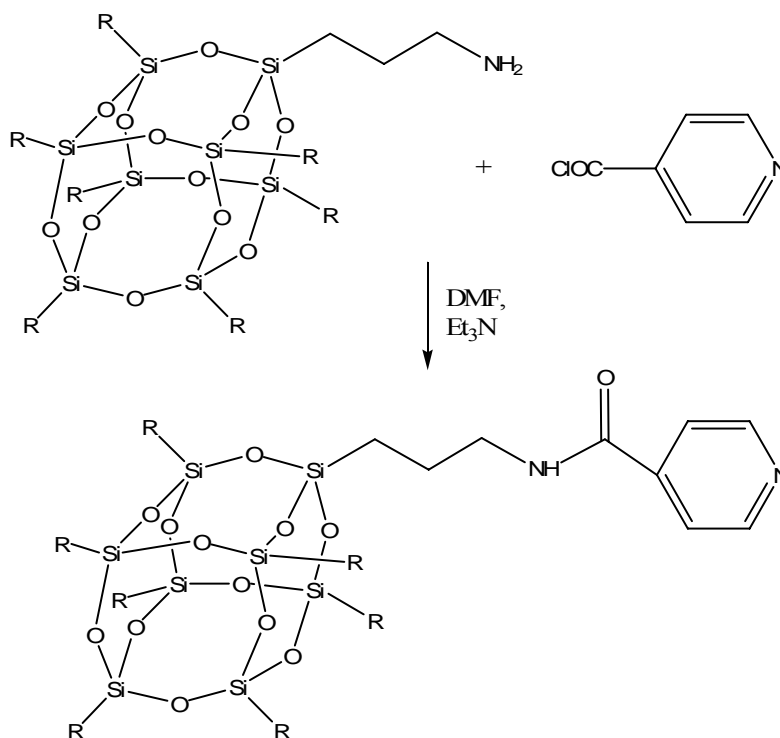


Figure 4.13. Synthesis of mono-pyridyl POSS (4.3)

¹H NMR of **4.3** exhibited isobutyl resonances at δ 0.60 (14H, iBu CH₂), 0.92-0.96 (42H, iBu CH₃) and 1.80-1.89 (7H, iBu CH₂). Propyl chain resonances were evident at δ 0.68-0.75 (2H, SiCH₂), 1.67-1.78 (2H, CH₂) and 3.45 (2H, CH₂N), resulting in downfield shifts of 0.17 and 0.88 ppm in the CH₂ and CH₂N resonances, relative to the corresponding resonances in mono-(3-aminopropyl)POSS. These shifts were again analogous to the downfield shifts observed in **4.2** (0.19 and 0.76 ppm) and the benzamide derivative (0.12 and 0.85 ppm), as discussed previously.³³ Resonances of the pyridyl moiety were apparent at δ 7.58-7.60 (2H, CH) and 8.72-8.74 (2H, CH), with the amide resonance observed at δ 6.24 (1H, NH).

4.6.2.5 Mono-porphyrin POSS

The desired POSS porphyrin was synthesised via the reaction of **4.3** with $[\text{Ru}(\text{C}\equiv\text{O})(\text{EtOH})(\text{TPP})]$ (**Figure 4.14**).

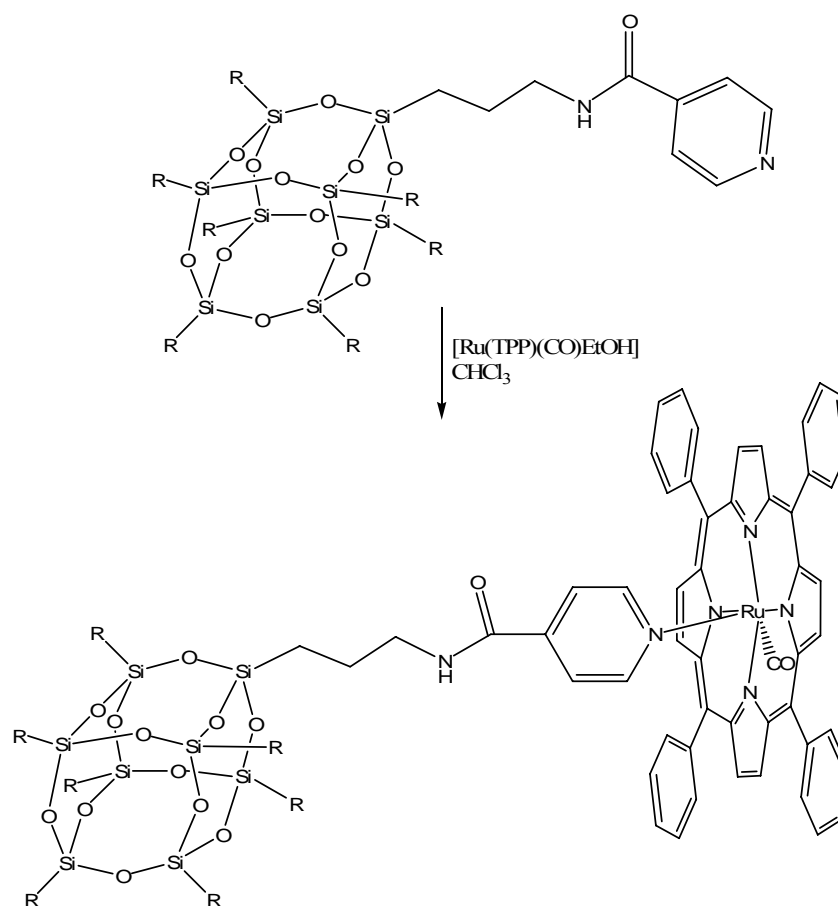


Figure 4.14. Synthesis of mono-porphyrin POSS (4.3)

The ^1H NMR spectrum of **4.3** exhibited significant variations in the majority of resonances, in comparison with those observed in **4.2**, associated with the large diamagnetic anisotropy of the porphyrin ring.³⁶ Non-equivalence of the resonances of the cage bound isobutyl groups was observed, with resonances apparent at δ 0.45 (d, $^3J_{\text{H-H}} = 6.9$ Hz, 4H, iBu CH_2), 0.55 (d, $^3J_{\text{H-H}} = 6.9$ Hz, 4H, iBu CH_2), 0.58-0.62 (m, 6H, iBu CH_2), 0.80 (d, $^3J_{\text{H-H}} = 6.6$ Hz, 12H, iBu CH_3), 0.91-0.97 (30H, iBu CH_3), 1.62-1.89 (m, 9H, pyridyl CH/iBu CH). Propyl chain resonances were apparent at δ 0.22-0.27 (Si CH_2) and 2.41-2.45 (CH_2N), with the remaining propyl resonance obscured. The propyl chain resonances were significantly shifted, relative to the corresponding resonances in **4.2**, with the Si CH_2 and CH_2N resonances being shifted upfield by 0.46 and 1.04 ppm, respectively, caused by the increased shielding

associated with the coordinated porphyrin. The α and β protons of the porphyrin bound pyridyl ligand also experienced increased shielding by the porphyrin ring-current, with the β resonance observed at δ 5.48-5.51 (2H), corresponding to an upfield shift of 2.10 ppm. The α resonance was expected to occur at approximately δ 1.6,³⁷ however this resonance was obscured. Comparable resonance shifts were exhibited in the literature for [Ru(TPP)(CO)(py-fp)] (7.03 and 2.17 ppm).^{27,28} The porphyrin moiety exhibited resonances of the phenyl rings at δ 7.64-7.74 (12H, *m/p* CH), 8.04-8.06 (4H, *o*-CH) and 8.20-8.23 (4H, *o*-CH), with the pyrrole resonance at δ 8.62 (8H, CH). Comparable porphyrin resonance positions were also present in [Ru(TPP)(CO)(py-fp)] (δ 5.80, 7.59, 7.70, 7.86, 8.21, 8.55).^{27,28}

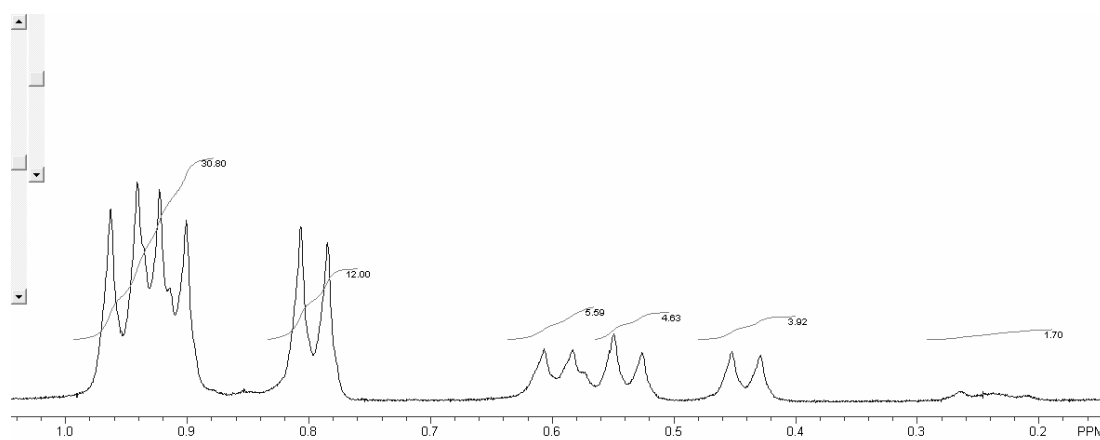


Figure 4.15. Non-equivalence in isobutyl resonances in ^{13}C NMR spectrum of mono-porphyrin POSS 4.4 in CDCl_3

4.6.3 ^{13}C NMR

The ^{13}C NMR resonances of all functionalised POSS compounds are summarised in **Table 4.2**.

4.6.3.1 (3-aminopropyl)POSS

As detailed previously in **Section 3.6.3.1**, ^{13}C NMR of **3.1** exhibited resonances of the cage bound isobutyl carbons at δ 24.01, 25.84 and 27.23, with propyl chain

Table 4.2. ^{13}C NMR of POSS porphyrin and precursor compounds

Compound	iBu CH ₂	SiCH ₂	CH ₂	CH ₂ N	Ph/Py	C=O	Porphyrin
3.1	24.01, 25.84, 27.23	9.36	22.65	44.90	-	-	-
4.1	-	-	-	-	126.85, 145.36, 145.62	165.22	-
4.2	22.46, 23.84, 25.68	9.49	23.06	42.25	126.81, 128.54, 131.29	167.46	-
4.3	22.62, 24.04, 25.83	9.65	23.09	42.58	120.97, 142.10, 150.72	165.62	-
4.4	22.46, 22.58, 22.69, 23.90, 23.94, 24.02, 25.67, 25.80, 25.84	9.24	29.84	42.05	128.96, 131.01	163.53	118.90, 121.77, 126.42, 126.74, 127.45, 128.96, 132.00, 134.13, 134.51, 140.01, 142.69, 143.76, 145.02, 180.35

resonances apparent at δ 9.36, 22.65 (CH_2) and 44.90 (CH_2N). These resonances were consistent with those detailed in the literature.³²

4.6.3.2 *Mono-phenyl POSS*

^{13}C NMR of **4.1** exhibited resonances of the cage bound isobutyl carbons at δ 22.46, 23.84 and 25.68, resulting in upfield shifts of 1.55, 2.00 and 1.55 ppm, relative to the corresponding resonances in mono-(3-aminopropyl)POSS. Comparable resonance shifts were also present in the literature for the benzamide derivative (1.5, 2.0 and 1.5 ppm), as discussed previously in **Chapter 3**.³³ Propyl chain resonances were observed at δ 9.49 (SiCH_2), 23.06 (CH_2), and 42.25 (CH_2NH), resulting in downfield shifts of 0.13 and 0.41 ppm in the SiCH_2 and CH_2 resonances and an upfield shift of 2.65 ppm in the CH_2N resonance, relative to the corresponding resonances in mono-(3-aminopropyl)POSS. Comparable resonance shifts were displayed in the benzamide derivative (0.1, 0.4, 2.6)³³ and the mono- and bis- POSS imide compounds detailed in **Chapter 3**. The aromatic resonances were displayed at δ 126.85, 145.36 and 145.62, with the carbonyl resonance apparent at δ 165.22.

4.6.3.3 *Isonicotinic acid chloride*

^{13}C NMR of **4.2** exhibited pyridyl resonances at δ 126.85, 145.36 and 145.62, with the carbonyl resonance evident at δ 165.22. These resonances were consistent with those detailed in the literature.³⁵

4.6.3.4 *Mono-pyridyl POSS*

^{13}C NMR of **4.3** exhibited resonances of the cage bound isobutyl carbons at δ 22.62, 24.04 and 25.83, resulting in upfield shifts of 1.39, 1.80 and 1.40 ppm, relative to the corresponding resonances in mono-(3-aminopropyl)POSS. Comparable resonance shifts were previously detailed for **4.2** (0.95, 2.00 and 1.55 ppm) and the benzamide derivative (1.0, 2.0 and 1.5 ppm).³³ Propyl chain resonances were evident at δ 9.65 (SiCH_2), 23.90 (CH_2) and 42.58 (CH_2N), resulting in downfield shifts of 0.29 and

0.44 ppm in the SiCH₂ and CH₂ resonances, with an upfield shift of 2.32 ppm apparent in the CH₂N resonance, relative to the corresponding resonances in mono-(3-aminopropyl)POSS. Comparable resonance shifts were displayed in **4.2** (0.13, 0.41, 2.65 ppm) and the benzamide derivative (0.1, 0.4, 2.6 ppm).³³ Pyridyl resonances were displayed at δ 126.81, 128.54, 131.29 and 134.97, with the carbonyl resonance observed at δ 167.46.

4.6.3.5 Mono-porphyrin POSS

The non-equivalence noted in the description of the ¹H NMR spectrum was also evident in the ¹³C NMR spectrum of **4.4** (**Figure 4.16**). The isobutyl resonances were apparent at δ 22.56, 22.64, 22.69, 23.90, 23.94, 24.02, 25.67, 25.80 and 25.84.

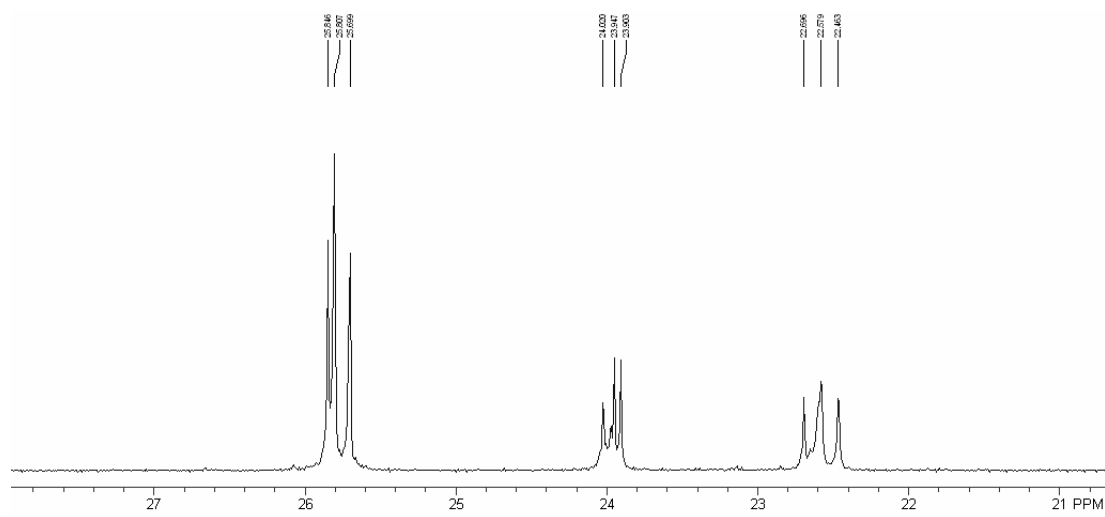


Figure 4.16. Non-equivalence in isobutyl resonances in ¹³C NMR spectrum of mono-porphyrin POSS 4.4 in CDCl₃

Propyl chain resonances were apparent at δ 9.23 (SiCH₂), 29.84 (CH₂) and 42.05 (CH₂N), resulting in downfield shifts of 0.26, 6.75 and 0.20 ppm, relative to the corresponding resonances in **4.3**, with the resonance shifts attributed to the large diamagnetic anisotropy of the adjacent porphyrin ring.³⁶ Resonances of the porphyrin moiety were evident at δ 118.90 (β -Py), 121.77, 126.42 (*m/p* CH), 126.74 (*m/p* CH), 127.45 (*m/p* CH), 128.96 (*m/p* CH), 132.00 (pyrrole), 134.13 (*o* CH), 134.51 (*o* CH), 140.00, 142.69 (porphyrin C), 143.76 (α -Py) and 145.02 (aromatic C), with resonance assignments confirmed by HETCOR analysis (**Figure 4.17**). The amide carbonyl resonance was apparent at δ 163.53, corresponding to an upfield shift of

3.93 ppm, relative to the corresponding resonance in **4.3**, with the resonance shift again attributed to the large diamagnetic anisotropy of the adjacent porphyrin ring.³⁶ The ruthenium carbonyl resonance was observed at δ 180.35, with the resonance position comparable to that present in other [Ru(P)(CO)(L)] compounds in the literature, where P = porphyrin and L = pyridyl containing ligand.^{27,28,38}

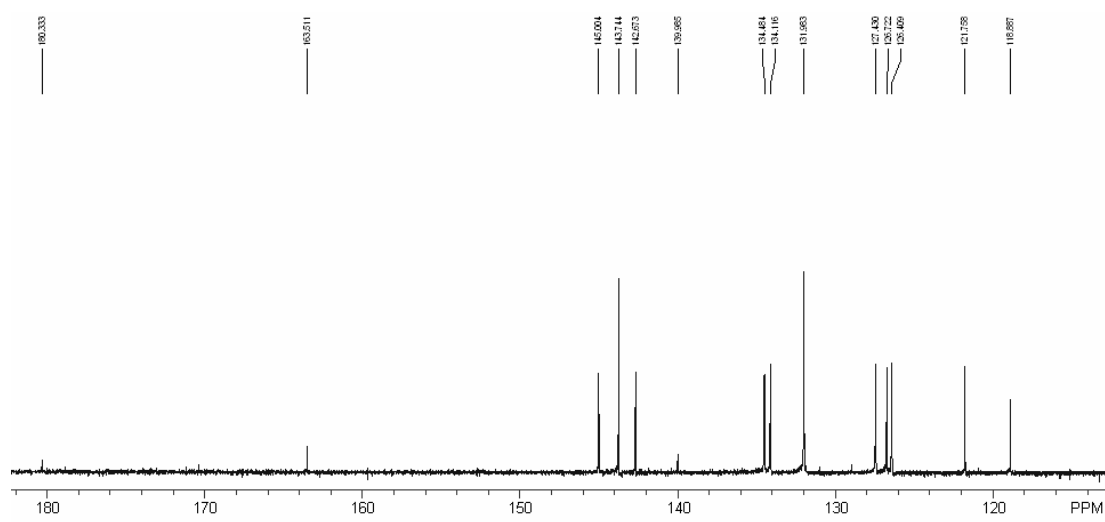


Figure 4.17. Aromatic region in ^{13}C NMR spectrum of mono-porphyrin POSS **4.4** in CDCl_3

4.6.4 ^{29}Si NMR

The ^{29}Si NMR resonances of all POSS compounds are summarised in **Table 4.3**. All compounds exhibited resonances characteristic of the monosubstituted POSS cage, indicating that the cage structure remained intact during reaction.

Table 4.3. ^{29}Si NMR of POSS porphyrin and precursor compounds

Compound	^{29}Si NMR
3.1	-67.64, -68.06, -68.26
4.1	-68.03, -68.04
4.3	-68.03, -68.28, -68.63
4.4	-68.22, -68.35, -68.40, -68.89

The ^{29}Si NMR spectrum of **4.4** exhibited resonances at δ -68.22, -68.35, -68.40 and -68.89 (**Figure 4.18**), with all other spectra being analogous in appearance.

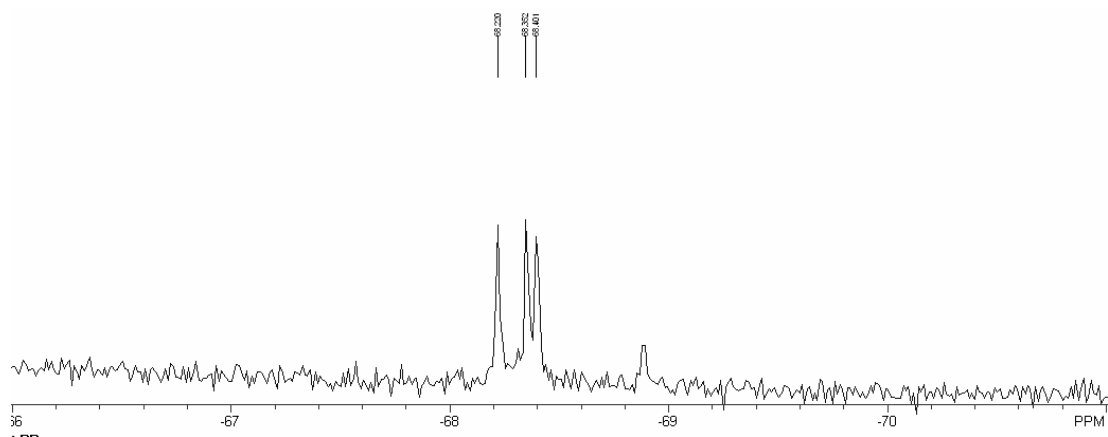


Figure 4.18. ^{29}Si NMR of mono-porphyrin POSS (4.4)

4.6.5 High Resolution ESI Mass Spectrometry

The theoretical and experimental high resolution ESI mass spectrometry results are depicted in **Table 4.4**. The close correlation between the experimental and theoretical results offered unequivocal confirmation of the formation of the desired compounds.

Table 4.4. ESI mass spectrometry of POSS porphyrin and precursor compounds

Compound	Experimental	Theoretical
3.1	874.3218	874.3126
4.1	1000.3290	1000.3290
4.3	1001.3245	1001.3243
4.4	1722.4757	1722.4763

4.6.6 Elemental Analysis of POSS Porphyrin & Precursor Compounds

The theoretical and experimental elemental analysis results are depicted in **Table 4.5**. The close correlation between the experimental and theoretical results offered further evidence of formation of the desired compounds.

Table 4.5. Elemental analysis results of POSS Porphyrin & Precursor Compounds

Compound	Experimental (C, H, N)	Theoretical (C, H, N)
4.2	46.38, 8.14, 1.06	46.63, 7.72, 1.43
4.3	44.23, 7.93, 2.15	45.36, 7.61, 2.86
4.4	57.40, 7.39, 3.11	57.18, 6.03, 4.88

4.6.7 Optical Properties of Mono-porphyrin POSS

4.6.7.1 UV-Vis Spectrum of Mono-porphyrin POSS

Porphyrins exhibit characteristic UV-Vis spectra, consisting of an intense absorption between 390-425nm, (the [B(0,0)] or Soret band), relating to the $S_0 \rightarrow S_2$ transition. Weaker bands (Q bands) are situated between 480-700 nm and pertain to the $S_0 \rightarrow S_1$ transition. Metalloporphyrins are generally more symmetrical than free-base porphyrins, hence their Q band spectra habitually consist of one or two bands, with multiple bands denoted as α [Q(1,0)] and β [Q(0,0)] bands, and the α band situated at a longer wavelength than the β band.¹

4.4 exhibited B and Q absorption bands at 412 and 532 nm, with molar extinction coefficients of 184459 and 16376, respectively (**Figure 4.19**).

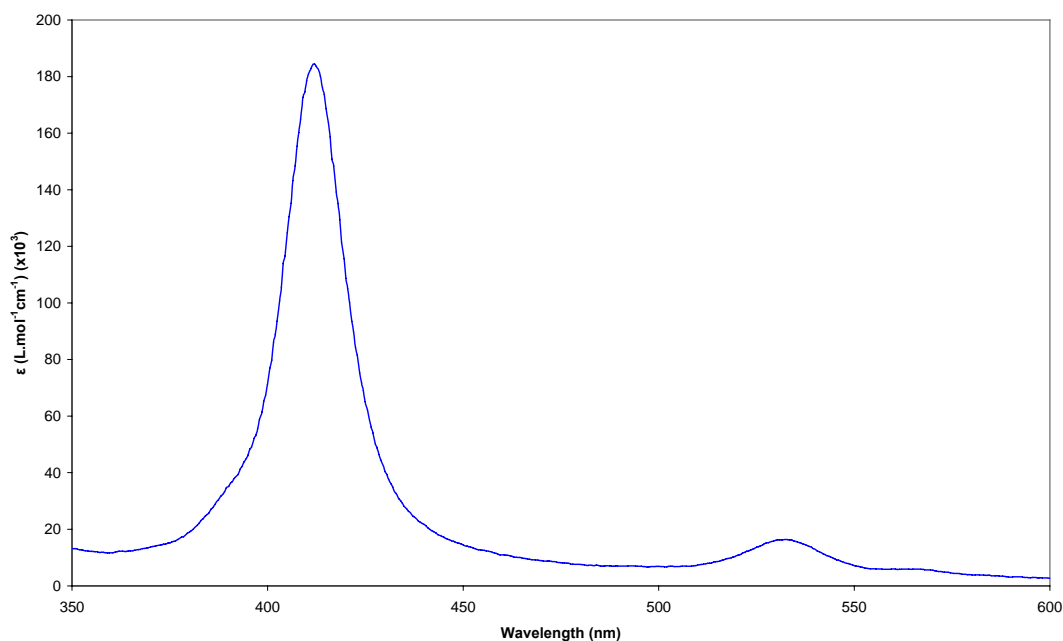


Figure 4.19. UV-Vis spectrum of POSS porphyrin **4.4** in dichloromethane

The absorption properties of the [Ru(TPP)(CO)L] series of compounds, where L = absent, EtOH, DMSO, pyridine and piperidine has been reported. Minor changes in the absorption maxima were evident, with a shift in the B band from 410-413 nm observed through the progression of the ligand series, coupled with analogous shifting in the Q(1,0) band (528-533 nm).^{39,40} The absorption maxima positions in **4.4** (412 and 532 nm) were therefore analogous to that of other pyridyl coordinated

ruthenium porphyrins, such as [Ru(TPP)(CO)(py)]^{26,39-41} (412 and 529 nm) and [Ru(TPP)(CO)(py-fp)] (412 and 531 nm).^{27,28}

The magnitudes of the molar extinction coefficients of the B and Q bands of 4.4 were comparable to that of similar compounds in the literature, such as (5,10,15,20-tetrakis(di-*tert*-butylphenyl)porphyrinato)ruthenium(II) carbonyl, which exhibited molar extinction coefficients of 177827 and 17782, respectively.³⁷

Ruthenium porphyrins exhibited similar behaviour to that of other typical inorganic chromophores, being dominated by the heavy ruthenium atom.⁴² The strong spin-orbit coupling, provided by the heavy metal centre, caused fast S₁→T₁ intersystem crossing, which prevented any measurable singlet-state fluorescence.^{42,43} Phosphorescence emission was not observed in degassed (sonicated) solution at ambient temperature.

4.7 Conclusions and Future Work

A range of POSS amides have been synthesised through the reaction of the desired acid chloride with mono(3-aminopropyl)POSS. The introduction of a pyridyl ligand on the periphery of the POSS cage was achieved through this synthetic process, followed by the coordination of a ruthenium tetraphenylporphyrin compound, in order to synthesise a POSS porphyrin compound. All compounds were characterised by ¹H, ¹³C and ²⁹Si NMR, FTIR, UV-Vis spectrophotometry and ESI mass spectrometry. The various methods of characterisation confirmed the formation of the desired compounds, with the POSS porphyrin found to exhibit comparable absorption properties to other pyridyl ligated ruthenium porphyrins.

The use of multi-hydroxy functionalised POSS would allow for the synthesis of a more soluble pyridyl precursor. Subsequent coupling of these precursors to metalloporphyrins offers a convenient pathway to multi-porphyrin functionalised POSS cages. Investigation of the optical properties should observe an increase in absorption associated with the multi-functionality.

Phosphorescence studies were unable to be performed under suitably inert, degassed conditions on the available instrumentation, and would allow for quantification of the optical properties and excited state lifetimes of the POSS porphyrin compounds.

4.8 References:

- (1) L. R. Milgron *The Colours of Life: An Introduction to the Chemistry of Porphyrins and Related Compounds*; Oxford University Press: New York, 1997.
- (2) A. D. Adler; F. R. Longo; J. D. Finarelli; J. Goldmacher; J. A.; L. Korsakoff *J. Org. Chem.* **1967**, *32*, 476.
- (3) P. Rothemund *J. Am. Chem. Soc.* **1936**, *58*, 625.
- (4) P. Rothemund *J. Am. Chem. Soc.* **1935**, *57*, 2010.
- (5) S. Mathew Honours Thesis, Flinders University, 2002.
- (6) A. Tsuda; S. Sakamoto; K. Yamaguchi; T. Aida *J. Am. Chem. Soc.* **2003**, *125*, 15722.
- (7) K. Li; D. I. Schuster; D. M. Guldi; M. A. Herranz; L. Echegoyen *J. Am. Chem. Soc.* **2004**, *126*, 3388.
- (8) F. T. Tat; Z. Zhou; S. Macmahon; F. Song; A. L. Rheingold; L. Echegoyen; D. I. Schuster; S. R. Wilson *J. Org. Chem.* **2004**, *69*, 4602.
- (9) A. J. Myles; N. R. Branda *J. Am. Chem. Soc.* **2001**, *123*, 177.
- (10) T. D. Lash; P. Chandrasekar *J. Am. Chem. Soc.* **1996**, *118*, 8767.
- (11) D. Sun; F. S. Tham; C. A. Reed; L. Chaker; M. Burgess; P. D. W. Boyd *J. Am. Chem. Soc.* **2000**, *122*, 10704.
- (12) P. A. Liddell; G. Kodis; A. L. Moore; T. A. Moore; D. Gust *J. Am. Chem. Soc.* **2002**, *124*, 7668.
- (13) T. Hasobe; P. V. Kamat; V. Troiani; N. Solladie; T. K. Ahn; S. K. Kim; D. Kim; A. Kongkanand; S. Kuwabata; S. Fukuzumi *J. Phys. Chem. B* **2005**, *109*, 19.
- (14) J. R. Darwent; A. Harriman; G. Porter; M.-C. Richoux *Coord. Chem. Rev.* **1982**, *44*, 833.
- (15) S. Funyu; T. Isobe; S. Takagi; D. A. Tryk; H. Inoue *J. Am. Chem. Soc.* **2003**, *125*, 5734.
- (16) S. T. Fujiwara; Y. Gushikem; C. A. Pessoa; S. Nakagaki *Electroanal.* **2005**, *17*, 783.
- (17) Y. Itagaki; K. Deki; S.-I. Nakashima; Y. Sadaoka *Sens. Act. B: Chem.* **2006**, *117*, 302.
- (18) M. A. Da Silva; D. C. De Olivieira; A. T. Papacidero; C. Mello; E. J. Nassar; K. J. Cuiffi; H. C. Saco *J. Sol-Gel Sci. Tech.* **2003**, *26*, 329.
- (19) K. Wada; D. Izuhara; M. Shiotsuki; T. Kondo; T. Mitsudo *Chem. Lett.* **2001**, *30*, 734.
- (20) H. C. L. Abbenhuis; R. A. van Santen; A. D. Burrows; M. T. Palmer; H. Kooijman; M. Lutz; A. L. Spek *Chem. Comm.* **1998**, 2627.
- (21) P. Braunstein; J. R. Galsworthy; B. J. Hendan; H. C. Marsmann *J. Organomet. Chem.* **1998**, *551*, 125.
- (22) K.-M. Kim; Y. Chujo *J. Mater. Chem.* **2003**, *13*, 1384.
- (23) B. Hong; T. P. S. Thoms; H. J. Murfee; M. J. Lebrun *Inorg. Chem.* **1997**, *36*, 6146.
- (24) H. J. Murfee; T. P. S. Thoms; J. Greaves; B. Hong *Inorg. Chem.* **2000**, *39*, 5209.
- (25) J. J. Bonnet; S. S. Eaton; G. R. Eaton; R. H. Holm; J. A. Albers *J. Am. Chem. Soc.* **1973**, *95*, 2141.

- (26) J. Rodriguez; C. Kirmaier; D. Holten *J. Am. Chem. Soc.* **1989**, *111*, 6500.
- (27) D. M. Guldi; T. Da Ros; P. Braiuca; M. Prato *Photochem. Photobiol. Sci.* **2003**, *2*, 1067.
- (28) T. Da Ros; M. Prato; D. M. Guldi; M. Ruzzi; L. Pasimeni *Chem. Eur. J.* **2001**, *7*, 816.
- (29) F. J. Feher; K. D. Wyndham; D. Soulivong; F. Nguyen *J. Chem. Soc., Dalton Trans.* **1999**, *9*, 1491.
- (30) P. Crews; J. Rodriguez; M. Jaspars *Organic Structure Analysis*; Oxford University Press: New York, 1998.
- (31) E. Alessio; S. Geremia; S. Mestroni; E. Iengo; I. Srnova; M. Slouf *Inorg. Chem.* **1999**, *38*, 869.
- (32) J. Carsten; K. Adolf 2003.
- (33) M. E. Wright; B. J. Petteys; A. J. Guenther; G. R. Yandek; L. C. Baldwin; C. Jones; M. J. Roberts *Macro.* **2007**, *40*, 3891.
- (34) Y. T. Park; C. H. Jung; K. W. Kim; H. S. Kim *J. Org. Chem.* **1999**, *64*, 8546.
- (35) K. I. Nattinen; K. Rissanen *Cryst. Growth Design* **2003**, *3*, 339.
- (36) S. S. Eaton; G. R. Eaton *Inorg. Chem.* **1977**, *16*, 72.
- (37) B. G. Maiya; N. Bampos; A. A. Kumar; N. Feeder; J. K. M. Sanders *New J. Chem.* **2001**, *25*, 797.
- (38) S. S. Eaton; G. R. Eaton *Inorg. Chem.* **1976**, *15*, 134.
- (39) L. M. A. Levine; D. Holten *J. Phys. Chem.* **1988**, *92*, 714.
- (40) K. M. Kadish; D. Chang *Inorg. Chem.* **1982**, *21*, 3614.
- (41) G. M. Brown; F. R. Hopf; J. A. Ferguson; T. J. Meyer; D. G. Whitten *J. Am. Chem. Soc.* **1973**, *95*, 5939.
- (42) F. Scandola; C. Chiorboli; A. Prodi; I. Iengo; E. Alessio *Coord. Chem. Rev.* **2006**, *250*, 1471.
- (43) A. Prodi; C. Chiorboli; F. Scandola; E. Iengo; E. Alessio; R. Dobraza; F. Wurthner *J. Am. Chem. Soc.* **2005**, *127*, 1454.

5 POSS BOUND PYRENE

5.1 Outline

This chapter details a details the properties and functionalisation of pyrene, followed by the synthesis and characterisation of the POSS pyrene derivative. Full experimental conditions, general characterisation techniques sample data are detailed in **Chapter 6**.

5.2 Pyrene

Pyrene possesses several interesting photophysical properties which make it suitable for fluorescent probe applications, notably the long lifetime of pyrene monomers and efficient excimer formation.¹ The vibronic structure in the fluorescence spectrum of pyrene was determined to be environmentally dependent, with polar solvents causing enhancement of the 0→0 band, whilst concurrently instigating reduction in intensity of the remaining bands. This variation in band intensity enabled the use of pyrene as a fluorophore to probe the critical micelle concentration of a variety of ionic and non-ionic surfactants.²⁻⁵

Pristine pyrene has previously been used as a fluorescent probe in order to investigate the sol-gel process. Incorporation of pyrene into a sol-gel starting solution enabled monitoring of the gelation process, local viscosity, solution polarity and, eventually, porosity of the final xerogel, through observation of the UV-Vis and fluorescence parameters.² Among the fluorescent probes, pyrene and perylene derivatives are advantageous due to the high quantum yield of fluorescence generally exhibited in dilute solutions combined with high photostability.^{6,7}

5.3 Silsesquioxane Bound Pyrene

Functionalised silsesquioxanes have been previously prepared in the synthesis of luminescent nanocomposites, with the incorporation of the pyrene group on the

periphery of POSS cages previously achieved through the Heck coupling of bromopyrene with octa(vinyl)POSS (**Figure 5.1**).^{8,9} Variations in the stoichiometry of bromopyrene to POSS affected the resultant substitution patterns. The use of eight equivalents of bromopyrene revealed a substitution range, determined via MALDI-ToF, of 4-10, with eight pyrene groups per POSS cage being the most abundant. The use of 24 equivalents of bromopyrene gave rise to a substitution range of 12-16, with fourteen pyrene groups per POSS cage being the most abundant. The presence of a number of substitutions higher than eight was indicative of di-substituted vinyl groups.¹⁰⁻¹² Silsesquioxane based pyrene hybrids have been reported as effective hole transport materials in organic light emitting diodes (OLED's), and are completely amorphous, enabling the formation of photoluminescent powders and films.^{8,9}

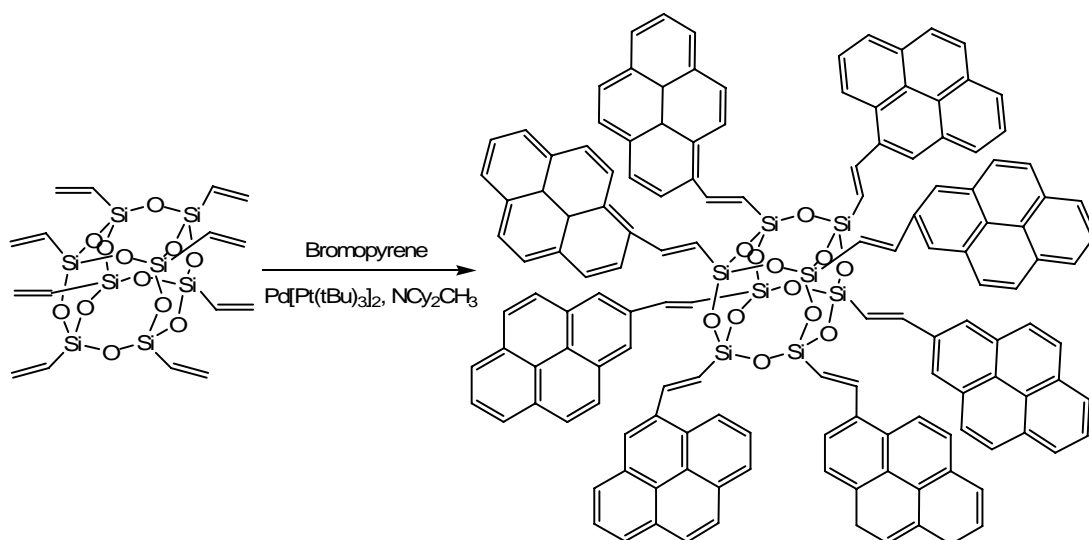


Figure 5.1. Synthesis of octa-pyrene substituted POSS^{8,9}

In order to avoid the uncontrollable stoichiometry of the product introduced by the Heck coupling method, an alternative synthetic pathway for the synthesis of pyrene substituted POSS was desired. It was envisaged that, similarly to the phenyl and pyridyl examples detailed earlier within **Chapter 4**, the reaction of pyrene acid chloride with an amino functionalised POSS would yield the desired POSS pyrene derivative.

5.4 Characterisation

Characterisation was performed by ^1H , ^{13}C and ^{29}Si NMR, UV-Vis and fluorescence spectrophotometry, Electrospray Ionisation (ESI) mass spectrometry and power limiting measurements, the details of which are detailed in **Chapter 6**.

5.4.1 FTIR

FTIR confirmed the presence of the amide functionality with amide band I (C=O stretching) present at 1632cm^{-1} and amide band II (N-H deformation) displayed at 1530cm^{-1} .¹³

5.4.2 ^1H NMR

The ^1H NMR resonances of all functionalised POSS compounds are summarised in **Table 5.1**.

5.4.2.1 (3-aminopropyl)POSS

As detailed in **Section 3.6.2.1**, ^1H NMR of (3-aminopropyl)POSS (**3.1**) exhibited resonances associated with the isobutyl chains of the POSS cage at δ 0.58-0.61 (16H, SiCH₂/iBu CH₂), 0.95 (42H, iBu CH₃) and 1.80-1.92 (7H, iBu CH), with propyl chain resonances at δ 1.50-1.58 (2H, CH₂) and 2.67 (2H, CH₂N), with the SiCH₂ resonance obscured. These resonances were consistent with those detailed in the literature.¹⁴

5.4.2.2 1-Pyrene Acid Chloride

1-Pyrene acid chloride was synthesised via the reaction of 1-pyrenecarboxylic acid in thionyl chloride (**Figure 5.2**).¹⁵ ^1H NMR exhibited pyrene resonances at δ 8.04-8.31 (m, 7H), 8.88-8.91 (d, $^3J_{\text{H-H}} = 9.0\text{ Hz}$) and 8.99-9.04 (d, $^3J_{\text{H-H}} = 9.9\text{ Hz}$), with these resonances consistent with those detailed in the literature.¹⁵

Table 5.1. ^1H NMR of mono-pyrene POSS (5.2) and precursor compounds

Compound	iBu	SiCH ₂	CH ₂	CH ₂ N	Pyrene
3.1	0.58-0.61, 0.95 d (6.6 Hz), ^a 1.80-1.92	-	1.50-1.58	2.67 t (7.2 Hz) ^a	-
5.1	-	-	-	-	8.04-8.31, 8.88-8.91 d (9.0 Hz) 8.99-9.04 d (9.9 Hz) ^a
5.2	0.60-0.63, 0.95-0.97, 1.87	0.74-0.79	Obs.	3.61-3.68	8.05-8.16, 8.22 d (7.8 Hz), 8.57 d (9.3 Hz) ^a

^a = $^3J_{\text{H-H}}$

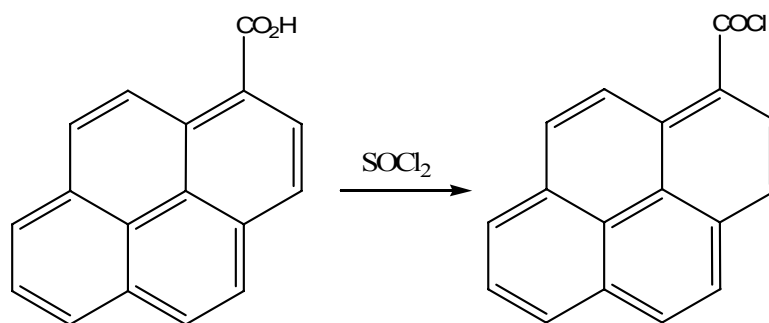


Figure 5.2. Synthesis of pyrene acid chloride (5.1)

5.4.2.3 Mono-pyrene POSS

The reaction of **5.1** and **3.1** yielded the desired mono-pyrene POSS product (**5.2**) (**Figure 5.3**).

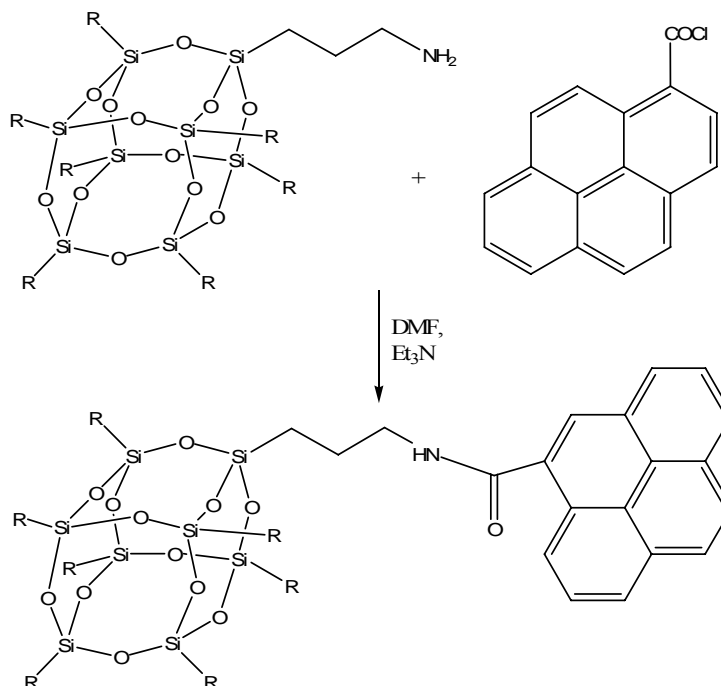


Figure 5.3. Synthesis of mono-pyrene POSS (5.2)

^1H NMR of **5.2** (**Figure 5.4**) exhibited the isobutyl resonances at δ 0.60-0.63 (14H, iBu CH_2), 0.95-0.97 (42H, iBu CH_3) and 1.87 (9H, CH_2 /iBu CH). Propyl chain resonances were observed at δ 0.74-0.79 (2H, SiCH_2) and 3.61-3.68 (2H, CH_2N), with the remaining CH_2 resonance obscured. Resonances indicative of the 1-substituted pyrene moiety were evident at δ 8.05-8.16 (m, 6H), 8.22 (d, 2H, $^3J_{\text{H-H}} = 7.8$ Hz) and 8.57 (d, 1H, $^3J_{\text{H-H}} = 9.3$ Hz).¹⁶

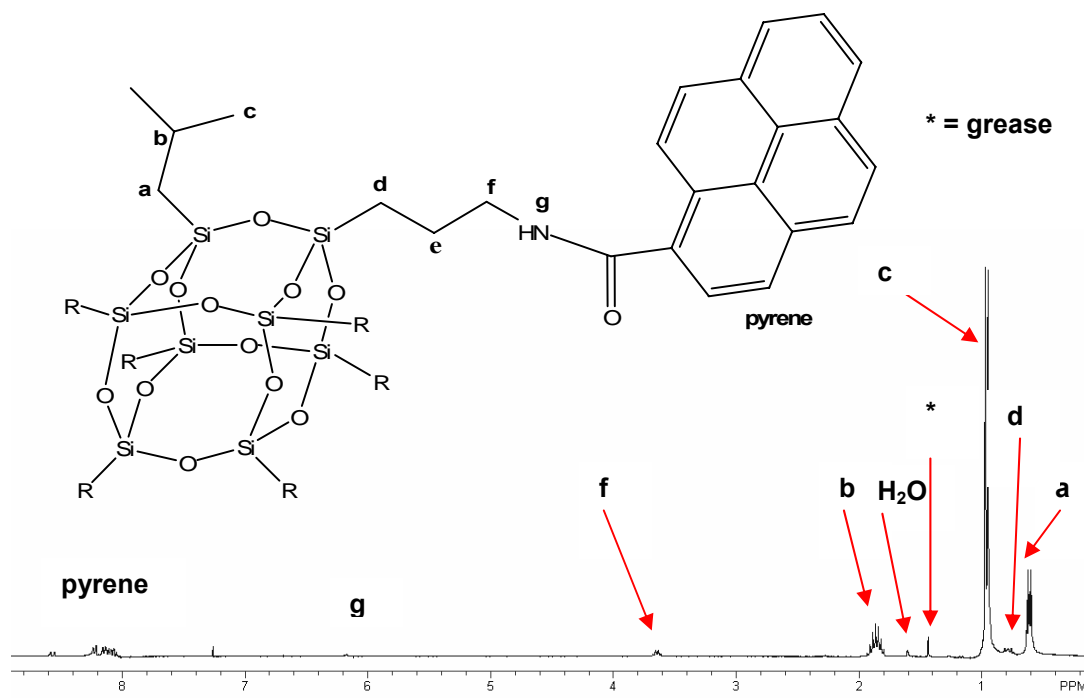


Figure 5.4. ^1H NMR of mono-pyrene POSS 5.2 (pictured) in CDCl_3

Downfield shifts of 0.16 and 0.94 ppm, respectively, were observed in the SiCH_2 and CH_2N resonances, relative to the corresponding resonances in (3-aminopropyl)POSS. Similar resonance shifts were evident in **4.1** (0.19 and 0.76 ppm) and **4.3** (0.17 and 0.88 ppm), as detailed in **Section 4.6.2**, and N-[3-(isobutylPOSS)propyl]-bis(benzyloxybenzamide)¹⁷ (0.12 and 0.85 ppm). The increased downfield shift of the CH_2N resonance was attributed to the enlarged deshielding effect experienced by the propyl chain resonance associated with the greater electron density of the pyrene functionality, in comparison to the phenyl, pyridyl and benzamide groups.

5.4.3 ^{13}C NMR

The ^{13}C NMR resonances of all functionalised POSS compounds are summarised in **Table 5.2**.

5.4.3.1 (3-aminopropyl)POSS

As detailed in **Section 3.6.3.1**, ^{13}C NMR exhibited resonances of the cage bound

Table 5.2. ^{13}C NMR of mono-pyrene POSS (5.2) and precursor compounds

Compound	iBu CH₂	SiCH₂	CH₂	CH₂N	Pyrene	C=O
3.1	24.01, 25.84, 27.23	9.36	22.65	44.90	-	-
5.1	-	-	-	-	123.88, 124.17, 126.79, 126.96, 127.19, 127.50, 130.18, 130.86, 131.30, 131.40, 131.86, 135.98	167.92
5.2	22.66, 24.00 25.85	9.79	23.41	42.72	124.57, 124.62, 125.84, 125.93, 126.47, 127.27, 128.75, 128.81, 130.91, 131.36, 131.65, 132.61	170.01

isobutyl carbons at δ 24.01, 25.84 and 27.23, with propyl chain resonances apparent at δ 9.36 (SiCH₂), 22.65 (CH₂) and 44.90 (CH₂N). These resonances were consistent with those detailed in the literature.¹⁴

5.4.3.2 1-Pyrene Acid Chloride

¹³C NMR exhibited resonances at δ 123.88, 124.17, 126.79, 126.96, 127.19, 127.50, 130.18, 130.86, 131.30, 131.40, 131.86 and 135.98, with the carbonyl resonance apparent at δ 167.92. These resonances were consistent with those detailed in the literature.¹⁵

5.4.3.3 Mono-pyrene POSS

¹³C NMR of **5.2** (**Figure 5.5**) exhibited the isobutyl resonances at δ 22.66, 24.00 and 25.85, resulting in upfield shifts of 1.35, 1.84 and 1.38 ppm, relative to the corresponding resonances in mono-(3-aminopropyl)POSS. Similar upfield resonance shifts were also present in **4.1** (0.95, 2.00, 1.55 ppm), **4.3** (1.39, 1.80, 1.40 ppm) and the benzamide derivative (1.0, 2.0 and 1.5 ppm).¹⁷ Propyl chain resonances were observed at δ 9.79 (SiCH₂), 23.41 (CH₂) and 42.72 (CH₂N), resulting in downfield shifts of 0.43 and 1.36 ppm in the SiCH₂ and CH₂ resonances, with an upfield shift of 2.18 ppm evident in the CH₂N resonance. Comparable resonance shifts were evident in **4.1** (0.13, 0.41, 2.65 ppm), **4.3** (0.29, 0.44, 2.32 ppm) and the benzamide derivative (0.1, 0.4, 2.6 ppm).¹⁷ The increased downfield shift of the SiCH₂ and CH₂ resonances, coupled with the reduced upfield shift of the CH₂N resonance was attributed to the increased deshielding experienced by the propyl chain, associated with the increased electron density associated of the pyrene moiety, in comparison to the phenyl, pyridyl and benzamide functionalities.

Resonances indicative of the 1-substituted pyrene moiety were evident at δ 124.57, 124.62, 125.84, 125.93, 126.47, 127.27, 128.75, 128.81, 130.91, 131.36, 131.65 and 132.61,¹⁸ with the carbonyl resonance observed at δ 170.01.

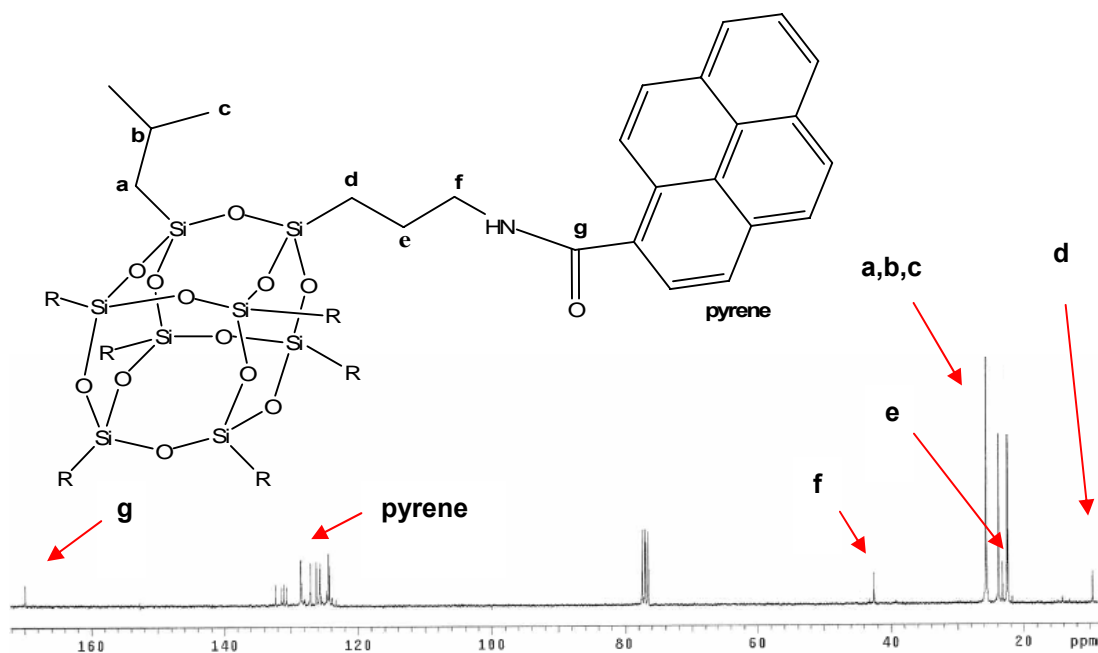


Figure 5.5. ^{13}C NMR of mono-pyrene POSS 5.2 (pictured) in CDCl_3

5.4.4 ^{29}Si NMR

^{29}Si NMR exhibited resonances characteristic of the monosubstituted POSS cage in **5.2** at δ -68.03, -68.26, -68.30 and -68.36 (Figure 5.6), indicating that the cage structure remained intact during reaction.

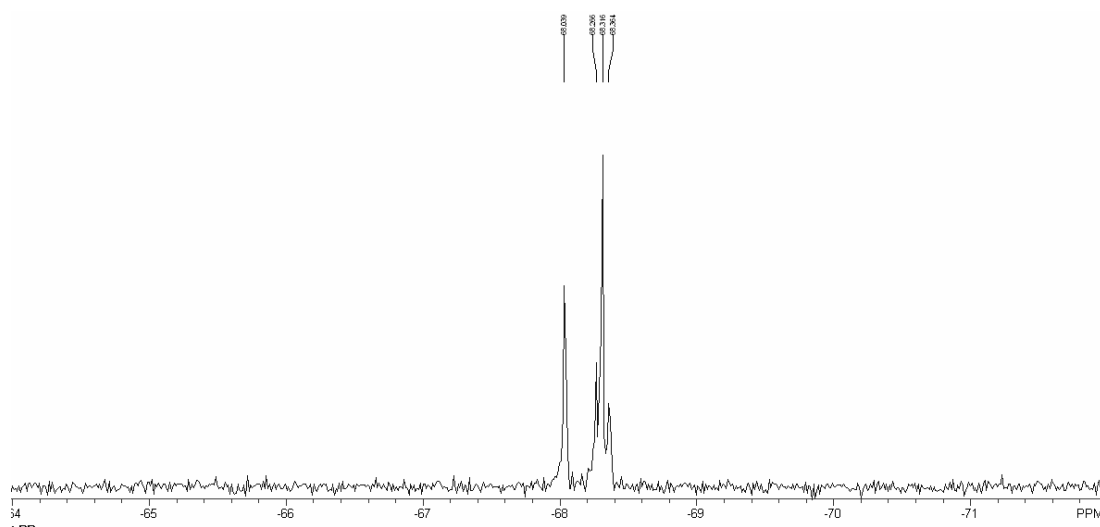


Figure 5.6. ^{29}Si NMR of mono-pyrene POSS 5.2 in (pictured) CDCl_3

5.4.5 High Resolution ESI Mass Spectrometry

High resolution ESI mass spectrometry of **5.2** exhibited a molecular ion, $[M+Na]^+$, at 1124.3595, compared to the theoretical value of 1124.3602, giving unequivocal evidence of the formation of the desired mono-pyrene POSS imide.

5.4.6 Elemental Analysis of Mono-pyrene POSS

The close correlation between the theoretical (52.28, 7.22, 1.27) and experimental (52.94, 6.52, 1.83) results of **5.2** offered further confirmation of the formation of the desired pyrene functionalised POSS compound.

5.4.7 Optical Properties of Mono-pyrene POSS

5.4.7.1 UV-Vis Spectrum of Mono-pyrene POSS

UV-Vis of **5.2** displayed absorption maxima at 332 and 344 nm, giving rise to molar extinction coefficients of 32635 and 44328, respectively (**Figure 5.7**). The absorption spectra of pyrene exhibited maxima at 232, 242, 252, 260, 272, 308, 320 and 336 nm, with each maxima attributed to a distinct vibronic band.^{4,19} **Figure 5.7** contains an overlay of the UV-Vis spectra of **5.2** and pyrene, with the molar extinction coefficient of pyrene divided by a factor of 2 to enable comparison of the absorption maxima positions.

Absorption maxima of mono- (345 nm), bis- (355 nm), tris- (365 nm) and tetrakis-substituted pyrenes (375 nm) were bathochromically shifted consecutively at intervals of 10nm, with respect to pyrene (336 nm).²⁰ The nature of this red shift was attributed to a reduction in the energy gap between the HOMO and LUMO following substitution.^{20,21} Analogously, the absorption maxima of **5.2** were bathochromically shifted by 12 and 10 nm, in comparison to the corresponding vibronic bands of pyrene (320 and 336 nm), characteristic of mono-substituted pyrene derivatives.^{4,19} The absorption spectrum of **5.2** was analogous to that exhibited by other mono-substituted pyrene derivatives, such as trimethylsilylpyrene, which displayed

comparable absorption maxima position (344 nm) and a similar molar extinction coefficient (51286).²⁰

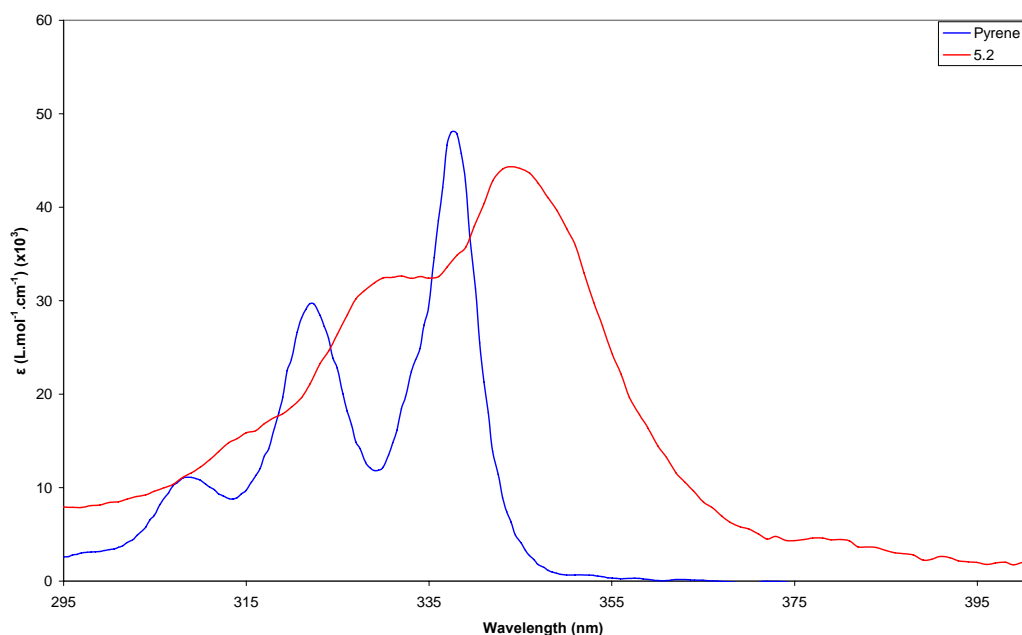


Figure 5.7. UV-VIS spectrum of mono-pyrene POSS (**5.2**) and pyrene in toluene

5.4.7.2 Steady State Spectrofluorometric Emission Study of Mono-pyrene POSS

Pyrene is one of the few condensed aromatics to exhibit vibronic bands in its fluorescence spectrum. Excitation of **5.2** ($\lambda_{\text{exc}} = 365\text{nm}$) yielded emission bands at 385, 404 and 425 nm (**Figure 5.8**), with a high quantum yield ($\Phi_{\text{F}} = 0.91$). The emission maxima position observed were similar to that exhibited by other mono-substituted pyrene derivatives, such as trimethylsilylpyrene, which exhibited an emission maxima at 394 nm (toluene).^{16,20}

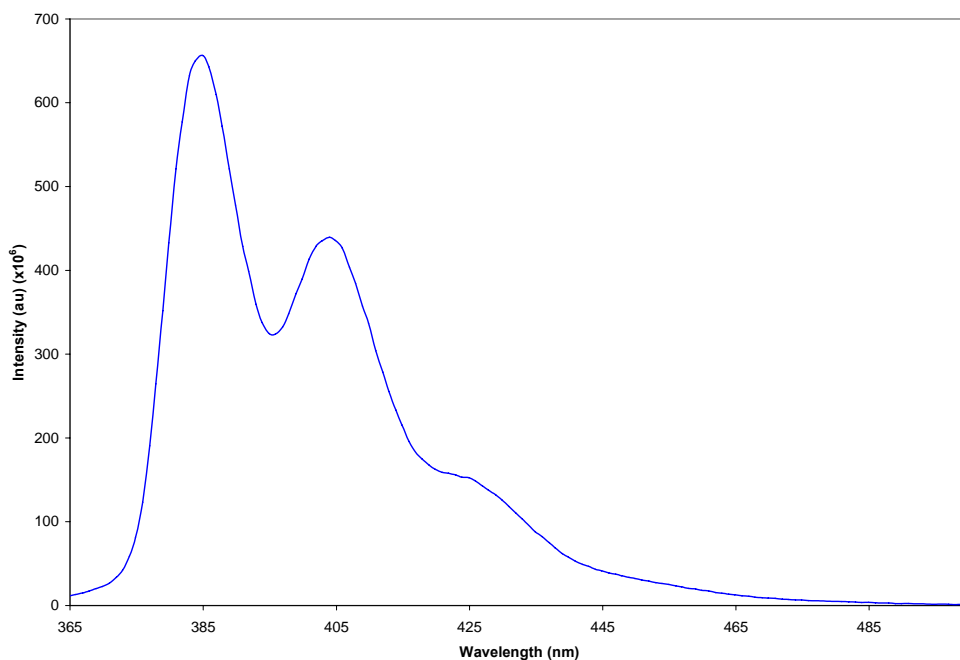


Figure 5.8. Emission spectrum of mono-pyrene POSS 5.2 in toluene ($\lambda_{\text{exc}} = 365\text{nm}$)

Elevated quantum yields have been observed in other functionalised pyrene derivatives, such as trimethylsilylpyrene ($\Phi_{\text{F}} = 0.8$)¹⁶ and oligo-ether functionalised pyrene⁶ (**Figure 5.9**), which exhibited a quantum yield approaching unity.

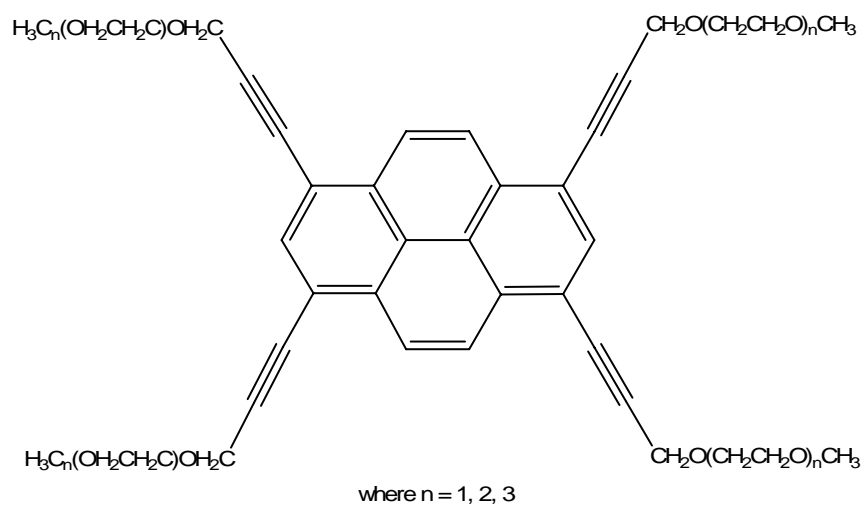


Figure 5.9. Oligo-ether functionalised pyrene⁶

5.5 Conclusions and Future Work

A mono-functionalised POSS pyrene compound has synthesised through the reaction of (3-aminopropyl)POSS with 1-pyrene acid chloride. The mono-pyrene POSS was characterised by ^1H , ^{13}C and ^{29}Si NMR, FTIR, UV-VIS and fluorescence spectrophotometry and ESI mass spectrometry. The various methods of characterisation confirmed the formation of the desired mono-pyrene POSS.

The synthetic pathway detailed within this chapter offered a convenient route to mono-functionalised pyrene POSS compounds. In order to synthesise multi-substituted derivatives, the employment of multi-hydroxy POSS derivatives, in preference to the amino compounds used within this chapter, will offer increased solubility through the ester spacer group. This reaction pathway will offer a convenient synthetic route to multi-functionalised POSS cages containing stoichiometrically defined number of pyrene functionalities in preference to the distribution ranges exhibited achieved via the Heck coupling pathway.

5.6 References:

- (1) K. Kalyanasundaram; J. K. Thomas *J. Am. Chem. Soc.* **1977**, *99*, 2039.
- (2) L. M. Ilharco; A. M. Santos; M. J. Silva; J. G. M. Martinho *Langmuir* **1995**, *11*, 2419.
- (3) Q. R. Huang; H. C. Kim; E. Huang; D. Mecerreyes; J. L. Hedrick; W. Volksen; C. W. Frank; R. D. Miller *Macro.* **2003**, *36*, 7661.
- (4) G. Basu Ray; I. Chakraborty; S. P. Moulik *J. Coll. Interf. Sci.* **2006**, *294*, 248.
- (5) N. Lebedeva; R. Ranganathan; B. L. Bales *J. Phys. Chem. B* **2007**, *111*, 5781.
- (6) V. de Halleux; W. Mamdouh; S. De Feyter; F. De Schryver; J. Levin; Y. H. Geerts *J. Photochem. Photobiol. A: Chem.* **2006**, *178*, 251.
- (7) S. I. Kawamura; T. Morita; S. Kimura *Sci. Tech. Adv. Mat.* **2006**, *7*, 544.
- (8) M. Y. Lo; C. Zhen; M. Lauters; G. E. Jabbour; A. Sellinger *J. Am. Chem. Soc.* **2007**, *129*, 5808.
- (9) Mee Yoon Lo; Kazunori Ueno; Hiroshi Tanabe; Sellinger, A. *The Chemical Record* **2006**, *6*, 157-168.
- (10) K. Itami; Y. Ushioji; T. Nokami; Y. Ohashi; J. Yoshida *Org. Lett.* **2004**, *6*, 3695.
- (11) K. Itami; Y. Ohashi; J. I. Yoshida *J. Org. Chem.* **2005**, *70*, 2778.
- (12) L. Botella; C. Najera *J. Org. Chem.* **2005**, *70*, 4360.
- (13) P. Crews; J. Rodriguez; M. Jaspars *Organic Structure Analysis*; Oxford University Press: New York, 1998.
- (14) J. Carsten; K. Adolf **2003**, WO03042223.
- (15) H. Yuasa; N. Miyagawa; T. Izumi; M. Nakatani; M. Izumi; H. Hashimoto *Org. Lett.* **2004**, *6*, 1489.
- (16) D. Declerq; P. Debelke; F. C. De Schryver; L. Van Meervelt; R. D. Miller *J. Am. Chem. Soc.* **1993**, *115*, 5702.
- (17) M. E. Wright; B. J. Petteys; A. J. Guenther; G. R. Yandek; L. C. Baldwin; C. Jones; M. J. Roberts *Macro.* **2007**, *40*, 3891.
- (18) R. W. Murray; M. Singh; N. P. Rath *Carcinogenesis* **1999**, *20*, 147.
- (19) Z. H. Khan; B. N. Khanna *J. Chem. Phys.* **1973**, *59*, 3015.
- (20) H. Maeda; Y. Inohue; H. Ishida; K. Mizuno *Chem. Lett.* **2001**, 1224.
- (21) V. Georgakilas; K. Kordatos; M. Prato; D. M. Guldi; M. Holzinger; A. Hirsch *J. Am. Chem. Soc.* **2002**, *124*, 760.

6 EXPERIMENTAL

6.1 Instrumentation

6.1.1 Nuclear Magnetic Resonance (NMR) Spectroscopy

^1H , ^{13}C and ^{29}Si NMR were recorded on a 300MHz Varian Gemini FT-NMR. Chemical shifts (δ) are reported in parts per million (ppm), with solvent peaks used as references for ^1H and ^{13}C NMR spectra. External tetramethylsilane was used as a reference for ^{29}Si NMR spectra. The solvent used was deuterated chloroform unless otherwise indicated. Abbreviations used in assigning spectra include: s, singlet; b, broad; d, doublet; t, triplet; q, quartet; sept, septet; n, nonet; m, multiplet; dd, doublet of doublets.

6.1.2 Fourier Transform Infra-Red (FTIR) Spectroscopy

FTIR spectra were obtained on a Nicolet Nexus 8700 FTIR spectrometer and data analysis was performed using Omnic 7.0 software. A Diffuse Reflectance Infra Red Transmission (DRIFT) spectroscopy accessory was used in combination with the FTIR for solid sample analysis. Approximately 2 mg of sample was ground with dried high purity potassium bromide (KBr) and placed in the DRIFT sample holder for analysis. Spectra were obtained from 650 to 4000 cm^{-1} , using a liquid nitrogen cooled MCT/A detector with an aperture of 33 and resolution of 4 cm^{-1} , over 256 scans. KBr was used to obtain the background spectra. Abbreviations used in the description of band intensities include: vs, very strong; s, strong; m, medium; w, weak.

6.1.3 Mass Spectrometry

Accurate mass ElectroSpray Ionisation (ESI) analysis was performed on a Bruker BioApex II 47e Fourier Transform Mass Spectrometer (FT-MS), using Xmass

Version 5.0 software at Monash University. ESI was used to determine the molecular mass of the samples. A capillary volt of 80 volts was used with a Shimadzu QP5050A GC-MS system, fitted with a solid probe. The probe was heated from 60 to 280 °C, at a heating rate of 15 °C/min.

6.1.4 Elemental Analysis

Elemental analyses samples were submitted to the analytical department of the University of Otago, New Zealand, for analysis of carbon, hydrogen and nitrogen contents.

6.1.5 UV-Vis Spectrophotometry

UV-Vis experiments were performed at an ambient temperature of 25 °C using a Varian Cary 50 Scan Spectrophotometer. The samples were analysed in a Quartz cuvette obtained from Starna Pty. Ltd.

6.1.6 Fluorescence Spectrophotometry

Steady-State Fluorescence experiments were conducted on a Varian Cary Eclipse Fluorescence Spectrophotometer equipped with a Varian single cell Peltier accessory used in conjunction with a Gilson MINIPULS3 peristaltic pump to aid temperature control of the sample. The samples held in a quartz cuvette obtained from Starna Pty. Ltd.

6.1.7 Power Limiting

Power limiting measurements were performed using a diode-Q-switched Nd:YLF laser which after frequency doubling of the output provided ~25 ns 523 nm pulses of microjoule energies. The experimental setup was constructed to be similar to the standard $f/5$ test bed used in the literature¹ and toluene solutions of the investigated compounds with concentrations adjusted to provide 70 % transmission at 523 nm

were examined in 1 mm glass cells. The transmission vs fluence curves were each constructed from several runs in which the incident pulse energy was varied and the fluence was additionally varied by scanning the sample position along the Z-axis. The shapes of open and closed aperture Z-scans obtained were used to calculate the fluence values.

6.1.8 Single Crystal X-ray Crystallography

X-ray crystallographic studies of selected crystals were carried out by Dr Brian Skelton at the University of Western Australia. Data were collected on a Bruker Smart CCD diffractometer at 100(2) K using CuK α radiation ($\lambda = 1.5418 \text{ \AA}$) to a Θ max) of 65.7028 $^\circ$. Absorption corrections were applied using the multiscan technique² giving maximum and minimum transmission coefficients T (min, max) (0.77705, 1). The solution and refinement was undertaken using the Xtal suite of programs.³ Reflections collected/unique: 18388/5745. R-factors R, R': 0.1774, 0.067.

6.1.9 Chromatography

Thin layer chromatography (TLC) was performed on pre-coated sheets of Merck silica gel 60 and visualised using visible or UV light (254 nm). Column chromatography was carried out under a positive pressure of nitrogen using Merck Kieselgel (230-400 mesh).

6.2 Chemicals

Commercially available chemicals were used without purification unless otherwise stated. R₇Si₇O₉(OH)₃ (where R = iBu, Cp, Ph) was purchased from Hybrid Plastics (Hattiesburg, MS). C₆₀ was purchased from SES Laboratories (Houston, TX) and used as received. [Ru(CO)(EtOH)(tetraphenylporphyrin)] was a gift from Simon Mathew (Flinders University). The remaining chemicals were obtained from Sigma-Aldrich. Solvents were purified and dried according to literature procedures.⁴

Chlorobenzene was distilled from calcium hydride, degassed via the freeze/pump/thaw method and distilled via standard Schlenk techniques.

6.3 Synthesis

6.3.1 POSS Fulleropyrrolidines: Synthetic Pathway 1

2-(4-bromophenyl)-1,3-dioxolane

2-(4-bromophenyl)-1,3-dioxolane was prepared according to the procedure outlined by Silverman *et al.*⁵ To a stirred solution of 4-bromobenzaldehyde (5 g, 40.9 mmol) in benzene (100 ml) was added ethylene glycol (4.6 ml, 81.8 mmol) and *p*-toluenesulfonic acid (100 mg). The solution was azeotropically distilled until no further water condensed, cooled and extracted with cold water/ethyl acetate. The organic layer was washed with brine, dried (Na₂SO₄) and the solvent evaporated *in vacuo*. Kugelrohr distillation of the residue yielded 4-bromophenyldioxolane as a colourless oil.

Yield = 5.2 g (75 %); ¹H NMR (CDCl₃): δ 4.06 (m, 4H, OCH₂CH₂O), 5.77 (s, 1H, OCHO), 7.38 (d, ³J_{H-H} = 8.0 Hz, 2H, CH), 7.51 (d, ³J_{H-H} = 8.0 Hz, 2H CH); ¹³C NMR (CDCl₃): δ 65.4 (OCH₂CH₂O), 103.1 (OCHO), 123.3, 128.3 (CC), 131.6 (CBr), 137.1 (CC).

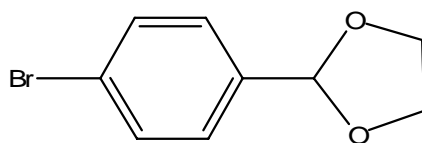


Figure 6.1. Structure of 4-Bromophenyldioxolane

Mono-vinyl POSS, R = *i*Bu (2.1)

Mono-vinyl POSS compounds were synthesised according to the literature procedure detailed by Shockey *et al.*⁶ The example where R = *i*Bu (2.1) is detailed herein. Vinyltrichlorosilane (2.0 ml, 15.7 mmol) in diethyl ether (20 ml) was added dropwise to a solution of *i*Bu₇Si₇O₇(OH)₃ (11.35 g, 14.2 mmol) and triethylamine (6.0 ml, 42.7

mmol) in diethyl ether (300 ml). The solution was stirred overnight and the residue extracted with diethyl ether. **2.1** was precipitated as a white solid via the addition of methanol.

Yield = 8.30 g (58 %); FTIR (KBr, cm^{-1}): 2957m, 2890m, 1464m, 1408m, 1257m, 1168m, 1116vs, 1022m, 971m, 944m, 839m, 815m, 741m; ^1H NMR (CDCl_3): δ 0.60 (m, 14H, CH_2), 0.94 (m, 42H, CH_3), 1.86 (n, 7H, $^3J_{\text{H-H}} = 10.2$ Hz, CH), 5.87-6.01 (m, 3H, $\text{CH}=\text{CH}_2$); ^{13}C NMR (CDCl_3): δ 22.64, 24.09, 25.90, 130.16, 136.03; ^{29}Si NMR (CDCl_3): δ -67.79, -68.26; $[\text{M}+\text{Na}]^+$ 865.2615 (865.2606 theory)

Mono-vinyl POSS, R = Ph (**2.2**)

Yield 2.74 g, 50 %; FTIR (KBr, cm^{-1}): 3073w, 3052w, 3028w, 2957w, 2922w, 1595w, 1490w, 1409w, 1109vs, 1049s, 1030s, 999m, 921w, 852w, 741m, 697m; ^1H NMR (CDCl_3): δ 5.85-6.20 (3H, m, $\text{CH}=\text{CH}_2$), 7.30-7.50 (21H, m, CH), 7.75-7.80 (14H, m, CH); ^{13}C NMR (CDCl_3): δ 127.89, 130.72, 134.34; ^{29}Si NMR (CDCl_3): δ -65.14, -78.88, -79.13; $[\text{M}+\text{Na}]^+$ 1005.0421 (1005.0415 theory)

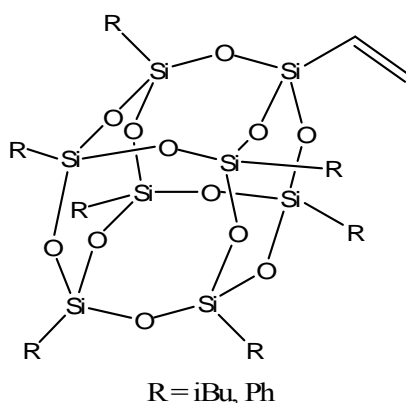


Figure 6.2. Structure of mono-vinyl POSS (**2.1**, **2.2**)

2-(4-(Dimethylsilyl)phenyl)-1,3-dioxolane (**2.3**)

2.3 was synthesised according to the literature procedure detailed by Morris *et al.*⁷ 4-(1,3-dioxolon-2-yl)phenylmagnesium bromide was prepared from Mg (1.02 g, 41.8 mmol) and 2-(4-bromophenyl)-1,3-dioxolane (9.58 g, 41.8 mmol) in THF (100 ml). Chlorodimethylsilane (4.54 ml, 41.8 mmol) in THF (25 ml) was added dropwise and

the solution stirred overnight. Sodium hydrogen carbonate (1 M in H₂O, 80 ml) was added and the solution extracted with diethyl ether (3 x 50 ml). The combined ether layers were washed with brine (60 ml), dried (MgSO₄) and concentrated *in vacuo*. The residue was purified by Kugelrohr distillation yielding **2.3** as a colourless oil.

Yield = 5.98 g (78 %); ¹H NMR (CDCl₃): δ 0.35 (d, ³J_{H-H} = 5.7 Hz, 6H, SiCH₃), 4.01 (m, 4H, OCH₂CH₂O), 4.44 (sept, ³J_{H-H} = 5.7 Hz, 1H, SiH), 5.85 (s, 1H, OCHO), 7.48 (d, ³J_{H-H} = 8.1 Hz, 2H, CH), 7.58 (d, ³J_{H-H} = 8.1 Hz, 2H, CH); ¹³C NMR (CDCl₃): δ -3.72 (SiCH₃), 65.39 (OCH₂CH₂O), 103.73 (OCHO), 125.39 (CH), 134.15 (CH), 138.75 (CSi), 139.00 (CCH); ²⁹Si NMR (CDCl₃): δ -17.60

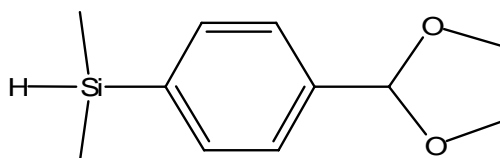


Figure 6.3. Structure of 2-(4-(Dimethylsilyl)phenyl)-1,3-dioxolane (**2.3**)

Mono-dioxolane POSS, R = iBu (**2.4**)

2.4 was synthesised via modification of the literature procedure reported by Morris *et al.*⁷ **2.3** (3.10 g, 16 mmol) and Karstedt's catalyst (50 μl) were added to a solution of **2.1** (7.00 g, 8.3 mmol) in diethyl ether (100 ml) and the solution was refluxed overnight. The crude green solution was filtered through silica and the filtrate was concentrated *in vacuo*. Excess **2.3** was removed by Kugelrohr distillation to yield the desired product as a viscous brown oil. In the case of R = Ph, the dioxolane was not isolated, due to partial deprotection of the dioxolane occurring *in situ*.

Yield = 5.67 g (68 %); FTIR (KBr, cm⁻¹): 2957m, 2888m, 1696m, 1586m, 1407m, 1370m, 1249m, 1206m, 1101vs, 896m, 870m, 836m, 754m, 692w; ¹H NMR (CDCl₃): δ 0.35 (m, 6H, SiCH₃), 0.61 (m, 14H, iBu CH₂), 0.97 (m, 42H, iBu CH₃), 1.86 (m, 7H, iBu CH), 4.04-4.14 (m, 4H, OCH₂CH₂O), 5.84 (s, 1H, CH), 7.49 (s, 2H, CH), 7.51 (s, 2H, CH); ¹³C NMR (CDCl₃): δ -3.53 (SiCH₃), 4.56 (O₃SiCH₂), 6.82 (CH₂Si), 22.65, 24.01, 25.83, 65.42 (OCH₂CH₂O), 103.86 (CH), 125.86, 133.80, 138.53, 140.57; ²⁹Si NMR (CDCl₃): δ -1.51 (SiC₄), -67.60, -68.04, -68.36 (RSiO₃);

$[M+Na]^+$ 1073.3510 (1073.3526 theory)

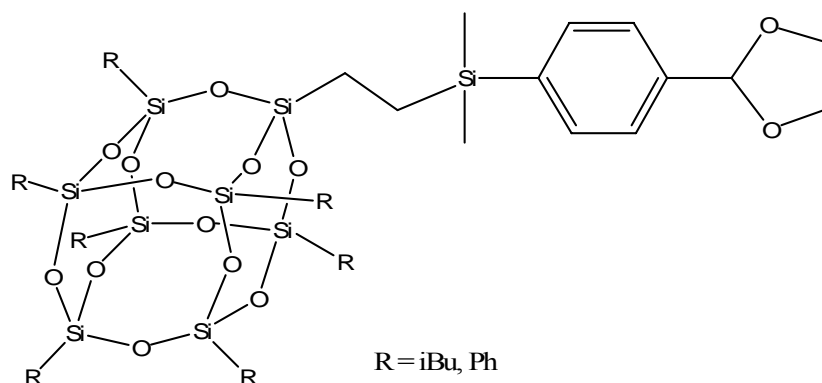


Figure 6.4. Structure of mono-dioxolane POSS (2.4)

Mono-aldehyde POSS, R = iBu (2.5)

The synthesis of mono-aldehyde POSS was achieved via modification of the literature procedure reported by Morris *et al.*⁷ The example of R = iBu (**2.5**) is described herein. **2.4** (1.026 g, 0.975 mmol) and pyridinium *p*-toluenesulfonate (2.5 mg, 0.01 mmol) were refluxed in acetone (50 ml) overnight. The solvent was removed *in vacuo* to yield a viscous oil, which was crystallised from ethanol to yield **2.5** as a white solid.

Yield = 0.172 g (18 %); $^1\text{H NMR}$ (CDCl_3): δ 0.29 (m, 6H, SiCH_3), 0.59 (d, $^3J_{\text{H-H}} = 9.9$ Hz, 14H, iBu CH_2), 0.95 (d, $^3J_{\text{H-H}} = 9.9$ Hz, 42H, iBu CH_3), 1.85 (sept, $^3J_{\text{H-H}} = 9.9$ Hz, 7H, iBu CH), 7.66 (d, $^3J_{\text{H-H}} = 12.0$ Hz, 2H, CH), 7.84 (d, $^3J_{\text{H-H}} = 12.0$ Hz, 2H, CH), 10.02 (s, 1H, CHO); $^{13}\text{C NMR}$ (CDCl_3): δ -3.27 (SiCH_3), 4.55 (SiCH_2), 6.70 (CH_2Si), 18.44, 22.62, 24.00, 25.80, 128.75, 134.25, 136.59, 148.30, 192.87 (CHO); $^{29}\text{Si NMR}$ (CDCl_3): δ -0.66 (SiC_4), -67.89, -68.03, -68.33 (RSiO_3)

Mono-aldehyde POSS, R = Ph (2.6)

Yield = 0.326 g (27 %); $^1\text{H NMR}$ (CDCl_3): δ 0.25 (SiCH_3), 0.69 - 0.74 (2H, m, CH_2), 0.89 - 0.94 (2H, m, CH_2), 7.34-7.58 (2H, m, CH), 7.73-7.80 (16H, m, CH), 9.97 (21H, CHO); $^{13}\text{C NMR}$ (CDCl_3): δ -3.79, (SiCH_3), 4.24 (SiCH_2), 6.51 (CH_2Si), 127.85, 128.60, 130.18, 130.43, 130.76, 134.05, 134.16, 136.12, 147.96, 192.62

(CHO); ^{29}Si NMR (CDCl_3): δ -0.54 (SiC_4), -65.12, -78.84, -79.16 (RSiO_3); $[\text{M}+\text{Na}]^+$ 1169.0200 (1169.1073 theory)

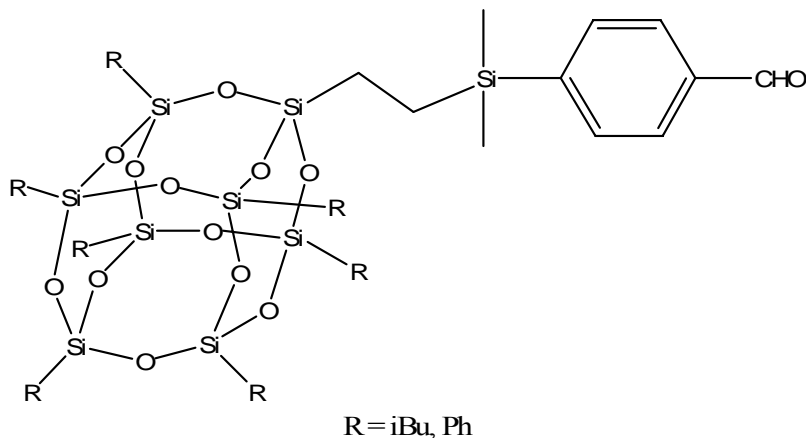


Figure 6.5. Structure of mono-aldehyde POSS (2.5, 2.6)

POSS Fulleropyrrolidine, R = iBu (2.7)

POSS fulleropyrrolidines were synthesised through modification of the literature procedure detailed by Prato *et al.*⁸ The example of R = iBu (2.7) is detailed herein. Mono-aldehyde POSS (137 mg, 0.14 mmol) was added to a solution containing C_{60} (100 mg, 0.14 mmol), N-methylglycine (25 mg, 0.28 mmol) and toluene (100 ml), and the solution was refluxed overnight. The solvent was removed *in vacuo* and the residue extracted with toluene and separated with flash chromatography (eluant hexane/dichloromethane). Evaporation of the brown fraction yielded the POSS-fulleropyrrolidine product as a brown solid.

Yield = 20 mg (9 %); FTIR (KBr, cm^{-1}): 2957m, 2870m, 2700m, 1463m, 1429w, 1401w, 1104vs, 1022s, 801s, 744m, 706w; ^1H NMR (CDCl_3): δ 0.24 (SiCH_3), 0.55-0.59 (m, 14H, iBu CH_2), 0.91-0.96 (m, 42H, iBu CH_3), 1.75-1.90 (m, 7H, iBu CH), 2.82 (s, 3H, NCH_3), 4.27 (d, 1H, $^3\text{J}_{\text{H-H}} = 14.1$ Hz, NCH), 4.93 (s, 1H, NCH), 4.99 (d, $^3\text{J}_{\text{H-H}} = 14.1$ Hz, 1H, NCH), 7.42 (d, $^3\text{J}_{\text{H-H}} = 11.4$ Hz, 2H, CH), 7.76 (d, $^3\text{J}_{\text{H-H}} = 11.4$ Hz, 2H, CH); ^{13}C NMR (CDCl_3): δ -3.56 and -3.47 (SiCH_3), 4.57 (SiCH_2), 7.09 (CH_2Si), 22.62, 24.00, 25.87 (iBu), 40.26 (NCH_3), 69.25 (CH_2), 70.25 (sp^3 C), 83.78 (CH), 127.75, 128.10, 128.35, 128.77, 129.69, 130.54, 134.00, 136.00, 136.87, 137.59, 139.56, 139.73, 139.99, 140.33, 141.66, 141.84, 142.10, 142.28, 142.72, 143.28, 144.55, 144.86, 145.42, 145.71, 145.92, 146.09, 146.04, 146.65, 147.00,

147.47, 153.62, 154.27, 156.41; ^{29}Si NMR (CDCl_3): δ -1.66 (SiC_4), -67.65, -68.13, -68.40 (RSiO_3); $[\text{M}]^+$ 1754.3888 (1754.3872 theory); elemental analysis: calcd (%) 69.81, 5.67, 0.46; found 69.10, 4.77, 0.80; UV-Vis λ_{max} (nm) (ϵ ($\text{M}^{-1}\text{cm}^{-1}$)) (toluene) 433 (3005), 705 (235); Fluorescence (λ_{exc} = 335 nm, toluene) 719 nm

POSS Fulleropyrrolidine, R = Ph (2.8)

Yield = 34 mg (14 %); FTIR (KBr, cm^{-1}): 3072w, 3050w, 3028w, 2953m, 2923m, 2780w, 1666w, 1594w, 1463w, 1430m, 1261w, 1247w, 1203w, 1134vs, 1109s, 1029m, 998m, 837w, 797w, 744m, 697m; ^1H NMR (CDCl_3): δ 0.23 (s, 6H, SiCH_3), 0.53-0.59 (m, 2H, SiCH_2), 0.82-0.90 (m, 2H, CH_2Si), 2.83 (s, 3H, NCH_3), 4.25-4.28 (m, 1H, NCH_2), 4.92 (s, 1H, NCHR), 4.98-5.00 (m, 1H, NCH_2), 7.34-7.49 (m, 23H, CH), 7.70-7.74 (m, 16H, CH); ^{13}C NMR (CDCl_3): δ -3.56 (SiCH_3), 4.21 (SiCH_2), 7.04 (CH_2Si), 40.14 (NCH_3), 68.84 (CH_2), 69.77 (sp^3 C), 83.47 (CH), 127.80, 128.60, 130.25, 130.45, 130.74, 133.91, 134.18, 134.20, 135.65, 136.76, 139.26, 139.81, 140.04, 141.09, 141.37, 141.57, 141.57, 141.72, 141.81, 142.05, 142.05, 142.12, 142.37, 142.44, 142.49, 142.59, 142.76, 142.91, 143.00, 144.21, 144.28, 144.46, 144.58, 145.11, 145.21, 145.41, 145.53, 145.60, 145.75, 145.79, 146.03, 146.17, 146.23, 147.19, 153.02; ^{29}Si NMR (CDCl_3): δ -1.19 (SiC_4), -65.28, -78.85, -78.92, -79.19 (RSiO_3); $[\text{M}]^+$ 1894.1723 (1894.1681 theory); elemental analysis: calcd (%) 70.29, 3.12, 0.75; found 72.87, 2.92, 0.74; UV-Vis λ_{max} (nm) (ϵ ($\text{M}^{-1}\text{cm}^{-1}$)) (toluene) 432 (4935), 705 (343); Fluorescence (λ_{exc} = 335 nm, toluene) 719 nm

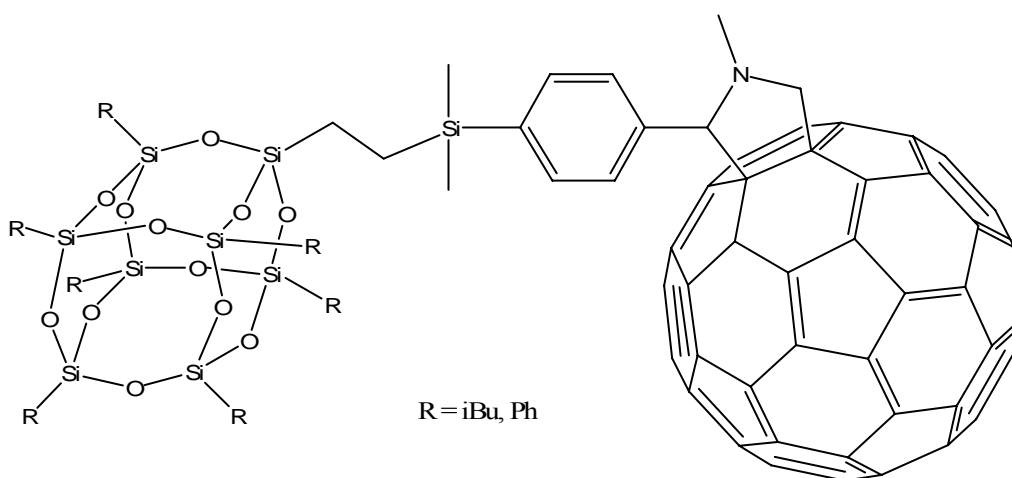


Figure 6.6. Structure of POSS fulleropyrrolidines (2.7, 2.8)

6.3.2 POSS Fulleropyrrolidines: Synthetic Pathway 2

Mono-benzyl chloride POSS, R = iBu (2.9)

Mono-benzyl chloride POSS was synthesised according to the method outlined by Wei *et al.*⁹ The example of R = iBu (2.9) is detailed herein. Trichloro[4-(chloromethyl)phenyl]silane (2.7 ml, 14 mmol) was added drop wise to a solution of iBu₇Si₇O₉(OH)₃ (10 g, 12.6 mmol) and triethylamine (6 ml, 43 mmol) in THF (30 ml). The reaction mixture was stirred overnight and then filtered through celite. The filtrate was added to a stirred solution of acetonitrile and the resultant precipitate was isolated by filtration and dried *in vacuo*.^{9,10}

Yield = 4.00 g (34 %); FTIR (KBr, cm⁻¹): 2954m, 2869m, 1465m, 1400w, 1366w, 1332w, 1230m, 1110vs, 1039m, 838m, 741m, 694w; ¹H NMR (CDCl₃): δ 0.58-0.62 (m, 16H, iBu CH₂), 0.93-0.97 (m, 42H, iBu CH₃), 1.85-1.91 (m, 7H, iBu CH), 4.59 (s, 2H, CH₂Cl), 7.39 (d, ³J_{H-H} = 7.50 Hz, 2H, CH), 7.64 (d, ³J_{H-H} = 7.50 Hz, 2H, CH); ¹³C NMR (CDCl₃): δ 22.37, 22.46, 23.85, 25.69, 46.09, 127.68, 132.13, 134.44, 139.28 ²⁹Si NMR (CDCl₃): δ -67.97, -68.26, -68.29, -68.49; [M+Na]⁺ 963.2536 (963.2529 theory)

Mono-benzyl chloride POSS, R = Cp (2.10)⁹

Yield = 2.42 g (46 %); FTIR (KBr, cm⁻¹): 2950m, 2865m, 1608m, 1108vs, 913m; ¹H NMR (CDCl₃): δ 0.99-1.04 (m, 7H, Cp), 1.52-1.56 (m, 42H, Cp), 1.76-1.78 (m, 14H, Cp), 4.60 (s, 2H, CH₂Cl), 7.40 (d, ³J_{H-H} = 7.8 Hz, 2H, CH), 7.67 (d, ³J_{H-H} = 7.8 Hz, 2H, CH); ¹³C NMR (CDCl₃): δ 22.22, 26.96, 27.02, 27.30, 46.13 (CH₂Cl), 127.70, 132.54, 134.49, 139.22; ²⁹Si NMR (CDCl₃): δ -67.81, -68.22, -79.61; [M+Na]⁺ 1047.2541 (1047.2529 theory)

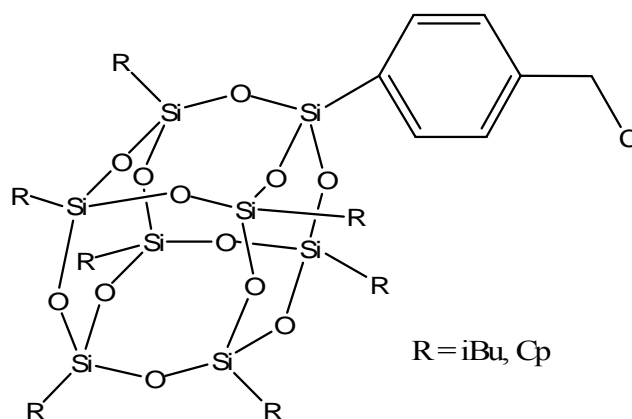


Figure 6.7. Structure of mono-benzyl chloride POSS (2.9, 2.10)

Mono-aldehyde POSS, R = iBu (2.11)

Mono-aldehyde POSS was synthesised according to the literature procedure reported by Wei *et al.*⁹ The example of R = iBu (**2.11**) is detailed herein. 4-Hydroxybenzaldehyde (0.14 g, 1.06 mmol) and potassium carbonate (0.32 g, 0.98 mmol) were stirred in DMF (10 ml) at 90 °C for 1 hour. **2.9** (1 g, 0.8 mmol) in THF (10 ml) was added drop wise over 30 minutes. Sodium iodide (0.14 g, 0.98 mmol) was added and the solution was refluxed overnight. The solution was diluted with water and extracted with chloroform (2 x 50 ml). The organic layer was washed with water (3 x 50 ml), dried (MgSO₄), filtered and evaporated. Methanol was added and the resultant precipitate was filtered and dried *in vacuo*.

Yield = 0.372 g (42 %); FTIR (KBr, cm⁻¹): 2954m, 2869m, 1697m, 1601m, 1579w, 1508w, 1465m, 1401w, 1383w, 1366w, 1332w, 1230m, 1110vs, 1038m, 1012m, 838m, 741m, 690m; ¹H NMR (CDCl₃): δ 0.63-0.66 (m, 16H, iBu CH₂), 0.94-0.99 (m, 42H, iBu CH₃), 1.83-1.93 (m, 7H, iBu CH), 5.17 (s, 2H, CH₂), 7.08 (d, ³J_{H-H} = 8.70 Hz, 2H, CH), 7.44 (d, ³J_{H-H} = 7.50 Hz, 2H, CH), 7.71 (d, ³J_{H-H} = 7.50 Hz, 2H, CH), 7.85 (d, ³J_{H-H} = 8.70 Hz, 2H, CH), 9.90 (s, 1H, CHO); ¹³C NMR (CDCl₃): δ 22.44, 22.48, 22.57, 23.03, 23.66, 25.68, 70.04, 114.81, 116.03, 129.61, 132.13, 132.46, 164.36 (C-O), 191.17 (C=O); ²⁹Si NMR (CDCl₃): δ -67.60, -68.23; [M+Na]⁺ 1049.3113 (1049.3130 theory).

Mono-aldehyde POSS, R = Cp (2.12)

Yield = 0.54 g (56 %); FTIR (KBr, cm^{-1}): 2950m, 2865m, 1699m, 1601m, 1579w, 1321w, 1253w, 1109vs, 941w, 830w, 806w; ^1H NMR (CDCl_3): δ 0.96-1.04 (m, 7H, Cp), 1.51-1.56 (m, 42H, Cp), 1.77 (m, 14H, Cp), 5.17 (s, 2H, CH_2), 7.08 (d, $^3J_{\text{H-H}} = 8.70\text{Hz}$, 2H, CH), 7.43 (d, $^3J_{\text{H-H}} = 7.50\text{ Hz}$, 2H, CH), 7.71 (d, $^3J_{\text{H-H}} = 7.50\text{ Hz}$, 2H, CH), 7.84 (d, $^3J_{\text{H-H}} = 8.70\text{ Hz}$, 2H, CH), 9.88 (s, 1H, CHO); ^{13}C NMR (CDCl_3): δ 22.44, 22.47, 27.20, 27.26, 27.60, 70.42, 115.42, 116.41, 126.74, 130.40, 132.25, 132.62, 134.72, 138.12, 163.68 (C-O), 190.74 (C=O); ^{29}Si NMR (CDCl_3): δ -67.54, -68.19, -79.12; $[\text{M}+\text{Na}]^+$ 1133.3134 (1133.3130 theory)

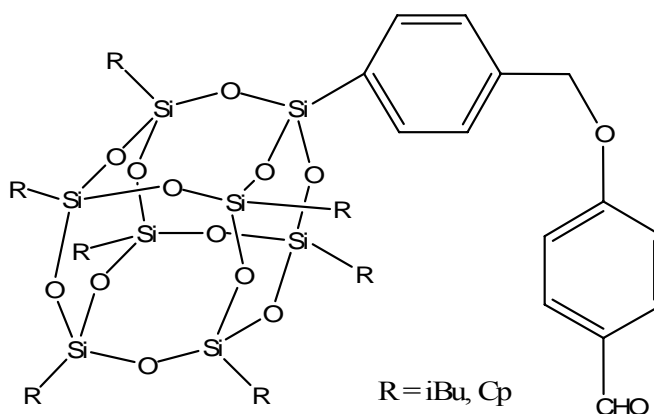


Figure 6.8. Structure of mono-aldehyde POSS (2.11, 2.12)

POSS Fulleropyrrolidine, R = iBu (2.13)

POSS fulleropyrrolidines were synthesised through modification of the literature procedure detailed by Prato *et al.*⁸ The example of R = iBu (2.13) is detailed herein. Mono-aldehyde POSS (310 mg, 0.28 mmol) was added to a solution containing C_{60} (100 mg, 0.14 mmol), N-methylglycine (25 mg, 0.28 mmol) and toluene (100 ml), and the solution was refluxed overnight. The solvent was removed *in vacuo* and the residue extracted with toluene and separated with flash chromatography (eluant hexane/dichloromethane). Evaporation of the brown fraction yielded the POSS-fulleropyrrolidine product as a brown solid.

Yield = 80 mg (54 %); FTIR (KBr, cm^{-1}): 2954m, 2905m, 2870m, 2779w, 1698w, 1600m, 1577w, 1512m, 1382w, 1366w, 1332w, 1261m, 1229m, 1110vs, 1035m, 833m, 803m, 743m; ^1H NMR (CDCl_3): δ 0.65-0.66 (m, 16H, iBu CH_2), 0.96-1.01 (m, 42H, iBu CH_3), 1.86-1.93 (m, 7H, iBu CH), 2.80 (s, 3H, NCH_3), 4.26-4.27 (m, 1H, NCH_2), 4.91 (s, 1H, NCH), 4.96-5.21 (m, 3H, CH_2O and NCH_2), 6.85-7.07 (m, 4H, CH), 7.43-7.50 (m, 2H, CH), 7.68-7.84 (m, 4H, CH); ^{13}C NMR (CDCl_3): δ 22.62, 22.71, 24.02, 25.86, 40.14, 69.15, 70.12, 83.32, 115.14, 126.75, 128.42, 128.50, 129.75, 129.91, 131.68, 132.54, 134.47, 135.95, 136.00, 136.74, 136.96, 139.07, 139.13, 139.19, 139.75, 140.09, 140.34, 141.32, 141.44, 141.72, 141.85, 142.01, 142.14, 142.21, 142.29, 142.43, 142.73, 142.84, 143.16, 143.32, 144.34, 144.80, 144.85, 145.32, 145.42, 145.45, 145.49, 145.65, 145.72, 145.95, 146.10, 160.30, 146.38, 146.48, 146.52, 146.68, 146.97, 147.47, 153.80, 154.27, 156.56, 159.04; ^{29}Si NMR (CDCl_3): δ -67.65, -68.26; $[\text{M}+\text{Na}]^+$ 1774.3790 (1774.3739 theory); elemental analysis: calcd (%) 69.81, 5.01, 0.77; found 70.36, 4.48, 0.79; UV-Vis λ_{max} (nm) (ϵ ($\text{M}^{-1}\text{cm}^{-1}$)) (toluene) 432 (2695), 706 (214); Fluorescence (λ_{exc} = 335 nm, toluene) 723 nm

POSS Fulleropyrrolidine, R = Cp (2.14)

Yield = 171mg (60 %); FTIR (KBr, cm^{-1}): 2949m, 2865m, 1699m, 1601m, 1579w, 1508m, 1451m, 1400w, 1321w, 1252m, 1114, 914m, 830m, 806m, 700w; ^1H NMR (CDCl_3): δ 1.03 (m, 7H, Cp), 1.54 (m, 42H, Cp), 1.78 (m, 14H, Cp), 2.80 (m, 3H, NCH_3), 4.25-4.27 (m, 1H, CH_2), 4.91-5.13 (m, 3H, CH and CH_2), 7.04 (m, 2H, CH), 7.43 (m, 4H, CH), 7.69 (m, 2H, CH); ^{13}C NMR (CDCl_3): δ 22.40, 27.13, 27.18, 27.46, 40.13, 69.12, 70.13, 83.28, 115.10, 126.75, 129.47, 129.88, 130.65, 132.02, 134.67, 135.92, 135.96, 136.71, 136.93, 138.94, 139.71, 120.06, 140.29, 141.42, 141.68, 141.81, 141.97, 142.11, 142.17, 142.25, 142.40, 142.69, 142.81, 143.13, 143.28, 144.53, 144.76, 144.85, 145.28, 145.38, 145.44, 145.61, 145.68, 145.91, 146.07, 146.26, 146.34, 146.43, 146.49, 146.65, 146.93, 147.23, 147.44, 153.76, 154.23, 156.50, 159.00; ^{29}Si NMR (CDCl_3): δ -66.22, -66.55; $[\text{M}+\text{Na}]^+$ 1880.3600 (1880.3603 theory); elemental analysis: calcd (%) 70.24, 4.82, 0.78; found 71.70, 4.28, 0.75; UV-Vis λ_{max} (nm) (ϵ ($\text{M}^{-1}\text{cm}^{-1}$)) (toluene) 433 (3028), 704 (260); Fluorescence (λ_{exc} = 335 nm, toluene) 721 nm

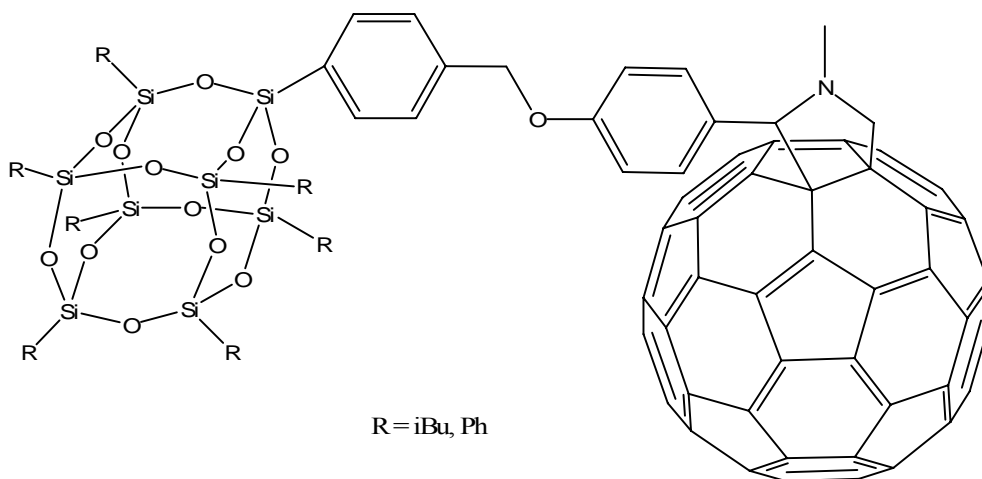


Figure 6.9. Structure of POSS Fulleropyrrolidines (2.13, 2.14)

6.3.3 POSS Iminofullerenes

Mono-benzyl azide POSS (2.15)

Sodium azide (1.10 g, 16.9 mmol) was added to a solution of **2.9** (1.62 g, 1.69 mmol) in DMF (40 ml) and the solution was refluxed overnight. The solution was cooled to room temperature, diluted with chloroform (150 ml), and washed with a NaHCO₃ solution (1 M, 2 x 100 ml) and water (2 x 100 ml). The organic layer was dried (Na₂SO₄) and the solvent removed *in vacuo* to yield **2.16** as a white solid.

Yield = 0.33 g (33 %); FTIR (KBr, cm⁻¹): 2954s, 2869m, 2099m, 1465m, 1399w, 1383w, 1366w, 1332w, 1230s, 1106vs, 1038m, 838m, 803w, 744m; ¹H NMR (CDCl₃): δ 0.57-0.67 (m, 14H, iBu CH₂), 0.95-0.99 (m, 42H, iBu CH₃), 1.85-1.93 (m, 7H, iBu CH), 4.36 (s, 2H, CH₂N₃), 7.33 (d, ³J_{H-H} = 7.8 Hz, 2H, CH), 7.69 (d, ³J_{H-H} = 7.8 Hz, 2H, CH); ¹³C NMR (CDCl₃): δ 22.59, 22.71, 23.28, 23.37, 24.05, 24.12, 55.93, 127.48, 134.67, 134.74, 137.55; ²⁹Si NMR (CDCl₃): δ -67.58, -68.24; [M+Na]⁺ 970.2937 (970.2933 theory)

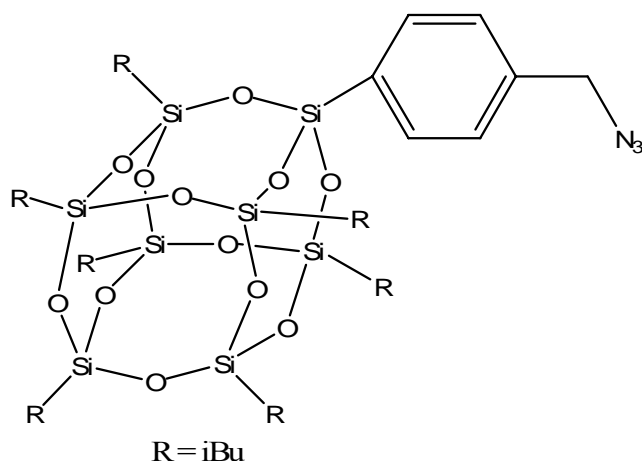


Figure 6.10. Structure of mono-benzyl azide POSS (2.17)

POSS Iminofullerene (2.16)

2.15 (266 mg, 0.28 mmol) was added to a solution of C₆₀ (0.2 g, 0.28 mmol) in chlorobenzene (100 ml) and the solution was refluxed overnight. The solvent was removed *in vacuo* and the residue was purified by flash chromatography (eluant hexane).

Yield = 82 mg (36 %); FTIR (KBr, cm⁻¹): 2955m, 2926m, 2906m, 2870m, 1606w, 1464w, 1400w, 1382w, 1365w, 1332w, 1262m, 1229w, 1168m, 1105vs, 1022m, 801s, 742m, 691w; ¹H NMR (CDCl₃): δ 0.63 - 0.68 (m, 16H, iBu CH₂), 0.91-0.99 (m, 42H, iBu CH₃), 1.85-1.93 (m, 7H, iBu CH), 4.98 (s, 2H, CH₂N), 7.78-7.80 (m, 4H, CH); ¹³C NMR (CDCl₃): δ 22.68, 22.74, 24.05, 25.88, 68.12, 128.25, 131.75, 134.69, 136.53, 137.31, 138.45, 138.76, 139.54, 139.63, 141.05, 141.71, 142.37, 142.92, 143.31, 143.36, 143.63, 144.05, 144.24, 144.51, 144.76, 144.92, 145.37, 146.52, 147.98, 152.74; ²⁹Si NMR (CDCl₃): δ -67.97, -68.25; [M]⁺ 1779.0801 (1779.0783 theory); elemental analysis: calcd (%) 70.78, 3.84, 0.74; found 69.29, 4.14, 0.75; UV-Vis λ_{max} (nm) (ε (M⁻¹cm⁻¹)) (toluene) 334 (23163), 698 (138); Fluorescence (λ_{exc} = 335 nm, toluene) 733 nm

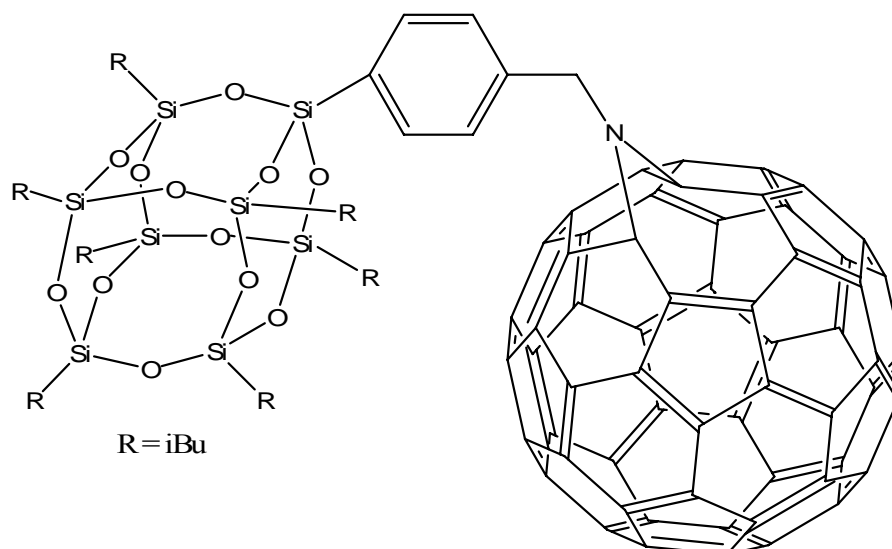


Figure 6.11. Structure of POSS iminofullerene (2.16)

6.3.4 POSS Imides

Mono-(3-aminopropyl)POSS (3.1)

Mono-(3-aminopropyl)POSS was synthesised according to the literature procedure reported by Carsten and Adolf.¹¹ (3-aminopropyl)triethoxysilane (3 ml, 12.8 mmol) was added to a solution of $i\text{Bu}_7\text{Si}_7\text{O}_9(\text{OH})_3$ (10 g, 12.6 mmol) in THF (20 ml). Tetrabutylammonium hydroxide was added (1 ml of 40 wt% solution) and the solution was stirred overnight. Methanol was added and the solution stirred for 4 hours. The resultant product was isolated by filtration and washed with acetone (2 x 20 ml) to yield **3.1** as a white powder.

Yield = 3.67 g (33 %); FTIR (KBr, cm^{-1}): 2953s, 2927s, 2870s, 1464m, 1399m, 1366m, 1331m, 1230s, 1168m, 1103vs, 1039w, 955w, 838m, 747m, 649w; ^1H NMR (CDCl_3): δ 0.58-0.61 (m, 7H, iBu CH_2), 0.95 (d, $^3J_{\text{H-H}} = 6.60$ Hz, 42H, iBu CH_3), 1.50-1.58 (m, 2H, CH_2), 1.80-1.92 (m, 7H, iBu CH), 2.67 (t, 2H, $^3J_{\text{H-H}} = 7.2$ Hz, 2H, CH_2N); ^{13}C NMR (CDCl_3): δ 9.36 (SiCH_2), 22.65 (CH_2), 24.01, 25.84, 27.23, 44.90 (CH_2N); ^{29}Si NMR (CDCl_3): δ -67.64, -68.06, -68.26; M^+ 874.3202 (874.3126 theory)

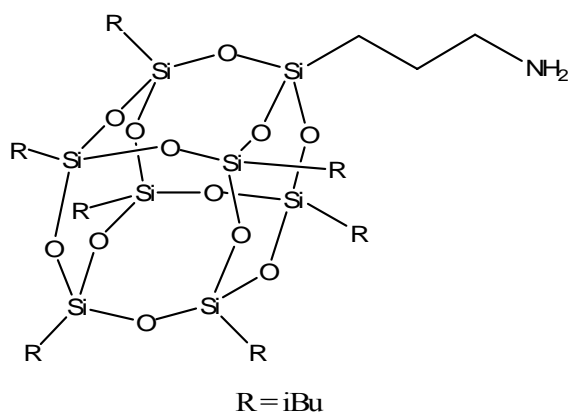


Figure 6.12. Structure of (3-aminopropyl)POSS (3.1)

Octa-(3-chloroammoniumpropyl)POSS (OAPS) (3.4)

Octa-(3-chloroammoniumpropyl)POSS was synthesised according to the literature procedure reported by Laine *et al.*¹⁴ (3-aminopropyl)triethoxysilane (15 ml, 83.8 mmol) was added to a solution of methanol (360 ml) and concentrated aqueous HCl (27 ml). The solution was stirred for six weeks and the resultant precipitate was collected by filtration and dried *in vacuo*.

Yield = 3.70 g (30 %); FTIR (KBr, cm^{-1}): 3007s, 2893s, 2031m, 1593m, 1513s, 1415w, 1393w, 1334w, 1309w, 1214m, 1146vs, 997m, 944m, 890w, 708m; ^1H NMR (D_2O): δ 0.80 (t, $^3J_{\text{H-H}} = 7.20$ Hz, 2H, SiCH₂), 1.77 (p, $^3J_{\text{H-H}} = 7.20$ Hz, 2H, CH₂), 2.99 (t, $^3J_{\text{H-H}} = 7.20$ Hz, 2H, CH₂N); ^{13}C NMR (D_2O): δ 8.08 (SiCH₂), 20.60 (CH₂CH₂CH₂), 41.68 (NCH₂); ^{29}Si NMR (D_2O): δ -66.65

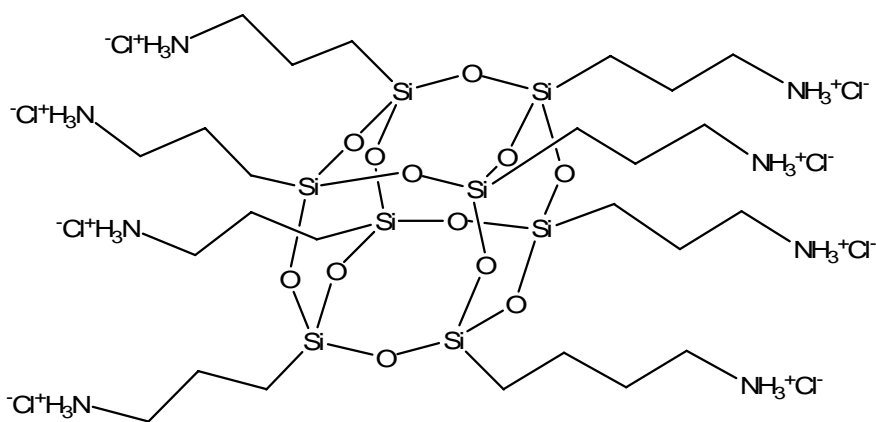


Figure 6.13. Structure of octa(3-chloroammoniumpropyl)POSS (3.4)

Mono-phthalic POSS imide (3.2)

All mono- and bis- POSS imides were synthesised according to the method for the mono-phthalic POSS imide (3.2) outlined below. Phthalic anhydride (166 mg, 1.12 mmol), **3.1** (3.918 g, 4.48 mmol) and imidazole (10 g, 14.7 mmol) were combined. The mixture was reacted in a microwave reactor for approximately 5 minutes, with homogenisation performed as required.¹³ Tetrahydrofuran (100 ml) and hydrochloric acid (100 ml, 3 M) were added and the solution stirred overnight. Diethyl ether (100 ml) was added and the organic layer was separated, washed with water (2 x 100 ml), dried (MgSO₄), filtered and the solvent removed *in vacuo*. The resultant solid was dissolved in the minimum amount of chloroform and methanol (150 ml) was added.

Yield = 173 mg (15 %); FTIR (KBr, cm⁻¹): 2954s, 2869m, 1776w, 1719m, 1465m, 1396m, 1366m, 1332m, 1230m, 1169m, 1109vs, 837m, 743m; ¹H NMR (CDCl₃): δ 0.57-0.65 (m, 16H, SiCH₂/iBu CH₂), 0.92-0.96 (m, 42H, iBu CH₃), 1.78-1.87 (m, 9H, CH₂/iBu CH), 3.67 (t, ³J_{H-H} = 7.20 Hz, 2H, CH₂N), 7.69-7.72 (m, 2H, CH), 7.84-7.86 (m, 2H, CH); ¹³C NMR (CDCl₃): δ 9.56 (SiCH₂), 22.14 (CH₂), 22.47, 23.85, 25.69 (iBu), 40.48 (CH₂N), 123.13 (CH), 132.20 (C-C), 133.80 (CH), 168.33 (C=O); ²⁹Si NMR (CDCl₃): δ -68.02, -68.36, -68.56; [M+Na]⁺ 1026.3072 (1026.3083 theory); elemental analysis: calcd (%) 46.62, 7.32, 1.39; found 46.38, 98.13, 1.06; UV-Vis λ_{max} (nm) ε (M⁻¹cm⁻¹): 294 (2356)

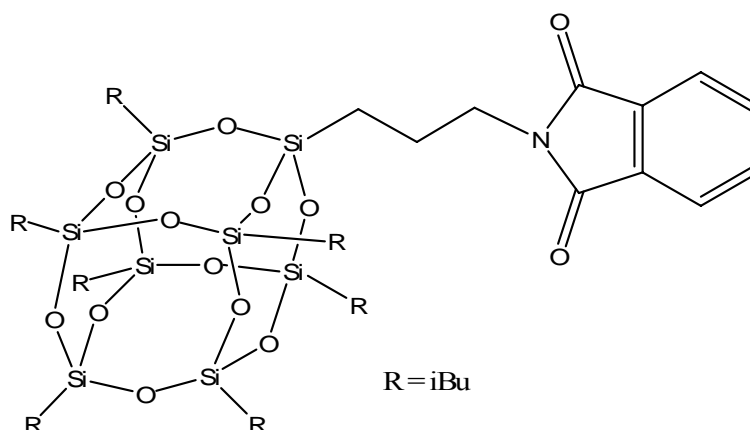


Figure 6.14. Structure of mono-phthalic POSS imide (3.2)

Bis-phthalic POSS imide (3.3)

Yield = 480 mg (37 %); FTIR (KBr, cm^{-1}): 2954m, 2870m, 1774w, 1727m, 1465m, 1391m, 1366m, 1332w, 1230m, 1112vs, 838m, 743m; ^1H NMR (CDCl_3): δ 0.57-0.60 (m, 32H, $\text{SiCH}_2/\text{iBu CH}_2$), 0.92-0.96 (m, 84H, iBu CH_3), 1.80-1.90 (m, 18H, $\text{CH}_2/\text{iBu CH}$), 3.72 (m, 4H, CH_2N), 8.27 (m, 2H, CH); ^{13}C NMR (CDCl_3): δ 9.56 (SiCH_2), 22.04 (CH_2), 22.47, 23.82, 25.67 (iBu), 41.09 (CH_2N), 118.06, 137.23, 166.18 ($\text{C}=\text{O}$); ^{29}Si NMR (CDCl_3): δ -68.01, -68.3, -68.51; $[\text{M}+\text{Na}]^+$ 1951.5829 (1951.5799 theory); elemental analysis: calcd (%) 45.02, 7.45, 1.39; found 44.78, 7.31, 1.45; UV-Vis λ_{max} (nm) ϵ ($\text{M}^{-1}\text{cm}^{-1}$): 309 (2357)

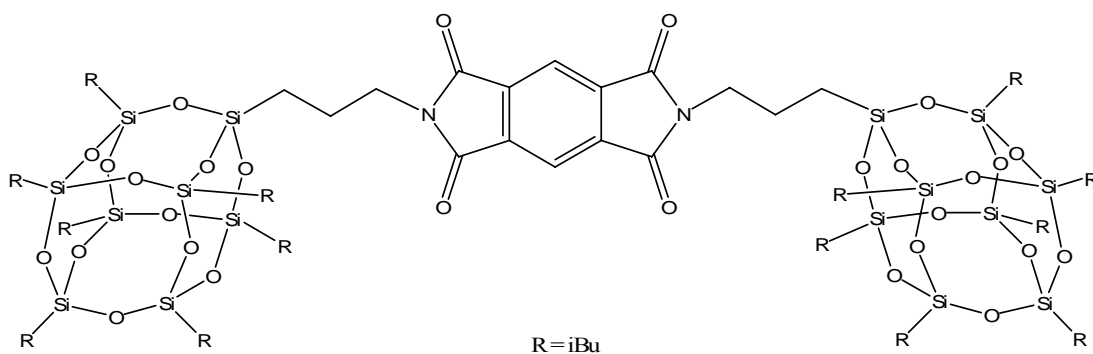


Figure 6.15. Structure of bis-phthalic POSS imide (3.3)

Octa-phthalic POSS imide (3.5)

Octa-phthalic POSS imide was synthesised according to the literature procedure reported by Laine *et al.*¹⁴ Phthalic anhydride (4.0 g, 27 mmol) and **3.4** (0.2 g, 0.15 mmol) were heated overnight at 150 °C. The flask was allowed to cool and chloroform (25 ml) was added. The solution was filtered, washed with chloroform and evaporated. The resultant white powder was dried *in vacuo*.

Yield = 87 mg (31 %); FTIR (KBr, cm^{-1}): 2963m, 1775m, 1713s, 1465m, 1437m, 1398m, 1370m, 1262m, 1096vs, 872m, 801s, 718m; ^1H NMR (CDCl_3): δ 0.62-0.68 (m, 16H, SiCH_2), 1.69-1.80 (m, 16H, CH_2), 3.59-3.64 (m, 16H, CH_2N), 7.57-7.61 (m, 16H, CH), 7.64-7.68 (m, 16H, CH); ^{13}C NMR (CDCl_3): δ 8.97 (SiCH_2), 21.85 (CH_2), 40.16 (CH_2N), 122.97, 132.25, 133.46, 168.17 ($\text{C}=\text{O}$); ^{29}Si NMR (CDCl_3): δ -67.61; $[\text{M}+\text{Na}]^{2+}$ 983.1506 (983.1516 theory); UV-Vis λ_{max} (nm) ϵ ($\text{M}^{-1}\text{cm}^{-1}$): 294 (85726)

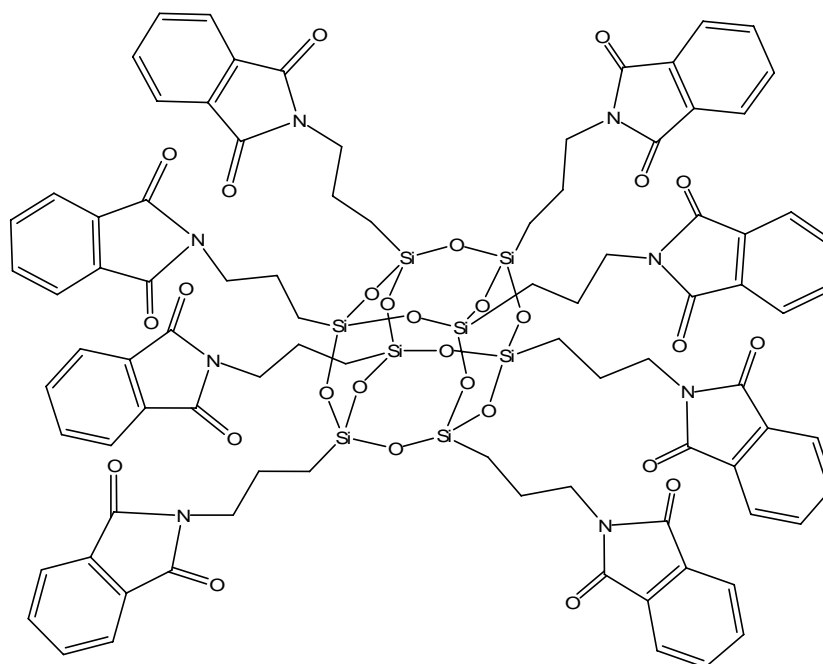


Figure 6.16. Structure of octa-phthalic POSS imide (3.5)

Mono-naphthalic POSS imide (3.6)

Yield = 107 mg (54 %); FTIR (KBr, cm^{-1}): 2954m, 2906w, 2870w, 1703m, 1671m, 1591w, 1465w, 1437w, 1386w, 1365w, 1344w, 1316w, 1261w, 1244m, 1230w, 1200w, 1168w, 1109vs, 1032w, 837w, 802w, 782w, 743w; ^1H NMR (CDCl_3): δ 0.57-0.61 (m, 14H, iBu CH_2), 0.70-0.76 (m, 2H, SiCH_2), 0.93-0.96 (m, 42H, iBu CH_3), 1.79-1.90 (m, 7H, iBu CH), 4.15 (t, $^3J_{\text{H-H}} = 6.6$ Hz, 4H, CH_2N), 7.73 (t, $^3J_{\text{H-H}} = 7.8$ Hz, 2H, CH), 8.18 (dd, $^3J_{\text{H-H}} = 8.40$ Hz, $^2J_{\text{H-H}} = 0.9$ Hz, 2H, CH), 8.58 (dd, $^3J_{\text{H-H}} = 7.80$ Hz, $^2J_{\text{H-H}} = 0.9$ Hz, 2H, CH); ^{13}C NMR (CDCl_3): δ 9.72 (SiCH_2), 21.55 (CH_2), 22.39, 22.50, 23.84, 25.68, (iBu), 42.69 (CH_2N), 122.81, 126.85, 128.15, 131.04, 131.55, 133.68, 163.98 (C=O); ^{29}Si NMR (CDCl_3): δ -68.05, -68.30, -68.40; $[\text{M}+\text{Na}]^+$ 1076.3229 (1076.3239 theory); elemental analysis: calcd (%) 48.97, 7.17, 1.33; found 48.31, 7.42, 1.43; UV-Vis λ_{max} (nm) ϵ ($\text{M}^{-1}\text{cm}^{-1}$): 335 (13846), 350 (15022); Fluorescence ($\lambda_{\text{exc}} = 335$ nm, CHCl_3) 362, 380, 390 nm ($\Phi_{\text{F}} = 0.02$)

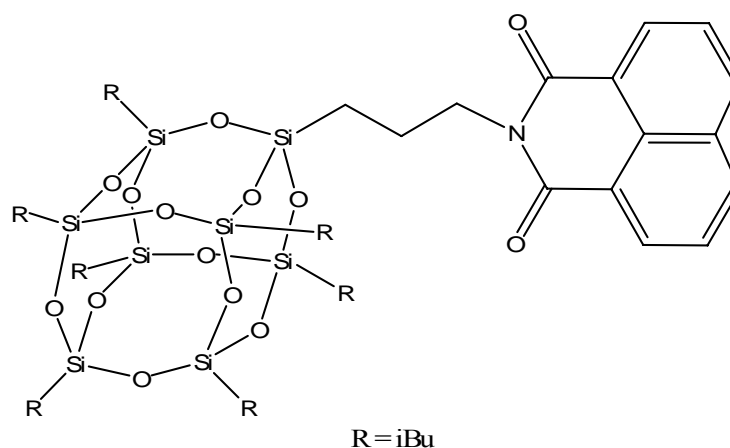


Figure 6.17. Structure of mono-naphthalic-POSS imide (3.6)

Bis-naphthalic POSS imide (3.7)

Yield = 368 mg (49 %); FTIR (KBr, cm^{-1}): 2954m, 2870m, 1709m, 1672m, 1465w, 1366w, 1333m, 1230m, 1112vs, 838w, 743m; ^1H NMR (CDCl_3): δ 0.57-0.61 (m, 28H, iBu CH_2), 0.69-0.75 (m, 4H, SiCH_2), 0.92-0.96 (m, 84H, iBu CH_3), 1.84 (n, $^3J_{\text{H-H}} = 6.3$ Hz, 18H, $\text{CH}_2/\text{iBu CH}$), 3.67 (t, $^3J_{\text{H-H}} = 7.20$ Hz, 4H, NCH_2), 8.76 (s, 4H, CH); ^{13}C NMR (CDCl_3): δ 9.72 (SiCH_2), 21.55 (CH_2), 22.47, 23.85, 25.68 (iBu), 43.16 (CH_2N), 126.68, 130.86, 162.71 ($\text{C}=\text{O}$); ^{29}Si NMR (CDCl_3): δ -68.03, -68.34, -68.54 [$\text{M}+\text{Na}$] $^+$ 2001.5946 (2001.5955 theory); elemental analysis: calcd (%) 46.02, 7.32, 1.41; found 46.31, 7.42, 1.43; UV-Vis λ_{max} (nm) ϵ ($\text{M}^{-1}\text{cm}^{-1}$): 342 (10084), 360 (15864), 381 (19153); Fluorescence ($\lambda_{\text{exc}} = 350$ nm, CHCl_3) 350, 386, 404 nm ($\Phi_{\text{F}} = 0.05$)

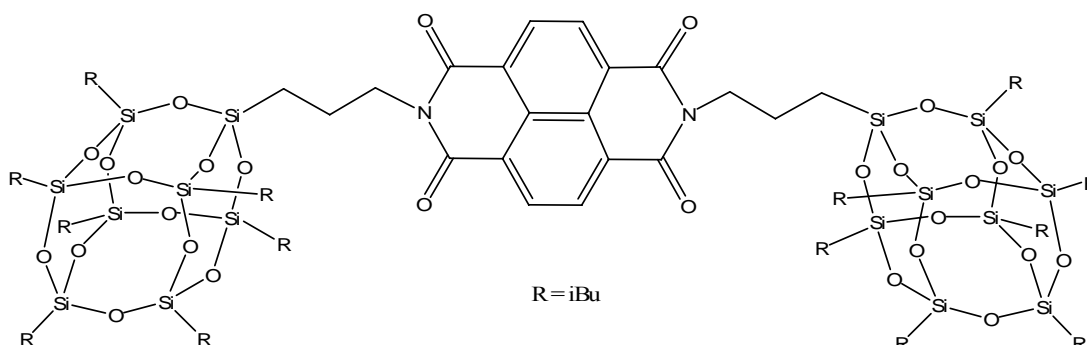


Figure 6.18. Structure of bis-naphthalic-POSS imide (3.7)

Biphenyl POSS imide (3.8)

Yield = 822 mg (88 %); FTIR (KBr, cm^{-1}): 2954m, 2870w, 1773w, 1721m, 1465m, 1391w, 1366w, 1332w, 1261w, 1230m, 1169w, 1110vs, 1038w, 839w, 802w, 742w; ^1H NMR (CDCl_3): δ 0.57-0.61 (m, 32H, $\text{SiCH}_2/\text{iBu CH}_2$), 0.93-0.96 (m, 84H, iBu CH_3), 1.85 (n, $^3J_{\text{H-H}} = 6.3$ Hz, 18H, $\text{CH}_2/\text{iBu CH}$), 3.70 (t, $^3J_{\text{H-H}} = 7.20$ Hz, 4H, CH_2N), 7.97 (s, 4H, CH), 8.10 (s, 2H, CH); ^{13}C NMR (CDCl_3): δ 9.58 (SiCH_2), 22.13 (CH_2), 22.37, 23.86, 25.69, (iBu), 40.71 (CH_2N), 121.99, 123.97, 131.94, 132.74, 133.38, 145.07, 167.74 (C=O); ^{29}Si NMR (CDCl_3): δ -68.06, -68.34, -68.44; $[\text{M}+\text{Na}]^+$ 2027.6108 (2027.6112 theory); elemental analysis: calcd (%) 46.67, 7.23, 1.40; found 45.76, 7.55, 1.04; UV-Vis λ_{max} (nm) ϵ ($\text{M}^{-1}\text{cm}^{-1}$): 259 (34628), 322 (7358); Fluorescence ($\lambda_{\text{exc}} = 320$ nm, CHCl_3) 389 nm ($\Phi_{\text{F}} = 0.07$)

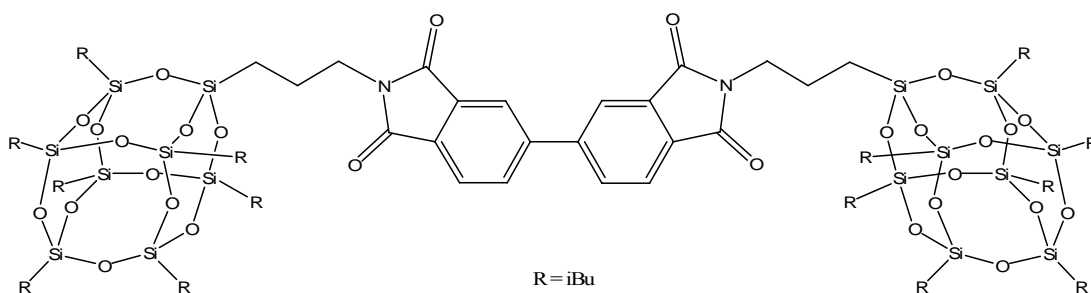


Figure 6.19. Structure of biphenyl POSS imide (3.8)

Perylene POSS imide (3.9)

Yield = 1.323 g (98 %); FTIR (KBr, cm^{-1}): 2954m, 2869m, 1700m, 1663m, 1595m, 1465w, 1404w, 1342w, 1229m, 1110vs, 837w, 811w, 746m; ^1H NMR (CDCl_3): δ 0.54-0.59 (m, 32H, $\text{SiCH}_2/\text{iBu CH}_2$), 0.93 (s, 84H, iBu CH_3), 1.83-1.90 (m, 18H, $\text{CH}_2/\text{iBu CH}$), 4.20 (m, 4H, CH_2N), 8.60 (br m, 8H, CH); ^{13}C NMR (CDCl_3): δ 9.78 (SiCH_2), 21.57 (CH_2), 22.49, 23.93, 25.69, (iBu), 42.94 (CH_2N), 123.08, 123.30, 126.27, 129.23, 131.29, 134.38, 163.11 (C=O); ^{29}Si (CDCl_3): δ -68.05, -68.14, -68.38; $[\text{M}+\text{Na}]^+$ 2127.6260 (2127.628 theory); elemental analysis: calcd (%) 49.06, 6.99, 1.33; found 49.10, 7.05, 1.53; UV-Vis λ_{max} (nm) (ϵ ($\text{M}^{-1}\text{cm}^{-1}$)) 459 (17157), 490 (48730), 526 nm (80877); Fluorescence ($\lambda_{\text{exc}} = 450$ nm, CHCl_3) 533, 575, 620 nm ($\Phi_{\text{F}} = 1.0$)

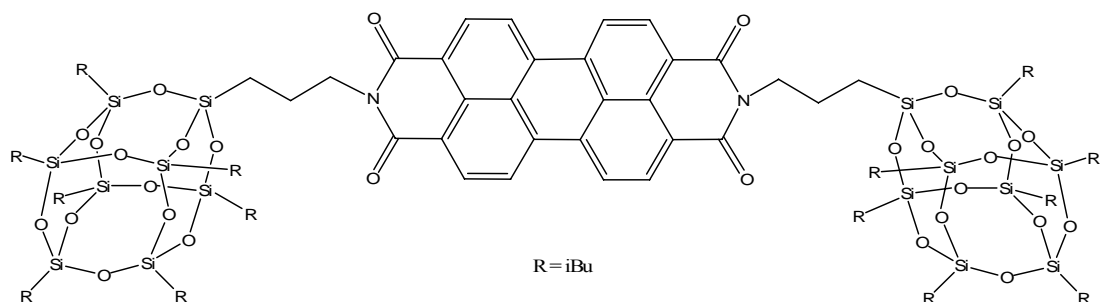


Figure 6.20. Structure of perylene POSS imide (3.9)

6.3.5 POSS Porphyrin

Mono-phenyl POSS (4.1)

Mono-phenyl POSS was synthesised according to the method detailed by Feher *et al.*¹⁵ Benzoyl chloride (0.26 ml, 2.2 mmol) was added drop wise to a solution of **3.1** (1 g, 1.14 mmol) in DMF (10 ml) and Et₃N (1.4 ml, 11 mmol) at 0 °C. The solution was stirred overnight and the crude product was precipitated by addition to 1 M HCl (50 ml) at 0 °C. The product was filtered, washed (H₂O, 10 ml), dissolved in DMSO (10 ml), precipitated into 1 M NaHCO₃ (50 ml), washed with water and dried *in vacuo* to yield a white solid.

Yield = 0.586 g (52 %); FTIR (KBr, cm⁻¹): 2953m, 2870m, 1637m, 1580w, 1544, 1464, 1401m, 1383m, 1366m, 1332m, 1230m, 1202m, 1168m, 1108vs, 837m, 746m, 693m; ¹H NMR (CDCl₃): δ 0.59-0.61 (m, 14H, iBu CH₂), 0.65-0.71 (m, 2H, SiCH₂), 0.94-0.96 (m, 42H, iBu CH₃), 1.69-1.79 (m, 2H, CH₂), 1.81-1.90 (m, 7H, iBu CH), 3.43-3.49 (m, 2H, CH₂N), 6.12 (br s, 1H, NH), 7.43-7.47 (m, 3H, CH), 7.74-7.63 (m, 2H, CH); ¹³C NMR (CDCl₃): δ 9.49, 22.46, 23.06, 23.84, 25.68, 42.25, 126.81, 128.54, 131.29, 167.46; ²⁹Si NMR (CDCl₃): δ -68.04, -68.30; [M+Na]⁺ 1000.3290 (theory 100.3290); elemental analysis: calcd (%) 46.38, 8.14, 1.06; found 46.63, 7.72, 1.43

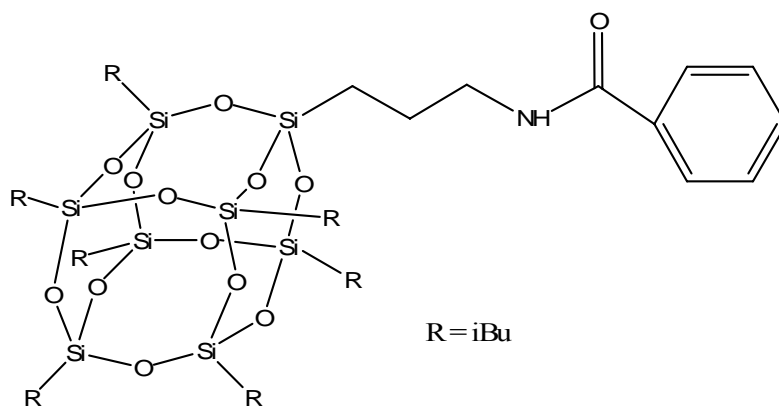


Figure 6.21. Structure of mono-phenyl POSS (4.1)

Isonicotinic acid chloride (4.2)

Isonicotinic acid was synthesised according to the method reported by Rissanen *et al.*¹⁶ Oxalyl chloride (2.02 g, 16.0 mmol) was added to a suspension of isonicotinic acid (2.5 g, 20.3 mmol) in toluene (50 ml) at 0 °C. After 1 hour the solution was warmed to ambient temperature and stirred overnight. The solution was filtered, washed with toluene (50 ml) and dried *in vacuo* to yield **4.2** as white powder.

Yield = 2.332 g (81 %); ¹H NMR (d₆ DMSO): δ 8.32 (d, ³J_{H-H} = 5.7 Hz, 2H, CH), 9.07 (d, ³J_{H-H} = 5.7 Hz, 2H, CH); ¹³C NMR (d₆ DMSO): δ 126.85, 145.36, 145.62, 165.22 (COCl)

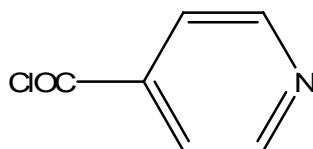


Figure 6.22. Structure of isonicotinic acid chloride (4.2)

Mono-pyridyl POSS (4.3)

4.2 (340 mg, 2.4 mmol) in pyridine (20 ml) was added dropwise to a solution of **3.1** (1 g, 1.14 mmol) in toluene (10 ml) and Et₃N (1 ml, 7.85 mmol) at 0 °C. The solution was stirred overnight and the amine salt was removed by filtration through celite. The filtrate was washed with 1 M HCl (2 x 20 ml), water (2 x 20 ml), dried (MgSO₄), filtered and concentrated *in vacuo* to yield a white solid.

Yield = 0.27 g (24 %); FTIR (KBr, cm^{-1}): 2954m, 2928m, 2906m, 2870m, 1677w, 1545w, 1465m, 1402w, 1383w, 1366w, 1332w, 1261w, 1230m, 1169m, 1110vs, 1038m, 839m, 803w, 744m; ^1H NMR (CDCl_3): δ 0.60 (d, $^3J_{\text{H-H}} = 6.9$ Hz, 14H, iBu CH_2), 0.68-0.75 (m, 2H, SiCH_2), 0.92-0.96 (m, 42H, iBu CH_3), 1.67-1.78 (m, 2H, CH_2), 1.80-1.89 (m, 7H, iBu CH), 3.45 (t, $^3J_{\text{H-H}} = 6.6$ Hz, 2H, CH_2N), 6.24 (m, 1H, NH), 7.58-7.60 (m, 2H, CH), 8.72-8.74 (m, 2H, CH); ^{13}C NMR (CDCl_3): δ 9.65, 22.62, 23.09 (CH_2), 24.04, 25.83, 42.58 (CH_2N), 120.97, 142.10, 150.72, 165.62 ($\text{C}=\text{O}$); ^{29}Si NMR (CDCl_3): δ -68.03, -68.28, -68.63; $[\text{M}+\text{Na}]^+$ 1001.3245 (1001.3243 theory); elemental analysis: calcd (%) 45.36, 7.61, 2.86; found 44.23, 7.93, 2.15; UV-Vis λ_{max} (ϵ ($\text{M}^{-1}\text{cm}^{-1}$)) (CHCl_3) 261 (3423)

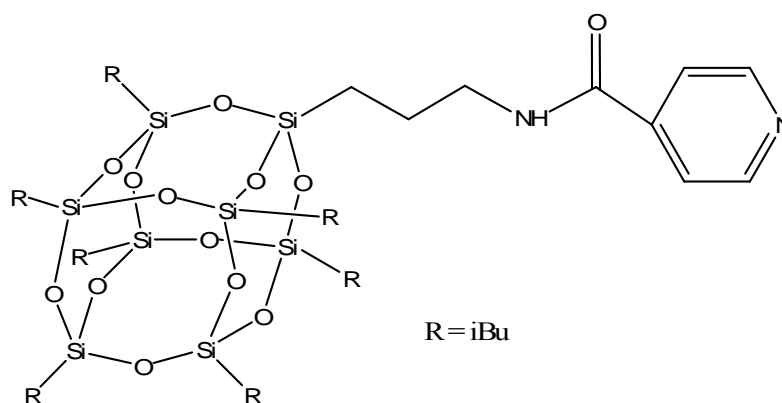


Figure 6.23. Structure of mono-pyridyl POSS (4.3)

POSS Porphyrin (4.4)

4.3 (12.2 mg, 0.0127 mmol) and $[\text{Ru}(\text{C}\equiv\text{O})(\text{EtOH})(\text{TPP})]$ (10 mg, 0.0127 mmol) were combined and stirred in CHCl_3 (10 ml) overnight. The resultant solution was concentrated under reduced pressure and the product was purified by column chromatography (alumina, eluant hexane: CHCl_3 , 3:1).

Yield = 21 mg (96 %); FTIR (KBr, cm^{-1}): 2956s, 2924s, 2869m, 1972s, 1679m, 1640m, 1629m, 1598m, 1529m, 1487w, 1464m, 1441w, 1402w, 1382w, 2366w, 1351w, 1332w, 1306w, 1263m, 1229m, 1207m, 1169m, 1106vs, 1020s, 1008s, 797s, 751m, 702m; ^1H NMR (CDCl_3): δ 0.22-0.27 (m, 2H, SiCH_2), 0.45 (d, $^3J_{\text{H-H}} = 6.9$ Hz, 4H, iBu CH_2), 0.55 (d, $^3J_{\text{H-H}} = 6.9$ Hz, 4H, iBu CH_2), 0.58-0.62 (m, 6H, iBu CH_2),

0.80 (d, $^3J_{\text{H-H}} = 6.6$ Hz, 12H, iBu CH₃) 0.91-0.97 (m, 30H, iBu CH₃), 1.62-1.89 (m, 7H, iBu CH), 4.21-4.24 (m, 2H, NCH₂), 5.48-5.50 (m, 2H, pyridyl), 7.64-7.74 (m, 12H, *m/p*-CH), 8.04-8.06 (m, 4H, *o*-CH), 8.20-8.23 (m, 4H, *o*-CH), 8.62 (s, 8H, pyrrole); ^{13}C NMR (CDCl₃): δ 9.24 (SiCH₂), 22.46, 25.58, 22.69, 23.90, 23.94, 24.02, 25.67, 25.80, 25.84, 29.84, 42.05, 118.90, 121.77, 126.42, 126.74, 127.45, 132.00, 134.13, 134.51, 140.01, 142.69, 143.76, 145.02, 163.53, 180.35; ^{29}Si NMR (CDCl₃): δ -68.22, -68.35, -68.40, -68.89; $[\text{M}+\text{Na}]^+$ 1722.4757 (1722.4763 theory); elemental analysis: calcd (%) 57.18, 6.03, 4.88; found 57.40, 7.39, 3.11; UV-VIS λ_{max} (ϵ (M⁻¹cm⁻¹)) (toluene) 412 (121995), 532 (9236)

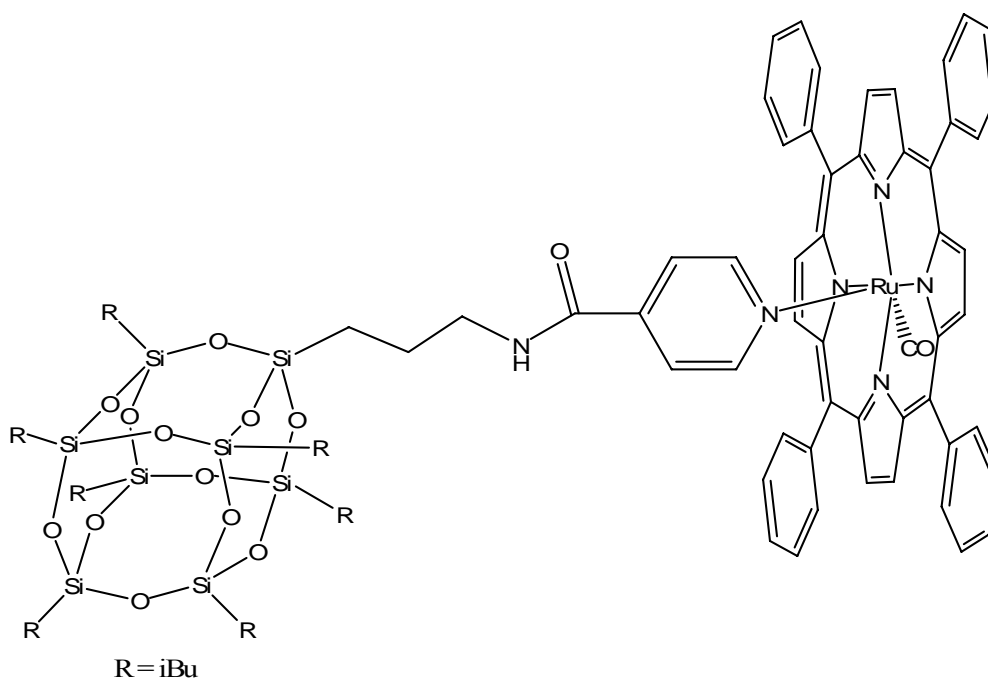


Figure 6.24. Structure of mono-porphyrin POSS (4.4)

6.3.6 POSS Pyrene

1-Pyrene acid chloride (5.1)

Pyrene acid chloride was synthesised according to the method outlined by Yuasa *et al.*¹⁷ A solution of 1-pyrenecarboxylic acid (549.0 mg, 2.23 mmol) in thionyl chloride (20 ml) was refluxed for 3 hours. Thionyl chloride was removed *in vacuo* to yield 1-pyrene acid chloride as a brown/yellow solid.

Yield = 582 g (99 %); ^1H NMR (CDCl_3): δ 8.04-8.31 (m, 7H, CH), 8.88-8.91 (d, 1H, $^3J_{\text{H-H}} = 9.0$ Hz, CH) 8.99-9.04 d (d, 1H, $^3J_{\text{H-H}} = 9.9$ Hz); ^{13}C NMR (CDCl_3): δ 123.88, 124.17, 126.79, 126.96, 127.19, 127.50, 130.18, 130.86, 131.30, 131.40, 131.86, 135.98, 167.92 (C=O)

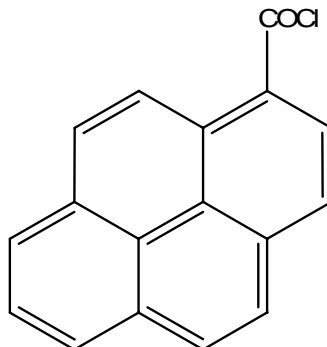


Figure 6.25. Structure of pyrene acid chloride

Mono-pyrene POSS (5.2)

1-pyrene acid chloride (365 mg, 1.3 mmol) in pyridine (20 ml) was added dropwise to a solution of mono-amino POSS (1 g, 1.14 mmol) in toluene (10 ml) and Et_3N (1 ml, 7.85 mmol) at 0 °C. The solution was stirred overnight and the amine salt was removed by filtration through celite. The filtrate was washed with 1 M HCl (2 x 20 ml), water (2 x 20 ml), dried (MgSO_4), filtered and concentrated *in vacuo* to yield a white solid.

Yield = 0.645 g (45 %); FTIR (KBr, cm^{-1}): 2954m, 2870m, 1632m, 1530m, 1465m, 1401w, 1383w, 1366m, 1331m, 1230m, 1168m, 1110vs, 1038m, 841m, 745m; ^1H NMR (CDCl_3): δ 0.60-0.63 (m, 7H, iBu CH_2), 0.74-0.79 (m, 2H, SiCH_2), 0.95-0.97 (m, 42H, iBu CH_3), 1.87 (n, $^3J_{\text{H-H}} = 6.6$ Hz, iBu CH), 3.61-3.68 (m, 2H, CH_2), 8.05-8.16 (m, 6H), 8.12 (d, $^3J_{\text{H-H}} = 9.3$ Hz, 2H), 8.57 (d, $^3J_{\text{H-H}} = 7.8$ Hz, 1H); ^{13}C NMR (CDCl_3): δ 9.79, 22.66, 23.41 (CH_2), 24.00, 25.85, 42.72 (CH_2), 124.57, 124.62, 125.84, 125.93, 126.47, 127.27, 128.75, 128.81, 130.91, 131.36, 131.65, 132.61, 170.01; ^{29}Si NMR (CDCl_3): δ -68.09, -68.27, -68.32, -68.36; $[\text{M}+\text{Na}]^+$ 1124.3595 (1124.3602 theory); elemental analysis: calcd (%) 52.28, 7.22, 1.27; found 52.94, 6.52, 1.83; UV-VIS λ_{max} (ϵ ($\text{M}^{-1}\text{cm}^{-1}$)) (toluene) 332 (18410), 346 (24770); Fluorescence ($\lambda_{\text{exc}} = 365$ nm, toluene) 385, 404, 425 nm ($\Phi_{\text{F}} = 0.91$)

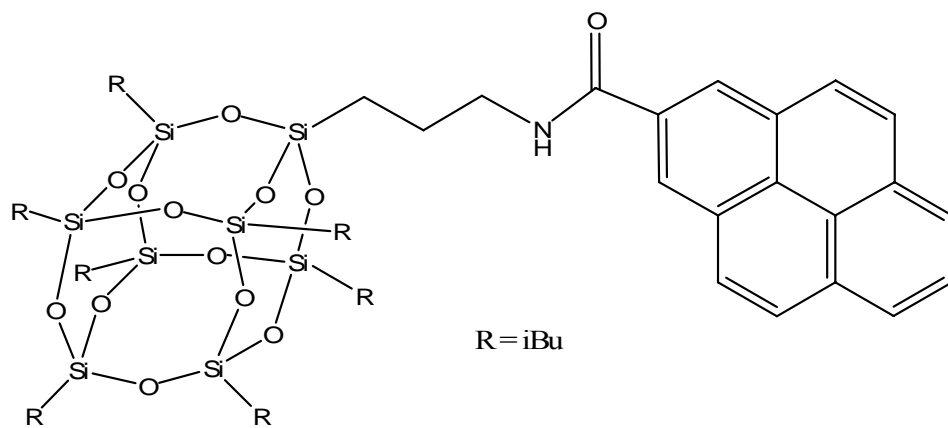


Figure 6.26. Structure of mono-pyrene POSS (5.2)

6.4 References:

- (1) Y. Morel; P. Najechalski; N. Sanz; A. Ibanez; C. Nguetack; C. Andraud; Baldeck, P. L. *Synth. Met.* **2000**, *109*, 215.
- (2) G. M. Sheldrick; University of Gottingen, Germany: 1996.
- (3) S. R. Hall; G. S. D. King; J. M. Stewart *The Xtal 3.5 User's Manual*; University of Western Australia: Perth, 1995.
- (4) W. L. F. Armarego; Chai, C. L. L. *Purification of Laboratory Chemicals*; Fifth ed.; Butterworth-Heinemann, 2003.
- (5) Y. Lee; Silverman, R. B. *Organic Letters* **2000**, *2*, 303.
- (6) E. G. Shockey; A. G. Bolf; P. F. Jones; J. J. Schwab; K. P. Chaffee; T. S. Haddad; J. D. Lichtenhan *Appl. Organomet. Chem.* **1999**, *13*, 311.
- (7) B. W. Manson; J. J. Morrison; P. I. Coupar; P.-A. Jarès; R. E. Morris *J. Chem. Soc., Dalton Trans.* **2001**, 1123.
- (8) M. Maggini; G. Scorrano; M. Prato *J. Am. Chem. Soc.* **1993**, *115*, 9798.
- (9) Leu, C. M.; Chang, Y. T.; Wei, K. H. *Macromolecules* **2003**, *36*, 9122-9127.
- (10) X. Yan Song; H. Ping Geng; Q. F. Li *Polymer* **2006**, *47*, 3049.
- (11) J. Carsten, K. A. 2003.
- (12) Liu, H.; Zhang, W.; Zheng, S. *Polymer* **2005**, *46*, 157-165.
- (13) Kacprzak, K. *Synthetic Communications* **2003**, *33*, 1499-1507.
- (14) M.-C. Gravel, C. Z., M. Dinderman, R. M. Laine *Appl. Organometal. Chem.* **1999**, *13*, 329.
- (15) F. J. Feher; K. D. Wyndham; D. Soulivong; F. Nguyen *J. Chem. Soc., Dalton Trans.* **1999**, *9*, 1491.
- (16) Nattinen, K. I.; Rissanen, K. *Crystal Growth & Design* **2003**, *3*, 339-353.
- (17) Yuasa, H.; Miyagawa, N.; Izumi, T.; Nakatani, M.; Izumi, M.; Hashimoto, H. *Org. Lett.* **2004**, *6*, 1489-1492.

7 CONCLUSIONS & FUTURE WORK

The overall aim of this thesis was to design synthetic methodologies in order to obtain a range of optically active polyhedral oligomeric silsesquioxane compounds. Therefore, POSS compounds were prepared with a range of optical functionalities, with the results summarised below.

7.1 POSS Fulleropyrrolidines

7.1.1 Conclusions

A variety of POSS fullerene compounds have been synthesised through the employment of two synthetic pathways; the cycloaddition of azomethine ylides to C_{60} and the addition of alkyl azides to C_{60} , to generate [6,6] closed fulleropyrrolidines and a [5,6] open iminofullerene. Power limiting measurements were performed on the POSS fullerene compounds, all of which exhibited essentially identical power limiting properties to that of C_{60} .

7.1.2 Future Work

The use of N-functionalised amino acids in the synthesis of POSS fulleropyrrolidines allow for the further functionalisation of the compound with polymerisable functionalities. This would allow the covalent linkage of the POSS fulleropyrrolidine to a range of polymers, the physical and optical properties of which would be able to be further investigated.

The synthesis of multi-functionalised POSS aldehydes, would allow for the synthesis of multi-fulleropyrrolidino POSS compounds. The use of octa-functionalised aldehydes was not investigated in this project, due to the large excess of aldehyde or azide required for the synthetic pathways of choice. This implied it was extremely unlikely that an octa-substituted product could be formed, with a range of substitutions that would be difficult to isolate the likely products. The use of bis- and tri-substituted POSS aldehydes would allow for the formation of the desired

fulleropyrrolidines.

Alternatively, the investigation of different synthetic pathways, such as the addition of unsymmetrical protected malonates, would allow for selective deprotection of one site. DCC mediated coupling would allow for the covalently link the POSS moieties and subsequent deprotection of the other reactive site on the malonates would, in theory, allow for the synthesis of mono-, tri- and possibly octa-functionalised POSS fullerenes, with free reactive sites for the attachment of polymerisable functionalities.

Fullerenes in polymer films or solid matrices display significantly weaker optical limiting responses than in solution. Therefore, in order to maintain a high level of optical limiting response in cross-linked polymeric systems, the attachment of alternative optical limiting compounds to POSS is required.

7.2 POSS Imides

7.2.1 Conclusions

A range of POSS imides have been synthesised through the condensation of POSS amines with a variety of mono and bis-anhydrides. The bis-POSS perylene diimide was also characterised by single crystal x-ray crystallography. The use of microwave radiation has been shown to offer a rapid, high yielding pathway to POSS imides. The naphtha and biphenyl POSS imides exhibited extremely weak fluorescence, whilst the perylene POSS imide displayed particularly strong fluorescence, with a quantum yield approaching unity.

7.2.2 Future Work

The formation of POSS polyimide hybrid materials has previously been investigated. The incorporation of the anhydrides used to synthesise mono-functional imides in this chapter could be applied on a multi-functional scale and the mechanical and physical properties examined. This would likely involve the use of another bis-

anhydride, in conjunction with a small amount of the perylene bis-anhydride to form the POSS imide product. It is expected that a reduction in the dielectric constant would occur, due to the presence of the porous POSS cages and the increase in free volume from the presence of the large, rigid POSS structure.⁵⁴¹

Incorporation of bay functionalised perylenes would allow for the formation of a variety of pigments, due to the disruption of the planarity and solid state packing of the perylene moieties.

Synthesis of a monosubstituted perylene anhydride and subsequent reaction with octa-aminopropyl POSS would enable the synthesis of octa-perylene functionalised POSS. This could be done in a variety of ways, through decarboxylation of one of the anhydride functionalities to form a perylene mono anhydride, or the reaction of one anhydride with a long chain amine, to increase the solubility of the desired product.

7.3 POSS Porphyrin

7.3.1 Conclusions

A range of POSS amides have been synthesised through the reaction of the desired acid chloride with mono(3-aminopropyl)POSS. The introduction of a pyridyl ligand on the periphery of the POSS cage was achieved through this synthetic process, followed by the coordination of a ruthenium tetraphenylporphyrin compound, in order to synthesise a POSS porphyrin compound. Mono-porphyrin POSS exhibited comparable absorption properties to other pyridyl ligated ruthenium porphyrins.

7.3.2 Future Work

The use of multi-hydroxy functionalised POSS would allow for the synthesis of a more soluble pyridyl precursor. Subsequent coupling of these precursors to metalloporphyrins offers a convenient pathway to multi-porphyrin functionalised

POSS cages. Investigation of the optical properties should observe an increase in absorption associated with the multi-functionality.

Phosphorescence studies were unable to be performed under suitably inert, degassed conditions on the available instrumentation, and would allow for quantification of the optical properties and excited state lifetimes of the POSS porphyrin compounds.

7.4 POSS Pyrene

7.4.1 Conclusions

A mono-functionalised POSS pyrene compound was synthesised through the reaction of (3-aminopropyl)POSS with 1-pyrene acid chloride. Mono-pyrene POSS was determined to be strongly fluorescent, exhibiting a high quantum yield of fluorescence.

7.4.2 Future Work

The use of multi-hydroxy functionalised POSS would allow for the synthesis of a more soluble multi-functionalised POSS pyrene compound. Investigation of the optical properties should observe an increase in absorption and bathochromic shift of the absorption maxima, associated with the multi-functionality.